

Helicopter SONAR Control

Cable Control for Helicopter Dipping SONAR
Operations in Hover using Incremental Nonlinear
Dynamic Inversion

Maarten A. J. Maurer



Helicopter SONAR Control

Cable Control for Helicopter Dipping SONAR Operations
in Hover using Incremental Nonlinear Dynamic Inversion

Thesis report

by

Maarten A. J. Maurer

To obtain the degree of Master of Science
at the Delft University of Technology
to be defended publicly on February 7, 2023 at 14:00

Thesis committee:

Chair:	Dr. M.D. Pavel
Supervisors:	Dr. ir. E. van Kampen Dr. M.D. Pavel
External examiner:	Dr. A. Sharpanskykh
Place:	Faculty of Aerospace Engineering, Delft
Project Duration:	October, 2021 - February, 2023
Student number:	4683455

An electronic version of this thesis is available at <http://repository.tudelft.nl/>.



Copyright © Maarten Maurer, 2023
All rights reserved.

Preface

I would like to thank my project supervisors Marilena Pavel and Erik-Jan van Kampen for guiding me through this project. They provided me with knowledge and inspiration throughout.
I also want to thank my friends for the discussions we had and the ideas that followed from that.
My final thanks go to my family for all the support during this project.

Contents

List of Figures	ix
List of Tables	xiii
1 Introduction	4
I Scientific Article	7
2 Cable Control for Dipping SONAR operations using INDI	8
2.1 Introduction	8
2.2 Cable + SONAR Model.	10
2.3 Wind and Turbulence Model.	13
2.4 Principle of NDI and INDI	14
2.5 Cable Controllers.	15
2.6 Simulation Cases.	17
2.7 Simulation Results	18
2.8 Conclusions.	23
II Preliminary Analysis	28
3 Literature Review	29
3.1 General Helicopter	29
3.2 Rotor and Actuator Dynamics	33
3.3 Dipping SONAR Missions	36
3.4 State-of-the-Art Helicopter-SONAR Modelling	39
3.5 Helicopter Automatic Flight Control Systems	43
3.6 INDI Control on Helicopters	49
4 Preliminary study : 3-DOF Helicopter Model	55
4.1 Problem Definition	55
4.2 Case 3-DOF-PH-HUB-CG	57
4.3 Case 3-DOF-PH-HUB-OFF	67
4.4 Case 3-DOF-SP-CG-HUB-OFF	71
4.5 Case 3-DOF-SP-OFF-HUB-OFF	79
4.6 Case 3-DOF-DP-OFF-HUB-OFF	84
4.7 Case 3-DOF-DP-OFF-HUB-OFF-SUB	90
4.8 Concluding Remarks of Preliminary Study for Helicopter Behaviour with Submerged Load	94
III Additional Results	95
5 6-DOF Suspension Cable + SONAR Model	96
5.1 Reference Frames	96
5.2 Assumptions	97
5.3 Kinematics	98
5.4 Force and Moment Equations	100
5.5 Solving for Dynamic System	102
5.6 Modelling Damping	102
5.7 Modelling of Aerodynamic Forces and Hydrodynamic	102
5.8 Cable Model Trim.	104

6	6-Degrees of Freedom SONAR Control	105
6.1	Simulation Cases	105
6.2	Simulation Data	105
6.3	Control Effectiveness	106
6.4	Tuning Process	106
6.5	Case 1: Pure Helicopter with Hub aligned with C.G.	106
6.6	Case 2: Pure Helicopter with Hub unaligned with C.G..	114
6.7	Case 3: Helicopter with Single Cable Section at C.G.	115
6.8	Case 4: Helicopter with Single Cable Section at Offset	121
6.9	Case 5: Helicopter with Multiple Cable Sections at Offset	124
6.10	Case 6: Helicopter with Multiple Cable Sections at Offset, Partially Submerged	129
6.11	Case 7: Helicopter with Multiple Cable Sections at Offset, Partially Submerged with Wind	138
6.12	Conclusions.	144
7	Sensitivity Analysis 6-DOF Cable Controller	147
7.1	Sensitivity to Changing Cable Length	147
7.2	Sensitivity to Amount of Cable Sections.	149
7.3	Conclusions Sensitivity Analysis.	150
8	Verification and Validation	151
8.1	Cable Model Verification	151
8.2	Cable Model Validation.	151
IV	Closure	154
9	Conclusion	155
9.1	Closing Remarks	155
9.2	Research Questions	156
10	Recommendations	159
	References	164
A	Partial Derivatives T, D, V and a_1	165
B	Partial Derivatives Single Pendulum	167
C	Partial Derivatives Double Pendulum	170
D	Simulation Data	175
E	Cable Model Verification	178

Nomenclature

List of Abbreviations

ACAH	Attitude command attitude hold
AFCS	Automatic flight control systems
ASW	Anti-submarine warfare
ATT	Attitude Hold
BS	Backstepping
CPL	Coupled
DCM	Direction cosine matrix
DI	Dynamic inversion
DOF	Degrees of freedom
DP	Double pendulum
IBS	Incremental backstepping
INDI	Incremental Nonlinear Dynamic Inversion
LPF	Low pass filter
LQR	Linear quadratic regulator
LVLH	Local vertical local horizontal
MIMO	Multiple inputs multiple outputs
MRAC	Model reference adaptive control
NDI	Nonlinear dynamic inversion
PCH	Pseudo control hedging
PH	Position hold
PH	Pure helicopter
PID	Proportional integral derivative
SAS	Stability augmentation system
SCAS	Stability control augmentation system
SISO	Single input single output
SMC	Sliding mode control
SONAR	Sound navigation and ranging

SP	Single pendulum
TRC	Translational rate command
UAV	Uninhabited aerial vehicle

Units

°	Degrees
Bft	Beaufort
C	Celsius
cm	Centimeter
ft	Feet
Hz	Herz
kg	Kilogram
kts	Knots
m	Meter
N	Newton
rad	Radians
s	Second

Constants

a_0	Coning angle [1/rad]
a_1	Longitudinal Flap angle [1/rad]
b_1	Lateral Flap angle [1/rad]
c	Chord of main rotor blade [m]
C_{D_i}	Drag coefficient load i 3-DOF model [-]
c_{l_α}	Average lift coefficient per angle of attack [1/rad]
$C_{T_{BEM}}$	Thrust coefficient from blade element theory [-]
$C_{T_{Glau}}$	Thrust coefficient from Glauert method [-]
C_T	Thrust coefficient [-]
D	Drag helicopter [N]

D_{angle}	Damping coefficient on angle [–]	R	Radius of rotor disk [m]
D_{rate}	Damping coefficient on rate [–]	r	Body yaw rate [rad/s]
e	Error [varies]	Re	Reynolds number [–]
f_0	Oscillation frequency Ziegler-Nichols tuning method [Hz]	s	Laplace domain constant [–]
F_c	Tension in cable between load 1 and helicopter [N]	S_i	Surface area load i 3-DOF model [m ²]
F_{c12}	Cable tension between loads 1 and 2 3-DOF model [N]	T	Thrust [N]
F_{ct_i}	Centrifugal force of load i 3-DOF model [N]	u	Longitudinal velocity in body frame [m/s]
h	Height of the rotor hub above the center of mass [m]	V	Free-stream velocity [m/s]
h_l	Distance of load hinge from center of mass in z-direction in body frame [m]	v	Lateral velocity in body frame [m/s]
I_B	Inertia of single main rotor blade [kgm ²]	W	Weight helicopter [N]
I_y	Inertia of Helicopter around the y-axis in body frame 3-DOF model [kgm ²]	w	Vertical velocity in body frame [m/s]
K_d	Derivative gain PID controller [varies]	x	x-direction [m]
K_i	Integral gain PID controller [varies]	x_h	Distance of rotor hub from center of mass in x-direction in body frame [m]
K_p	Proportional gain PID controller [varies]	x_l	Distance of load hinge from center of mass in x-direction in body frame [m]
K_{max}	Critical gain Ziegler-Nichols tuning method [–]	y	y-direction [m]
L	Characteristic length scale [m]	z	z-direction [m]
l_c	Length cable [m]	c.g.	Center of mass
l_i	Cable length pendulum i 3-DOF model [m]	g	Gravitational constant [m/s ²]
l_i	Length cable section i 6-DOF model [m]	Greek Symbols	
m	Mass helicopter 3-DOF model [kg]	α_c	Angle of attack of control plane 3-DOF model [rad]
m_i	Mass cable section i 6-DOF model [kg]	α_d	Angle of attack of disk plane 3-DOF model [rad]
m_i	Mass of pendulum i 3-DOF model [kg]	\bar{v}	Virtual control input [varies]
n	Number of cable sections [–]	β	Flap angle, positive around positive y-direction of helicopter body [1/rad]
p	Body roll rate [rad/s]	Δ	Small change [–]
q	Pitch rate [rad/s]	δ	Small increment [varies]
Q_i	Generalised forces of system i (Lagrange method) [Nm · rad]	ϵ	Angle of incidence of velocity [rad]
		γ	Lock number [–]
		λ_0	Normalised uniform inflow velocity main rotor [–]
		λ_c	non-dimensional inflow velocity of the control plane as caused by flight velocity [–]

λ_i	Non-dimensional induced velocity [–]
λ_{0tr}	Normalised uniform inflow velocity tail rotor [–]
μ	Dynamic viscosity of fluid [Ns/m^2]
μ	Main rotor advance ratio [–]
ν	Kinematic viscosity of fluid [m^2/s]
Ω	Rotational rate of rotor [rad/s]
ω	Main rotor angular rate [rad/s]
ω_n	Natural frequency [Hz]
ϕ	Roll angle [rad]
ϕ_i	Longitudinal angle of cable section i relative to local vertical [rad]
ψ	Rotational position of blade [rad]
ψ	Yaw angle [rad]
ρ	Air density [kg/m^3]
ρ_w	Water density [kg/m^3]
ρ_{air}	Air density [kg/m^3]
ρ_{s_i}	Effective density for cable section s_i [kg/m^3]
σ	Standard deviation [varies]
τ	Main rotor inflow derivative [s]
τ	Time constant [s]
$\tau_{d_{i_{angle}}}$	Torque created by damping angle component section i [Nm]
$\tau_{d_{i_{rate}}}$	Torque created by damping rate component section i [Nm]
τ_{lag}	Time constant first order filter [s]
θ	Pitch angle [rad]
θ_0	Collective pitch main rotor [rad]
θ_c	Cyclic Pitch, positive around negative y-direction of helicopter body 3-DOF model [rad]
θ_i	Longitudinal angle of cable section i relative to local vertical [rad]
θ_{0tr}	Tail rotor collective [rad]

θ_0	Main rotor collective [rad]
θ_{1c}	Lateral cyclic [rad]
θ_{1s}	Longitudinal cyclic [rad]
ζ	Damping ratio [–]
$C_{D_{s_i}}$	Drag coefficient cable section s_i [–]

Subscripts

0	Attachment point of cable
f	Filtered
A	LVLH frame
att	Attitude
B	Body frame
c	Commanded
f	Fuselage
OFF	offset
pos	Position
u	Longitudinal body velocity
v	Lateral velocity in body frame
vel	Velocity
w	Vertical velocity in body frame
Load	External load

Matrices

I	Identity matrix [–]
J_{s_i}	Inertia matrix cable section s_i in LVLH frame [kgm^2]
$R(\phi_i, \theta_i)$	Rotation matrix for cable section i [–]
$G(\bar{x})$	Control effectiveness matrix [varies]
$h(\bar{x})$	Output function [varies]

Vectors

\bar{v}_{p_i}	Linear velocity vector hinge p_i [m/s]
\bar{v}_{s_i}	Linear velocity vector cable section s_i [m/s]
\bar{v}_{wind}	Linear wind velocity [m/s]
$\bar{\omega}_{s_i}$	Rotational rate vector cable section s_i [rad/s]

$\bar{\Theta}_{s_i}$	Rotation vector cable section s_i [rad]	\bar{r}_i	Cable section i vector [m]
\bar{a}_{p_i}	Linear acceleration vector hinge p_i [m/s^2]	\bar{S}_{s_i}	Surface area vector cable section s_i [m^2]
\bar{a}_{s_i}	Linear acceleration vector cable section s_i [m/s^2]	\bar{u}	Input vector [varies]
\bar{F}_{AE_i}	Aerodynamic or hydrodynamic force vector section i [N]	\bar{x}	State vector [varies]
\bar{p}_i	Cable hinge i position vector [m]	$\dot{\bar{\omega}}_{s_i}$	Rotational acceleration vector cable section s_i [rad/s^2]
		$\dot{\bar{x}}$	State vector derivative [varies]

List of Figures

3.1	A rescue helicopter used by the dutch coast guard [11]	29
3.2	An NH90 military helicopter in a dipping SONAR mission used by the dutch navy [36]	29
3.3	Rigid rotor connection	31
3.4	Teetering rotor connection	31
3.5	Fully articulated rotor connection	31
3.6	Swash plate mechanism	31
3.7	Diagram illustrating the flapping angle β and the coning angle a_0 [22].	34
3.8	Diagram illustrating the longitudinal disc-tilt a_1 [22].	34
3.9	Helicopter dipping SONAR manoeuvre	36
3.10	Discrete cable model for longitudinal motion (left) and lateral motion (right)	41
3.11	Control response in heavy turbulence with controller [53]	45
3.12	Control response gust turbulence with controller [57]	47
3.13	Block diagram of general INDI-controlled system.	50
3.14	Poles of closed-loop system based on eigenvalue λ [24].	52
3.15	Cyclic control of the INDI controlled pure helicopter from case 1.	53
3.16	Collective control of the INDI controlled pure helicopter from case 1.	53
3.17	Comparison between INDI controller and PID controller for disturbed pure helicopter trimmed at $V = 1m/s$	53
4.1	Body and LVLH reference frames	56
4.2	Diagram of case 3-DOF-PH-HUB-CG in body frame.	57
4.3	Trim curve for case 3-DOF-PH-HUB-CG	59
4.4	Response of linear and non-linear hovering helicopter model case 3-DOF-PH-HUB-CG to input disturbance on cyclic of 1 degree for 5 seconds.	61
4.5	Pole-Zero map of linearised system for case 3-DOF-PH-HUB-CG, trimmed at $V = 1$ m/s.	62
4.6	Response of controlled hovering helicopter case 3-DOF-PH-HUB-CG to input disturbance on cyclic of 1 degree for 5 seconds.	66
4.7	Cyclic control of the controlled hovering helicopter case 3-DOF-PH-HUB-CG to input disturbance on cyclic of 1 degree for 5 seconds.	66
4.8	Collective control of the controlled hovering helicopter case 3-DOF-PH-HUB-CG to input disturbance on cyclic of 1 degree for 5 seconds.	66
4.9	Diagram of case 3-DOF-PH-HUB-OFF in x_B frame.	67
4.10	Trim curve for case 3-DOF-PH-HUB-OFF where the rotor hub is located at different offsets of $x_{h,m}$ in x_B direction.	68
4.11	Response of linear and non-linear hovering helicopter model case 3-DOF-PH-HUB-OFF to input disturbance on cyclic of 1 degree for 5 seconds.	69
4.12	Pole-Zero map of linearised system for case 3-DOF-PH-HUB-OFF, trimmed at $V = 1$ m/s.	70
4.13	Response controlled hovering helicopter case 3-DOF-PH-HUB-OFF to input disturbance on cyclic of 1 degree for 5 seconds.	71
4.14	Cyclic control of the controlled hovering helicopter case 3-DOF-PH-HUB-OFF to input disturbance on cyclic of 1 degree for 5 seconds.	71
4.15	Collective control of the controlled hovering helicopter case 3-DOF-PH-HUB-OFF to input disturbance on cyclic of 1 degree for 5 seconds.	71
4.16	Diagram of case 3-DOF-SP-CG-HUB-OFF in x_B frame.	72
4.17	Diagram of single pendulum model.	73
4.18	Trim curve for case 3-DOF-SP-CG-HUB-OFF.	74
4.19	Response of linear and non-linear hovering helicopter model case 3-DOF-SP-CG-HUB-OFF to input disturbance on cyclic of 1 degree for 5 seconds.	76
4.20	Pole-Zero map of linearised system for case 3-DOF-SP-CG-HUB-OFF, trimmed at $V = 1$ m/s.	77

4.21	Response controlled hovering helicopter case 3-DOF-SP-CG-HUB-OFF to input disturbance on cyclic of 1 degree for 5 seconds.	78
4.22	Cyclic control of the controlled hovering helicopter case 3-DOF-SP-CG-HUB-OFF to input disturbance on cyclic of 1 degree for 5 seconds.	79
4.23	Collective control of the controlled hovering helicopter case 3-DOF-SP-CG-HUB-OFF to input disturbance on cyclic of 1 degree for 5 seconds.	79
4.24	Diagram of hcase 3-DOF-SP-OFF-HUB-OFF.	79
4.25	Trim curve for case 4, where the single pendulum is offset with the c.g.	80
4.26	Response of linear and non-linear hovering helicopter model case 3-DOF-SP-OFF-HUB-OFF to input disturbance on cyclic of 1 degree for 5 seconds.	82
4.27	Pole-Zero map of linearised system for case 4, trimmed at $V = 1$ m/s.	83
4.28	Response controlled hovering helicopter case 3-DOF-SP-OFF-HUB-OFF to input disturbance on cyclic of 1 degree for 5 seconds.	84
4.29	Cyclic control of the controlled hovering helicopter case 3-DOF-SP-OFF-HUB-OFF to input disturbance on cyclic of 1 degree for 5 seconds.	84
4.30	Collective control of the controlled hovering helicopter case 3-DOF-SP-OFF-HUB-OFF to input disturbance on cyclic of 1 degree for 5 seconds.	84
4.31	Diagram of case 3-DOF-DP-OFF-HUB-OFF.	85
4.32	Diagram of the double pendulum model.	85
4.33	Trim curve for case 3-DOF-SP-OFF-HUB-OFF.	86
4.34	Response of linear and non-linear hovering helicopter + double pendulum model case 3-DOF-DP-OFF-HUB-OFF to input disturbance on cyclic of 1 degree for 5 seconds.	88
4.35	Pole-Zero map of linearised system for case 3-DOF-DP-OFF-HUB-OFF.	89
4.36	Response controlled hovering helicopter case 3-DOF-DP-OFF-HUB-OFF to input disturbance on cyclic of 1 degree for 5 seconds.	90
4.37	Cyclic control of controlled hovering helicopter case 3-DOF-DP-OFF-HUB-OFF to input disturbance on cyclic of 1 degree for 5 seconds.	90
4.38	Collective control of controlled hovering helicopter case 3-DOF-DP-OFF-HUB-OFF to input disturbance on cyclic of 1 degree for 5 seconds.	90
4.39	Response of linear and non-linear hovering helicopter + double pendulum model case 3-DOF-DP-OFF-HUB-OFF-SUB to input disturbance on cyclic of 1 degree for 5 seconds.	91
4.40	Pole-Zero map of linearised system for case 3-DOF-DP-OFF-HUB-OFF-SUB.	92
4.41	Response controlled hovering helicopter case 3-DOF-DP-OFF-HUB-OFF-SUB with double pendulum at an offset w.r.t the c.g. of the helicopter with load 2 submerged to input disturbance on cyclic of 1 degree for 5 seconds.	93
4.42	Cyclic control of controlled hovering helicopter case 3-DOF-DP-OFF-HUB-OFF-SUB with double pendulum at an offset w.r.t the c.g. of the helicopter with load 2 submerged to input disturbance on cyclic of 1 degree for 5 seconds.	93
4.43	Collective control of controlled hovering helicopter case 3-DOF-DP-OFF-HUB-OFF-SUB with double pendulum an offset w.r.t the c.g. of the helicopter with load 2 submerged to input disturbance on cyclic of 1 degree for 5 seconds.	93
5.1	Sequence of rotations from A-frame to k-frame of a cable section i	96
5.2	section frame of reference (k-frame) for a cable section i	96
5.3	Reference frames for suspension cable with 2 sections and SONAR attached to helicopter.	97
5.4	Diagram of vectors \bar{r} and hinge locations \bar{p}_i in the A -frame for three cable sections.	100
5.5	Free body diagram of 2 suspension cable sections in the x_A - z_A plane.	101
5.6	Drag coefficient for different shapes vs. Reynolds number.[9]	104
6.1	Configuration 6-DOF pure helicopter for case 1 in body frame of reference.	106
6.2	Block diagram for INDI ACAH controller	108
6.3	Block diagram for PID ACAH controller	108
6.4	Response of inner loop INDI ACAH controller.	108
6.5	Response of outer loop INDI ACAH controller.	108
6.6	Response of PID ACAH controller.	108
6.7	Block diagram for NDI TRC controller	109

6.8	Block diagram for INDI TRC controller	109
6.9	Response of u - and v -component TRC controller for INDI ACAH.	110
6.10	Response of u - and v -component TRC controller for PID ACAH.	110
6.11	Response of w -component TRC controller for INDI ACAH.	110
6.12	Response of w -component TRC controller for PID ACAH.	110
6.13	Block diagram position hold controller	111
6.14	Response of position hold controller for INDI ACAH.	112
6.15	Response of position hold controller for PID ACAH.	112
6.16	Response of position hold controller for INDI ACAH.	112
6.17	Response of position hold controller for PID ACAH.	112
6.18	Position response of both the ACAH INDI and ACAH PID controllers to step input on disturbance velocity of $4kts$	113
6.19	Attitude response of both the ACAH INDI and ACAH PID controllers to step input on disturbance velocity of $4kts$	113
6.20	Control inputs relative to trim of both the ACAH INDI and ACAH PID controllers to step input on disturbance velocity of $4kts$	114
6.21	Configuration 6-DOF pure helicopter for case 2 in body frame of reference.	114
6.22	Configuration 6-DOF pure helicopter for case 3 in body frame of reference.	116
6.23	Block diagram for cable control through helicopter attitude	118
6.24	Block diagram for INDI cable controller using cable control through helicopter attitude	118
6.25	Block diagram for PID cable controller using cable control through helicopter attitude	119
6.26	Cable angle response for INDI controller case 3, given a step input in commanded cable angle.	120
6.27	Cable angle response for PID controller case 3, given a step input in commanded cable angle.	120
6.28	Control inputs relative to trim for PID controller case 3, given a step input in commanded cable angle.	120
6.29	Cable angle response for disturbance case 3, given a filtered 4 kts step input in wind.	121
6.30	Control inputs relative to trim for disturbance case 3, given a filtered 4 kts step input in wind.	121
6.31	Sonar ground velocity response for disturbance case 3, given a filtered 4 kts step input in wind.	121
6.32	Configuration 6-DOF pure helicopter for case 4 in body frame of reference.	122
6.33	Cable angle response for disturbance case 4, given a filtered 4 kts step input in wind.	124
6.34	Configuration 6-DOF pure helicopter for case 5 - case 7 in body frame of reference.	124
6.35	Controller architecture case 5	126
6.36	Block diagram INDI cable controller case 5	126
6.37	Block diagram PID cable controller case 5	127
6.38	Response cable angle with INDI cable controller	127
6.39	Response cable angle with PID cable controller	127
6.40	Response of cable angle with INDI and PID controller to a step input on wind of $4kts$	128
6.41	Control inputs from INDI and PID controller from a step input on wind of $4kts$	128
6.42	Response cable angle with INDI cable controller through attitude control	131
6.43	Response of helicopter attitude from trim with INDI cable controller through attitude control	131
6.44	Response of body velocities with with INDI cable controller through attitude control	131
6.45	Control inputs from trim to helicopter with with INDI cable controller through attitude control	131
6.46	Response cable angle with INDI cable controller through velocity control	132
6.47	Response of helicopter attitude from trim with INDI cable controller through velocity control	132
6.48	Response of body velocities with with INDI cable controller through velocity control	132
6.49	Control inputs from trim to helicopter with with INDI cable controller through velocity control	132
6.50	Controller architecture cable control through helicopter position	133
6.51	Cable controller block diagram for control through helicopter position	133
6.52	Response cable angle with INDI cable controller through position control	134
6.53	Response of helicopter attitude from trim with INDI cable controller through position control	134
6.54	Response of body velocities with with INDI cable controller through position control	134
6.55	Control inputs from trim to helicopter with with INDI cable controller through position control	134
6.56	Cable angle response to a $4kts$ wind using different control strategies	135
6.57	SONAR ground velocity squared response to a $4kts$ wind using different control strategies	135
6.58	Body velocity response to a $4kts$ wind using different control strategies	135

6.59 Helicopter attitude response relative to trim to a <i>4kts</i> wind using different control strategies	135
6.60 Cable angle response using PID controller for case 6	136
6.61 Helicopter attitude response using PID controller for case 6	136
6.62 Cable angle response to a 4kts wind using PID and INDI control for case 6	136
6.63 SONAR ground velocity response to a 4kts wind using PID and INDI control for case 6	136
6.64 Control inputs from trim to helicopter with a 4kts wind using PID and INDI control for case 6	137
6.65 Gust velocities for a wind of 10 kts.	138
6.66 SONAR ground velocity response at 10 kts wind.	138
6.67 Cable angle response at 10 kts wind.	139
6.68 SONAR angular rate response at 10 kts wind.	139
6.69 Gust velocities for a wind of 20 kts.	140
6.70 SONAR ground velocity response at 20 kts wind.	140
6.71 Cable angle response at 20 kts wind.	140
6.72 SONAR angular rate response at 20 kts wind.	140
6.73 Gust velocities for a wind of 30 kts.	141
6.74 SONAR ground velocity response at 30 kts wind.	141
6.75 Cable angle response at 30 kts wind.	142
6.76 SONAR angular rate response at 30 kts wind.	142
6.77 SONAR ground velocity response at 17m/s step in wind.	144
6.78 Cable angle response at 17 m/s step in wind	144
7.1 SONAR ground velocity response at 30 kts wind for 250m long cable.	148
7.2 SONAR ground velocity response at 30 kts wind for 500m long cable.	148
7.3 SONAR ground velocity response at 30 kts wind for 750m long cable.	149
7.4 SONAR ground velocity response at 30 kts wind for 750m long cable with 25 cable sections.	149
7.5 SONAR ground velocity response at 30 kts wind for 750m long cable with 75 cable sections.	149
8.1 Validation cable shape when dropping cable	152
8.2 Validation cable angle when dropping cable	152
8.3 Validation cable shape when in 40 m/s wind	152
8.4 Validation cable angle when in 40 m/s wind	152
8.5 Validation cable shape when in 40 m/s wind submerged	153
8.6 Validation cable angle when in 40 m/s wind submerged	153

List of Tables

1	Simulation Cases for the 6-DOF hovering helicopter controller	2
3.1	Effect of PID-gains on response of system [25]	43
3.2	PID tuning with Ziegler-Nichols method [13]	43
4.1	Modelling cases for the 3-DOF model, each increasing the level of complexity.	55
4.2	Simulation data throughout the six simulation cases	57
4.3	Poles of linearised system for case 3-DOF-PH-HUB-CG, trimmed at $V = 1$ m/s	62
4.4	Poles of the linearised pure helicopter model with the rotor hub offset the c.g. of the helicopter trimmed at $V = 1$ m/s.	70
4.5	Poles of case 3-DOF-SP-CG-HUB-OFF, where the linearised single pendulum model with the pendulum attached at the c.g. of the helicopter trimmed at $V = 1$ m/s.	77
4.6	Poles of the linearised single pendulum model with the pendulum attached at an offset w.r.t the c.g. of the helicopter trimmed at $V = 1$ m/s.	83
4.7	Poles of the linearised double pendulum model case 3-DOF-DP-OFF-HUB-OFF.	89
4.8	Poles of the linearised double pendulum model with the pendulum attached at an offset w.r.t the c.g. of the helicopter trimmed at $V = 1$ m/s with load 2 submerged.	92
6.1	Simulation Cases for the 6-DOF hovering helicopter controller	105
6.2	Control method control loops	107
6.3	Trim data Case 1	107
6.4	Gains for ACAH Controller Case 1.	109
6.5	Gains for TRC Controller Case 1.	111
6.6	Gains for Position hold Controller Case 1.	112
6.7	Trim data Case 1 vs. 2	115
6.8	Trim data Case 2 and 3	117
6.9	Gains for Cable Controller Case 3.	120
6.10	Trim data Case 2 and 3	123
6.11	Trim data Case 4 vs. 5	125
6.12	Gains for Cable Controllers Case 5.	128
6.13	Trim data Case 5 vs. 6	130
6.14	Gains for Cable Controllers Case 6.	137
6.16	Performance metrics Cable controllers for a wind of 10 kts.	139
6.17	Performance metrics Cable controllers for a wind of 20 kts.	141
6.18	Performance metrics Cable controllers for a wind of 30 kts.	143
6.15	Trim data Case 6 vs. 7 trimmed at a wind of 33 kts	146
7.1	Performance metrics Cable controllers for a wind of 30 kts, compared to cable length.	148
7.2	Performance metrics Cable controllers for a wind of 30 kts with 750m long cable, compared to better resolution cable model.	150
D.1	Simulation data Bö-105 Helicopter obtained from supervisor	176
D.2	Cable and SONAR Data used throughout 6-DOF simulations. Note that when a variable has multiple values, different values are used for this variable throughout the cases.	177

Summary

Sound navigation and ranging (SONAR) is a technology primarily used in water to map underwater surface features, or detect submarine vehicles. It can be installed on both ships or helicopters. A dipping SONAR is a SONAR device that is suspended below a helicopter, and lowered into the water periodically to take measurements in order to detect submarines. The most notable advantage of dipping sonar is that helicopters can move faster than a ship, meaning that it can take measurements over a much larger area in a shorter amount of time. Also the quick deployment of multiple helicopters can increase the detection chance of a submarine. Moreover, since the SONAR is not attached to a moving ship, there is no Doppler effect due to ship motion nor noise pollution generated by the ship's engines that would typically be there with ship based SONAR. However, if the helicopter or the cable moves, the SONAR will move as well, adding a Doppler effect due to helicopter or cable motion. The main challenge for dipping SONAR therefore lies in controlling the helicopter such that the SONAR is kept still in the water to reduce Doppler effects on the SONAR for the duration of a dip, in potentially rough conditions.

During a dipping SONAR mission, the transducer is lowered to depths ranging up to 2500 ft from a hovering helicopter at an altitude of 50-300 ft above the water. Dipping can take a long time, but is assumed to take no longer than 5 minutes.

Based on the mission requirements combined with a lack of available information about SONAR motion requirements, the following controller requirements have been defined:

1. The translational rates of the SONAR shall not exceed $1m/s$ in all directions with the SONAR submerged at a depth of 60m and sea state of 5 for 5 minutes.
2. The rotational rates of the SONAR shall not exceed $1^\circ/s$ in all directions with the SONAR submerged at a depth of 60m and sea state of 5 for 5 minutes.
3. The SONAR shall reach steady state within 60 seconds in all axes after a step input gust of 0 to 7 Bft with the SONAR submerged at a depth of 60m.

The suspension cable is the largest uncertainty in the helicopter-cable system. This is due to its ability to deform due to both environmental conditions such as wind as well as helicopter motion. This deformation results in changing dynamics of the cable, and the SONAR. This makes control of the SONAR difficult, since its dynamics are uncertain.

Throughout literature, many different control methods are proposed for stabilizing helicopters either with or without load. Each of them having benefits and drawbacks. Despite this large variety of different methods, it is still common to find gain scheduled classical controllers. Such controllers are developed using linearised models of the vehicle to determine the gains, and are scheduled for specific flight conditions. The main reason for using such controllers is its structured loop design which makes them easy to verify and hence certify.

In this thesis, incremental nonlinear dynamic inversion (INDI) is used to control the cable. This is done to remove the complex cable dynamics from the cable controller. INDI is the incremental approach to Nonlinear Dynamic Inversion (NDI), which is a control method where the feedback of the controller is such that the dynamics of the system are linear globally. The main advantage of NDI is that it inverts the dynamics of the system, linearising it. However, for it to function properly, perfect model knowledge is required. This means that, in order to make this method practical, either the model must be updated continuously, or the modelling error must be found. The latter is done in [48] and [60]. Because of this, NDI is called a model-based approach.

INDI moves from a model based NDI approach to a sensor based approach, by using sensor measurements instead of the system model. Generally, only the control effectiveness is required. It has also already been applied to helicopter control systems in [42], [43] and [51] as proof of concept.

Using INDI for controlling the cable removes the required knowledge of the dynamics of the suspension cable, simplifying the control task greatly. Therefore, this research aims to use INDI as control method for

a system with a hovering helicopter and a dipping SONAR. It will be compared to a classical PID controller to judge its performance and to determine whether it is a feasible control method for dipping SONAR missions.

From this, the following main research question of this thesis arises:

How does an INDI controller compare to PID control in keeping a dipping SONAR stationary while hanging under a hovering helicopter during a dipping SONAR mission?

This question is answered throughout this report.

In this research, an 8 degrees-of-freedom (DOF) helicopter model was used. This includes 6-DOF body motion and 2-DOF quasi-dynamic rotor inflow for the main and tail rotor. This model was applied to a dipping SONAR configuration. A suspension cable + SONAR model was modelled from scratch. This was done by modelling the cable as a number of rigid links attached by friction-less hinges. The environment model used is a von Karman turbulence model. With these models, simulations were performed in order to simulate the behaviour of a helicopter with a dipping SONAR in turbulent conditions.

The controllers designed were cable angle controllers. These controllers control the cable angle at the helicopter attachment point relative to the local vertical. The idea behind this is that the helicopter knows nothing about what is happening below it. This means that it is assumed that there are no sensors on the cable, nor on the SONAR about its position, velocity or rotation relative to the helicopter. Both an INDI cable controller and a PID cable controller were designed. They were tuned to show similar output when subjected to a single step input in wind of 4 kts. This way, the comparison between them is fair, and differences are less likely due to gain tuning.

Simulation was done in step via the means of simulation cases, each case increasing in complexity. The cases are presented in Table 1. The column helicopter model indicates where the main rotor hub is located relative to the center of mass. The cable model column indicates how many cable sections are used. For cases 1 and 2, no load is assumed so no cable sections apply. Column Load location indicates where the attachment point of the cable is located. Medium indicates the medium in which the cable model is modelled. The idea behind this approach is to build up the problem in a systematic way.

Table 1: Simulation Cases for the 6-DOF hovering helicopter controller

Case	Helicopter Model	Cable Model	Load Location	Medium	Disturbances
1	Rotor hub aligned with c.g.	-	-	-	-
2	Rotor hub at offset	-	-	-	-
3	Rotor hub at offset	Single cable section + SONAR	c.g. of helicopter	Air	-
4	Rotor hub at offset	Single cable section + SONAR	At offset	Air	-
5	Rotor hub at offset	5 cable sections + SONAR	At offset	Air	-
6	Rotor hub at offset	5 cable sections + SONAR	At offset	Air + water	-
7	Rotor hub at offset	5 cable sections + SONAR	At offset	Air + water	Aerodynamic

The main conclusion of this thesis is that cable control using INDI performs better at stabilising the SONAR than PID does under turbulent conditions with wind up to 20 kts in terms of control use and SONAR velocity. However, due to the way the cable controller is designed in this work, either controller could fail if the helicopter gets blown away too far from the cable sections that are submerged, which was the case for 30 kts. In this research, the cable controller has as goal to keep the angle of the cable at the attachment point to the helicopter constant. Thus, changing wind will inevitably result into translation commands to the helicopter in order to keep this angle constant. A position controller proved to work better under the high wind and high turbulent conditions of 30 kts wind. It seems that improvements could be made by either finding a way to vary the desired cable angle based on the turbulence or to find a controller that incorporates cable control and helicopter position hold together in order to keep the helicopter position somewhat constant, yet move slightly to stabilise the cable to changing wind conditions.

Moreover, simulation showed that the requirements could be met by both the PID and the INDI controllers up to 20 kts wind. It was also found that shorter cables are more limiting than longer cables. This is due to the higher drag of longer cables and the lower natural frequency of longer cables.

It is recommended that future steps could use measurements of the SONAR states if possible and controlling the SONAR, rather than the cable angle at the helicopter. The major advantage here would be that for INDI, the complex cable dynamics could be largely ignored. The difficulty here, however, lies in determining what the control effectiveness is in such a case, as the cable shape influences the control effectiveness. Also, in [12] and [53] discuss the use of an active cargo hook, which essentially is a moving platform underneath the helicopter to which the cable is attached. According to [12], this is more stable than when using the helicopter to move around. The use of an active cargo hook could be the solution to staying in the same position while stabilising the suspension cable using the active cargo hook.

Finally, it is recommended to improve the fidelity of the models used in this research. There were some things, however, that were not modelled, which could change the behavior of the controller. These are sensor measurements and actuator dynamics. The cable model could be improved by adding a more realistic damping model. Currently, the damping is assumed to be linear and depends on the angle between cable sections and the relative angular velocity between these two. The coefficients used for damping were based on guesswork in order to ensure a stable simulation. Having a realistic damping of the cable would make the motion of the cable more realistic. Also, the sensitivity analysis showed that there are large peaks in the vertical SONAR velocity. It is thought that a lack of drag on the cable in this direction is the cause of this. Adding a more refined drag model would show whether this is the case. The fidelity of the wind model could be improved by adding varying wind with altitude, since wind and gusts are different close to the water's surface than at altitude. It would also be interesting to add a wave model, a sea current model and to have wind interact with the waves in order to see the effects this has on the cable's behaviour.

Introduction

Sound navigation and ranging (SONAR) is a technology primarily used in water to map underwater surface features, or detect submarine vehicles. It can be installed on both ships or helicopters. A dipping SONAR is a SONAR device that is suspended below a helicopter, and lowered into the water periodically to take measurements in order to detect submarines. The most notable advantage of dipping sonar is that helicopters can move faster than a ship, meaning that it can take measurements over a much larger area in a shorter amount of time. Also the quick deployment of multiple helicopters can increase the detection chance of a submarine. Moreover, since the SONAR is not attached to a moving ship, there is no Doppler effect due to ship motion nor noise pollution generated by the ship's engines that would typically be there with ship based SONAR. However, if the helicopter or the cable moves, the SONAR will move as well, adding a Doppler effect due to helicopter or cable motion. The main challenge for dipping SONAR therefore lies in controlling the helicopter such that the SONAR is kept still in the water to reduce Doppler effects on the SONAR for the duration of a dip, in potentially rough conditions.

The suspension cable is the largest uncertainty in the helicopter-cable system due to its ability to deform due to both environmental conditions such as wind as well as helicopter motion. This deformation results in changing dynamics of the cable, and the SONAR and makes control of the SONAR problematic, since its dynamics are uncertain.

In this thesis, incremental nonlinear dynamic inversion (INDI) is used to control the cable. This is done to remove the complex cable dynamics from the cable controller. INDI is the incremental approach to Nonlinear Dynamic Inversion (NDI), which is a control method where the feedback of the controller is such that the dynamics of the system are linear globally. The main advantage of NDI is that it inverts the dynamics of the system, linearising it. However, for it to function properly, perfect model knowledge is required. This means that, in order to make this method practical, either the model must be updated continuously, or the modelling error must be found. The latter is done in [48] and [60]. Because of this, NDI is called a model-based approach.

INDI moves from a model based NDI approach to a sensor based approach, by using sensor measurements instead of the system model. Generally, only the control effectiveness is required. It has also already been applied to helicopter control systems in [42], [43] and [51] as proof of concept.

Using INDI for controlling the cable removes part of the required knowledge of the dynamics of the suspension cable, simplifying the control task greatly. Therefore, this research aims to use INDI as control method for a system with a hovering helicopter and a dipping SONAR. It will be compared to a classical PID controller to judge its performance and to determine whether it is a feasible control method for dipping SONAR missions.

Research Formulation

Research Questions

The main research goal is to find an INDI controller, capable of keeping a dipping SONAR still during a dipping SONAR mission. This goal was provided by the project supervisor. In order to compare the performance of such a controller, this controller will be compared to a conventional PID controller. From

this, the following main research question arises:

How does an INDI controller compare to PID control in keeping a dipping SONAR stationary while hanging under a hovering helicopter during a dipping SONAR mission?

In order to answer this main question, the following sub-questions have been defined:

Sub-question 1: What does a dipping SONAR mission look like?

Sub-question 1.1: What is dipping SONAR?

Sub-question 1.2: What manoeuvres are expected?

Sub-question 1.3: What environmental conditions are expected?

Sub-question 1.4: What are the requirements of the controller?

Sub-question 1.5: What are the controller performance metrics?

Sub-question 2: What are the dynamic characteristics of a helicopter during a dipping SONAR mission?

Sub-question 2.1: What are the rotor dynamics?

Sub-question 2.2: What are the actuator dynamics?

Sub-question 2.5: What is the state of the art in helicopter modelling with a slung load?

Sub-question 2.3: How does a pure helicopter behave (without any suspended load)?

Sub-question 2.4: How does a submerged load change helicopter behaviour?

Sub-question 3: What is the state of the art in helicopter automatic flight control systems?

Sub-question 3.1: What different control methodologies exist?

Sub-question 3.2: What different control modes exist?

Sub-question 3.3: What are their advantages/disadvantages?

Sub-question 3.4: Why choose INDI as control strategy?

Sub-question 4: How to design an INDI controller for a helicopter with a dipping SONAR?

Sub-question 4.1: How does INDI work?

Sub-question 4.2: What is the controlled variable?

Sub-question 4.3: How is INDI currently used in control systems?

Sub-question 4.4: How to design the outer loop controller?

Sub-question 5: What models will be used?

Sub-question 5.1: What model is used for the helicopter?

Sub-question 5.2: What model is used for the suspension cable?

Sub-question 5.3: What model is used for the SONAR?

Sub-question 5.4: What model is used for the environment?

Sub-question 6: How does an INDI controller perform for a helicopter with a dipping SONAR compared to PID?

Sub-question 6.1: What sensors are required to make it work?

Sub-question 6.2: What are the requirements of the sensors?

Sub-question 6.3: How robust is INDI to flapping dynamics?

Sub-question 6.4: How robust is INDI to actuator dynamics?

Research Objective

The main research objective is to find an INDI controller, capable of keeping a dipping SONAR still during a dipping SONAR mission.

In order to achieve this main objective, five sub-goals have to be reached:

1. Obtain the models of the system. These are the helicopter model, the suspension cable model, the SONAR model and the environment model.
2. Design a PID controller for this system.
3. Design an INDI controller for this system.
4. Implementation into simulation. Simulation is done using Matlab, in which all models and the controllers will be combined into the final system.
5. Compare performance between the two designed controllers and determining whether the INDI controller is suitable.

Structure of the Report

The goal of this report is to provide an overview of the work done in this Thesis in order to find the solution to the main research question of how an INDI controller performs to a PID controller in a dipping SONAR mission. This report is laid out as follows: First, the scientific article is provided in Part I. Then, the preliminary analysis is provided in Part II, which contains a brief description of the control mechanisms of a general helicopter in Section 3.1, a literature overview of helicopter rotor dynamics as well as actuator dynamics in Section 3.2, a description of dipping SONAR missions as well as the controller requirements in Section 3.3, the different modelling methods found in literature in Section 3.4, the state of the art in helicopter automatic control systems in Section 3.5 and the working principle of INDI in Section 3.6. In Chapter 4, a 3-degree-of-freedom model is presented with INDI and PID controllers stabilizing the helicopter and the load as a preliminary analysis.

In Part III, the additional results are presented. Here, the suspension cable + SONAR model are presented in Chapter 5. The 6-degrees-of-freedom cable control cases are given in Chapter 6. A sensitivity analysis is performed in Chapter 7. Finally, a verification and validation is provided in Chapter 8. The conclusions and recommendations are given in Part IV.

Part I

Scientific Article

Cable Control for Dipping SONAR Operations using Incremental Nonlinear Dynamic Inversion

M. Maurer*, E. van Kampen, M. D. Pavel

Delft University of Technology, Faculty of Aerospace Engineering, Kluyverweg 1, 2629 HS Delft, The Netherlands

Control of a helicopter with a deployed dipping sound navigation and ranging (SONAR) is no trivial task due to the complex dynamics of the suspension cable. The cable can change shape, which influences the effect of water, wind and the motion of the helicopter itself. To control such a system, a control method is needed that can cope with these complex dynamics. In this paper, an investigation is performed on how to model and control a helicopter and a dipping SONAR through the suspension cable using incremental nonlinear dynamic inversion (INDI) as well as a comparison between the use of INDI and linear proportional integral derivative (PID) control. The controller uses only the cable states at the attachment point of the cable to the helicopter in order to determine the control inputs to the helicopter. This means that only these measurements are needed and no complex model of the cable is required for control. This reduces model dependency of the controller. The control system is simulated in different wind conditions in order to analyse its performance in turbulent conditions, where the cable changes shape constantly. It was found that, although INDI performs better than PID control at low wind speeds, an INDI position hold controller appeared to perform better than an INDI cable controller at high wind speeds.

Keywords: *Helicopter, Dipping SONAR, Helicopter slung load, Nonlinear Control, Incremental nonlinear dynamic inversion, Cable control*

I. Introduction

Sound navigation and ranging (SONAR) is a technology primarily used in water to map underwater surface features, or detect submarine vehicles. It can be installed on both ships or helicopters. Dipping SONAR is a SONAR installed on a helicopter, and is lowered into the water periodically to take measurements in order to detect submarines. The most notable advantage of dipping sonar is that helicopters move faster than ships, making them capable of taking measurements over a larger area in a shorter amount of time. Also the quick deployment of multiple helicopters can increase the detection chance of a submarine. For optimum SONAR performance, the SONAR must be kept still [1][2][3]. Dipping SONAR experiences no Doppler effect due to ship motion nor noise pollution generated by the ship's engines that would typically be there with ship based SONAR. However, if the helicopter or the cable moves, the SONAR will move as well, adding a Doppler effect due to helicopter or cable motion. When hovering, the SONAR transducer is lowered into the water to take measurements. This is done at an altitude of 50-300 ft [4] and transducer is lowered to depths of 0 to 2500 ft [4] [5]. After measurements are done, the transducer is lifted back up out of the water before flying to a next location. The duration of a dip is unknown to the author, but is assumed to take no more than 5 minutes. Also, although the exact conditions in which dipping SONAR is used was not found in literature, it was observed that in many cases, a sea state of 4-5 was taken for maritime helicopter operations as a worst-case scenario. Mainly due to on-deck operations such as maintenance, take-off and landing. Hence, a sea state of 4-5 was chosen as a worst-case scenario. This corresponds to waves between 2.5 and 4.0m high. Such waves are also found in wind conditions of 5-7 Bft, or 17-33 kts wind [6]. The main challenge for dipping SONAR therefore lies in controlling the helicopter such that the SONAR is kept still in the water to reduce Doppler effects on the SONAR for the duration of a dip, in potentially rough conditions.

The suspension cable is the largest uncertainty in the helicopter-cable system. This is due to its ability to deform due to both environmental conditions such as wind, waves or helicopter motion. This deformation results in changing dynamics of the cable, and the SONAR. This makes both control as well as modelling of the cable and SONAR problematic, since its dynamics are uncertain. Often, the suspension cable and load are simplified to a pendulum hanging from

*Corresponding author. E-mail address: maarten.maurer@gmail.com

a helicopter ([7], [8], [9], [10], [11]). This is due to the pendulum-like behaviour of such load configurations. It makes positioning tasks for such configurations difficult [9] and may cause instabilities due to pilot induced oscillations ([7],[12]). Moreover, the pendulum mode couples easily with the helicopter dutch roll [8]. Because of this, reducing the pendulum motion receives much attention in literature.

The main assumption that drives this simplification is that the wire is always taught. This is a reasonable assumption to make if the helicopter is flying through air. Unfortunately, if the hovering, disturbances will cause the cable to deform. Additionally, in order to study the effect of cable motion on the SONAR, flexibility of the cable must be modelled. In [13], the cable model is considered as a distributed parameters system expressed as partial differential equations with boundary conditions. Based on the Hamilton's principle, the suspension cable dynamic equations are derived. In [3] and [2], the suspension cable is modelled as a discrete cable system. In [2], two modelling methods are proposed: A discrete cable model and a lumped model. The discrete model uses many rigid sections, where the lumped cable model is a simplified double pendulum model. The discrete model in [3] is similar to the discrete cable model in [3]: Each link is regarded as a rigid link. The force conditions are analysed for every section such that the differential equation of each section can be established.

Controlling a helicopter with a hanging load is not new and is applied in a number of fields, such as construction, firefighting, cargo transport, etc. Many different control methods have been identified for stabilisation of the helicopter and load. Linear control methods are popular ([14],[15],[16]) due to the fact that it is easy to verify such controllers (and hence certify) and the fact that it is structured in loops [17]. Interestingly, [16] uses controls the position of the hook underneath the helicopter, rather than the helicopter itself. This has an advantageous effect on the stability with cable angle feedback as explained in [18]. However, it is more conventional to use helicopter motion to control the cable angle instead. The main problem, however, with linear control is the fact that it in principle only works for linear systems. Aircraft in general, and especially helicopters are highly non-linear, which means that this control strategy will not work for a non-linear helicopter model. To work around this, gain scheduling is used, but is generally a very time-consuming and tedious approach for control engineering.

To overcome this, other control methods have been identified for stabilisation of the helicopter and load. Dynamic Inversion (DI), or nonlinear dynamic inversion (NDI) is a method where the feedback of the controller is such that the dynamics of the vehicle are linear globally. An example of application of DI to a helicopter system is presented in [19]. Unfortunately, any modelling errors will directly impact the performance of the controller or even cause instability. In order to make this method practical, either the model must be updated continuously, or the modelling error must be found ([20], [21]). Other control methods such as robust control [22], backstepping control ([23],[24]), Model reference adaptive control [25], sliding mode control ([26],[27]), delayed load feedback [7], fuzzy control ([28], [29] [3]) and input shaping ([12],[9],[30]) are control methods that have also been applied to helicopter systems with or without load.

Recently, A new type of control appeared: Incremental control, and especially incremental nonlinear dynamic inversion (INDI). This type of control uses sensor knowledge instead of model knowledge. INDI is hence robust to model uncertainties, which is a problem with NDI. However, INDI requires having sensors measuring the states fast enough. This makes it a perfect candidate for nonlinear highly coupled vehicles such as helicopters. Incremental nonlinear dynamic inversion is a control method that has already been applied to helicopter control systems in [31] and [32] as proof of concept.

The contribution of this paper is an application of incremental nonlinear dynamic inversion (INDI) to a helicopter dipping SONAR system as well as a way to model a suspension cable combined with a pre-existing 8 degrees-of-freedom helicopter model. The INDI controller is compared to a classical PID controller to judge its performance and to determine whether it is a feasible control method for dipping SONAR missions. The paper is structured as follows: First, the helicopter+cable model and wind model used are given in section II and section III. This is followed by the basic principles of INDI in section IV. The design of the cable controllers is discussed in section V. The simulation cases are explained in section VI with the simulation results in section VII. The main conclusions are in section VIII. Additionally, an appendix is available, showing a derivation of the cable model.

Nomenclature

Abbreviations

<i>ACAH</i>	=	Attitude command attitude hold
<i>DOF</i>	=	Degrees of freedom
<i>DI</i>	=	Dynamic Inversion
<i>INDI</i>	=	Incremental nonlinear dynamic inversion
<i>LPF</i>	=	Low pass filter
<i>LVLH</i>	=	Local horizontal local vertical
<i>PID</i>	=	Proportional derivative integral
<i>NDI</i>	=	Nonlinear dynamic inversion
<i>SONAR</i>	=	Sound navigation and ranging
<i>TRC</i>	=	Translational rate command

Variables

\bar{a}	=	Linear acceleration vector [m/s^2]
C_D	=	Drag coefficient of cable section [-]
D_{angle_c}	=	Damping constant cable angle [Nm/deg]
D_{damp}	=	Damping vector cable hinges [Nm]
D_{rate_c}	=	Damping constant cable rate [Nms/deg]
\bar{F}_{AE}	=	Drag vector [N]
$f(\bar{x})$	=	state matrix [varies]
G	=	Control effectiveness matrix [varies]
$h(\bar{x})$	=	Output function [varies]
I	=	Identity matrix [-]
J	=	Inertia matrix [kgm^2]
l_i	=	Length cable section i [m]
m	=	Mass [kg]
n	=	Number of cable sections [-]
\bar{p}	=	Cable hinge position vector [m]
R	=	Main rotor radius [m]
\bar{r}	=	Cable hinge direction vector [m]
\bar{S}	=	Surface area vector in LVLH frame [m^2]
\bar{T}	=	Cable attachment force vector [N]
t	=	Time [s]
\bar{u}	=	Control input vector [varies]
u,v,w	=	Body velocity in x-, y-, z-direction [m/s]
V	=	Velocity [m/s]
\bar{W}	=	Weight vector [N]
x_h, y_h, h	=	Main rotor hub location from c.g. [m]
x_l, y_l, h_l	=	Load attachment location from c.g. [m]
\bar{x}	=	State vector [varies]
$\dot{\bar{x}}$	=	Derivative state vector [varies]
\bar{y}	=	Output vector [varies]
x,y,z	=	Helicopter position in x-, y-, z-direction [m]

Greek Symbols

Δ	=	Small change [-]
ζ	=	Damping ratio [-]
$\bar{\Theta}$	=	Orientation vector in LVLH frame [rad]
θ_0	=	Collective input [rad]
θ_{0tr}	=	Tail rotor collective input [rad]
θ_{1c}	=	Lateral cyclic input [rad]
θ_{1s}	=	Longitudinal cyclic input [rad]
\bar{v}	=	Linear velocity vector [m/s]
\bar{v}	=	Virtual control input [varies]
ρ	=	Density [kg/m^3]
σ	=	Standard deviation [varies]
$\bar{\tau}$	=	Torque vector [Nm]
$\dot{\psi}, \dot{\theta}, \dot{\phi}$	=	yaw, pitch, roll rate in LVLH frame [rad]
$\ddot{\psi}, \ddot{\theta}, \ddot{\phi}$	=	yaw, pitch, roll acceleration in LVLH frame [rad]
ψ, θ, ϕ	=	yaw, pitch, roll angle in LVLH frame [rad]
$\bar{\omega}$	=	Angular rate in LVLH frame [rad/s]
$\dot{\bar{\omega}}$	=	Angular acceleration in LVLH frame [rad/s^2]

Subscripts

0	=	Initial condition
1	=	First cable section
<i>air</i>	=	Air
<i>angle</i>	=	Due to cable bending
<i>att</i>	=	Attitude
<i>c</i>	=	Commanded
<i>c</i>	=	Cable
<i>f</i>	=	Fuselage
<i>f</i>	=	filtered
<i>i</i>	=	Index
<i>p</i>	=	Cable hinge
<i>pos</i>	=	Position
<i>rate</i>	=	Due to cable bending rate
<i>si</i>	=	Cable section i
<i>s</i>	=	SONAR
<i>vel</i>	=	Velocity
<i>w</i>	=	Water
<i>x</i>	=	x-direction
<i>y</i>	=	y-direction
<i>z</i>	=	z-direction

II. Helicopter + Cable + SONAR Model

A. Basic Principles

The suspension cable + SONAR is modelled as a set of rigid links that can rotate with respect to each other. The cable is divided into n sections and the SONAR is added at the end of the cable. This means that effectively the system is an

$n + 1$ (n cable sections + SONAR) pendulum system. The idea behind this approach is that the behaviour of the cable becomes more real, the more cable sections there are. Thus, the desired accuracy could be achieved by choosing enough cable sections. A pre-existing 8 degrees-of-freedom (DOF) helicopter model was used. This includes 6-DOF body motion and 2-DOF quasi-dynamic rotor inflow for the main and tail rotor. The configuration of the load at the helicopter is presented in Figure 2. An illustration of the suspension cable model is given in Figure 1. For reference, the linear velocity and the linear accelerations are indicated for the first cable section.

B. Assumptions

The cable model makes use of several assumptions:

- Each cable section is assumed to be rigid. This means that rigid body dynamics apply.
- Each cable section is assumed to have the same parameters for mass, size, shape, etc.
- Cable stretch is assumed to be small, and is thus neglected.
- Cable sections are assumed to rotate in two directions only. They are allowed to rotate around the lateral axes (x and y) of the cable sections and not the longitudinal axis. This essentially means that bending is modelled, but twist is not.
- The SONAR is assumed to behave as any other cable section, albeit with different parameters. It is therefore modelled as a cable section in the dynamic system.
- The center of mass is assumed to be in the geometric center of a cable section.
- The cable section is assumed to be a smooth circular cylinder when computing the drag.
- The cable attachment point is assumed to be a free hinge, meaning that no friction or damping is present here.
- Cable hinges carry no torque, but produce a damping torque depending on relative angle and angular rate.
- Cable damping is assumed to be linear with respect to bending angular rate and bending angle.
- Submerged cable sections are assumed to not experience wind velocities.
- Aerodynamic drag is assumed to act on the center of mass of the cable section.

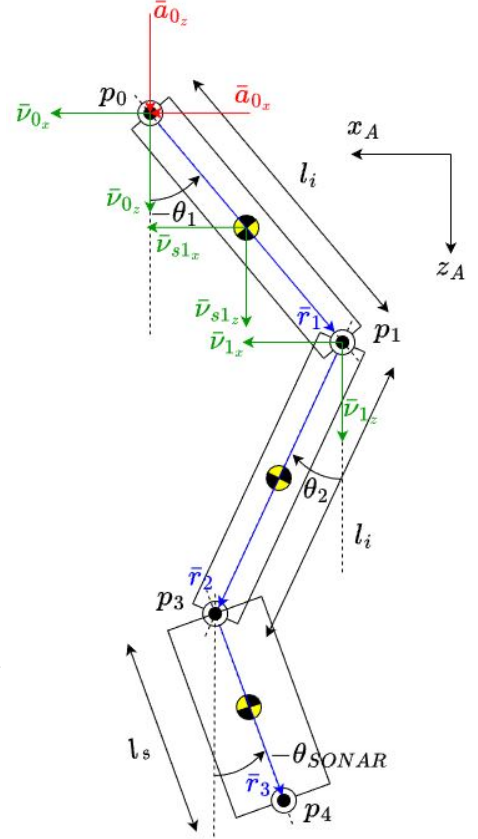


Fig. 1 Illustration 6-DOF of suspension 2 sections cable + SONAR.

C. Dynamic System

The direction vector from one cable hinge to another is represented by (1).

$$\bar{r}_i = \bar{p}_i - \bar{p}_{i-1} \quad (1)$$

Taking the derivative of this vector yields the linear velocity from one hinge to another. This is represented by (2). Note that the vector $\bar{\omega}_{s_i}$ is the rotational rate vector of the cable section. The angular acceleration of a cable hinge is found in (3) by taking the derivative of the linear velocity. The linear acceleration of a cable section at the center of mass is then given by (4). Note that $\dot{\bar{\omega}}_{s_i}$ is the angular acceleration vector of a cable section.

$$\bar{a}_{p_i} = \bar{a}_{p_{i-1}} + \dot{\bar{\omega}}_{s_i} \times \bar{r}_i + \bar{\omega}_{s_i} \times \bar{v}_i \quad (3)$$

$$\bar{a}_{s_i} = \bar{a}_{p_{i-1}} + \dot{\bar{\omega}}_{s_i} \times \frac{1}{2} \bar{r}_i + \bar{\omega}_{s_i} \times \frac{1}{2} \bar{v}_i \quad (4)$$

Rearranging terms in (4) yields an expression for the angular acceleration of a cable section $\dot{\bar{\omega}}_{s_i}$. Doing this for all cable sections yields a dynamic system is set up. Solving the system (see Appendix A), yields the linear dynamic system in (5). Note that the variables $A_{\dot{\bar{\omega}}}$, $B_{\dot{\bar{\omega}}}$, $A_{\bar{a}_s}$, $B_{\dot{\bar{\omega}}}$, $B_{\bar{a}_s}$, $B_{\dot{\bar{\omega}}}$, $C_{\bar{a}_s}$, $C_{\dot{\bar{\omega}}}$ and $D_{\dot{\bar{\omega}}}$ are intermediate matrix solutions from Appendix A. D_{damp} is the cable section damping, which is explained further below. Note that all angles are taken in the A-frame, the local vertical local horizontal (LVLH) frame.

$$\dot{\bar{\omega}}_s = (A_{\dot{\bar{\omega}}} - B_{\dot{\bar{\omega}}} A_{\bar{a}_s})^{-1} [B_{\dot{\bar{\omega}}} B_{\bar{a}_s} \bar{v}_p + B_{\dot{\bar{\omega}}} C_{\bar{a}_s} \bar{a}_{p_0} + C_{\dot{\bar{\omega}}} + D_{\dot{\bar{\omega}}} + D_{damp}] = [\ddot{\phi}_{s_i}, \ddot{\theta}_{s_i}, \ddot{\psi}_{s_i}]^T \quad (5)$$

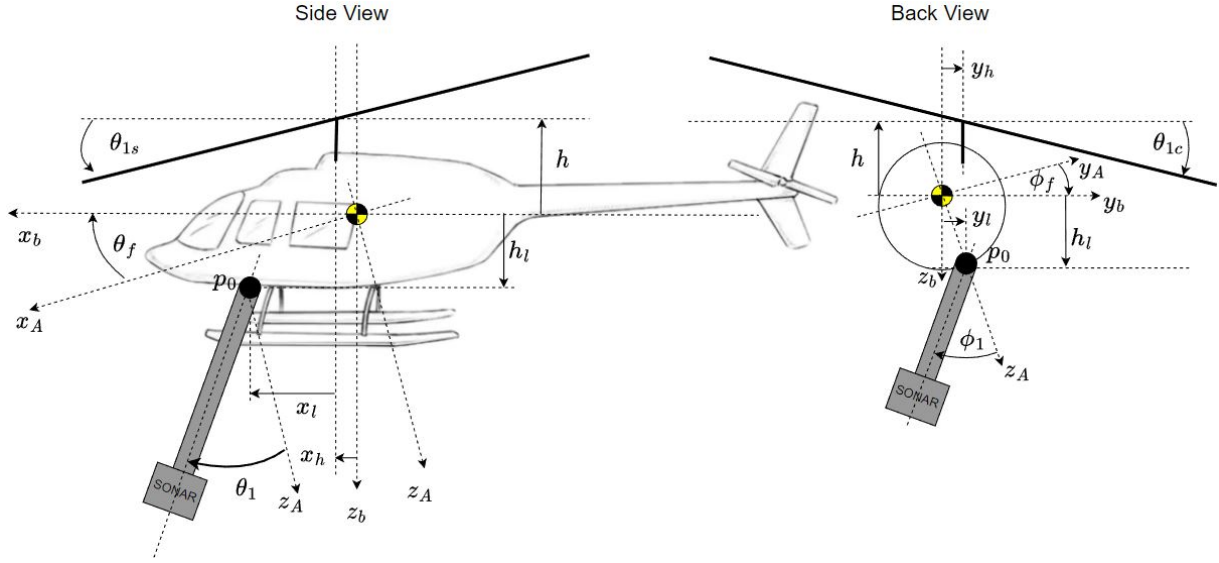


Fig. 2 Configuration 6-DOF of helicopter with suspension and cable attached.

D. Cable Damping

Cable damping is added to both model the resistance of the cable to bending as well as removing energy from the system. The latter is necessary since simulation is done in discrete steps and it was found that if no damping is added, occasional overshoots added energy to the cable system.

Damping is modelled as a torque produced by two components: A component due to the angular deflection between two sections and a torque produced due to the relative angular rate between two sections. The two components of the damping are given in (6) and (7). Note that the subscript s_i indicates a property of cable section i . Torque is denoted with τ .

$$\bar{\tau}_{d_{angle}} = D_{angle_c} (\bar{\Theta}_{s_i} - \bar{\Theta}_{s_{i-1}}) \quad (6) \quad \bar{\tau}_{d_{rate}} = D_{rate_c} (\bar{\omega}_{s_i} - \bar{\omega}_{s_{i-1}}) \quad (7)$$

The two damping constants D_{angle_c} and D_{rate_c} are scalars that indicate how much torque is produced for a deflection in the cable or a relative angular rate between two sections. Note that if the sections get smaller, the damping constants have to be reduced since the effect of the damping torque on the angular acceleration increases when the moment of inertia decreases. Therefore, the damping constants are reduced by a factor of n^3 when modelling more than 1 section. This is done since the moment of inertia of a cable section scales with n^{-3} . Since the SONAR size remains equal though, the damping constants of the SONAR are kept constant, with changing n .

The damping matrix is computed as in (8). Note that the damping in the first column is zero. This is since it is assumed that the cable is free to rotate at the attachment hinge of the helicopter. However, there is a case to be made to include a damping due to angular rate, since this technically produces friction and hence damping.

$$D_{damp} = D_{angle_c} \begin{bmatrix} 0 & \Theta_2 - \Theta_1 & \Theta_3 - \Theta_2 & \dots & \Theta_{n+1} - \Theta_n \end{bmatrix}^T + D_{rate_c} \begin{bmatrix} 0 & \bar{\omega}_2 - \bar{\omega}_1 & \bar{\omega}_3 - \bar{\omega}_2 & \dots & \bar{\omega}_{n+1} - \bar{\omega}_n \end{bmatrix}^T \quad (8)$$

E. Cable Drag

The effects of cable drag are also modelled. This is especially important since the drag on the cable changes when submerged. The equation used for drag is (9). Note that here \odot indicates element-wise multiplication. $\bar{F}_{AE_{s_i}}$ is the drag force vector experienced by cable section i . The density ρ_{s_i} is the effective fluid density experienced by the cable section. \bar{v}_{s_i} is the linear velocity of the center of mass of cable section i , $C_{D_{s_i}}$ is the drag coefficient of section i . S_{s_i} is the surface area vector of the cable section (or SONAR) rotated to the LVLH frame.

$$\bar{F}_{AE_{s_i}} = \frac{1}{2} \rho_{s_i} \bar{v}_{s_i} \odot \bar{v}_{s_i} C_{D_{s_i}} \bar{S}_{s_i} \quad (9)$$

Conditions for submerging

The cable sections experience drag, which is different depending on whether a cable section is submerged or not. If a cable section is submerged, the density of the fluid is higher than when emerged, which changes the drag by a large amount.

If the top hinge p_{i-1} of the cable section i is not submerged, but the bottom hinge p_i is submerged, the amount of each section that is submerged will determine the "effective density" of the fluid the section is going through, which is the average of the amount the section is submerged. In (10), the equation for the effective density is given. Note that this only applies to the section that is partially submerged. Sections that are emerged use the air density $\rho_{air} = 1.225 \text{ kgm}^3$ and the sections that are submerged use the water density $\rho_W = 997 \text{ kgm}^3$. This is the case when the z-position of the bottom hinge of a section is positive or the top hinge negative. Note that in this equation, only the z-position of the hinge positions matters as this is negative if the section is emerged and positive if submerged (Hence only the third entry for p is relevant).

$$\rho_{s_i} = \frac{\rho_w \cdot p_i(3) - \rho_{air} \cdot p_{i-1}(3)}{p_i(3) - p_{i-1}(3)} \quad (10)$$

It is also important to note that wind is only applied to sections that are emerged. If a section is submerged, it is assumed that it does not experience wind. If a section is partially submerged, the wind is applied via the same principle in (10), where the densities are replaced by the wind velocities.

III. Wind and Turbulence Model

In this paper, wind plays a big role by acting as a disturbance on the helicopter and the cable. Therefore, a wind and turbulence model is used throughout the simulations done in this research.

A. Constant Wind

Constant wind is, as the name implies, an air velocity that is added to the helicopter and the cable sections emerged from the water. The direction of this wind is taken always in the x -direction (so head on) of the helicopter at $t = 0$ (so before any yaw changes occur). The wind velocities used range from 4 kts to 30 kts, depending on the simulation.

B. Turbulence Model

For the turbulence, a von Karman turbulence model is used. For simplicity, the von Karman Wind Turbulence Model block from Matlab Simulink is used. The settings used for this block are found in Table 1. Specification is the military reference, which affects the application of turbulence scale lengths in the lateral and vertical directions, specified as MIL-F-8785C, MIL-HDBK-1797, or MIL-HDBK-1797B[33]. MIL-HDBK-1797 contains the flying quality requirements of piloted aircraft.

Table 1 Turbulence Model Settings in Matlab Simulink

Units	Metric (MKS)
Specification	MIL-HDBK-1797
Model Type	Contiuous Von Karman (+q +r)
Wind speed at 6m defines the low-altitude intensity	v_{trim}
Wind direction at 6m (degrees clockwise from north)	0
Probability of exceedance of of high altitude intensity	10^{-2} -Light
Scale length at medium/high altitudes (m)	762
Wingspan (m)	$2R$
Band limited noise sample time (sec)	0.1
Noise seeds [ug vg wg pg]	[23341 23342 23343 23344]

Interesting to note here is that for the wind speed at low altitude, the trimmed wind velocity is used. This is " v_{trim} ". Also, as wingspan, the diameter of the main rotor was used (diameter is $2R$). As for the justification of the settings, it should be noted that no attempts were made to get a perfectly accurate turbulence model. For the problem at hand, designing a controller, it was found to be of more importance to have a turbulence model that is somewhat accurate. Therefore, the settings of this block could be argued with. The inputs for this block are the altitude, velocity and the direction cosine matrix. For these, the values from the helicopter are used. The gust velocities obtained from this block are then applied everywhere on the helicopter and cable system, except for the sections submerged in water. This could

also be argued with, since the gusts experienced at the altitude of the helicopter (approximately 60m throughout this thesis) can be very different than those just over the surface of the water. Additionally, the rotational rates produced from this block are not used.

IV. Principle of NDI and INDI

In this section, the basic principle of non-linear dynamic inversion (NDI) and incremental non-linear dynamic inversion (INDI) is explained. Consider a nonlinear system that is affine in the input in (11).

$$\begin{aligned}\dot{\bar{x}} &= f(\bar{x}) + G(\bar{x})\bar{u} \\ \bar{y} &= \bar{h}(\bar{x})\end{aligned}\quad (11)$$

Where the function $f(\bar{x})$ contains the change in states due to the current state, $G(\bar{x})$ is the control effectiveness matrix and $h(\bar{x})$ is the output function. Each of these components can be nonlinear.

INDI is the incremental version of NDI, of which the principle is to create a control input based on the desired change of the states. By rearranging the terms in (11), the control input can be computed using (12).

$$\bar{u} = G^{-1}(\bar{x}) (\bar{v} - f(\bar{x})) \quad (12)$$

Where \bar{v} is the desired change of state, or the virtual control input. From this equation, it is clear where the model dependency comes from. An NDI controller will need accurate descriptions of the functions $G(\bar{x})$ and $f(\bar{x})$. If any model errors exist, the system is given by (13), where $\Delta f(\bar{x})$ and $\Delta G(\bar{x})$ are the modelling errors in the model and control effectiveness respectively.

$$\dot{\bar{x}} = f(\bar{x}) + \Delta f(\bar{x}) + [G(\bar{x}) + \Delta G(\bar{x})] \bar{u} \quad (13)$$

Inserting the NDI control law in (12) into (13) then yields (14).

$$\dot{\bar{x}} = \Delta f(\bar{x}) - \Delta G(\bar{x})G^{-1}(\bar{x})f(\bar{x}) + [I + \Delta G(\bar{x})G^{-1}(\bar{x})] \bar{v} \quad (14)$$

As shown, there are more terms present in the state change than just the desired change \bar{v} . Depending on the model uncertainties, these components could cause degraded performance, or even instability.

This is also the major shortcoming of NDI. Fortunately, this problem can be solved by using adaptive controllers, or by performing online system identification.

Another method of avoiding this shortcoming is by using incremental NDI, or INDI. INDI assumes that the control input can be updated fast enough, such that the change of states is only dependent on the change in input (see (3)).

Consider the Taylor series expansion of the nonlinear function of the state derivative (11) in (15), which can be reduced to (16) when neglecting higher order terms.

$$\dot{\bar{x}} = \dot{\bar{x}}_0 + \frac{\partial}{\partial \bar{x}} [f(\bar{x}) + G(\bar{x})\bar{u}] \Big|_{\bar{x}_0, u_0} (\bar{x} - \bar{x}_0) + \frac{\partial}{\partial \bar{u}} G(\bar{x})\bar{u} \Big|_{\bar{x}_0, u_0} (\bar{u} - \bar{u}_0) + H.O.T. \quad (15)$$

$$\dot{\bar{x}} \approx \dot{\bar{x}}_0 + \frac{\partial}{\partial \bar{x}} f(\bar{x}_0)(\bar{x} - \bar{x}_0) + G(\bar{x}_0)(\bar{u} - \bar{u}_0) \quad (16)$$

As can be seen from (16), the second component on the right-hand side approaches zero if the sampling frequency increases, since $(\bar{x} - \bar{x}_0) \rightarrow 0$ when the sampling frequency increases. Furthermore, it is important to note that the dynamics of the vehicle and the control inputs must be separated in time, also known as the timescale separation. Under normal circumstances, the rotor dynamics are indeed much faster than the vehicle dynamics and it can therefore be assumed that the difference in states is zero, with a nonzero difference in actuator inputs. In mathematical terms, this means that the change in state can be approximated as (17), where the change in state is only dependent on the input to the system. Rearranging terms, and using an incremental input $\Delta \bar{u}$ yields (18).

$$\dot{\bar{x}} \approx \dot{\bar{x}}_0 + G(\bar{x}_0)(\bar{u} - \bar{u}_0) \quad (17) \qquad \Delta \bar{u} = G^{-1}(\bar{x}_0)(\bar{v} - \dot{\bar{x}}_0) \quad (18)$$

An illustration of an INDI-controlled system is presented in a block diagram in Figure 3.

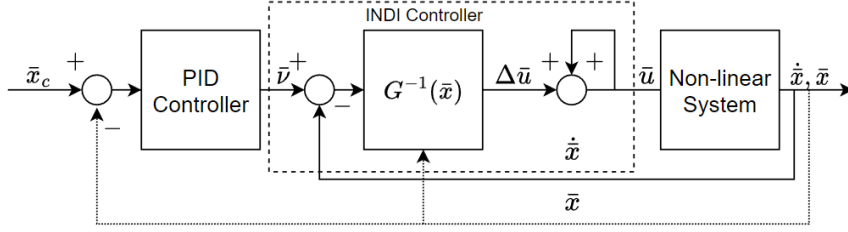


Fig. 3 Block diagram of general INDI-controlled system.

As is apparent from (18), the input of the system is no longer dependent on the non-linear feedback model of the vehicle which is the major downside of NDI. On the other hand, there is an increased dependency on the measurements taken or state estimations of the system \hat{x}_0 . This also means that the states must be either measurable directly or indirectly. Another uncertainty can still exist in the control effectiveness matrix $G(\bar{x}_0)$.

Assuming an uncertainty of ΔG in the system and applying INDI as is done in (13) and (14), yields (19).

$$\dot{\hat{x}} = \bar{v} + \Delta G(\bar{x}_0)G^{-1}(\bar{x}_0)\bar{v} - \Delta G(\bar{x}_0)G^{-1}(\bar{x}_0)\dot{\hat{x}}_0 \quad (19)$$

When still assuming a high sampling rate, the difference between two state changes is negligible and $\dot{\hat{x}} \approx \dot{\hat{x}}_0$, meaning that (20) holds and $\dot{\hat{x}} = \bar{v}$ when the sampling frequency is high enough.

$$[I + \Delta G(\bar{x}_0)G^{-1}(\bar{x}_0)] \dot{\hat{x}} = [I + \Delta G(\bar{x}_0)G^{-1}(\bar{x}_0)] \bar{v} \quad (20)$$

This means that INDI is robust to model uncertainties, even in the control effectiveness matrix. However, INDI requires having sensors measuring the states fast enough.

V. Cable Controller Design

Cable control is done using the motion of the helicopter itself. The reasoning behind controlling the cable rather than the SONAR directly is because it is assumed that the helicopter does not know where the SONAR is relative to the helicopter position. Hence, the cable angle is the only known for the helicopter about the SONAR motion.

A. Helicopter Control Design

Without cable controller, the helicopter uses 3 control loops: The attitude command attitude hold (ACAH) as inner loop to control helicopter attitude, the translational rate command (TRC) around it to control body velocities and the position hold as the final outer loop to control helicopter position. There are 2 different controllers tuned: An INDI controller and a PID controller. The control method for each loop is provided in Table 2. The reason for using NDI in the TRC loop is that the relationship in the TRC is almost only kinematic. The choice for using INDI for w comes from the idea to use INDI in the most inner loop of the controller. The TRC for w controls the main rotor collective θ_0 , meaning that it is in the most inner loop. Tuning is done by sending a step command signal to the controller and have the PID and the INDI controller show the same out response to that step input. This way, both controllers perform the same under that condition.

Table 2 Control method control loops

Controller	INDI	PID
ACAH ψ_f	INDI	PID
ACAH θ_f	INDI	PID
ACAH ϕ_f	INDI	PID
TRC u	NDI	NDI
TRC v	NDI	NDI
TRC w	INDI	NDI
Position hold x	PID	PID
Position hold y	PID	PID
Position hold z	PID	PID

B. Cable Control Strategies

In this paper, 3 different control strategies for cable control were investigated:

- 1) Cable control through helicopter attitude. This strategy was chosen as a candidate since the attitude controls the direction in which the helicopter accelerates. Since the acceleration of the attachment point from the cable is present in the dynamic equations (5), using acceleration of the vehicle to control the angular acceleration of the cable seemed trivial. The block diagram of this control strategy is provided in Figure 4.

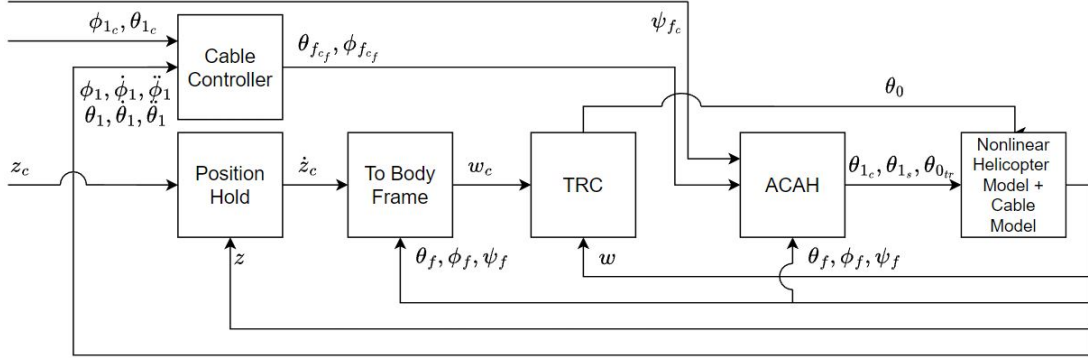


Fig. 4 Control architecture for cable control through helicopter attitude.

- 2) Cable control through helicopter velocity. Using the velocity of the helicopter was chosen since the velocity of the helicopter is essentially one integral further away from the acceleration. It was thought that this may be more stable than the previous strategy. The block diagram of this control strategy is provided in Figure 5.

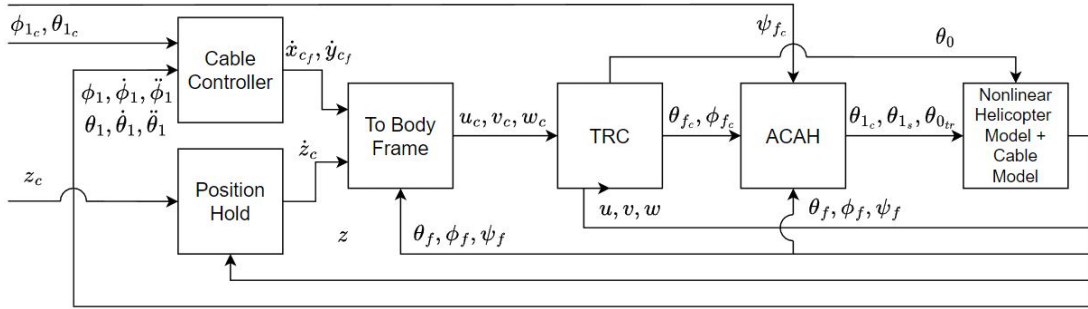


Fig. 5 Control architecture for cable control through helicopter velocity.

- 3) Cable control through helicopter position. Using the helicopter position was chosen as a candidate to go another integral further away from the cable dynamics to see whether this improved or degraded the performance of the controllers. The block diagram of this control strategy is provided in Figure 6.

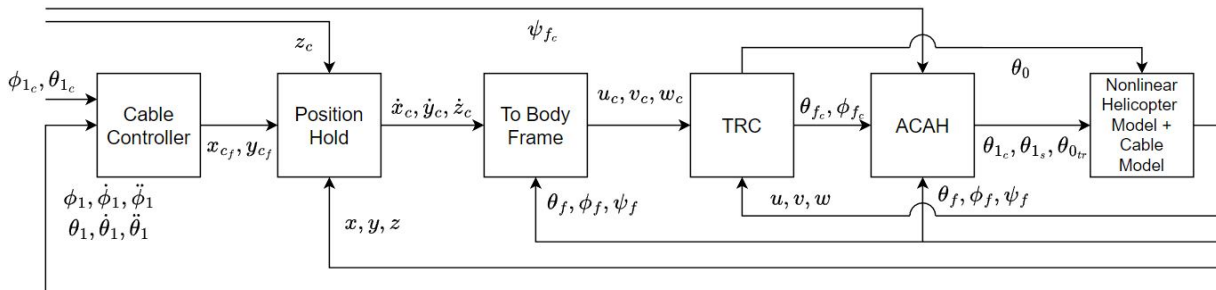


Fig. 6 Control architecture for cable control through helicopter position.

C. Cable Controller

The cable controller can be either a PID or an INDI controller with the architecture described in Figure 7 for the INDI controller and Figure 8 for the PID controller. Both the INDI and PID controller follow a two-loop structure, where the outer loop controls the cable angle, and the inner loop the cable angular rate. However, the INDI controller has an extra loop controlling the angular acceleration of the cable. G^{-1} is the control effectiveness. This is essentially the inverse of the partial derivative of the cable angular acceleration with respect to either the helicopter attitude, velocity or position, depending on the control strategy. u is the control input to the cable system, which is the commanded attitude, velocity or position. Note the addition of low pass filters (LPF). These were used to smooth the in and output signals of the cable controllers. They are also used on the feedback of the control input in the INDI controllers for synchronisation. For the simulation cases explained in the following section, it is important to note that there are two different low-pass filters used: LPF_1 and LPF_2 . These are both first order lag filters, but with different time constants. The subscript f indicates that the signal is filtered. The subscript c indicates that the signal is a command signal.

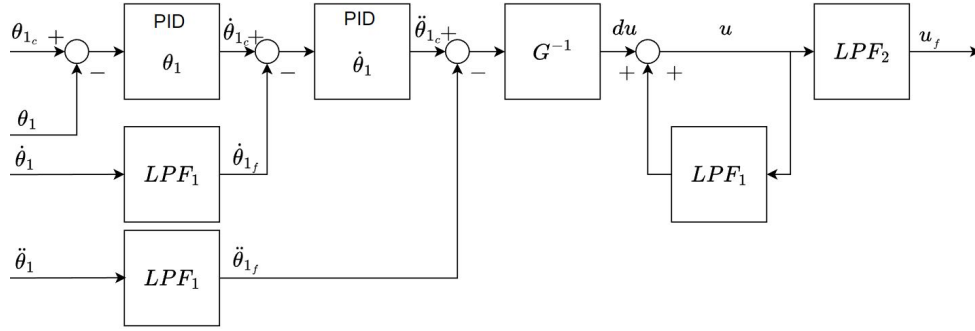


Fig. 7 Control architecture for INDI cable control.

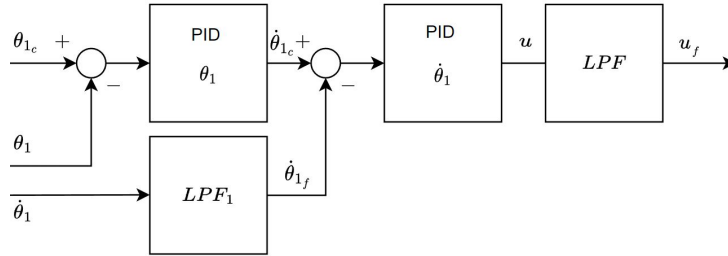


Fig. 8 Control architecture for PID cable control.

PID and INDI controllers are tuned in such a way that their response to a step input in commanded cable angle of -1° showed approximately the same response (approximately, since an exact match was not possible). In order to assess this, both controllers were tuned to show a second order response with a natural frequency of ω_n and a damping ratio of ζ .

VI. Simulation Cases

This research was performed in different cases, increasing the complexity of the system at each case. The final goal of this exercise is to have a controller capable of reducing the velocity of a hanging SONAR to zero, given a disturbance found during dipping SONAR mission conditions. At the same time, the helicopter is required to hover, but it is allowed to translate. The cases are presented in Table 3. The column helicopter model indicates where the main rotor hub is located. The cable model column indicates how many cable sections are used. For cases 1 and 2, no load is assumed so no cable sections apply. Column Load location indicates where the attachment point of the cable is located. Medium indicates the medium in which the cable model is modelled. For cases 3-5, this is air, meaning that the cable is not submerged. For cases 6 and 7, this is air+water, meaning that the cable is partially submerged. The disturbance column indicates the disturbances modelled in the environment. This is either constant wind or constant wind with gusts.

Table 3 Simulation Cases for the 6-DOF helicopter controller

Case	Helicopter Model	Cable Model	Load Location	Medium	Disturbances
1	Rotor hub aligned with c.g.	-	-	-	Constant wind
2	Rotor hub at offset	-	-	-	Constant wind
3	Rotor hub at offset	Single cable section + SONAR	c.g. of helicopter	Air	Constant wind
4	Rotor hub at offset	Single cable section + SONAR	At offset	Air	Constant wind
5	Rotor hub at offset	5 cable sections + SONAR	At offset	Air	Constant wind
6	Rotor hub at offset	5 cable sections + SONAR	At offset	Air + water	Constant wind
7	Rotor hub at offset	5 cable sections + SONAR	At offset	Air + water	Constant wind + Gusts

VII. Simulation Results

A. Cases 1 and 2: Pure Helicopter

Cases 1 and 2 have no load attached to the helicopter. The disturbance response was assessed by subjecting both tuned controllers to a step input in wind of 4 kts in the longitudinal direction. The response of the helicopter position and its attitude are presented in Figure 9 and Figure 10 for both the PID and the INDI controller. The position appears to have a steady state error for both controllers, although it is smaller for the PID controller. This steady state error is caused by the fact that the position hold controller is a PID without an integral. Interestingly, the PID controller reaches steady state quicker than the INDI controller. Likely due to the attitude controller with the initial pitch-up of the helicopter in the first second after the disturbance starts. The INDI controller pitches back more than the PID. At $t = 0$, the reference body velocity is 0 m/s from the position hold controller. Therefore, as soon as the wind is added, the initial response of the TRC controller is to compensate for the velocity of the wind and bring it back to zero, hence the pitch-up. The INDI controller appears to compensate for wind more quickly than the PID controller.

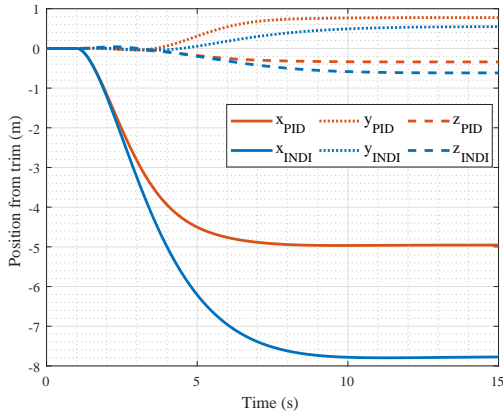


Fig. 9 Position response of both the ACAH INDI and ACAH PID controllers to step input on disturbance velocity of 4 kts .

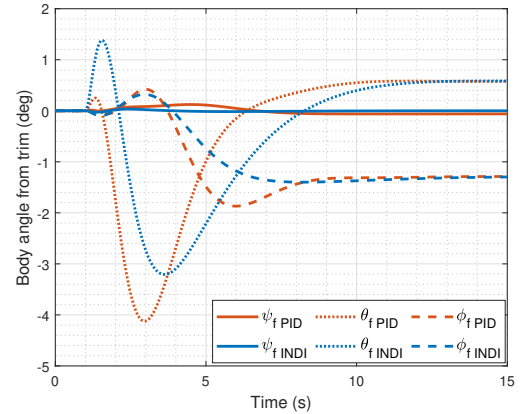


Fig. 10 Attitude response of both the ACAH INDI and ACAH PID controllers to step input on disturbance velocity of 4 kts .

B. Cases 3 and 4: Single Cable Section

In cases 3 and 4 a load was attached, consisting only of 1 cable section and the SONAR. First at the c.g. of the helicopter in case 3, then at an offset of $x_l = 0.5\text{ m}$ in front of the c.g. and $h_l = 1\text{ m}$ below the c.g. in case 4. These were then compared by subjecting both tuned controllers to a step input in wind similar to cases 1 and 2. The cable angle response is shown in Figure 11. The cable angles are larger for the PID, than the INDI controller. The SONAR ground velocity is presented in Figure 12. Here, it becomes clear that the INDI controller is better than the PID controller at keeping the

lateral velocity low, given a longitudinal wind disturbance. This means that the INDI controller is better at decoupling longitudinal and lateral modes. Interestingly, the change in load location did not influence the performance of the controller from case 3 to 4, since the cable angle response was observed to be the same as in case 3.

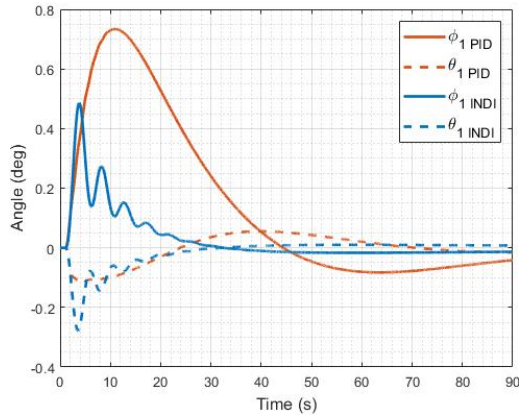


Fig. 11 Cable angle response for disturbance case 3, given a filtered 4 kts step input in wind.

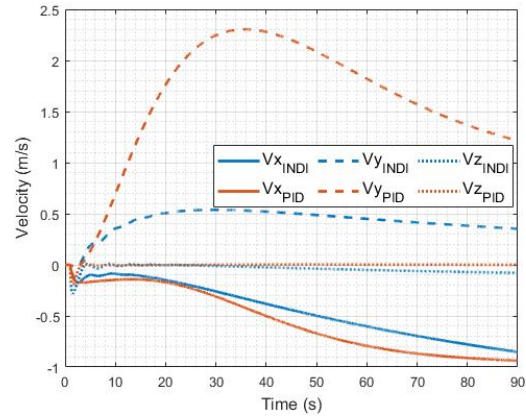


Fig. 12 Sonar ground velocity response for disturbance case 3, given a filtered 4 kts step input in wind.

C. Case 5: Flexible Cable

Case 5 is the same as case 4, yet with a longer cable and 5 cable sections. The function of this case is to observe the change from a rigid to a flexible cable. Comparing was done in the same way as in cases 1-4. Changing from a rigid to a flexible cable had a large influence on the response of the controlled system. It was not possible to use cable control through attitude in this case due to oscillations, hence cable control through velocity was used. The response of the cable angle and control inputs are presented in Figure 13 and Figure 14. The PID controller is unstable under the given disturbance. It is not able to compensate for the added wind. The INDI controller on the other hand is capable of maintaining control. However, a vibration is present in the controls. These vibrations are caused by the oscillations of the first cable section. Such oscillations could be removed by making the controller slower. Either by increasing the time constant of the filters used or by reducing the gains of the controller. Furthermore, it was found that these vibrations are present when the air velocity in that direction is small. This means that drag has a damping effect on the cable sections. Nevertheless, it shows that the INDI controller is more capable of adapting to the new situation of added wind.

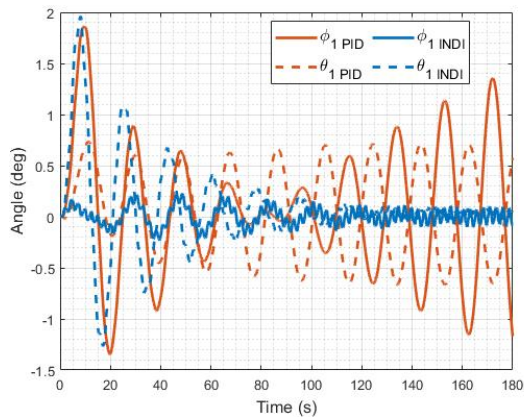


Fig. 13 Response of cable angle with INDI and PID controller to a step input on wind of 4 kts

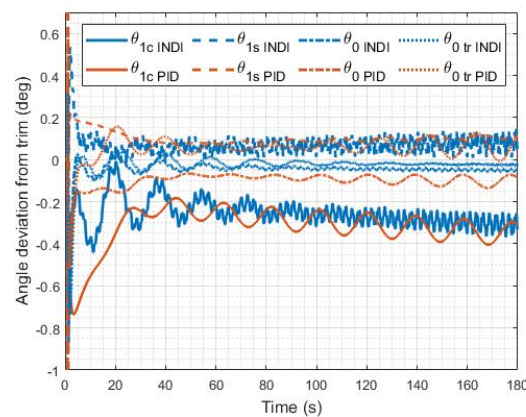


Fig. 14 Control inputs from INDI and PID controller from a step input on wind of 4 kts

D. Case 6: Submerged Cable

Case 6 adds the concept of submergence. With a trimmed altitude of 60m and a total cable length of 120m, half the cable is submerged and the other half emerged in zero wind conditions. The addition of water drag, instead of air drag in case 5, causes more damping to the cable. Case 6 also introduces 3 control strategies that are tested in order to find out what control strategy works best for dipping SONAR missions. There 3 control strategies are: cable control through helicopter attitude, cable control through helicopter velocity and cable control through helicopter position. As the name suggests, the first strategy uses the cable controller to obtain a reference attitude for the helicopter to follow in order to control the cable as in cases 3 and 4. The second uses the velocity, as done in case 5. The final strategy uses the controller to obtain a reference position.

The response of the cable angle, SONAR ground velocity, body velocities and helicopter attitude to a constant wind disturbance are presented in Figure 15 - Figure 18. Observing the cable angles, it is clear that the cable controller through helicopter attitude shows the smallest angle deviation to a $4kts$ wind and it reaches a 0° angle faster. However, the cross-coupling between the longitudinal and lateral angles appears to be larger for the control strategy using attitude control than the other two strategies. In order to determine what strategy is best for dipping SONAR missions, it can be reasoned that the amount of velocity deviation is most important. Observing the SONAR velocity, the control strategy using helicopter attitude performs the best, by having the lowest velocity deviation. The reason why cable control through attitude control performs better, is likely due to the wind velocity not being present in the controller loop. In the other two control strategies, the body velocity is within the control loop via the TRC controller. Since there is initially no body velocity (there is no wind after all) and the cable is straight, the reference body velocity is zero. This means that once the wind hits, the reference velocity is still close to zero, meaning that the controller will move the helicopter such that the body velocity is reduced to zero, before the cable controller or position hold controller can match the wind velocity. This can be seen in Figure 17, where the control strategies using velocity and position decrease the body velocity initially, before matching the roughly 1.8 m/s in u direction.

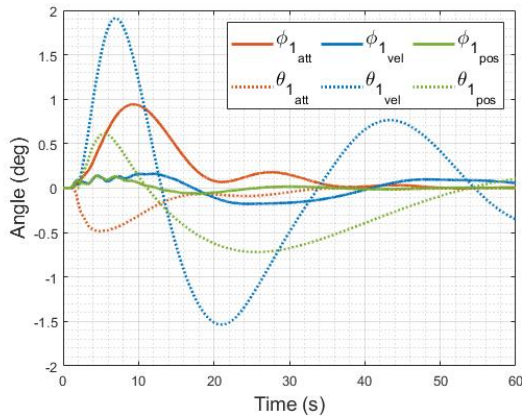


Fig. 15 Cable angle response to a $4kts$ wind using different control strategies

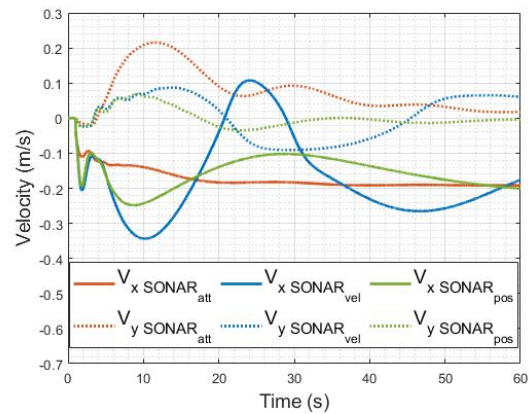


Fig. 16 SONAR ground velocity squared response to a $4kts$ wind using different control strategies

Choosing cable control through helicopter attitude as the better control strategy, the response of both the PID and the INDI controllers are shown in Figure 19 and Figure 20. As shown, the INDI controller is more capable of keeping the SONAR velocity low than the PID. However, the PID controller's response is more smooth. Looking at the cable angle response, the same can be said. This suggests that INDI is better at stabilising the SONAR under these conditions.

E. Case 7: Submerged Cable with Turbulence

In case 7, turbulence is added to observe the controller performance under high wind turbulent conditions. The simulation is run for 300 seconds, to see the behaviour of the controller in a turbulent environment over a long time. Also, unlike the previous cases, the cable controllers are assessed based on the following performance metrics: the standard deviation of the control inputs, mean sonar velocity and standard deviation of the SONAR velocity. These will say something about the efficiency of the controller, the changes in SONAR velocity and the drift of the SONAR. The

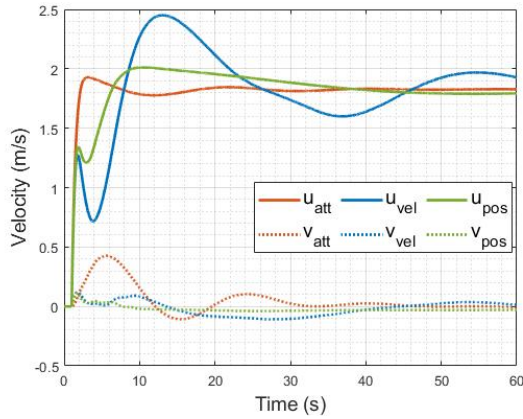


Fig. 17 Body velocity response to a 4kts wind using different control strategies

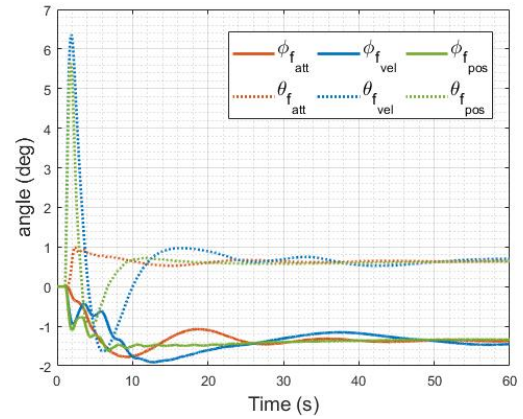


Fig. 18 Helicopter attitude response relative to trim to a 4kts wind using different control strategies

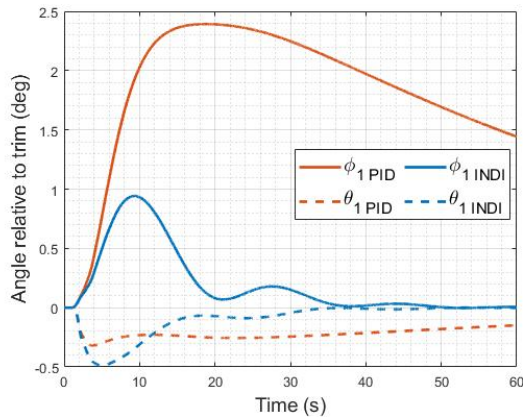


Fig. 19 Cable angle response to a 4kts wind using PID and INDI control for case 6

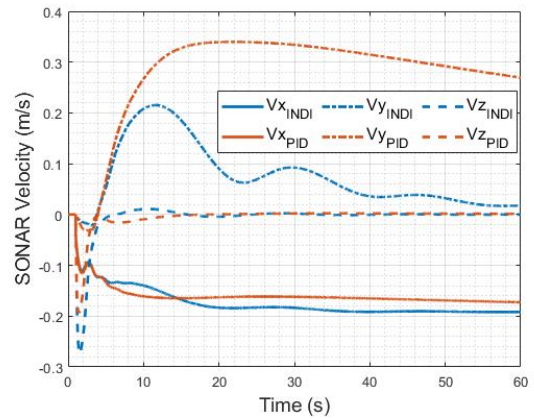


Fig. 20 SONAR ground velocity response to a 4kts wind using PID and INDI control for case 6

simulation performance metrics are presented in Table 4 with the SONAR velocity responses in Figure 21-Figure 23.

From simulation for 10kts wind, it follows that, although the PID controller from case 6 is capable of controlling the disturbed system, it does so using more control than the INDI controller, constantly oscillating. This is also clear from the performance metrics. When looking at the standard deviation of the SONAR velocity, the PID and INDI perform roughly equal. The mean of the SONAR velocity is similar.

During simulation of 20kts wind, it was found that the controller could not handle the disturbances. The controller was trying to correct for the disturbances too aggressively. To counter this, the gains for the ACAH controllers have been lowered by a factor of 3. The gains for the TRC controllers for the vertical body velocity w were lowered by a factor 5. This hurts the performance of the ACAH and TRC controller, but it is necessary to reject the disturbance. The gains of the other controllers were left unchanged. This change was done for both the PID and the INDI controller.

When running the simulation with the re-tuned controllers, the performance metrics in Table 4 were found. From these metrics, it becomes clear that the performance of both the PID and the INDI controller worsened in all aspects, accompanied with a higher control use. This is also observed in Figure 22, where the SONAR velocity reaches higher values. Judging by the controller performance metrics, the INDI controller performs better than the PID, except at the mean of the SONAR velocity in x-direction.

30 kts wind is about the highest wind that would be encountered at a sea state of 4-5. During simulation, it was found that both the PID and INDI controller had trouble controlling the cable. Generally, there were no issues, until the helicopter got blown away far from its initial position in a short time. This meant that sometimes the helicopter would change position quickly, but the cable system is much slower. As a result, the helicopter would pull the cable completely straight, with the cable angle changing quickly. The cable pulls back the helicopter and changes angle quickly. The helicopter makes corrections at the same time in an attempt to keep the cable angle constant. This results in an aggressive correction of the helicopter and cable.

The source of this behaviour was not found, but it is likely that drifting of the helicopter is the source of this behaviour, since the other two wind velocities (10 and 20 kts) did not show this issue. To figure out whether this is the case, the position hold controller from case 2 is used for the INDI controller. The gains for the TRC and ACAH remain reduced (see 20 kts). Using this controller, the helicopter position barely drifted and the previous phenomena disappeared. This suggests that it was indeed caused by fast drifting of the helicopter relative to the cable. Also, the cable angle remained somewhat constant during this simulation. This suggests that a position hold might perform equal or better in high wind conditions. Therefore, the position hold case for INDI is included into Table 4, for comparison with the PID and INDI cable controller.

With respect to control use, the position hold controller performs worst here, likely because it is fighting the wind much more than the other two controllers. Keeping the cable angle constant requires flying with the gusts, whereas keeping constant position requires fighting the wind. With respect to SONAR velocity, the position hold controller performs best, with the smallest standard deviation of the SONAR velocity and the smallest mean in almost all directions. This is because the helicopter is set to hold the same position, keeping the mean of the SONAR velocity close to zero. This is also the case for the standard deviation.

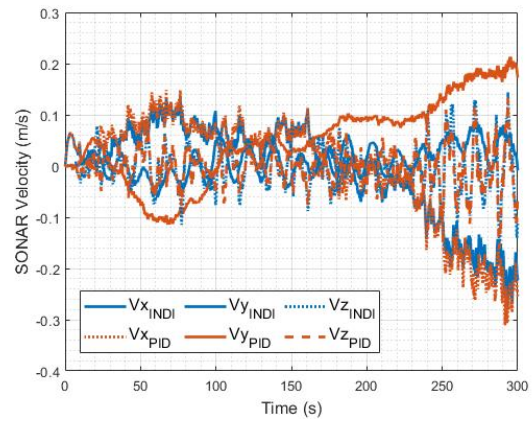


Fig. 21 SONAR ground velocity response at 10 kts wind.

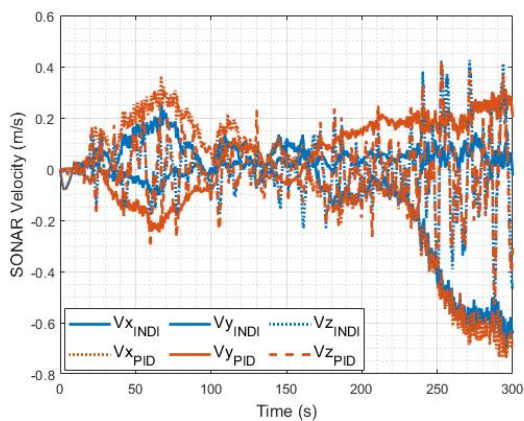


Fig. 22 SONAR ground velocity response at 20 kts wind.

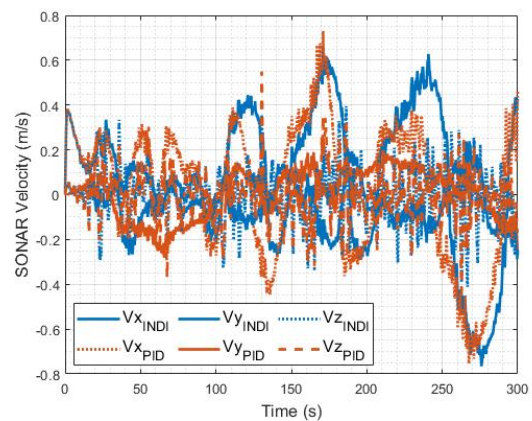


Fig. 23 SONAR ground velocity response at 30 kts wind.

Table 4 Performance metrics Cable controllers for a wind of 30 kts.

standard deviation controls (deg)	$\sigma_{\theta_{1c}}$	$\sigma_{\theta_{1s}}$	σ_{θ_0}	$\sigma_{\theta_{0rr}}$
INDI 10 kts	0.05	0.013	0.07	0.23
INDI 20 kts	0.11	0.06	0.25	0.69
INDI 30 kts	0.19	0.19	0.44	0.56
INDI position hold 30 kts	0.30	0.24	0.53	1.36
PID 10 kts	0.06	0.02	0.08	0.25
PID 20 kts	0.12	0.12	0.26	0.67
PID 30 kts	0.22	0.15	0.38	0.37
standard deviation V_{SONAR} (m/s)	$\sigma_{V_{SONARx}}$	$\sigma_{V_{SONARy}}$	$\sigma_{V_{SONARz}}$	
INDI 10 kts	0.09	0.03	0.04	
INDI 20 kts	0.23	0.04	0.12	
INDI 30 kts	0.35	0.09	0.37	
INDI position hold 30 kts	0.18	0.11	0.28	
PID 10 kts	0.10	0.08	0.04	
PID 20 kts	0.27	0.14	0.12	
PID 30 kts	0.38	0.10	0.32	
mean V_{SONAR} (m/s)	\bar{V}_{SONARx}	\bar{V}_{SONARy}	\bar{V}_{SONARz}	
INDI 10 kts	-0.01	0.01	-0.00	
INDI 20 kts	-0.09	0.02	-0.00	
INDI 30 kts	0.04	0.01	-0.02	
INDI position hold 30 kts	-0.02	-0.00	-0.00	
PID 10 kts	-0.01	0.05	-0.00	
PID 20 kts	-0.07	0.05	-0.01	
PID 30 kts	0.07	0.01	-0.03	

VIII. Conclusions

The goal of this paper is to apply INDI to a helicopter with a dipping SONAR. The main strength of INDI is that it uses minimal model knowledge in order to control a system. In order to assess the performance of the controller, it was compared to classical PID control. The main conclusion of this paper is cable control using INDI performs better at stabilising the SONAR than PID does at low constant wind speeds and under turbulent conditions with wind up to 20 kts. However, due to the way the cable controller works, either controller could fail if the helicopter gets blown away too far from the cable sections that are submerged, which was the case for 30 kts. In this research, the cable controller has as goal to keep the angle of the cable constant. Thus, changing wind will inevitably result into move commands to the helicopter in order to keep this angle constant. A position controller proved to work better under the high wind and high turbulent conditions of kts wind. Thus future work could aim to find a controller that incorporates cable control and position hold together in order to keep the helicopter position somewhat constant, yet move slightly to stabilise the cable to changing wind conditions.

A. Cable Model Derivation

This appendix contains the derivation of the suspension cable model with three cable sections. The goal of this exercise is to find a general expression for the cable model given any amount of cable sections. For reference, a free-body-diagram is provided for a cable with 2 sections.

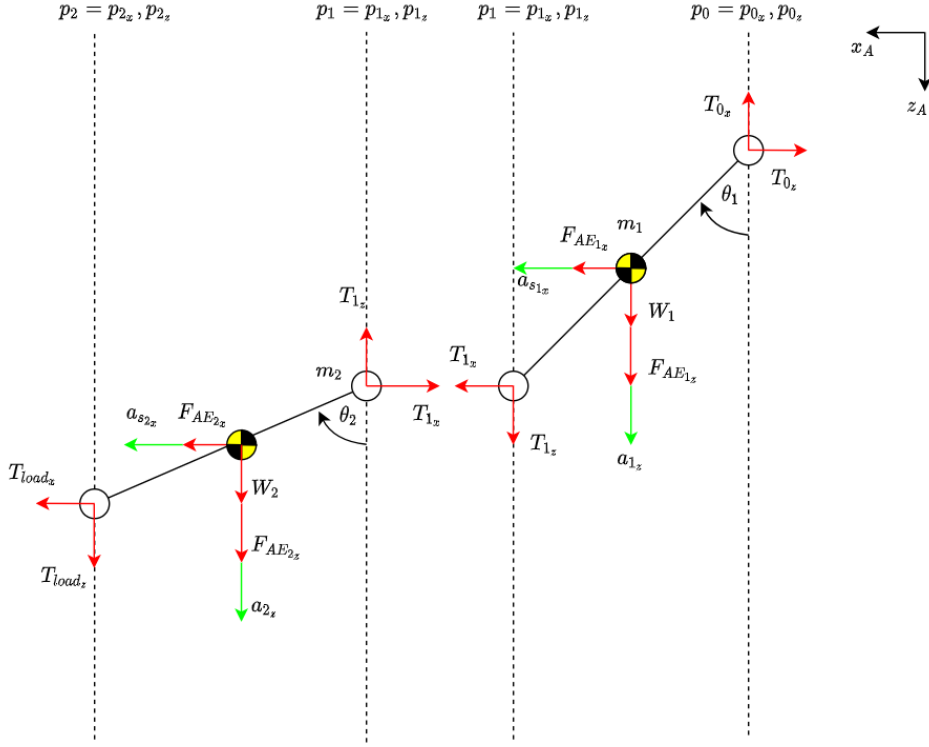


Fig. 24 Free body diagram of 2 suspension cable sections in the x_A - z_A plane.

A. Derivation

The force equations for three cable sections are presented in (21).

$$m_1 \bar{a}_{s_1} = \bar{T}_1 - \bar{T}_0 + \bar{W}_1 + \bar{F}_{AE_1}, m_2 \bar{a}_{s_2} = \bar{T}_2 - \bar{T}_1 + \bar{W}_2 + \bar{F}_{AE_2}, m_3 \bar{a}_{s_3} = \bar{T}_{load} - \bar{T}_2 + \bar{W}_3 + \bar{F}_{AE_3} \quad (21)$$

The torque equations are presented in (22)

$$\begin{aligned} J_{s_1} \dot{\bar{\omega}}_{s_1} &= \bar{\tau}_{s_1} - \bar{\omega}_{s_1} \times J_{s_1} \bar{\omega}_{s_1} = \frac{1}{2} \bar{r}_1 \times (\bar{T}_0 + \bar{T}_1) - \bar{\omega}_{s_1} \times J_{s_1} \bar{\omega}_{s_1} \\ J_{s_2} \dot{\bar{\omega}}_{s_2} &= \bar{\tau}_{s_2} - \bar{\omega}_{s_2} \times J_{s_2} \bar{\omega}_{s_2} = \frac{1}{2} \bar{r}_2 \times (\bar{T}_1 + \bar{T}_2) - \bar{\omega}_{s_2} \times J_{s_2} \bar{\omega}_{s_2} \\ J_{s_3} \dot{\bar{\omega}}_{s_3} &= \bar{\tau}_{s_3} - \bar{\omega}_{s_3} \times J_{s_3} \bar{\omega}_{s_3} = \frac{1}{2} \bar{r}_3 \times (\bar{T}_2 + \bar{T}_{load}) - \bar{\omega}_{s_3} \times J_{s_3} \bar{\omega}_{s_3} \end{aligned} \quad (22)$$

The force equations can be rewritten as such to obtain equations for the connection forces \bar{T} . This is shown in (23).

$$\bar{T}_0 = -m_1 \bar{a}_{s_1} + \bar{T}_1 + \bar{W}_1 + \bar{F}_{AE_1}, \bar{T}_1 = -m_2 \bar{a}_{s_2} + \bar{T}_2 + \bar{W}_2 + \bar{F}_{AE_2}, \bar{T}_2 = -m_3 \bar{a}_{s_3} + \bar{T}_{load} + \bar{W}_3 + \bar{F}_{AE_3} \quad (23)$$

Before inserting into the torque equations, the sum of forces is computed first in (24).

$$\begin{aligned} \bar{T}_0 + \bar{T}_1 &= -m_1 \bar{a}_{s_1} + 2\bar{T}_1 + \bar{W}_1 + \bar{F}_{AE_1} \\ &= -m_1 \bar{a}_{s_1} - 2m_2 \bar{a}_{s_2} - 2m_3 \bar{a}_{s_3} + 2\bar{T}_{load} + \bar{W}_1 + 2\bar{W}_2 + 2\bar{W}_3 + \bar{F}_{AE_1} + 2\bar{F}_{AE_2} + 2\bar{F}_{AE_3} \\ \bar{T}_1 + \bar{T}_2 &= -m_2 \bar{a}_{s_2} + 2\bar{T}_2 + \bar{W}_2 + \bar{F}_{AE_2} \\ &= -m_2 \bar{a}_{s_2} - 2m_3 \bar{a}_{s_3} + 2\bar{T}_{load} + \bar{W}_2 + 2\bar{W}_3 + \bar{F}_{AE_2} + 2\bar{F}_{AE_3} \\ \bar{T}_2 + \bar{T}_{load} &= -m_3 \bar{a}_{s_3} + 2\bar{T}_{load} + \bar{W}_3 + \bar{F}_{AE_3} \end{aligned} \quad (24)$$

The cross product in the moment equations (22) can be replaced by introducing two new variables $P_{i \rightarrow i+1}$ and $\bar{\Omega}_{s_i}$, which are the cross product matrices as shown in (25) and (26).

$$P_{i \rightarrow i+1} = \begin{bmatrix} 0 & -r_{i+1z} & r_{i+1y} \\ r_{i+1z} & 0 & -r_{i+1x} \\ -r_{i+1y} & r_{i+1x} & 0 \end{bmatrix} \quad (25) \quad \bar{\Omega}_{s_i} = \begin{bmatrix} 0 & -\bar{\omega}_{s_{iz}} & \bar{\omega}_{s_{iy}} \\ \bar{\omega}_{s_{iz}} & 0 & -\bar{\omega}_{s_{ix}} \\ -\bar{\omega}_{s_{iy}} & \bar{\omega}_{s_{ix}} & 0 \end{bmatrix} \quad (26)$$

With these variables, the moment equations (22) can be rewritten to

$$J_{s_1} \dot{\omega}_{s_1} = \frac{1}{2} P_{0 \rightarrow 1} (\bar{T}_0 + \bar{T}_1) - \bar{\Omega}_{s_1} J_{s_1} \bar{\omega}_{s_1}; J_{s_2} \dot{\omega}_{s_2} = \frac{1}{2} P_{1 \rightarrow 2} (\bar{T}_1 + \bar{T}_2) - \bar{\Omega}_{s_2} J_{s_2} \bar{\omega}_{s_2}; J_{s_3} \dot{\omega}_{s_3} = \frac{1}{2} P_{2 \rightarrow 3} (\bar{T}_2 + \bar{T}_{load}) - \bar{\Omega}_{s_3} J_{s_3} \bar{\omega}_{s_3} \quad (27)$$

By inserting (24) into (27), the intermediate solution is found in (28).

$$\begin{bmatrix} J_{s_1} & 0 & 0 \\ 0 & J_{s_2} & 0 \\ 0 & 0 & J_{s_3} \end{bmatrix} \begin{bmatrix} \dot{\omega}_{s_1} \\ \dot{\omega}_{s_2} \\ \dot{\omega}_{s_3} \end{bmatrix} = \begin{bmatrix} -\frac{1}{2} m_1 P_{0 \rightarrow 1} & -m_2 P_{0 \rightarrow 1} & -m_3 P_{0 \rightarrow 1} \\ 0_{3 \times 3} & -\frac{1}{2} m_2 P_{1 \rightarrow 2} & -m_3 P_{1 \rightarrow 2} \\ 0_{3 \times 3} & 0_{3 \times 3} & -\frac{1}{2} m_3 P_{2 \rightarrow 3} \end{bmatrix} \begin{bmatrix} \bar{a}_{s_1} \\ \bar{a}_{s_2} \\ \bar{a}_{s_3} \end{bmatrix} + \begin{bmatrix} -\bar{\Omega}_{s_1} J_{s_1} \bar{\omega}_{s_1} \\ -\bar{\Omega}_{s_2} J_{s_2} \bar{\omega}_{s_2} \\ -\bar{\Omega}_{s_3} J_{s_3} \bar{\omega}_{s_3} \end{bmatrix} + \begin{bmatrix} P_{0 \rightarrow 1} [\bar{T}_{load} + \frac{1}{2} \bar{W}_1 + \bar{W}_2 + \bar{W}_3 + \frac{1}{2} \bar{F}_{AE1} + \bar{F}_{AE2} + \bar{F}_{AE3}] \\ P_{1 \rightarrow 2} [\bar{T}_{load} + \frac{1}{2} \bar{W}_2 + \bar{W}_3 + \frac{1}{2} \bar{F}_{AE2} + \bar{F}_{AE3}] \\ P_{2 \rightarrow 3} [\bar{T}_{load} + \frac{1}{2} \bar{W}_3 + \frac{1}{2} \bar{F}_{AE3}] \end{bmatrix} \quad (28)$$

$$A_{\dot{\omega}} \dot{\omega}_s = B_{\bar{a}_s} \bar{a}_s + C_{\dot{\omega}} + D_{\dot{\omega}}$$

From the kinematic relationships, the equation for the linear accelerations $\bar{a}_{s_1} - \bar{a}_{s_3}$. First, the kinematic relations for the hinge positions in (29). Note that the cross-products are substituted, and that: $A \times B = -B \times A$.

$$\begin{aligned} \bar{a}_{p_1} &= \bar{a}_{p_0} + \dot{\omega}_{s_1} \times r_1 + \bar{\omega}_{s_1} \times (v_{p_1} - v_{p_0}) \\ &= \bar{a}_{p_0} - P_{0 \rightarrow 1} \dot{\omega}_{s_1} + \bar{\Omega}_{s_1} (v_{p_1} - v_{p_0}) \\ \bar{a}_{p_2} &= \bar{a}_{p_1} + \dot{\omega}_{s_2} \times r_2 + \bar{\omega}_{s_2} \times (v_{p_2} - v_{p_1}) \\ &= \bar{a}_{p_0} - P_{0 \rightarrow 1} \dot{\omega}_{s_1} - P_{1 \rightarrow 2} \dot{\omega}_{s_2} + \bar{\Omega}_{s_1} (v_{p_1} - v_{p_0}) + \bar{\Omega}_{s_2} (v_{p_2} - v_{p_1}) \\ \bar{a}_{p_3} &= \bar{a}_{p_2} + \dot{\omega}_{s_3} \times r_3 + \bar{\omega}_{s_3} \times (v_{p_3} - v_{p_2}) \\ &= \bar{a}_{p_0} - P_{0 \rightarrow 1} \dot{\omega}_{s_1} - P_{1 \rightarrow 2} \dot{\omega}_{s_2} - P_{2 \rightarrow 3} \dot{\omega}_{s_3} + \bar{\Omega}_{s_1} (v_{p_1} - v_{p_0}) + \bar{\Omega}_{s_2} (v_{p_2} - v_{p_1}) + \bar{\Omega}_{s_3} (v_{p_3} - v_{p_2}) \end{aligned} \quad (29)$$

Secondly, the kinematic relations for the center of mass positions of each section in (30).

$$\begin{aligned} \bar{a}_{s_1} &= \bar{a}_{p_0} + \dot{\omega}_{s_1} \times \frac{1}{2} r_1 + \bar{\omega}_{s_1} \times \frac{1}{2} (v_{p_1} - v_{p_0}) = \bar{a}_{p_0} - \frac{1}{2} P_{0 \rightarrow 1} \dot{\omega}_{s_1} + \frac{1}{2} \bar{\Omega}_{s_1} (v_{p_1} - v_{p_0}) \\ \bar{a}_{s_2} &= \bar{a}_{p_1} + \dot{\omega}_{s_2} \times \frac{1}{2} r_2 + \bar{\omega}_{s_2} \times \frac{1}{2} (v_{p_2} - v_{p_1}) = \bar{a}_{p_1} - \frac{1}{2} P_{1 \rightarrow 2} \dot{\omega}_{s_2} + \frac{1}{2} \bar{\Omega}_{s_2} (v_{p_2} - v_{p_1}) \\ \bar{a}_{s_3} &= \bar{a}_{p_2} + \dot{\omega}_{s_3} \times \frac{1}{2} r_3 + \bar{\omega}_{s_3} \times \frac{1}{2} (v_{p_3} - v_{p_2}) = \bar{a}_{p_2} - \frac{1}{2} P_{2 \rightarrow 3} \dot{\omega}_{s_3} + \frac{1}{2} \bar{\Omega}_{s_3} (v_{p_3} - v_{p_2}) \end{aligned} \quad (30)$$

Combining these two relations yields the following system

$$\begin{bmatrix} \bar{a}_{s_1} \\ \bar{a}_{s_2} \\ \bar{a}_{s_3} \end{bmatrix} = \begin{bmatrix} -\frac{1}{2} P_{0 \rightarrow 1} & 0 & 0 \\ -P_{0 \rightarrow 1} & -\frac{1}{2} P_{1 \rightarrow 2} & 0 \\ -P_{0 \rightarrow 1} & -P_{1 \rightarrow 2} & -\frac{1}{2} P_{2 \rightarrow 3} \end{bmatrix} \begin{bmatrix} \dot{\omega}_{s_1} \\ \dot{\omega}_{s_2} \\ \dot{\omega}_{s_3} \end{bmatrix} + \begin{bmatrix} \frac{1}{2} \bar{\Omega}_{s_1} & 0 & 0 \\ \bar{\Omega}_{s_1} & \frac{1}{2} \bar{\Omega}_{s_2} & 0 \\ \bar{\Omega}_{s_1} & \bar{\Omega}_{s_2} & \frac{1}{2} \bar{\Omega}_{s_3} \end{bmatrix} \begin{bmatrix} (v_{p_1} - v_{p_0}) \\ (v_{p_2} - v_{p_1}) \\ (v_{p_3} - v_{p_2}) \end{bmatrix} + \begin{bmatrix} I_{3 \times 3} \\ I_{3 \times 3} \\ I_{3 \times 3} \end{bmatrix} \bar{a}_{p_0} \quad (31)$$

$$\bar{a}_s = A_{\bar{a}_s} \dot{\omega}_s + B_{\bar{a}_s} \bar{v}_p + C_{\bar{a}_s} \bar{a}_{p_0}$$

Substituting (31) into (28) then yields the final expression for the angular acceleration in (32). Note the addition of a matrix D_{damp} in the last row. This matrix is added at the end to take into account damping due to cable motion.

$$\begin{aligned} A_{\dot{\omega}} \dot{\omega}_s &= B_{\dot{\omega}} \bar{a}_s + C_{\dot{\omega}} + D_{\dot{\omega}} \\ &= B_{\dot{\omega}} (A_{\bar{a}_s} \dot{\omega}_s + B_{\bar{a}_s} \bar{v}_p + C_{\bar{a}_s} \bar{a}_{p_0}) + C_{\dot{\omega}} + D_{\dot{\omega}} \\ (A_{\dot{\omega}} - B_{\dot{\omega}} A_{\bar{a}_s}) \dot{\omega}_s &= B_{\dot{\omega}} B_{\bar{a}_s} \bar{v}_p + B_{\dot{\omega}} C_{\bar{a}_s} \bar{a}_{p_0} + C_{\dot{\omega}} + D_{\dot{\omega}} \\ \dot{\omega}_s &= (A_{\dot{\omega}} - B_{\dot{\omega}} A_{\bar{a}_s})^{-1} [B_{\dot{\omega}} B_{\bar{a}_s} \bar{v}_p + B_{\dot{\omega}} C_{\bar{a}_s} \bar{a}_{p_0} + C_{\dot{\omega}} + D_{\dot{\omega}} + D_{damp}] \end{aligned} \quad (32)$$

This linear system can now be used to compute the angular acceleration of each cable section, given the state of the system and the acceleration of the attachment point \bar{a}_{p_0} . Also note that the matrices in (28) and (31) follow a very clear pattern, which is exploited to find a generalised solution for any amount of links system.

References

- [1] Guy, C. R., Williams, M. J., and Gilbert, N. E., “ASW Helicopter/SONAR Dynamics Mathematical Model,” *sixth european rotorcraft and powered lift aircraft forum*, , No. 45, 1980.
- [2] Gian Pietro, A. S., “Automatic Flight Control System: Autopilot Cable Hover Mode Computer Aided Design and Assessment,” 1989.
- [3] Wang, X., Wang, X., Xie, R., and Zheng, Y., “Design of helicopter cable-orientation control system based on finite-element modeling,” *Lecture Notes in Computer Science (including subseries Lecture Notes in Artificial Intelligence and Lecture Notes in Bioinformatics)*, Vol. 7506 LNAI, No. PART 1, 2012, pp. 313–322. https://doi.org/10.1007/978-3-642-33509-9_{_}30.
- [4] “ASW Helicopters,” 2011. URL <https://www.globalsecurity.org/military/systems/aircraft/rotary-asw.htm>.
- [5] Thales, “FLASH & Compact FLASH dipping sonars SONICS sonobuoy processing system,” 2002.
- [6] “Wind,” 2022-01-04. URL <http://www.bom.gov.au/marine/knowledge-centre/reference/wind.shtml>.
- [7] Bisgaard, M., La Cour-Harbo, A., and Bendtsen, J. D., “Swing damping for helicopter slung load systems using delayed feedback,” *AIAA Guidance, Navigation, and Control Conference and Exhibit*, , No. August, 2009. <https://doi.org/10.2514/6.2009-5795>.
- [8] Marguerettaz, P., and Guglieri, G., “Simulation of helicopter dynamics with external suspended loads,” *37th European Rotorcraft Forum 2011, ERF 2011*, 2011, pp. 348–359.
- [9] Potter, J., Singhose, W., and Costelloy, M., “Reducing swing of model helicopter sling load using input shaping,” *IEEE International Conference on Control and Automation, ICCA*, 2011, pp. 348–353. <https://doi.org/10.1109/ICCA.2011.6138048>.
- [10] Krishnamurthi, J., and Horn, J. F., “Helicopter slung load control using lagged cable angle feedback,” *Journal of the American Helicopter Society*, Vol. 60, No. 2, 2015, pp. 1–12. <https://doi.org/10.4050/JAHS.60.022011>.
- [11] Wang, H., Liu, Y., Lin, C., and Zhou, Y., “Modeling and Simulation of a Slung-load System for the Helicopter,” *Proceedings of the 31st Chinese Control and Decision Conference, CCDC 2019*, 2019, pp. 1148–1153. <https://doi.org/10.1109/CCDC.2019.8833478>.
- [12] Bisgaard, M., La Cour-Harbo, A., and Bendtsen, J. D., “Input shaping for helicopter slung load swing reduction,” *AIAA Guidance, Navigation and Control Conference and Exhibit*, , No. August, 2008. <https://doi.org/10.2514/6.2008-6964>.
- [13] Chen, M., Ren, Y., and Liu, J., “Antidisturbance Control for a Suspension Cable System of Helicopter Subject to Input Nonlinearities,” *IEEE Transactions on Systems, Man, and Cybernetics: Systems*, Vol. 48, No. 12, 2018, pp. 2292–2304. <https://doi.org/10.1109/TSMC.2017.2710638>.
- [14] Lee, D. J., and Bang, H., “Model-free LQ control for unmanned helicopters using reinforcement learning,” *International Conference on Control, Automation and Systems*, , No. 6, 2011, pp. 117–120.
- [15] Riboldi, C. E., Trainelli, L., Capocchiano, C., and Cacciola, S., “A model-based design framework for rotorcrafttrim control laws,” *43rd European Rotorcraft Forum, ERF 2017*, Vol. 1, 2017, pp. 487–501.
- [16] Singh, A., Enciu, J., and Horn, J. F., “Slung load stabilization across the flight envelope using an active cargo hook,” *AIAA Scitech 2019 Forum*, , No. January, 2019. <https://doi.org/10.2514/6.2019-0821>.
- [17] Ivler, C. M., Tischler, M. B., and Powell, J. D., “Cable angle feedback control systems to improve handling qualities for helicopters with slung loads,” *AIAA Guidance, Navigation, and Control Conference 2011*, , No. August, 2011, pp. 1–27. <https://doi.org/10.2514/6.2011-6686>.
- [18] Dukes, T. A., “Maneuvering Heavy Sling Loads Near Hover Part I: Damping the Pendulus Motion,” , 1973.
- [19] PRASAD, J., and LIPP, A., “Synthesis of a helicopter nonlinear flight controller using approximate model inversion,” 1992. <https://doi.org/10.2514/6.1992-4468>.
- [20] Sahani, N. A., and Horn, J. F., “Adaptive model inversion control of a helicopter with structural load limiting,” *Journal of Guidance, Control, and Dynamics*, Vol. 29, No. 2, 2006, pp. 411–420. <https://doi.org/10.2514/1.13391>.
- [21] Wei, W., “Adaptive control based flying quality design for helicopters,” *43rd European Rotorcraft Forum, ERF 2017*, Vol. 1, 2017, pp. 474–486.

- [22] Liu, L., Chen, M., Li, T., and Wang, H., “Composite Anti-Disturbance Reference Model L 2- L Control for Helicopter Slung Load System,” *Journal of Intelligent and Robotic Systems: Theory and Applications*, Vol. 102, No. 1, 2021. <https://doi.org/10.1007/s10846-020-01276-z>.
- [23] Younes, A. Y., Jarrah, M. A., and Sukkarieh, S., “Adaptive integral backstepping controller for an autonomous rotorcraft,” *2009 6th International Symposium on Mechatronics and its Applications, ISMA 2009*, 2009. <https://doi.org/10.1109/ISMA.2009.5164795>.
- [24] Yan, K., Wu, Q., and Chen, M., “Robust adaptive backstepping control for unmanned autonomous helicopter with flapping dynamics,” *IEEE International Conference on Control and Automation, ICCA*, 2017, pp. 1027–1032. <https://doi.org/10.1109/ICCA.2017.8003202>.
- [25] Ertuğrul, T., Adli, M. A., and Salamci, M. U., “Model reference adaptive control design for helicopters using gain scheduled reference models,” *Proceedings of the 2016 17th International Carpathian Control Conference, ICCCC 2016*, 2016, pp. 182–187. <https://doi.org/10.1109/CarpathianCC.2016.7501090>.
- [26] Ashitha Varghese, T., and Mija, S. J., “Sliding Mode Control Based Design for a 6-DOF Miniature Helicopter in Hovering Flight Mode,” *2019 IEEE 5th International Conference on Mechatronics System and Robots, ICMSR 2019*, 2019, pp. 59–63. <https://doi.org/10.1109/ICMSR.2019.8835471>.
- [27] Gao, H., Gao, Z., Deng, Y., and Zhao, Z., “Design of sliding mode control system for automatic transition and hover of helicopter,” *2017 3rd IEEE International Conference on Control Science and Systems Engineering, ICCSSE 2017*, , No. 1, 2017, pp. 102–105. <https://doi.org/10.1109/CCSSE.2017.8087903>.
- [28] Sasaki, M., Ishida, H., Katsuno, T., and Ogasawara, A., “Learning fuzzy logic controller for hovering a helicopter,” *Annual Conference of the North American Fuzzy Information Processing Society - NAFIPS*, 1998, pp. 25–28. <https://doi.org/10.1109/NAFIPS.1998.715522>.
- [29] Lower, M., Szlachetko, B., and Krol, D., “Fuzzy flight control system for helicopter intelligence in hover,” *Proceedings - 5th International Conference on Intelligent Systems Design and Applications 2005, ISDA '05*, Vol. 2005, 2005, pp. 370–374. <https://doi.org/10.1109/ISDA.2005.48>.
- [30] Adams, C., Potter, J., and Singhose, W., “Modeling and input shaping control of a micro coaxial radio-controlled helicopter carrying a suspended load,” *International Conference on Control, Automation and Systems*, 2012, pp. 645–650.
- [31] Pavel, M. D., “Mathematical modeling of tandem helicopters with external sling loads for piloted simulation,” *Collection of Technical Papers - 2007 AIAA Modeling and Simulation Technologies Conference*, Vol. 1, No. August, 2007, pp. 570–587. <https://doi.org/10.2514/6.2007-6617>.
- [32] Pavel, M. D., Shanthakumaran, P., Chu, Q., Stroosma, O., Wolfe, M., and Cazemier, H., “Incremental nonlinear dynamic inversion for the apache AH-64 helicopter control,” *Journal of the American Helicopter Society*, Vol. 65, No. 2, 2020, pp. 1–16. <https://doi.org/10.4050/JAHS.65.022006>.
- [33] “Von Karman Wind Turbulence Model (Continuous),” , 2023-01-23. URL <https://www.mathworks.com/help/aeroblks/vonkarmanwindturbulencemodelcontinuous.html>.

Part II

Preliminary Analysis

*This part has been assessed for the course AE4020 Literature Study.

3

Literature Review

3.1. General Helicopter

This chapter contains a general overview of different helicopter missions, configurations and their control mechanism. Although no research questions are answered in this chapter, it acts as a chapter to familiarize with the concept of helicopter control.

3.1.1. Different Helicopter Applications

Nowadays, helicopters can be found in many places and perform both civilian and military missions. Civilian applications can include:

- Search and rescue by the coast guard
- Fighting wildfires
- Cargo transport to remote areas
- Passenger transportation
- Medical emergencies
- Police surveillance
- Disaster evacuations
- etc.



Figure 3.1: A rescue helicopter used by the dutch coast guard [11]

Military applications can include:

- Troop transport
- Military cargo transport
- Military evacuations
- Fire support
- Naval surveillance
- Anti Submarine Warfare (ASW)
- etc.



Figure 3.2: An NH90 military helicopter in a dipping SONAR mission used by the dutch navy [36]

Helicopters are vehicles that can perform manoeuvring tasks no other aircraft can currently do. These include manoeuvres such as hover, flying sideways or backwards and VTOL. This enables helicopters to

fly missions that would otherwise not be possible.

3.1.2. Helicopter Configurations

There are many different helicopter configurations. A general overview of the most common configurations is given below. Most helicopters have a single rotor, but some helicopters have two, as is listed below.

Single Main Rotor

This is the most common type of helicopter. It has, as the name implies, a single main rotor. This means that it needs an anti-torque device in the tail in the form of a tail rotor. This means that some of the power provided by the powerplant has to be allocated to the tail rotor.

Tandem Rotor

The tandem rotor helicopter is a helicopter that uses two rotors, typically spinning opposite to each other. This removes the need of an extra anti-torque device in the form of a tail rotor. This means that all of the power provided by the powerplant can be allocated to generating lift. The downside of such configurations is that the power transmission is more complex with such helicopters, and the rotors must be placed such that they don't collide. Such configurations are only used for large helicopters.

Coaxial

A coaxial helicopter is a helicopter with two counter-rotating rotors on a single mast. Just as with tandem rotor helicopters, there is no need for an extra anti-torque device. The stacking also enables this configuration to be used on smaller helicopters. The downside of this configuration is the fact that due to the wake interaction between both rotors, the drag produced is rather large.

Intermeshing Rotors

Intermeshing rotor helicopters have two counter rotating intermeshing main rotors located side by side. These rotors are synchronised to avoid collision. These configurations also require no extra anti-torque devices due to the counter rotating rotors.

Tilt-rotor

A tilt-rotor helicopter is a helicopter that can tilt its rotors forwards or backwards in such a way that it can use its rotors as propellers in forward flight, and as rotors during hover. This enables an airplane/helicopter hybrid configuration. It belongs to the family of compound rotor aircraft. Compound helicopters are helicopters with (usually wings) to increase the speed at which the helicopter can fly.

3.1.3. Helicopter Controls

There are three major components that determine the control of the helicopter. These are the main rotor and the tail rotor.

Main Rotor

The main rotor is a collection of rotor blades attached to a hub located at the top of the helicopter. Due to the nature of the blade motion, the blades need some freedom to move relative to the hub to remove excessive forces and moments. For this, three additional degrees of freedom are provided to the rotor. These are lead/lag, flapping and rotation around the longitudinal axis. There are multiple ways to provide these degrees of freedom:

- **Rigid rotor:** Rigid rotor systems are systems where there are neither flapping nor lead/lag hinges present (see Figure 3.3). Instead, the blades themselves bend to accommodate for these motions. A rigid rotor system is mechanically less complex due to the lack of hinges, but require a more complex blade structure. Moreover, this system results in higher vibrations in the vehicle due to the lack of damping provided by the hinges[15].
- **Semi-rigid rotor:** A semi-rigid rotor system typically contains 2 rotor blades that are rigidly attached to the rotor hub (see Figure 3.4). This hub is free to tilt relative to the shaft of the main rotor via the use of a teetering or flapping hinge. There is no lead/lag hinge present, meaning that those

forces are absorbed in the bending of the rotor blades. Rotation about the pitch axis is possible via a feathering hinge.

- **Fully articulated rotor:** A fully articulated rotor has hinges for all three axes for each blade (see Figure 3.5). This allows each blade to flap, lead/lag or feather independent of the other rotor blades. This removes the forces and moments on the shaft associated with these motions.

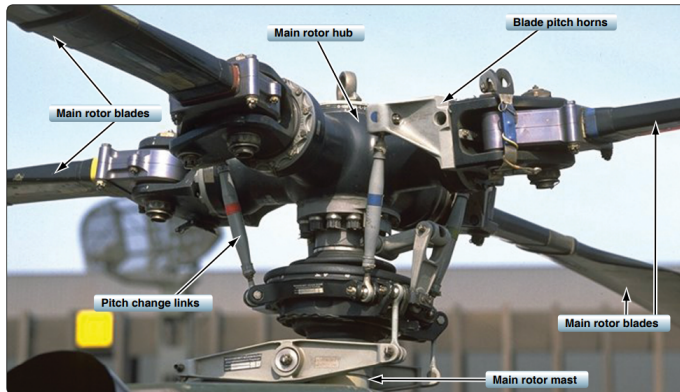


Figure 3.3: Rigid rotor connection [15].

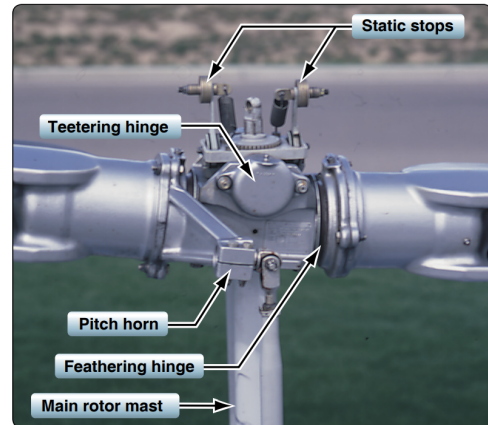


Figure 3.4: Teetering rotor connection [15].

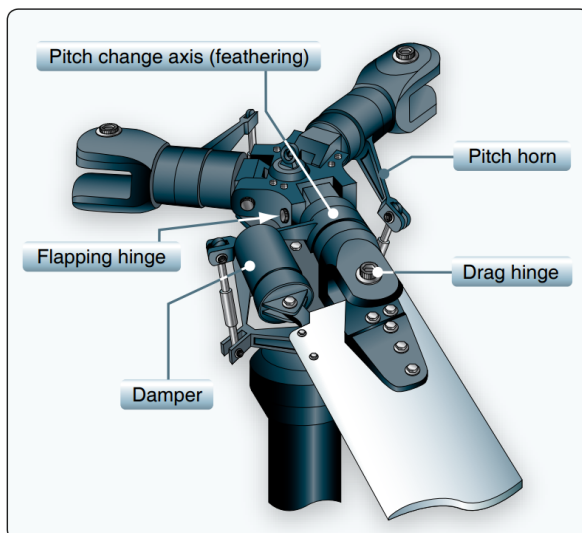


Figure 3.5: Fully articulated rotor connection [15].

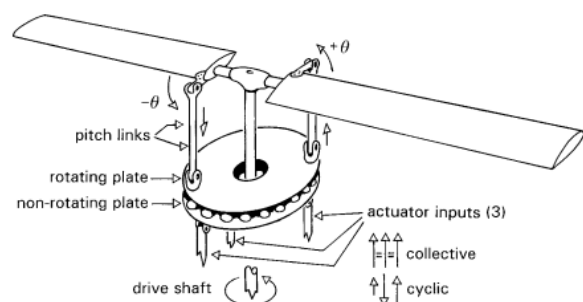


Figure 3.6: Swash plate mechanism [41]

Controlling the direction of the thrust of the main rotor is done via the swash plate. The purpose of this component is to transfer control inputs from the non-rotating helicopter to the rotating rotor blades. A schematic of this component is illustrated in Figure 3.6. As shown, the pitch links are connected via two plates to the actuator inputs. One rotating, and one non-rotating plate, connected together via bearings such that they can slide over each other freely.

The swash plate can be moved up or down via the collective pitch lever. This causes the pitch links also move up or down, changing the pitch angle of all rotor blades (hence the name collective pitch). This influences the amount of lift generated by the blade, and hence the thrust of the rotor.

The swash plate can also be tilted using the cyclic pitch lever, causing changes the pitch angle of a blade depending on where it is on its rotation (hence the name cyclic pitch). This causes changes in lift force at different positions around the shaft, effectively controlling the direction of the thrust.

Tail Rotor

Helicopters with a single main rotor require a tail rotor as an anti-torque device. Since the powerplant exerts a torque on the main rotor, there is an equal and opposite torque acting on the helicopter. This is why an anti-torque device is needed. The tail rotor collective pitch can be adjusted via the pedals. By adjusting the pitch angle of the tail rotor blades, the thrust is changed and hence the torque provided by the tail.

3.1.4. Concluding Remarks

As mentioned at the start of this chapter, this chapter acts as a familiarisation to the concept of helicopter operations and control. First, the application fields of helicopters have been listed. After that, different helicopter configurations have been looked at. Finally, the control mechanism behind the main and tail rotor has been explained.

3.2. Rotor and Actuator Dynamics

This chapter contains an overview of the rotor dynamics of the main rotor of a helicopter. As will be made clear in later chapters, INDI is a control method that is (like any incremental control system) sensitive to time delays. Therefore, it is important to have an understanding of where delays might arise. Rotor dynamics can be a source of delay. Therefore, it is important to have an understanding of how the rotor behaves. Additionally, in order to simulate the effect of a hanging load from a helicopter, some basic rotor dynamics are included in the helicopter model. A simple flapping model is therefore presented in this chapter.

3.2.1. Rotor Dynamics

This section contains the basic principles about rotor dynamics as well as a simple flapping model for the 3-DOF model developed later in this report.

Basic Rotor Behaviour

Helicopter rotors rotate at large rates, creating a big centrifugal force on the blade. This is the driving force that keeps the blade straight when in flight. When disturbing the blade during rotation, an oscillation will occur. This oscillation is called flapping.

Flapping is a complex phenomena that is dependent on not only the properties of the blades, but also the motion of the shaft, the control inputs given, and aerodynamic disturbances. One of the most important properties of the rotor blade is the Lock number γ given by Equation 3.1. This is a non-dimensional scaling coefficient, giving the ratio of aerodynamic to inertia forces acting on a rotor blade[41]. The smaller this number, the stiffer the blade is to aerodynamic forces.

$$\gamma = \frac{\rho c c_{l_\alpha} R^4}{I_B} \quad (3.1)$$

With

- ρ - air density
- c - chord of blade
- c_{l_α} - slope of lift coefficient with angle of attack
- R - radius of blade
- I_B - inertia of blade

Computing the Lock number is not trivial, as typical blades have complex mass distributions and multiple airfoils blended into a single blade.

Rotation of the rotor shaft must be taken into account as well. If the helicopter rotates, due to the gyroscopic nature, coriolis-effects act on the motion of the rotor blades. Furthermore, when considering aerodynamic effects, the complex nature of the flapping motion becomes clear. Flapping is harmonic, meaning that there is recurring motion in the blades per rotation. Taking only forward velocity into account, and neglecting drag forces, a second order dynamic appears. This is a constant coning effect, a first-order dynamic motion that repeats once per rotation and a second order dynamic called differential coning [41]. Typically, higher order dynamics are present in flapping motion.

It seems that in deriving the time delays caused by flapping dynamics, the main difficulty lies in modelling or estimating what these harmonic motions are and what their magnitude is. Time delays are the time needed for the disk plane to adjust to its new position forced by the cyclic and collective control setting. On the blades, this will result in a disturbed motion with a damped oscillation of a certain order. This means that it may be necessary to include higher order dynamics to have an accurate enough model of the flapping motion to derive time delays in the system.

Simple Flapping Model

In this section, the Fourier transformation of the flapping dynamics are presented. These equations (Equation 3.2-Equation 3.5) are derived via the method found in [22].

The Fourier approximation for the blade flapping angle is given by Equation 3.2, with as coefficients Equation 3.3-Equation 3.5 representing the coning angle, the longitudinal disc-tilt and lateral disc-tilt. Note that only the first order dynamics are taken into account, higher order dynamics are neglected from these equations. This means that no differential coning is present, nor higher order harmonics. Furthermore, the flap angle β is taken in the control plane of reference[22].

$$\beta = a_0 - a_1 \cos(\psi) - b_1 \sin(\psi) \tag{3.2}$$

$$a_0 = \frac{\gamma}{8} \theta_0 (1 + \mu^2) - \frac{\gamma}{6} (\lambda_c + \lambda_i) \tag{3.3}$$

$$a_1 = \frac{\frac{8}{3} \mu \theta_0 - 2\mu (\lambda_c + \lambda_i) - \frac{16q}{\gamma \Omega}}{1 - \frac{1}{2} \mu^2} \tag{3.4}$$

$$b_1 = \frac{\frac{4}{3} \mu a_0 - \frac{q}{\Omega}}{1 + \frac{1}{2} \mu^2} \tag{3.5}$$

This flapping model is simple, but useful in the development of a 3-DOF model of a helicopter with a partially submerged load. Furthermore, this flapping angle model is also be used to find the thrust coefficient of the rotor. This is presented in Equation 3.6[22].

$$C_{T_{BEM}} = \frac{1}{4} c_{l\alpha} \sigma \left[\frac{2}{3} \theta_0 \left(1 + \frac{3}{2} \mu^2 \right) - (\lambda_c + \lambda_i) \right] \tag{3.6}$$

As illustration of the angles β , a_0 and a_1 , figures Figure 3.7 (see bottom) and Figure 3.8 (see top right) are provided to show their physical meaning.

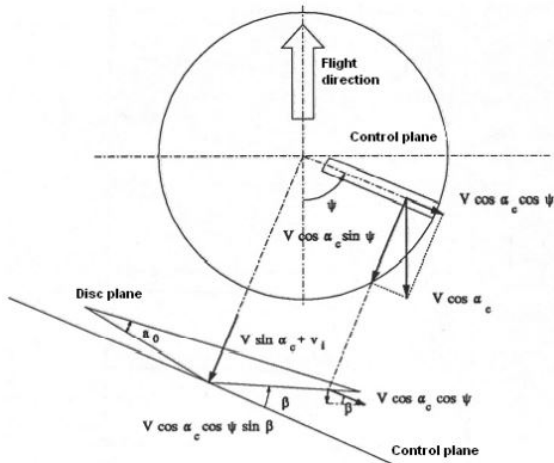


Figure 3.7: Diagram illustrating the flapping angle β and the coning angle a_0 [22].

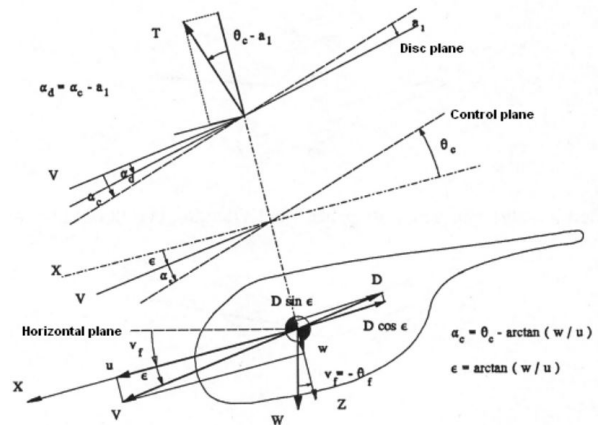


Figure 3.8: Diagram illustrating the longitudinal disc-tilt a_1 [22].

3.2.2. Actuator Dynamics

Since the actuators of the helicopters are a mechanical system, there are some dynamics regarding commanded input and commanded output. Since this research is mainly focused on control, the actuators will be modelled as a first order lag filter with a certain value of τ_{lag} , that can be changed to adjust the speed of the dynamics of the actuators. With this, the robustness of both controllers can be tested with changing system conditions, especially for the case with non-perfect actuator systems.

The transfer function of a first order lag filter is as follows:

$$H_{lag}(s) = \frac{1}{\tau_{lag}s + 1} \quad (3.7)$$

Additionally, the actuators have a certain operational range in which they function. These are the saturation limits of the main rotor collective, cyclic and tail rotor collective. These saturations are non-linear and will have to be taken into account when developing the controllers.

Saturation of controls is a well known problem for control systems. Especially when integrators are present, the control system may compensate for the saturation of the controllers when it is not necessary. This leads to degraded performance. In [51], pseudo control hedging is used to account for the effect of control saturation (more on this in [27]). This method sends a reverse control signal back to the control input equal to the exceeded control signal. This balances the control input. Other methods could be anti-windup for example.

3.2.3. Concluding Remarks

This section briefly covered the blade flapping dynamics of the main helicopter rotor. First, a general explanation about basic rotor behaviour was given. This was followed by presenting a simple flapping model from [22], which is also used in the 3-DOF helicopter model used in Chapter 4. Finally, the actuator dynamics have been discussed. The helicopter controls will be modelled as a first order lag filter, to simulate the slowness of the actuator dynamics.

3.3. Dipping SONAR Missions

In this chapter, a general description of a dipping SONAR mission can be found. This includes a description of the mission, environmental conditions and the SONAR dimensions. After that, controller requirements are defined. In order to find those requirements, performance metrics are defined first, after which the controller requirements are stated. Unfortunately, specific numbers for these requirements cannot be found. Likely due to the confidentiality related to military assets. Therefore, numbers have been assumed which can be changed in later stages.

3.3.1. Dipping SONAR

A dipping SONAR is a SONAR device that is suspended below a helicopter, and lowered into the water periodically to take measurements in order to detect submarines. There are two types of SONAR: Active SONAR and passive SONAR. Active SONAR sends sound pulses through the water. This pulse will bounce off of objects and returns back to the SONAR device, which is then received. The properties of this signal (time until return and Doppler shift) will then yield a distance, a bearing and a relative velocity to the detected objects. Passive SONAR does not send pulses and only listens for signals. It is not possible to find the distance to an object using passive SONAR, unless using multiple sensors [61].

Mission Description A Dipping SONAR mission has three distinct phases for each dip: A transition from cruise to hover, hovering and a transition from hover back to cruise. This is illustrated in Figure 3.9. During the hover, the SONAR transducer is lowered into the water to take measurements. Hovering is done at an altitude of 50-300 ft [4]. The transducer is lowered to depths of 0 to 2500 ft [4] [54]. When that is done, the transducer is lifted back up out of the water, before transitioning back to a cruise again to fly to a next location. The duration of a dip is unknown to the author, and will therefore be assumed to be no more than 5 minutes.

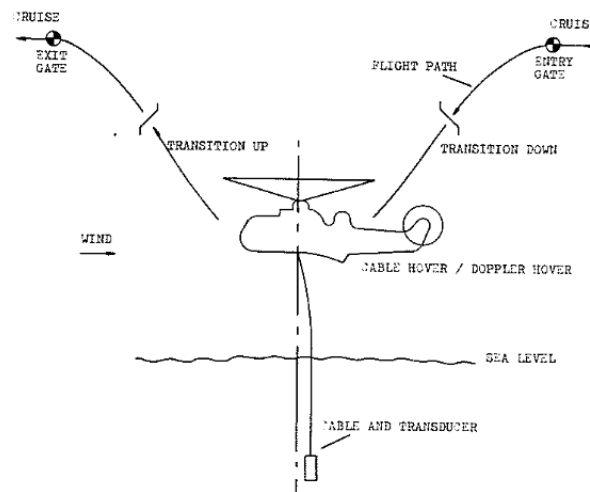


Figure 3.9: Helicopter dipping SONAR manoeuvre [19]

For optimum SONAR performance, the motion of the helicopter is used to keep the SONAR still [19][17][57]. The main difficulty associated with this task is the motion of the suspension cable. This cable can bend and swing due to aerodynamic forces and sea currents. It is therefore difficult to determine the velocity and exact orientation of the SONAR from within the helicopter. In literature, the cable angle and cable angle rate are typically used as an estimate.

Environmental Conditions

In the maritime industry, limitations on helicopter operations at sea are measured in sea states. This is a scale from 1-8, that classifies wave height, and by extension is a measure of the weather. Although, no direct link was found in literature between dipping SONAR missions and sea states, it was observed that in many cases, a sea state of 4-5 was taken for maritime helicopter operations. Mainly due to on-deck

operations such as maintenance, take-off and landing. A sea state of 4-5 corresponds to waves between 2.5 and 4.0m high. Such waves are also found in wind conditions of 5-7 Bft, or 17-33 kts wind [62]. It was also observed that operations are limited by sea state due to emergency landing procedures. The mean sea current speeds are found to be very slow (0.05-0.5 m/s) and decreasing with depth [40].

Dipping SONAR Dimensions

Additionally, from the product datasheet from dipping SONAR manufacturers L3HARRIS and armelsan, dipping SONAR can have dimensions of 1.2-5.2m high and a diameter of 2.6m [21] and can have a mass of up to 270 kg [20].

3.3.2. Controller Requirements

The performance requirements of the to-be-designed automatic controllers are presented in this section. For this, first the performance metrics of the controller are discussed in Section 3.3.2. These metrics will determine which controller performs best. After that, the controller requirements are presented in Section 3.3.2. These requirements are based on the mission specifications from Section 3.3.1.

Performance metrics

In order to compare the different controllers, performance metrics have to be specified. In this particular case, it is important to emphasize on what is important for the controller in order to fulfill the mission. The SONAR must be kept as still as possible. This means that the velocity of the SONAR must be kept as small as possible. This to keep the position of the SONAR at roughly the same position, while keeping Doppler shift effects low.

One way to measure the velocity changes is via statistics. The mean of the velocities will yield the average drift of the SONAR, whereas the standard deviation says something about the oscillatory nature of the motion. A large mean will show that the SONAR drifts from the original position at a high rate, which is also used as a performance metric. A high standard deviation means a larger variation in velocity, and thus classifies in worse performance.

Additionally, it is important to consider the control usage of the controller. If the controller uses the full control authority range, it could be considered a less efficient controller as it requires more energy to perform the same task. Here too, the standard deviation can be used as a metric for the amount of control usage. A high standard deviation signifies large control input variations and can therefore be used as a metric for control input efficiency.

To summarize, the controllers will be judged on three metrics:

- Standard deviation of the velocity of the SONAR;
- Mean of the velocity of the SONAR;
- Standard deviation of the control inputs.

Controller Requirements

This section presents the requirements for the controller. Unfortunately, there is not much information present in literature about the motion requirements for dipping SONAR missions. Therefore, assumptions are made about the allowable motion of the SONAR. For the determination of the requirements, it is assumed that the SONAR is not allowed to have translational rates of over $1m/s$ in all axes and rotational rates of over $1^\circ/s$ in all axes. Since there are no available numbers, these numbers are found by guessing. As depth, a depth of 60m is chosen. The main reason for this is that shorter cables are more limiting than longer cables due to slower motion and higher drag. Moreover, a requirement is made about the settling time of the controller after a step input. This requirement is set since a dip should be executed in a relatively short period of time. This means that the motion of the SONAR shall be suppressed in a timely manner. For this, a settling time of 60 seconds is taken. The step input simulates a strong gust acting on the helicopter and suspension cable. Additionally, it is assumed that a dip takes no longer than 5 minutes. The requirements regarding environmental conditions follow from Section 3.3.1. This leads to the following three main requirements:

1. The translational rates of the SONAR shall not exceed $1m/s$ in all directions with the SONAR submerged at a depth of 60m, a constant sea current of $0.5m/s$ and sea state 5 for 5 minutes.
2. The rotational rates of the SONAR shall not exceed $1deg/s$ in all directions with the SONAR submerged at a depth of 60m, a constant sea current of $0.5m/s$ and sea state 5 for 5 minutes.
3. The SONAR shall reach steady state within 60 seconds in all axes after a step input gust of 0 to 7 Bft with the SONAR submerged at a depth of 60m, a constant sea current of $0.5m/s$.

3.3.3. Concluding Remarks

This chapter contains a description of dipping SONAR missions as well as the metrics and requirements for the controller performance. From the mission description, it was found that dipping takes place in hover, at low altitudes. Furthermore, it seems that dipping takes no longer than 5 minutes per dip. The environmental conditions are not known exactly, but are deduced from literature. It seems that helicopter operations take place up to sea state 4-5, which is quite rough. The dimensions of the SONAR are also deduced from manufacturer datasheets.

The performance metrics of the controller will be the standard deviation of the velocity of the SONAR, its mean and the standard deviation of the control inputs. The metrics on the velocity will provide a measure of how much the sonar swings. The metric on the control inputs will provide a measure of the efficiency of the controller.

Combining the knowledge from the mission and the environmental conditions, 3 requirements have been specified for the helicopter controller. These are found in Section 3.3.2. Note that the limits on the linear and rotational velocities are very uncertain. No sources have been found discussing such limits, hence these numbers are taken as an initial guess.

3.4. State-of-the-Art Helicopter-SONAR Modelling

In this chapter, an overview will be given of different modelling methods to model a helicopter in combination with a SONAR. To the authors knowledge, there is not a lot of recent literature that addresses this specific configuration. On the other hand, a lot of recent literature can be found about a similar problem, namely a slung load configuration. This is a configuration where a heavy load is suspended from a helicopter for cargo transport. In this situation, a lot of focus lies in the interaction between the helicopter and the suspended load, and to keep the suspended load stable. In dipping SONAR missions, the suspended load is not that heavy, meaning that the effect of the SONAR on the helicopter won't be that large. Nevertheless, this configuration is interesting due to its close resemblance with the problem at hand. This chapter is divided into 3 sections: Section 3.4.1 addresses different methods to model a helicopter system with a hanging load. Section 3.4.2 covers different suspension cable models and Section 3.4.3 will discuss the modelling of the SONAR briefly.

3.4.1. Helicopter Slung Load Models

In this section, an overview will be given about the state of the art with regards to the modelling of a helicopter carrying a suspended load. It was found that especially in older literature, there is a lot of emphasis on simple models. There were two main reasons for this:

First, especially in the 60s and 70s, there was a need for stabilisation of helicopters with a hanging load. Therefore, much effort was put into understanding the basic stability principles of suspended loads from helicopters ([12], [35], [38]). This need for understanding called for very simple models, since simple models are easier to understand the basic principles of that phenomena.

The second reason was that computers at that time were not very powerful. Therefore, simple models that require little computing power were desirable since they were cheaper to use.

Pendulum models

Because of this need for simple models, the first hanging load models were pendulum models. For helicopters carrying a heavy load, this is a logical choice, due to the nature of the motion. For heavy loads, this is the most important motion and it is also a very large disturbance acting on the helicopter. Therefore it would make sense to stabilize this motion in order to stabilize the load.

In various literature, these models are used to simulate the movement of a hanging load below a helicopter. In [35], the suspended load is modelled as a compound pendulum. In [18], the load is modelled as a point mass on a constant length, mass-less rigid link below the helicopter's center of mass, which is effectively also a compound pendulum. A somewhat different approach is taken in [12]. Here, the load is still modelled as a pendulum, but the load is not attached to the center of mass. This is because this paper addresses the stability analysis of different configurations and feedback options. [38] presents three different models for a helicopter with a slinging load: a simple helicopter model that is simply a disk, a rigid body with a disk rotor and a rigid body with an articulated rotor. This was also done to study the dynamic stability, but this time with at varying levels of complexity.

Even today, with better understood concepts and more powerful computers, the pendulum model is still used quite often in literature ([32], [56], [29], [44], [37]). As mentioned before, the pendulous motion is the main motion of the hanging load and also the most disturbing to the helicopter. Therefore, it makes sense to address this motion in particular.

It is important to note that pendulum models are probably not very useful for the problem at hand. This has multiple reasons: First of all, one should consider that the objective of the control system is not to stabilize the helicopter itself, but keep the load still in the water. This means that the motion of the helicopter is more a disturbance on the load than the other way around. Secondly, the load is not that heavy. Dipping SONAR weight in the order of 300 kg [2], which is small compared to modern-day military helicopters which can have a mass of 10500 kg (NH90 helicopter)[39]. Therefore, more complex models are needed. Nevertheless, a pendulum model is a good approximation of the motion of the problem at hand.

Rigid Body Models

More complex models than the pendulum models are rigid body models. Rigid body models differ from the pendulum models in the sense that a rigid body has more degrees of freedom (6) than a point mass (3).

In [7], a suspended load system is modelled using only rigid bodies. Constraints are added using constraint equations which follow from the assumption that the wire remains constant under nominal conditions. With those constraint functions, the Udwadia-Kalaba Equation is used to obtain equations of motion. The Udwadia-Kalaba equation describes the motion of a constrained mechanical system and is based on Gauss's principle of least constraint.

In [42], a mathematical model of tandem helicopters with a sling load is presented. Here, both the helicopter and the load are treated as rigid bodies. The equations of motion are found using force and moment equilibrium. This model also includes first order rotor dynamics, which is useful for the development of the dipping SONAR helicopter model.

Existing Models

In [29] and [53] an already existing helicopter model of the UH-60 Apache helicopter is used. This is a non-linear blade element model of the H-60 class helicopter. Such models are high-fidelity models that can track many degrees of freedom. Usually, these models are made by manufacturers in order to model the behaviour of their vehicle.

Trim Conditions

Trimming a helicopter model is not straight forward. For a 3-DOF model, it is possible to trim the helicopter and a hanging load analytically. For a 6-DOF model, this is unfortunately not possible. Therefore, according to [42], the helicopter-load system can be trimmed in 4 steps:

1. Trim the load with the helicopter in a neutral state;
2. Trim the helicopter with the trimmed load from step 1;
3. Trim the load again with the trimmed helicopter from step 2;
4. Trim the helicopter and the load together.

Trimming is done numerically. This means that the trim of the load and the helicopter are computed iteratively until the results converge to a single solution.

Helicopter Model Selection

For the helicopter model, an existing 6-DOF rigid body model will be used. This model will be obtained via the project supervisor. This alleviates the need to develop a new model, and it is already verified.

3.4.2. Cable Model

The cable model is a very important part of the total system model as the cable is responsible for transmitting the movement of the helicopter to the hanging load. The problem with the cable, however, is that it is flexible and can move freely due to disturbances such as wind, sea current and of course the helicopter motion. The three main methods found in literature are either rigid cables, discrete cables or continuous cable models. Each increasing complexity from the latter. These are discussed briefly further below.

Rigid Cable Models

Rigid cable models are models that assume that the cable always remains straight like a solid rigid beam. This is, however, almost never the case, but is a very good approximation if the wire is taught all the time. Nonetheless, it is a model that simplifies the equations of motion a lot, since the motion of the payload can simply be described as a simple pendulum.

Discrete Cable Models

The suspension cable can be modelled as a discrete system as is done in [17] and [58]. In such a model, the cable is divided into small rigid sections. Each section has its own equations of motion.

In [17], two different models are proposed: A discrete cable model and a lumped model. The discrete model is a model with many sections, whereas the lumped model is a simplified double-pendulum model. The discrete model is very similar to the model described in [58], which is described further below. The

lumped double pendulum model has two masses: one emerged and one submerged. The mass of the emerged part being the mass of the emerged part of the cable and the submerged mass being the mass of the submerged cable and the SONAR. This was done due to the limitations of computation power in the late 80s. Although much simpler than the discrete model, the accuracy of the model was still quite well.

In [58], a discrete model is proposed as shown in Figure 3.10, here illustrated with just 3 sections. The linear equations of motion of this cable model are given by Equation 3.8.

$$\begin{aligned}\dot{\bar{x}}_1 &= A_1 \bar{x}_1 + B_{11} \bar{u}_1 + B_{12} \bar{d} \\ \dot{\bar{x}}_2 &= A_2 \bar{x}_2 + B_2 \bar{u}_2\end{aligned}\quad (3.8)$$

Here, x is the state vector, u is the projected helicopter ground velocity and d is the steady state wind velocity, or water current velocity. The state vector contains the longitudinal angles θ_k and lateral angles ϕ_k , where k indicates the index of each section. These angles are relative to the local horizontal and the local vertical axis. Matrices A and B are the state matrix and the input matrix respectively, and the subscripts ij indicate the column within the matrices ($i=1$ for longitudinal motion and $i=2$ for lateral motion, $j=1$ for helicopter velocity and $j=2$ for wind/current velocity).

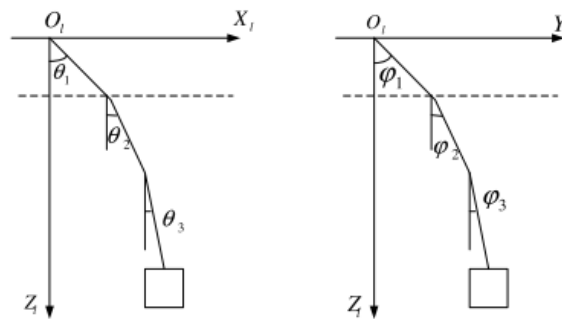


Figure 3.10: Discrete cable model for longitudinal motion (left) and lateral motion (right) [58]

Each link is regarded as a steel resistance bar with well distributed physical parameters. There is no bending moment between the cable sections and there is no transport of torque between the sections. The force conditions are analysed for every section such that the differential equation of each section can be established. There is a large similarity between this model and the double pendulum model. The difference being the amount of sections in the model. Discrete models like this have the major advantage that they can be solved iteratively and as detailed as desired, making them very attractive.

To make the model more realistic, a spring-damper could be added to simulate the effects of cable stretching and bending. Furthermore, the rotation along the cable axis (cable twist) can not be modelled using a hinged discrete cable model. To model cable twist, some spring-damper must be added to a cable link.

Continuous Cable Models

Next to the rigid cable and the discrete model, continuous cable are also used to model the behaviour of the cable in response to helicopter motion. In [10], the equations of motion of a suspension cable is derived using Hamilton's principle. This paper addresses the problem of using boundary control to remove disturbances acting on a hanging load. The major advantage of such a model is that the position of the cable is known at every point along the wire. It also enables the cable to have continuous properties, such as mass distributions that vary smoothly along the cable.

Cable Model Assumptions

In literature, many assumptions are made with regards to the cable properties. Some papers simplify the problem by disregarding the mass of the wire, the aerodynamic/hydrodynamic forces or the buoyancy of the cable ([29], [56], [53]). In the interest of solving the problem at hand, it is important to also model these effects, meaning that they cannot be assumed to not exist. However, for simplicity, buoyancy is neglected.

The elasticity of the cable is sometimes also neglected ([7]). Due to the relatively low mass of the SONAR, this assumption could be valid. Therefore, it is important to note that the following points of interest will likely be included in the final model of the suspension cable:

- The suspension cable will have a mass;
- The suspension cable will not experience buoyancy;
- The suspension cable will not experience elasticity;
- The suspension cable will experience aerodynamic and hydrodynamic drag forces;
- Turbulence effects (from the rotor, wind and current) on the cable will be neglected.

Cable Model Selection

The cable model used in designing the controller will be a discrete cable model. The main reason for this is the iterative nature, and the simplicity that follows from it. The main disadvantage of using such a model is that some properties of the cable are neglected. Especially the nature of how a cable bends is different when using a discrete model compared to a continuous model. To account for this discrepancy, addition of a spring-damper will be considered if necessary.

3.4.3. Modelling The SONAR

In order to model the effects of the helicopter motion on the SONAR, a model of the SONAR is also required. The SONAR can be modelled as a rigid body hanging from a helicopter. In [56], the problem of a submerged load is taken into account into the model. The first thing that needs to be addressed is the fact that the load is subject to buoyancy. This means that the load will appear to be lighter than it actually is. Also, depending on the mass distribution of the SONAR, this could introduce moments around the hinge-points of the cable, forcing the SONAR in an alternate rotation than perfectly straight. It is however assumed that the SONAR is symmetric, and that it would naturally stay in its upright position. The second point of interest is the difference in velocity between the air above the water and the current velocity of the water. This will cause different drag forces and therefore different cable displacements. The final thing addressed is the difference in density of the water. This is important since this means that dragging the load underwater will produce different drag forces. Drag forces will also cause a moment around the hinge point.

3.4.4. Concluding Remarks

This chapter gives an overview of a literature study about the modelling methods of helicopter configurations with a hanging load. This includes models of the helicopter itself, the suspension cable and the load. For each of these, an overview is presented of what is done in literature, as well as a choice on what method will be used in later stages of the research. For the helicopter, a 6-DOF rigid body model is used that will be provided by the thesis supervisor. The suspension cable model will be a discrete cable model with rigid links. The SONAR will be modelled as a rigid body.

3.5. Helicopter Automatic Flight Control Systems

In this chapter, an overview will be provided about the state of the art in helicopter automatic flight control systems (AFCS). This will be done by first discussing classical PID control, followed by an overview of the different control modes of a helicopter. After that, an overview of other control methods. Finally, the choice of control method will be discussed.

3.5.1. PID control

PID control is a control method found in many different systems. It is a linear control system that is relatively simple to apply to a system. PID stands for proportional integral derivative and relates to the feedback signal of the system. The basic principle of PID control is to multiply each of these signals (be it either the value of the output, its derivative or the integral or a combination of these) with a certain gain K , to form the feedback signal.

$$u(t) = K_p e(t) + K_i \int_0^t e(\tau) d\tau + K_d \frac{de(t)}{dt} \quad (3.9)$$

Here, K_p , K_i and K_d are the proportional, integral and derivative gain respectively. u is the control input to the system and e is the error signal. This error signal is the difference between the desired input and the current output of the system. Each of the different gains have different effects on the response of the system. These effects are summarised in Table 3.1.

Table 3.1: Effect of PID-gains on response of system [25]

	Rise Time	Overshoot	Settling Time	Steady State Error
K_p	Decrease	Increase	Small Change	Decrease
K_i	Decrease	Increase	Increase	Decrease
K_d	Small Change	Decrease	Decrease	No Change

Tuning

Finding the required gain for the controller is a process called tuning. This is not trivial, and there may be many PID's that satisfy the desired response characteristics. One method of computing the desired gains can be Ziegler-Nichols method, given in Table 3.2. Here, K_{max} is the proportional gain where the system becomes unstable for $K_i, K_d = 0$ and f_0 is the oscillation frequency.

Table 3.2: PID tuning with Ziegler-Nichols method [13]

	K_p	K_i	K_d
P Controller	$0.5 K_{max}$	0	0
PI Controller	$0.45 K_{max}$	$1.2 f_0$	0
PID Controller	$0.6 K_{max}$	$2.0 f_0$	$0.125 f_0$

Another method that can be used to tune a controller is a method called pole placement. With this method, the gains of the controller are chosen such that the response follows a certain behaviour. For a second order system for example, the gains could be chosen such that it has a certain natural frequency and a damping. This can typically be done analytically for systems of lower degree. For higher order systems, the gains can be found either empirically, or by using an approximation of the system by finding the dominant response of the system, and tuning it to that response.

Full state feedback is also a linear control method that has strong similarities with PID control. With this method, the feedback from the controller is some value K with the state of the vehicle. This method is very useful if the entire state of the system is known, or could be estimated. The main benefit of this method is that pole placement can be used to tune the gains K .

The main benefit of using PID control is the possibility of using it in control loops. Given the dynamic model, it is relatively easy to design a PID for it and prove that it is stable. The main problem with it is the fact that in principle it only works for linear systems. Aircraft in general, and especially helicopters are highly non-linear, which means that this control strategy will not work for a non-linear helicopter model. To work around this, a model is typically linearised around a certain flight condition, for which a PID controller can be derived. This brings another problem, namely the fact that a linear model is only valid near the linearisation point. This means that for a different flight condition, a different set of gains is necessary to control the helicopter. In other words, in order to use PID control for a helicopter or any non-linear system, the gains must be derived at all flight conditions in order to make the controller valid over the entire flight envelope and have the controller switch between gains depending on its flight state. This is called gain scheduling and was an early method of adaptive control [17]. Gain scheduling is generally a very time-consuming and tedious approach for control engineering.

Another problem with PID-control is that it is very model dependent and generally only works for single input single output (SISO) systems. Having an accurate model of a system can be very difficult, forcing major simplifications in models. This has a direct impact on the performance of the designed controller. Furthermore, a helicopter is not a SISO system, but has coupled responses between controls. This further degrades the performance of a PID controller.

Nevertheless, it is a very powerful control method that is still popular and is also used in helicopter control systems to this day. The main reason for this is the fact that it is easy to verify such controllers (and hence certify) and the fact that it is structured in loops [26].

3.5.2. Control Modes

Autopilots for helicopters contain three main operational modes: these are attitude hold, coupled and stability augmentation system [55].

Attitude Hold (ATT)

Attitude Hold is a control mode that, as the name implies, keeps the pitch and roll attitude of the helicopter fixed against disturbances.

Coupled (CPL)

Coupled is a flight control mode that is a combination of the ATT mode and a lateral and/or vertical flight director mode. Lateral commands are usually needed for navigation and vertical modes are primarily air data commands.

In [43], it was found that the stability control augmentation system (SCAS) of the Apache AH-64D helicopter contains the following control modes: **Attitude Command Attitude Hold (ACAH)**, which keeps the helicopter at a specified attitude. **Translational Rate Command (TRC)**, which makes the helicopter translate at a specified speed. **Position Hold (PH)**, **Heading Hold** and **Altitude Hold**.

In literature, other control modes are proposed. The most interesting listed below:

Hover Mode:

A hover mode in literature seems very similar to the SAS mode in autopilots. This mode would improve handling qualities during hover. This is especially important when manoeuvring with a hanging load below the helicopter. In [17], an automatic cable hover mode is presented specifically designed to keep a dipping SONAR still in the water. This control system uses classical control and gain scheduling.

Automatic Transition Mode:

In [16], An automatic transition and hover mode for a helicopter is proposed. The idea behind this controller is a controlled descend and deceleration to a hover at a given altitude. The controller proposed is based on sliding mode control. Such a control mode could be very useful for dipping SONAR missions for approach and departure of a certain dipping location. Keeping a certain altitude above water can be difficult at low altitudes. This is due to the varying height of the water surface when there are waves present. This particular problem is addressed in [58]. To solve it, a Kalman filter is used together with measurement data from accelerometers and the radio altimeter.

Automatic Load Positioning:

In [28], An automatic positioning system for a helicopter with a hanging load is presented. This too is based on a classical control structure, but with three different control loops: The most inner loop is an Attitude Command Attitude Hold controller that sets the attitude of the helicopter to a certain reference value. The loop around it is a translational rate command loop, which computes a reference attitude based on a desired horizontal ground speed. The final loop is the automatic load positioning loop, which computes the desired

horizontal ground speed, based on the cable angle, its rate and the load position. The gains were computed for different cable lengths, and using a linear reference model.

3.5.3. Other Control Methods

In this section, an overview is given of different control methods found in literature to control a helicopter with or without a hanging load. Since these do not belong to a particular flight mode, they are listed here.

Linear Quadratic Regulator (LQR)

Linear Quadratic Regulator is, just like classical control, a linear control method. It is a control method that computes the gains of the linear controller using a cost function and optimising the gains to minimise the cost function. The main advantages of using LQR over classical control are the fact that this control method can be applied to MIMO systems and that the gains are optimised. It still has the same drawbacks from being a linear controller in its limited region of validity.

In [30], LQR is used in combination with reinforced learning to an unmanned helicopter. By using reinforced learning, model dependency is reduced, since the Q-function necessary for gain computation is estimated. An LQR control law in order to trim a helicopter is proposed in [47]. Gain scheduling is used to allow using the controller for more flight conditions. LQR control is used in [53] to stabilise a hanging load in high-speed flight. Interestingly, the LQR controller controls the position of the hook underneath the helicopter, rather than the helicopter itself. This has an advantageous effect on the stability with cable angle feedback as explained in [12]. Here, it was found that feedback to the suspension point is more effective than to the rotor. The LQR controller also uses gain scheduling to broaden the flight envelope. The response in heavy turbulence of this controller is presented in Figure 3.11. Note that the angles are relative to the helicopter body.

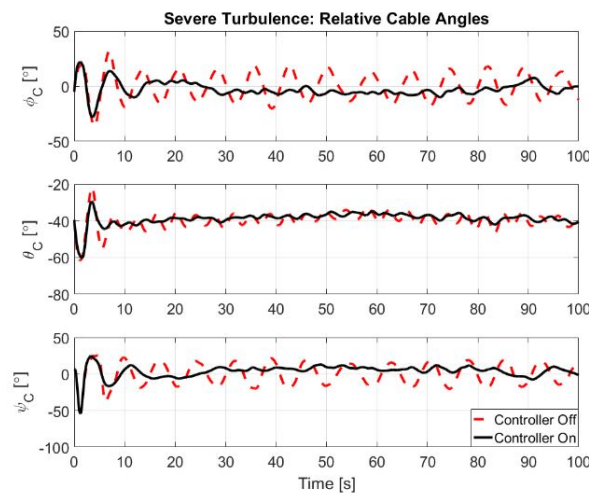


Figure 3.11: Control response in heavy turbulence with controller [53]

Dynamic Inversion (DI)

Dynamic Inversion, or nonlinear dynamic inversion (NDI) is a method where the feedback of the controller is such that the dynamics of the vehicle are linear globally. This has the major advantage that linear control can then be applied to control the linear system. The main advantage of this method is that control of a non-linear system is very straight forward and simple. An example of application of DI to a helicopter system is presented in [45]. The main drawback of this method is the requirement of an accurate vehicle model. Any modelling errors will directly impact the performance of the controller or even cause instability. This means that, in order to make this method practical, either the model must be updated continuously, or the modelling error must be found. The latter is done in [48] and [60]. In [48], a neural network is used to estimate the modelling error and in [60] a Kalman filter is used to estimate the disturbance acting on the helicopter. The linear system is then tuned using pole placement.

Incremental Nonlinear Dynamic Inversion (INDI)

INDI is the incremental version of NDI. The great advantage of using the incremental approach is that accurate model knowledge is no longer required, but this is replaced with measurements. This makes this method very powerful. INDI is proposed as a control method for helicopters in literature. A thesis that investigates the use of an INDI controller for a helicopter performing basic manoeuvres was found in [52]. It has a cascaded control structure. It uses PCH to work around control input saturation. It also addresses the problem with obtaining the angular accelerations. It proposes different methods. A predictive filter yields the best results, but needs to be trained for multiple flight conditions. Finite difference is adopted as a consequence. Regular NDI is used for attitude controller. The final loop is a navigational controller that uses approximate dynamic inversion. In [43], different INDI controllers for an AH-64 helicopter are proposed. Damping, filtering and synchronisation was attempted to improve the robustness of the controller. In the end, synchronisation using a delay in the control inputs yielded the best results.

Robust Control

In [32] a disturbance observed $L_2 - L_\infty$ controller for a helicopter with a slung load is presented. Stability of $L_2 - L_\infty$ control is guaranteed using Lyapunov stability. The addition of a disturbance observer improves the performance of the controller significantly, as it is capable of estimating the disturbance on the helicopter. The controller depends on a linear model of the helicopter and the disturbance is a set of sinusoidal functions.

Backstepping (BS)

Backstepping is a very powerful control method that stabilizes a system in a very systematic way. Starting from the dynamic system, the control law can be defined recursively, until the dynamic input is designed. By using Lyapunov's theory, stability is guaranteed at each step. Backstepping is also applied to rotorcraft systems in literature. In [64] an adaptive integral backstepping controller for controlling a UAH is proposed. Adaption is used to remove modelling errors. The control law is developed by recursively applying Lyapunov stability criteria. This also yields criteria for the model error estimation. An adaptive backstepping controller that uses a simplified vehicle model and uses a disturbance observer to eliminate effects of unknown disturbances is proposed in [63]. A boundary controller that uses backstepping to reduce vibrations in a suspension wire hanging from a helicopter is introduced in [46]. Disturbance is rejected by using a disturbance observer.

Incremental Backstepping (IBS)

The incremental version of backstepping, where a discrete control input is derived at each step is presented in [23]. A first order rotor model is used to estimate the induced velocity of the rotor. The control input is derived using Lyapunov. Then, the virtual control is defined such that an incremental nonlinear dynamic inversion (INDI) control response is achieved. A disturbance observer is designed in order to find the disturbance acting on the system. Comparison with INDI is made. IBS with a disturbance observer appears to have no steady state error with constant wind, whereas INDI does.

Model Reference Adaptive Control (MRAC)

MRAC is a method that changes the control inputs of the vehicle such that the vehicle follows the behaviour of a known model. In this case, that is a gain scheduled PID controller. This is done in [14]. Stability of MRAC is guaranteed using Lyapunov, given some constraints. The controller is an LQR controller and its parameters are found using the ricatti equation. Uses the model of the BO-105 as reference and uses the MRAC controller to control the LYNX as if it were a BO105. The adaptive rule changes the gains of the LQR such that it matches the known model.

Sliding Mode Control

Sliding mode control is a control method that drives the system states from an initial state onto a pre-designed sliding surface. One of the major down-sides of SMC is chattering which can seriously harm control actuators. A sliding mode controller for a small-scale helicopter is proposed in [3]. The sliding surface is designed using a linear control method. Three different reaching laws are proposed, which essentially is the control law. Each law has a different speed to reach the steady state. A sliding mode controller to transition from forward flight and a certain altitude to hover at a certain altitude was proposed

in [16]. This is especially useful in transition from forward flight to hover for dipping.

Delayed Feedback

Delayed load feedback is used in a controller in the work from [8] in combination with input shaping on a model helicopter. The idea of delaying the feedback is to align the control input signals with the motion of the load. It is done as a replacement of a standard PD controller. Selecting the properties of the controller depend on the gain and time delay chosen. Depending on the system, having some offset could have significant changes in performance.

Fuzzy Control

Fuzzy control is a control method that uses very simple IF-THEN logic. Examples of applications of such controllers to helicopters can be found in [49], [33] and [57]. In [49], a neural network is used to learn the weights of the membership functions. The combination of these membership functions will then determine the control response of the controller. [33] presents a fuzzy logic controller for hover of a small-scale helicopter. Here, the weights of the membership functions were measured empirically. A fuzzy-logic controller to stabilize a hanging load below a helicopter is used in [57], specifically with a submerged load. Here, a fuzzy logic controller is used in combination with a PID is used. The fuzzy logic controller brings the cable angle error to within a certain threshold, the PID is then used to remove the steady state error. This is due to fuzzy logic not having an integrator-like rule. The weights of the membership functions are found using the weighted average method. Another interesting feature of this controller is the so-called universe contraction-expansion of the controller. This essentially means that the weights are scaled to a function depending on the size of the error. The control response of this controller is shown in Figure 3.12.

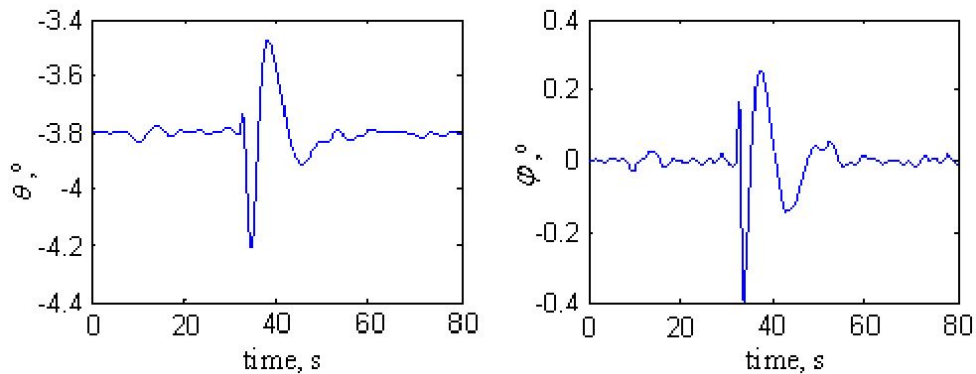


Figure 3.12: Control response gust turbulence with controller [57]

Input Shaping

Input shaping is a control method that uses control pulses in order to stabilize a system. This method can be found in cranes. The main principle behind it is to send input pulses at the exact right time to cancel out motion. The main difficulty lies in finding the exact frequency of the motion. For hanging load systems, this could be the pendulum motion, as this is the main motion of heavy loads.

An input shaping controller for a small-scale helicopter with a suspended load is proposed in [6]. Here, the frequency of the oscillation is also one of the main difficulties in using input shaping. The performance of an input shaping controller degrades quickly when the frequency is not exactly right. Even when using the derivative of the oscillation, the controller is only marginally more robust. A frequency estimator is used to estimate the frequency of the oscillation, and the small-scale helicopter is able to perform a tracking task while keeping oscillations low. The use of an input shaper is also investigated in [44] to reduce the swing of a hanging load from a small-scale helicopter. It largely validates the use of a UM-ZV shaper to reduce swing on an approximate model of the model helicopter. Reference [1] is an extension of [44]. It again shows the response of the helicopter to a regular ZV shaper. The helicopter model was found empirically using motion cameras.

3.5.4. Choice of Control Method

The main goal of this thesis is to find an INDI controller capable of performing dipping SONAR missions. Before beginning the design of such a controller, it is important to have knowledge of other control methods as well as knowing the advantages/disadvantages of the chosen control method. The advantages of INDI are clear: it is a model-free approach, meaning that exact model knowledge is not required. A more in-depth explanation of the working of INDI can be found in Section 3.6.

3.6. INDI Control on Helicopters

This chapter acts as an introduction to the concept of INDI. The working principle behind this control method is presented in Section 3.6.1. This is done via a derivation of the control input via this method. After that, a literature overview of INDI as a control system and its stability is given in Section 3.6.2 and Section 3.6.3. Finally, an application of INDI is done in Section 3.6.4 with case 3-DOF-PH-HUB-CG from Chapter 4 to show the difference between INDI and PID control.

3.6.1. Working Principle INDI

For a nonlinear system that is affine in the input, the equations of motion can be expressed as in Equation 3.10([5], [50]).

$$\begin{aligned}\dot{\bar{x}} &= f(\bar{x}) + G(\bar{x})\bar{u} \\ \bar{y} &= \bar{h}(\bar{x})\end{aligned}\quad (3.10)$$

Where the function $f(\bar{x})$ contains the change in states due to the current state, $G(\bar{x})$ is the control effectiveness matrix and $h(\bar{x})$ is the output function. Each of these components can be nonlinear.

INDI is the incremental version of NDI, of which the principle is to create a control input based on the desired change of the states. By rearranging the terms in Equation 3.10, the control input can be computed using Equation 3.11.

$$\bar{u} = G^{-1}(\bar{x})(\bar{v} - f(\bar{x}))\quad (3.11)$$

Where \bar{v} is the desired change of state, or the virtual control input. From this equation, it is clear where the model dependency comes from. An NDI controller will need accurate descriptions of the functions $G(\bar{x})$ and $f(\bar{x})$. If any model errors exist, the system is given by Equation 3.12, where $\Delta f(\bar{x})$ and $\Delta G(\bar{x})$ are the modelling errors in the model and control effectiveness respectively.

$$\dot{\bar{x}} = f(\bar{x}) + \Delta f(\bar{x}) + [G(\bar{x}) + \Delta G(\bar{x})]\bar{u}\quad (3.12)$$

Inserting the NDI control law of Equation 3.11 into Equation 3.12 then yields Equation 3.13.

$$\dot{\bar{x}} = \Delta f(\bar{x}) - \Delta G(\bar{x})G^{-1}(\bar{x})f(\bar{x}) + [I + \Delta G(\bar{x})G^{-1}(\bar{x})]\bar{v}\quad (3.13)$$

As shown, there are more terms present in the state change than just the desired change \bar{v} . Depending on the model uncertainties, these components could cause degraded performance, or even instability.

This is also the major shortcoming of NDI. Fortunately, this problem can be solved by using adaptive controllers, or by performing online system identification.

Another method of avoiding this shortcoming is by using incremental NDI, or INDI. INDI assumes that the control input can be updated fast enough, such that the change of states is only dependent on the change in input (see Figure 3.13). This comes, however, at the cost of required state derivative measurements.

Consider the Taylor series expansion of the nonlinear function of the state derivative Equation 3.10 in Equation 3.14, which can be reduced to Equation 3.15 when neglecting higher order terms.

$$\dot{\bar{x}} = \dot{\bar{x}}_0 + \left. \frac{\partial}{\partial \bar{x}} [f(\bar{x}) + G(\bar{x})\bar{u}] \right|_{x_0, u_0} (\bar{x} - \bar{x}_0) + \left. \frac{\partial}{\partial \bar{u}} G(\bar{x})\bar{u} \right|_{x_0, u_0} (\bar{u} - \bar{u}_0) + H.O.T.\quad (3.14)$$

$$\dot{\bar{x}} \approx \dot{\bar{x}}_0 + \frac{\partial}{\partial \bar{x}} f(\bar{x}_0)(\bar{x} - \bar{x}_0) + G(\bar{x}_0)(\bar{u} - \bar{u}_0)\quad (3.15)$$

As can be seen from Equation 3.15, the second component on the right-hand side approaches zero if the sampling frequency increases, since $(\bar{x} - \bar{x}_0) \rightarrow 0$ when the sampling frequency increases. Furthermore, it is important to note that the dynamics of the vehicle and the control inputs must be separated in time, also known as the timescale separation. Under normal circumstances, the rotor dynamics are indeed much faster than the vehicle dynamics and it can therefore be assumed that the difference in states is zero, with a nonzero difference in actuator inputs. In mathematical terms, this means that the change in state can be approximated as Equation 3.16, where the change in state is only dependent on the input to the system.

$$\dot{\hat{x}} \approx \dot{\hat{x}}_0 + G(\bar{x}_0)(\bar{u} - \bar{u}_0) \quad (3.16)$$

Rearranging terms, and using an incremental input $\Delta\bar{u}$ yields Equation 3.17.

$$\Delta\bar{u} = G^{-1}(\bar{x}_0)(\bar{\nu} - \dot{\hat{x}}_0) \quad (3.17)$$

An illustration of an INDI-controlled system is presented in a block diagram in Figure 3.13.

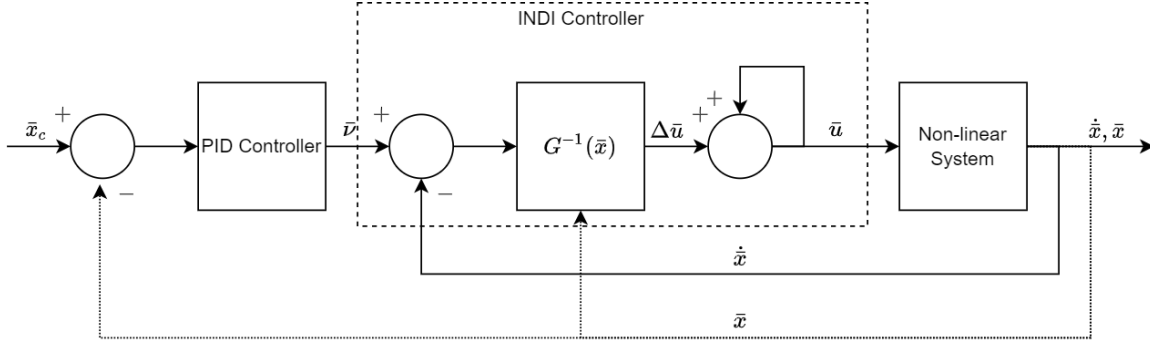


Figure 3.13: Block diagram of general INDI-controlled system.

As is apparent from Equation 3.17, the input of the system is no longer dependent on the non-linear feedback model of the vehicle which is the major downside of INDI. On the other hand, there is an increased dependency on the measurements taken or state estimations of the system $\dot{\hat{x}}_0$. This also means that the states must be either measurable directly or indirectly. Another uncertainty can still exist in the control effectiveness matrix $G(\bar{x}_0)$.

Assuming an uncertainty of ΔG in the system and applying INDI as is done in Equation 3.12 and Equation 3.13, yields Equation 3.18.

$$\dot{\hat{x}} = \bar{\nu} + \Delta G(\bar{x}_0)G^{-1}(\bar{x}_0)\bar{\nu} - \Delta G(\bar{x}_0)G^{-1}(\bar{x}_0)\dot{\hat{x}}_0 \quad (3.18)$$

When still assuming a high sampling rate, the difference between two state changes is negligible and $\dot{\hat{x}} \approx \dot{\hat{x}}_0$, meaning that Equation 3.19 holds and $\dot{\hat{x}} = \bar{\nu}$ when the sampling frequency is high enough.

$$[I + \Delta G(\bar{x}_0)G^{-1}(\bar{x}_0)] \dot{\hat{x}} = [I + \Delta G(\bar{x}_0)G^{-1}(\bar{x}_0)] \bar{\nu} \quad (3.19)$$

This means that INDI is robust to model uncertainties, even in the control effectiveness matrix. However, INDI requires having sensors measuring the states fast enough.

3.6.2. State of the Art in INDI as a Flight Control System

INDI as a flight control system is already discussed in literature, especially in recent years.

In [50], a robust flight control system is designed that uses angular acceleration predictions. The controller is designed for a general UAV that has a tail and an elevator. There are three distinct assumptions made within this control strategy. These are the time-scale separation. It is considered that this effect can be included as an additional uncertainty in the system. The second assumption is that the actuators are ideal, which is typically not the case, but is necessary in order for the first assumption to be correct. The final assumption is that the sensors used contain no biases, have no errors and no delays. In order to work around the issue of time delays, a predictive filter is proposed to anticipate for time delays in the measured angular accelerations. The advantage of such a filter is that the effect of time delay is reduced, but more model knowledge is required, since the predictive filter needs model knowledge.

In [31], an INDI control law is proposed that does not control the position of the actuators, but their rate. From their results, the vehicle was able to use the actuators more effectively using this scheme, than using pure INDI.

INDI has also a practical use in fault-tolerant control. Fault-tolerant control is a control scheme where the controller is capable of appropriately handling with either broken or missing control surfaces. References [65], [66] and [34] investigate the use of INDI under such circumstances, and INDI seems very robust in such circumstances.

Another possible problem with INDI could be the saturation of control inputs. For this, multiple solutions are proposed in literature. In [66], anti-windup is used in order to handle flight control with faulty actuators. Anti-windup is a method that reduces control overshoots if actuator saturation limits are reached.

INDI as a control mechanism for helicopters has also already been investigated in literature. An investigation is performed on the implementation of an INDI controller for the Apache AH-64 helicopter in [43]. It was found that normal INDI is not stable for this helicopter. The control inputs became saturated, and the helicopter oscillated and was unstable. This problem was solved by reducing the inverse of the control effectiveness matrix.

When investigating further, it was found that there was a time delay between the control input and the control response of the main rotor. To compensate for this time delay, a lead filter was proposed to the control input to synchronise the response of the helicopter with the input. Another proposal was done to add a lag filter to the feedback to synchronise both the input signal and the angular acceleration signal. The time delay is thought to be caused by the flapping dynamics of the main rotor. This has not been included into this work, but should be of interest when implementing INDI for helicopters in the future.

3.6.3. Stability of INDI

As illustrated in Section 3.6.1, INDI is very robust to model uncertainties as long as the sampling frequency is large enough. However, it is uncertain how large is large enough. Furthermore, INDI relies on infinitely fast actuators which do not exist.

Reference [24] investigates this issue in particular by first finding the time delay margin τ^* for INDI. This time delay τ is the sampling time of the sensors. For SISO systems, this margin was found to be Equation 3.20. MIMO systems can be decomposed to multiple SISO systems, which then follows the same criteria. Note that for MIMO systems, the eigenvalue λ can be complex, whereas a SISO system only has scalar values. β indicates the influence of the dynamics due to the states \bar{x} .

$$\tau > \tau^* = (1/\lambda\beta) \quad (3.20)$$

Another finding is that when introducing the actuator dynamics to the system, the stability of the closed loop system also changes as shown in Figure 3.14[24]. The two limits are found to be $\lambda = \infty$ and $\lambda = \tau/2(r + \tau_a)$, where $r = \tau/\tau_a$.

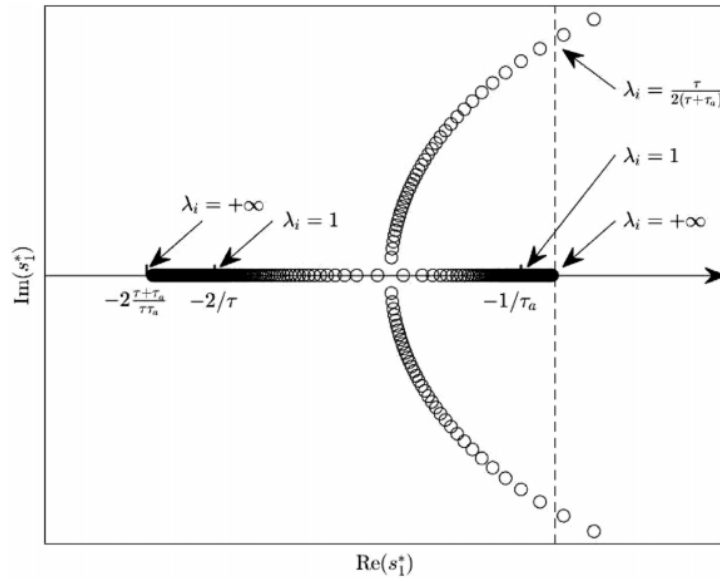


Figure 3.14: Poles of closed-loop system based on eigenvalue λ [24].

It was noted that when $\lambda = 1$, the model exactly matches the estimated control effectiveness of the system. However, if λ decreases, the dominant pole moves further away from the imaginary axis, resulting a more stable system. Therefore, it seems as if underestimating the control effectiveness matrix, yields a better transient response. This was also verified with simulations.

Another assumption made in INDI is the time-scale separation. In [59] an INDI control scheme is proposed that does not use this assumption and is valid for any degree system. Unlike what is done in typical literature, the time-scale separation part is not omitted from the equations. Lyapunov stability is then used to prove stability of the system.

3.6.4. Example Problem

In this section, an example of is presented where an INDI controller controls the pure helicopter in case 3-DOF-PH-HUB-CG from the preliminary work. The controller follows a cascaded control structure as shown in Figure 3.13. This means that the velocity is controlled using the attitude, the attitude using the pitch rate, and the pitch rate via the pitch acceleration. Note that there is both an NDI and an INDI controller present. The NDI controller uses the estimated $\frac{\partial \dot{u}}{\partial \theta_f}$ to compute the required attitude for the desired velocity change. The INDI controller inverts the attitude dynamics.

The control effectiveness matrix is updated each step with the current states by deriving the partial derivatives presented in Equation 4.14. In this case, only the cyclic control is used to adjust the horizontal velocity of the helicopter. The vertical speed w is still controlled using the PID from Section 4.2. The linear PID controllers for the INDI controller were tuned empirically, and found to be:

- Airspeed controller: $K_{P_u} = 0.2$, $K_{I_u} = 0$ and $K_{D_u} = 0.8$
- Attitude controller: $K_{P_{\theta_f}} = 1$, $K_{I_{\theta_f}} = 0$ and $K_{D_{\theta_f}} = 0.2$
- Pitch rate controller: $K_{P_q} = 1$, $K_{I_q} = 0$ and $K_{D_q} = 0.8$

The gains for the PID controller were:

- Airspeed controller: $K_{P_u} = -0.05$, $K_{I_u} = 0$ and $K_{D_u} = 0$
- Attitude controller: $K_{P_{\theta_f}} = -0.35$, $K_{I_{\theta_f}} = 0$ and $K_{D_{\theta_f}} = 0.26$

The disturbance acting on this system is, just as in the pure helicopter PID case, a constant 1° cyclic control input at the 10 second mark for 5 seconds. The controller is not activated before $t = 15$ seconds, and is activated after this time.

The response of the helicopter to the INDI and the PID controller is presented in Figure 3.17, with the control inputs in Figure 3.15 and Figure 3.16.

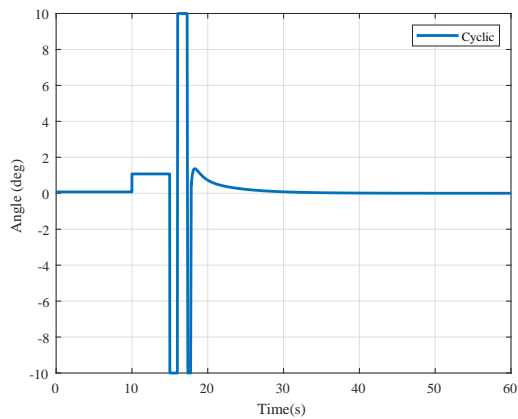


Figure 3.15: Cyclic control of the INDI controlled pure helicopter from case 1.

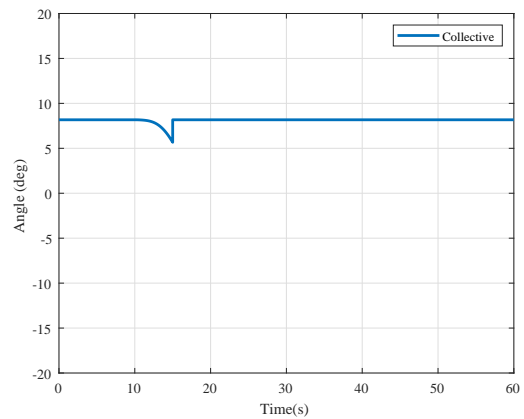


Figure 3.16: Collective control of the INDI controlled pure helicopter from case 1.

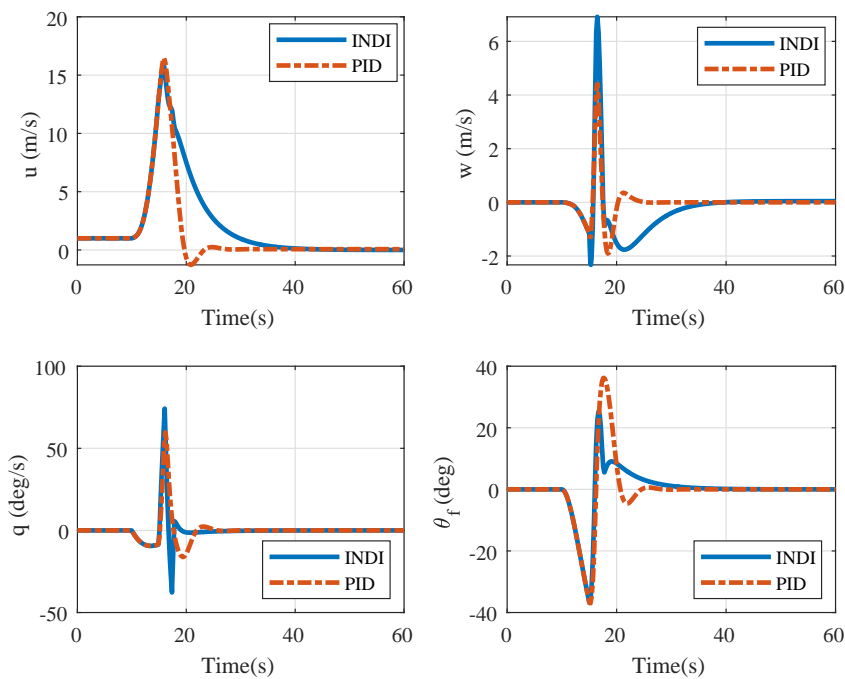


Figure 3.17: Comparison between INDI controller and PID controller for disturbed pure helicopter trimmed at $V = 1\text{m/s}$.

Observing the responses of both the PID controller and the INDI controller, two things become apparent. First of all, it seems that the INDI controller is more damped than the PID controller. This could, however, also be attributed bad controller tuning. The second observation that can be made is that the INDI controller seems to control very aggressively. The reason for this is that actuator dynamics are not taken into account, and perfect actuators are assumed with saturations at $\pm 10^\circ$. It seems that for this particular case, both controllers appear to have a stable result with the PID controller converging a bit faster.

3.6.5. Concluding Remarks

This section covered the working principle behind INDI as a control system, a literature of its uses as a flight control system, an overview of its stability and an example use-case using the 3-DOF model from Chapter 4.

The working principle behind INDI is moving from model dependency to sensor dependency. As was shown in the derivation, the model of the vehicle based on the current states can be ignored for finding the required control inputs. Instead, the control effectiveness and the derivative of the states are needed. This requires accurate sensors or estimation methods. Fortunately, it was shown that as the sampling frequency increases, the state derivative approaches the virtual control input.

The idea of using INDI as a flight control system is not new. It is proposed in multiple research papers where its applications are divers. Research is done on general flight control as well as fault-tolerant control. The stability of INDI was debatable, since it is based on the idea of having a large enough sampling frequency, yet the required size is unknown. In literature, the stability of INDI was investigated as to find the limits for the sampling time. Furthermore, INDI is based on the assumption of the time-scale separation. This assumption is also tested in literature.

From the results of the example problem, it became clear that the INDI controller appears more damped than the PID controller. The INDI controller also seems to control more aggressively, This is due to the lack of actuator dynamics in the controlled system. The PID controller also appears to provide a quicker response.

4

Preliminary study : 3-DOF Helicopter Model

This chapter contains the derivation of a 3 degrees of freedom model of a helicopter with a hanging load partially submerged in water. This is done to primarily get an understanding of the dynamics of the helicopter with a partially submerged load. Furthermore, it is interesting to see the effects of different configuration choices of the helicopter and the effects of different load models: A single pendulum and a double pendulum. Finally, it is attempted to design a PID controller to stabilise the load. This is done to see how well such a controller can stabilise a helicopter and can be used to compare PID control to INDI control. The model is derived in 6 steps each at a higher level of complexity than the latter. This is done to make distinctions between different configuration choices and see their effects. The 6 cases are provided in Table 4.1. The rotor hub location indicates the x-location of the hub in body frame. The load Model indicates what load is suspended from the helicopter, the load location indicates where the hinge of the load is located and the medium indicates in what medium the load is travelling. Air + Water indicating a partially submerged load. This chapter is structured as follows: First, problem is defined in Section 4.1. This includes the reference frames, the major model assumptions made and the simulation data used. Then, the 6 different cases are covered. For each configuration, the equations of motion are derived. After that, the model is trimmed and linearised using the Jacobian. This is followed by a stability analysis and the design of a PID and INDI controller. Finally, some concluding remarks are made in Section 4.8.

Table 4.1: Modelling cases for the 3-DOF model, each increasing the level of complexity.

3-DOF Model Cases				
Case	Rotor Hub Location	Load Model	Load Location	Medium
3-DOF-PH-HUB-CG	c.g.	-	-	-
3-DOF-PH-HUB-OFF	offset	-	-	-
3-DOF-SP-CG-HUB-OFF	offset	Single Pendulum	c.g.	Air
3-DOF-SP-OFF-HUB-OFF	offset	Single Pendulum	offset	Air
3-DOF-DP-OFF-HUB-OFF	offset	Double Pendulum	offset	Air
3-DOF-DP-OFF-HUB-OFF-SUB	offset	Double Pendulum	offset	Air + Water

4.1. Problem Definition

4.1.1. Reference frames

For the 3-DOF model, 2 reference frames are used. These are illustrated in Figure 4.1.

- LVLH Frame: The local vertical local horizontal frame is centered in the c.g. of the helicopter and is denoted with the subscript A . The x_A axis points towards the front of the helicopter (the nose when the fuselage angle is 0), the z_A axis towards the ground and y_A such that a right-handed system is achieved.

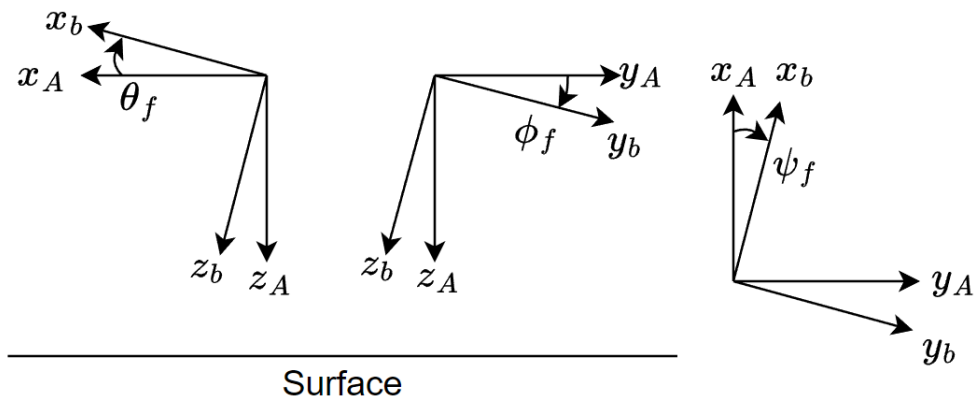


Figure 4.1: Body and LVLH reference frames

- **Body Frame:** The body frame is centered in the c.g. of the helicopter and is also attached to the helicopter. It is denoted by subscript B . The x_B axis points towards the nose and the z_B axis towards the bottom of the helicopter and the y_B axis such that it is a right-handed system. The B frame is therefore the A frame rotated the fuselage angle θ_f around the y_A axis.

4.1.2. Assumptions

For each specific case, the following assumptions are used:

1. Initial horizontal flight. This means that the helicopter is assumed to not move in the z_A direction initially. It can move in both x_A and z_A direction due to disturbances;
2. All angles are assumed small when trimming the aircraft;
3. The load angle is assumed small when computing the virtual work of the drag of the load.

4.1.3. Simulation Data

In Table 4.2, the simulation data used throughout this chapter is presented. There are a few notes to be made. In the cases where offsets are ignored, these offsets are set to zero. Furthermore, the chord c and blade inertia I_B are only used to compute the lock number. Additionally, the drag coefficient and the frontal surface area of the helicopter are combined together in the variable CDS . Constant τ is the time constant for dynamic inflow, since quasi-steady flow is assumed. The helicopter data belongs to the Bo-105 helicopter.

Table 4.2: Simulation data throughout the six simulation cases

Bo-105 Helicopter Data			Environment Data			Load Data		
Variable	Value	Unit	Variable	Value	Unit	Variable	Value	Unit
m	2200	kg	g	9.81	m/s^2	m_1	100	kg
I_y	4973	kgm^2	ρ	1.225	kg/m^3	m_2	300	kg
I_B	231.7	kgm^2	ρ_w	997	kg/m^3	x_l	0.5	m
R	4.91	m				h_l	1.0	m
x_h	-0.08	m				l_1	30	m
h	1.48	m				l_2	30	m
c	0.27	m				S_1	1	m^2
CDS	1.5	m^2				S_2	1	m^2
Ω	44.4	rad/s				C_{D_1}	0.5	-
cl_α	6.113	rad^{-1}				C_{D_2}	0.5	-
σ	0.07	-						
γ	5.0717	-						
τ	0.1	-						

4.2. Case 3-DOF-PH-HUB-CG

4.2.1. Configuration

The configuration of the pure helicopter with the rotor hub aligned with the c.g. of the helicopter in vertical direction is shown in Figure 4.2. It is shown in the body frame. Also, the forces acting on the helicopter and the variables used are given.

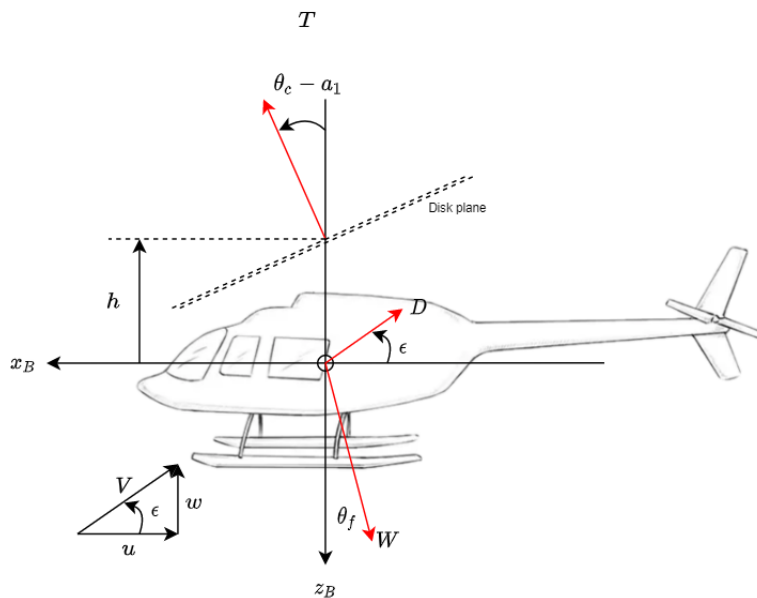


Figure 4.2: Diagram of case 3-DOF-PH-HUB-CG in body frame.

4.2.2. Equations of Motion

The set of equations of motion can be found using force equilibrium of the forces in Figure 4.2 and are given by Equation 4.1-Equation 4.4 [22] respectively.

$$\dot{u} = \frac{T}{m} \sin(\theta_c - a_1) - \frac{D}{m} \frac{u}{V} - g \sin(\theta_f) - qw \quad (4.1)$$

$$\dot{w} = -\frac{T}{m} \cos(\theta_c - a_1) - \frac{D}{m} \frac{w}{V} + g \cos(\theta_f) + qu \quad (4.2)$$

$$\dot{q} = -\frac{Th}{m} \sin(\theta_c - a_1) \quad (4.3)$$

$$\dot{\theta}_f = q \quad (4.4)$$

With:

$$\sin(\epsilon) = \frac{w}{V}; \cos(\epsilon) = \frac{u}{V} \quad (4.5)$$

4.2.3. Trimming

The trimmed aircraft condition is found by setting all equations of motion equal to zero[22]. Furthermore, the assumption is made that all angles are small and forward flight is assumed. This means that $\epsilon = \theta_f$. Also, quasi-steady inflow is assumed. These assumptions lead to the following conclusions: From Equation 4.3, it follows that $\theta_c = a_1$. Inserting this into Equation 4.1 leads to: $\tan(\theta_f) = -\frac{D}{W}$. This result then yields: $T = \sqrt{W^2 + D^2}$, when plugged into Equation 4.2.

The induced velocity of the rotor can be found numerically using the expression for the thrust coefficient according to the method of Glauert in Equation 4.6[22].

$$C_{T,Glauert} = 2\lambda_i \sqrt{\left(\left(\frac{V}{\Omega R} \cos(\alpha_d)\right)^2 + \left(\frac{V}{\Omega R} \sin(\alpha_d) + \lambda_i\right)^2\right)} \quad (4.6)$$

With the small angles assumption, the following expressions hold:

$$\alpha_c = \theta_c - \tan^{-1}\left(\frac{w}{u}\right) \approx \theta_c - \frac{w}{u} = \theta_c - \theta_f \quad (4.7)$$

$$\mu = \frac{V \cos(\alpha_c)}{\Omega R} \approx \frac{V}{\Omega R} \quad (4.8)$$

$$\lambda_c = \frac{V \sin(\alpha_c)}{\Omega R} \approx \mu a_1 - \mu \theta_f \quad (4.9)$$

With:

$$\alpha_d = \alpha_c - a_1 = -\theta_f = \frac{D}{W} \quad (4.10)$$

With the expression of the thrust coefficient from blade element theory in Equation 4.11[22], and the expression of the longitudinal flapping angle a_1 in Equation 4.12, it is possible to derive a linear set of equations as in Equation 4.13. The values of a_1 and θ_0 can then be computed very straightforward. Note that in this situation, the cyclic is equal to the flapping angle a_1 , hence both control inputs are known.

$$C_{T,BEM} = c_{l\alpha} \frac{\sigma}{4} \left[\frac{2}{3} \theta_0 \left(1 + \frac{3}{2} \mu^2 \right) - (\lambda_c + \lambda_i) \right] \quad (4.11)$$

$$a_1 = \theta_c = \frac{\frac{8}{3} \mu \theta_0 - 2\mu(\lambda_c + \lambda_i)}{1 - \frac{1}{2} \mu^2} \quad (4.12)$$

$$\begin{bmatrix} 1 + \frac{3}{2} \mu^2 & -\frac{8}{3} \mu \\ -\mu & \frac{2}{3} + \mu^2 \end{bmatrix} \begin{bmatrix} \theta_c \\ \theta_0 \end{bmatrix} = \begin{bmatrix} -2\mu^2 \alpha_d - 2\mu \lambda_i \\ \frac{4}{\sigma} \frac{C_T}{c_{l\alpha}} + \mu \alpha_d + \lambda_i \end{bmatrix} \quad (4.13)$$

Following the above procedure, a trim curve can be produced for various flight speeds as is shown in Figure 4.3. Note that for hover only the trim condition close to $V = 0$ is important. It makes sense that in order to go faster, the cyclic must be tilted further forwards. It is also interesting to see that at first, the collective decreases due to the increased massflow through the rotor, but at some point the collective also needs to increase due to the cyclic pointing further and further forward.

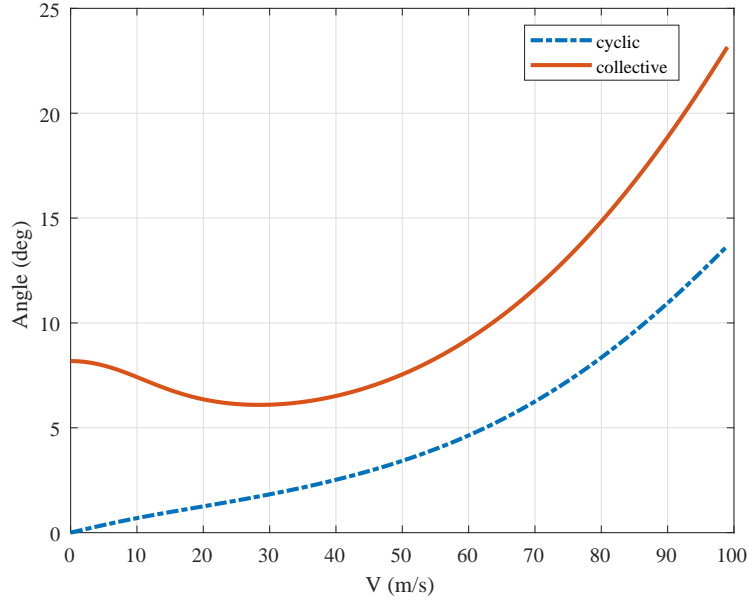


Figure 4.3: Trim curve for case 3-DOF-PH-HUB-CG

4.2.4. Model Linearisation

The non-linear model is linearised in order to assess its stability. It will also help when designing the controllers later on. Linearisation is done by computing the Jacobian of the linear system with respect to the states and the inputs around a trimmed condition. The linear system is then given by Equation 4.14.

$$\begin{bmatrix} \dot{u} \\ \dot{w} \\ \dot{q} \\ \dot{\theta}_f \end{bmatrix} = \begin{bmatrix} \frac{\partial \dot{u}}{\partial u} & \frac{\partial \dot{u}}{\partial w} & \frac{\partial \dot{u}}{\partial q} & \frac{\partial \dot{u}}{\partial \theta_f} \\ \frac{\partial \dot{w}}{\partial u} & \frac{\partial \dot{w}}{\partial w} & \frac{\partial \dot{w}}{\partial q} & \frac{\partial \dot{w}}{\partial \theta_f} \\ \frac{\partial \dot{q}}{\partial u} & \frac{\partial \dot{q}}{\partial w} & \frac{\partial \dot{q}}{\partial q} & \frac{\partial \dot{q}}{\partial \theta_f} \\ \frac{\partial \dot{\theta}_f}{\partial u} & \frac{\partial \dot{\theta}_f}{\partial w} & \frac{\partial \dot{\theta}_f}{\partial q} & \frac{\partial \dot{\theta}_f}{\partial \theta_f} \end{bmatrix} \begin{bmatrix} u \\ w \\ q \\ \theta_f \end{bmatrix} + \begin{bmatrix} \frac{\partial \dot{u}}{\partial \theta_c} & \frac{\partial \dot{u}}{\partial \theta_0} \\ \frac{\partial \dot{w}}{\partial \theta_c} & \frac{\partial \dot{w}}{\partial \theta_0} \\ \frac{\partial \dot{q}}{\partial \theta_c} & \frac{\partial \dot{q}}{\partial \theta_0} \\ \frac{\partial \dot{\theta}_f}{\partial \theta_c} & \frac{\partial \dot{\theta}_f}{\partial \theta_0} \end{bmatrix} \begin{bmatrix} \theta_c \\ \theta_0 \end{bmatrix} \quad (4.14)$$

The Individual partial derivatives from Equation 4.14 are given by Equation 4.15-Equation 4.18. These are derived by computing the partial derivatives of Equation 4.1-Equation 4.4. Note that the subscript *PH* indicates that this partial derivative holds for a pure helicopter. This is for cases 3-DOF-PH-HUB-CG and 3-DOF-PH-HUB-OFF. The partial derivatives of T , D , V and a_1 are found in Appendix A.

Partial Derivatives of \dot{u}

$$\begin{aligned}
\left(\frac{\partial \dot{u}}{\partial u}\right)_{PH} &= \frac{\partial T \sin(\theta_c - a_1)}{\partial u} \frac{1}{m} - \frac{T}{m} \cos(\theta_c - a_1) \frac{\partial a_1}{\partial u} - \frac{\partial D}{\partial V} \frac{\partial V}{\partial u} \frac{u}{mV} - \frac{D}{mV} + \frac{Du}{mV^2} \frac{\partial V}{\partial u} \\
\left(\frac{\partial \dot{u}}{\partial w}\right)_{PH} &= \frac{\partial T \sin(\theta_c - a_1)}{\partial w} \frac{1}{m} - \frac{T}{m} \cos(\theta_c - a_1) \frac{\partial a_1}{\partial w} - \frac{\partial D}{\partial V} \frac{\partial V}{\partial w} \frac{u}{mV} + \frac{Du}{mV^2} \frac{\partial V}{\partial w} - q \\
\left(\frac{\partial \dot{u}}{\partial q}\right)_{PH} &= -\frac{T}{m} \cos(\theta_c - a_1) \frac{\partial a_1}{\partial q} - w \\
\left(\frac{\partial \dot{u}}{\partial \theta_f}\right)_{PH} &= -g \cos(\theta_f) \\
\left(\frac{\partial \dot{u}}{\partial \theta_c}\right)_{PH} &= \frac{\partial T \sin(\theta_c - a_1)}{\partial \theta_c} \frac{1}{m} + \frac{T}{m} \cos(\theta_c - a_1) \left(1 - \frac{\partial a_1}{\partial \theta_c}\right) \\
\left(\frac{\partial \dot{u}}{\partial \theta_0}\right)_{PH} &= \frac{\partial T \sin(\theta_c - a_1)}{\partial \theta_0} \frac{1}{m} - \frac{T}{m} \cos(\theta_c - a_1) \frac{\partial a_1}{\partial \theta_0}
\end{aligned} \tag{4.15}$$

Partial Derivatives of \dot{w}

$$\begin{aligned}
\left(\frac{\partial \dot{w}}{\partial u}\right)_{PH} &= -\frac{\partial T \cos(\theta_c - a_1)}{\partial u} \frac{1}{m} - \frac{T}{m} \sin(\theta_c - a_1) \frac{\partial a_1}{\partial u} - \frac{\partial D}{\partial V} \frac{\partial V}{\partial u} \frac{w}{mV} + \frac{Dw}{mV^2} \frac{\partial V}{\partial u} + q \\
\left(\frac{\partial \dot{w}}{\partial w}\right)_{PH} &= -\frac{\partial T \cos(\theta_c - a_1)}{\partial w} \frac{1}{m} - \frac{T}{m} \sin(\theta_c - a_1) \frac{\partial a_1}{\partial w} - \frac{\partial D}{\partial V} \frac{\partial V}{\partial w} \frac{w}{mV} - \frac{D}{mV} + \frac{Dw}{mV^2} \frac{\partial V}{\partial w} \\
\left(\frac{\partial \dot{w}}{\partial q}\right)_{PH} &= -\frac{T}{m} \sin(\theta_c - a_1) \frac{\partial a_1}{\partial q} + u \\
\left(\frac{\partial \dot{w}}{\partial \theta_f}\right)_{PH} &= -g \sin(\theta_f) \\
\left(\frac{\partial \dot{w}}{\partial \theta_c}\right)_{PH} &= -\frac{\partial T \cos(\theta_c - a_1)}{\partial \theta_c} \frac{1}{m} + \frac{T}{m} \sin(\theta_c - a_1) \left(1 - \frac{\partial a_1}{\partial \theta_c}\right) \\
\left(\frac{\partial \dot{w}}{\partial \theta_0}\right)_{PH} &= -\frac{\partial T \cos(\theta_c - a_1)}{\partial \theta_0} \frac{1}{m} - \frac{T}{m} \sin(\theta_c - a_1) \frac{\partial a_1}{\partial \theta_0}
\end{aligned} \tag{4.16}$$

Partial Derivatives of \dot{q}

$$\begin{aligned}
\left(\frac{\partial \dot{q}}{\partial u}\right)_{PHCG} &= -\frac{\partial T h \sin(\theta_c - a_1)}{\partial u} \frac{1}{I_y} + \frac{Th}{I_y} \cos(\theta_c - a_1) \frac{\partial a_1}{\partial u} \\
\left(\frac{\partial \dot{q}}{\partial w}\right)_{PHCG} &= -\frac{\partial T h \sin(\theta_c - a_1)}{\partial w} \frac{1}{I_y} + \frac{Th}{I_y} \cos(\theta_c - a_1) \frac{\partial a_1}{\partial w} \\
\left(\frac{\partial \dot{q}}{\partial q}\right)_{PHCG} &= \frac{Th}{I_y} \cos(\theta_c - a_1) \frac{\partial a_1}{\partial q} \\
\left(\frac{\partial \dot{q}}{\partial \theta_f}\right)_{PHCG} &= 0 \\
\left(\frac{\partial \dot{q}}{\partial \theta_c}\right)_{PHCG} &= -\frac{\partial T h \sin(\theta_c - a_1)}{\partial \theta_c} \frac{1}{I_y} - \frac{Th}{I_y} \cos(\theta_c - a_1) \left(1 - \frac{\partial a_1}{\partial \theta_c}\right) \\
\left(\frac{\partial \dot{q}}{\partial \theta_0}\right)_{PHCG} &= -\frac{\partial T h \sin(\theta_c - a_1)}{\partial \theta_0} \frac{1}{I_y} + \frac{Th}{I_y} \cos(\theta_c - a_1) \frac{\partial a_1}{\partial \theta_0}
\end{aligned} \tag{4.17}$$

Partial Derivatives of $\dot{\theta}_f$

$$\begin{aligned}
\left(\frac{\partial \dot{\theta}_f}{\partial u}\right)_{PH} &= \left(\frac{\partial \dot{\theta}_f}{\partial w}\right)_{PH} = \left(\frac{\partial \dot{\theta}_f}{\partial \theta_f}\right)_{PH} = \left(\frac{\partial \dot{\theta}_f}{\partial \theta_c}\right)_{PH} = \left(\frac{\partial \dot{\theta}_f}{\partial \theta_0}\right)_{PH} = 0 \\
\left(\frac{\partial \dot{\theta}_f}{\partial q}\right)_{PH} &= 1
\end{aligned} \tag{4.18}$$

The resultant linear system is given in Equation 4.19.

$$\begin{bmatrix} \dot{u} \\ \dot{w} \\ \dot{q} \\ \dot{\theta}_f \end{bmatrix} = \begin{bmatrix} -0.014 & 0.000 & 0.697 & -9.810 \\ 0.000 & -0.984 & 1.000 & 0.000 \\ 0.008 & 0.000 & -0.456 & 0.000 \\ 0.000 & 0.000 & 1.000 & 0.000 \end{bmatrix} \begin{bmatrix} u \\ w \\ q \\ \theta_f \end{bmatrix} + \begin{bmatrix} 9.810 & -0.120 \\ 0.984 & -142.976 \\ -6.423 & 0.079 \\ 0.000 & 0.000 \end{bmatrix} \begin{bmatrix} \theta_c \\ \theta_0 \end{bmatrix} \quad (4.19)$$

To verify the correctness of the linear model, the response of both the linear and the nonlinear model are plotted when subjected to a disturbance. For this verification, both models are trimmed at a forward velocity of 1 m/s. The disturbance is a 1 degrees increase in cyclic control relative to trim at the 5 second mark. After 5 more seconds, the cyclic control is brought back to the trimmed value. The simulation results are presented in Figure 4.4. As shown, both the linear system approximates the nonlinear system very well until about 15 seconds, but diverges quickly after that. That is to be expected. The response of the system is unstable, which will be discussed in Section 4.2.5. Also note the two vertical dotted lines. these indicate the start and end of the disturbance.

Furthermore, the vertical velocity w diverges quickly. This is due to linearisation. As shown in Equation 4.19, \dot{w} is very dependent on q . This is due to the $+qu$ component in the equations of motion. Since the helicopter is trimmed around a $V = 1$ m/s, this value is almost equal to 1. In the nonlinear system, this component scales with the actual u , hence \dot{w} is in the nonlinear system differently dependent on u , depending on the value of u . \dot{u} has this same problem with w , but since horizontal flight is assumed, w is small anyway, hence this effect does not propagate that much.

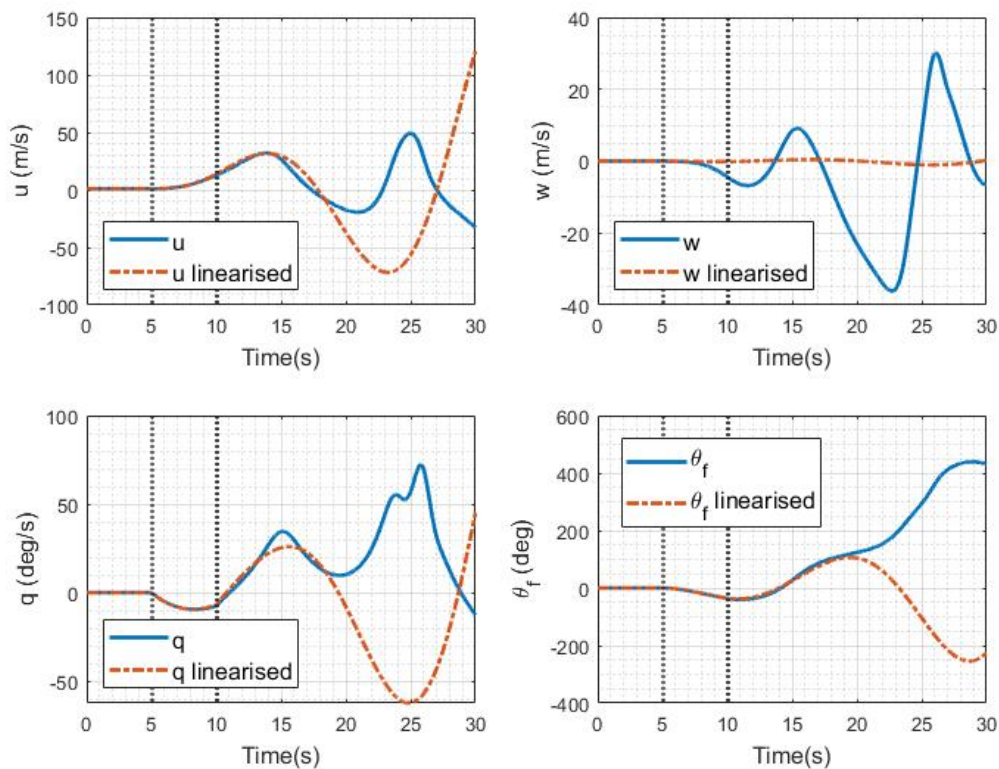


Figure 4.4: Response of linear and non-linear hovering helicopter model case 3-DOF-PH-HUB-CG to input disturbance on cyclic of 1 degree for 5 seconds.

4.2.5. Stability Analysis

Stability of the helicopter is assessed by obtaining the poles of the linearised system. The poles of this system are given in Table 4.3, with their location plotted in Figure 4.5. Note that the phugoid mode of the

helicopter model is unstable. This was also observed when verifying the linear model. This is also expected.

Table 4.3: Poles of linearised system for case 3-DOF-PH-HUB-CG, trimmed at $V = 1$ m/s

Pole	Real part	Complex part	Mode
1	-0.985	0.000	-
2	-0.657	0.000	Short Period
3	0.094	0.339	Phugoid
4	0.094	-0.339	Phugoid

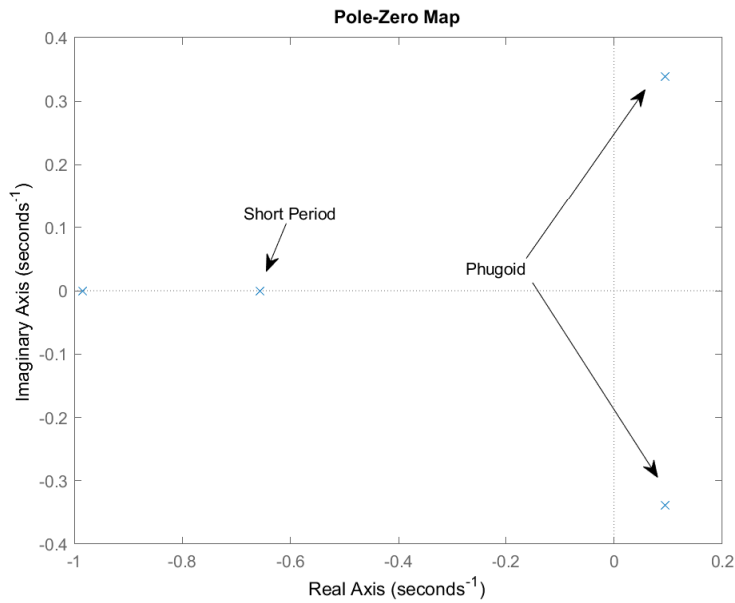


Figure 4.5: Pole-Zero map of linearised system for case 3-DOF-PH-HUB-CG, trimmed at $V = 1$ m/s.

4.2.6. Controller Design

In this section, a controller will be designed in order to control the unstable helicopter model. This is done in 3 steps. First, a pitch angle θ_f controller is designed, after that, a horizontal body velocity u controller is designed. Finally, a controller for the vertical body velocity w is designed.

Pitch angle θ_f controller

The pitch angle controller will have two variants: a PID and an INDI controller. These will have different control laws and gains, and has to be designed separately,

From Equation 4.19, the following assumptions can be made: Since u will remain small, its effect on the pitch rate will be negligible. This is also the case for the influence of the collective pitch. Therefore, the second derivative of the fuselage angle (or \dot{q}) can be approximated as in Equation 4.20.

$$\ddot{\theta}_f = \dot{q} = \frac{\partial \dot{q}}{\partial u} u + \frac{\partial \dot{q}}{\partial q} q + \frac{\partial \dot{q}}{\partial \theta_c} \theta_c + \frac{\partial \dot{q}}{\partial \theta_0} \theta_0 \approx \frac{\partial \dot{q}}{\partial q} q + \frac{\partial \dot{q}}{\partial \theta_c} \theta_c = \frac{\partial \dot{q}}{\partial q} \dot{\theta}_f + \frac{\partial \dot{q}}{\partial \theta_c} \theta_c \quad (4.20)$$

PID controller

For the linear PID controller, the decision is made to make it a PD controller. The reason for this is that the body velocity u is used as an outer loop for this controller, meaning that the integral term is redundant for this controller.

This means that the control law becomes: $\theta_c = K_p \theta_f + K_d \frac{d}{dt} (\theta_f)$. Note that the second

subscript _c after θ_f indicates "commanded", since θ_{f_c} is the reference pitch angle for the pitch angle controller. This control law leads to Equation 4.21.

$$\ddot{\theta}_f = \frac{\partial \dot{q}}{\partial q} \dot{\theta}_f + \frac{\partial \dot{q}}{\partial \theta_c} K p_{\theta_f} \theta_{f_c} + \frac{\partial \dot{q}}{\partial \theta_c} K d_{\theta_f} \dot{\theta}_{f_c} - \frac{\partial \dot{q}}{\partial \theta_c} K p_{\theta_f} \theta_f - \frac{\partial \dot{q}}{\partial \theta_c} K d_{\theta_f} \dot{\theta}_f \quad (4.21)$$

Going to the laplace domain, yields the transfer function of the fuselage angle w.r.t. to its reference value in Equation 4.22.

$$\frac{\theta_f(s)}{\theta_{f_c}(s)} = \frac{\frac{\partial \dot{q}}{\partial \theta_c} K p_{\theta_f}}{s^2 - \left(\frac{\partial \dot{q}}{\partial q} + \frac{\partial \dot{q}}{\partial \theta_c} K d_{\theta_f} \right) s + \frac{\partial \dot{q}}{\partial \theta_c} K p_{\theta_f}} = \frac{\omega_n^2}{s^2 + 2\zeta\omega_n s + \omega_n^2} \quad (4.22)$$

Since this is a simple second order system, the poles are found using Equation 4.23, where ω_n is the natural frequency of the response and ζ the damping ratio.

$$p_{1,2} = -\zeta\omega_n \pm \omega_n \sqrt{\zeta^2 - 1} \quad (4.23)$$

The values for the gains can then be derived to be:

$$K p_{\theta_f} = \frac{\omega_n^2}{\frac{\partial \dot{q}}{\partial \theta_c}}; K d_{\theta_f} = -\frac{2\zeta\omega_n + \frac{\partial \dot{q}}{\partial q}}{\frac{\partial \dot{q}}{\partial \theta_c}} \quad (4.24)$$

Choosing $\omega_n = 1.5 \text{ rad.s}$ $\zeta = .5\sqrt{2}$, yields a set of gains equal to $K p_{\theta_f} = -0.35, K d_{\theta_f} = -0.26$.

INDI controller

The INDI controller has a slightly different structure than the PID controller. It is a 2-loop controller where the inner loop controls the pitch rate, and the outer loop the pitch angle. This means that its transfer function is different as well, and thus its required gains too.

The principle behind INDI is that the state derivative changes fast enough, such that the only change in its derivative is caused by the control input. This means that the derivative of the pitch rate becomes Equation 4.25, and the inverse of the system will thus be inverse of the partial derivative, which is simply $\frac{\partial \theta_c}{\partial \dot{q}}$.

$$\ddot{\theta}_f = \dot{q} = \frac{\partial \dot{q}}{\partial \theta_c} \theta_c \quad (4.25)$$

Now, by multiplying the control input with the model inverse, the control loop becomes a double integral, meaning that the controller design is now linear, and a linear controller can be used. As control law, Equation 4.26 is used with the reference pitch rate is $K p_{\theta_f} (\theta_{f_c} - \theta_f)$.

$$\theta_c = K p_q \frac{\theta_c}{\dot{q}} (K p_{\theta_f} (\theta_{f_c} - \theta_f) - \dot{q}) \quad (4.26)$$

Going to the Laplace domain for the inner pitch rate loop, and rearranging terms, Equation 4.27 is obtained.

$$\frac{q(s)}{q_c(s)} = \frac{K_{p_q}}{s + K_{p_q}} \quad (4.27)$$

The outer loop of the controller is the controller for the attitude angle θ_f . Since the pitch rate is the derivative of the pitch angle, this loop is also an integral, and the transfer function becomes Equation 4.28.

$$\frac{\theta_f(s)}{\theta_{f_c}(s)} = \frac{K_{p_q} \frac{q(s)}{q_c(s)}}{s + K_{p_q} \frac{q(s)}{q_c(s)}} \quad (4.28)$$

Filling Equation 4.27 into Equation 4.28 yields a second order transfer function with Equation 4.29 as denominator. Choosing derivative gains of 0, yields a solution equal to $K_{p_{\theta_f}} = \frac{\omega_n}{2\zeta}$ and $K_{p_q} = 2\zeta\omega_n$. With $\omega_n = 1.5$ and $\zeta = 0.5\sqrt{2}$, this is equal to 1.06 and 2.12 respectively.

$$s^2 + K_{p_q}s + K_{p_{\theta_f}}K_{p_q} = s^2 + 2\zeta\omega_n s + \omega_n^2 \quad (4.29)$$

Horizontal body velocity u controller

Now the controller for the horizontal body velocity is designed. This is a controller in a loop around the pitch angle controller. Note that this controller is a PID, regardless whether the pitch angle controller is a PID or an INDI. However, there is some difference in determining the gains, since the control law for the pitch angle controller is different. Therefore, the u controller for the PID has a different derivation of the gains than for the INDI pitch angle controller.

Here too, when observing the linear system in Equation 4.19, certain parts of the model can be removed. The contribution of u on \dot{u} is negligible since u will remain small. This is also the case for the collective pitch. This leaves Equation 4.30 as a simplified model.

$$\dot{u} = \frac{\partial \dot{u}}{\partial u}u + \frac{\partial \dot{u}}{\partial q}q + \frac{\partial \dot{u}}{\partial \theta_f}\theta_f + \frac{\partial \dot{u}}{\partial \theta_c}\theta_c + \frac{\partial \dot{u}}{\partial \theta_0}\theta_0 \approx \frac{\partial \dot{u}}{\partial q}q + \frac{\partial \dot{u}}{\partial \theta_f}\theta_f + \frac{\partial \dot{u}}{\partial \theta_c}\theta_c \quad (4.30)$$

PID controller

Inserting the control law for the pitch angle controller and going to the laplace domian yields the transfer function of u with respect to θ_{f_c} Equation 4.31.

$$\frac{u(s)}{\theta_{f_c}(s)} = \frac{1}{s} \left[\left(\frac{\partial \dot{u}}{\partial q} + \frac{\partial \dot{u}}{\partial \theta_c}Kd_{\theta_f} \right) s + \left(\frac{\partial \dot{u}}{\partial \theta_f} + \frac{\partial \dot{u}}{\partial \theta_c}Kp_{\theta_f} \right) \right] \frac{\theta_f(s)}{\theta_{f_c}(s)} + Kp_{\theta_f} \frac{\partial \dot{u}}{\partial \theta_c} + Kd_{\theta_f} \frac{\partial \dot{u}}{\partial \theta_c} s \quad (4.31)$$

The control law for u will be a PD controller, with control law: $\theta_{f_c} = Kp_u(u_c - u) + Kd_u \frac{d}{dt}(u_c - u)$. Inserting this into Equation 4.31 and rearranging terms will yield the transfer function of $u(s)$ w.r.t. $u_c(s)$, and results in a 4th order transfer function with the following denominator:

$$k_1Kd_us^4 + [1 + k_1Kp_u + k_2Kd_u]s^3 + [2\zeta\omega_n + k_2Kp_u + k_3Kd_u]s^2 + [\omega_n^2 + k_3Kp_u + k_4Kd_u]s + k_4Kp_u \quad (4.32)$$

with

$$\begin{aligned} k_1 &= \frac{\partial \dot{u}}{\partial \theta_c}Kd_{\theta_f} \\ k_2 &= \frac{\partial \dot{u}}{\partial \theta_c}Kp_{\theta_f} + 2\frac{\partial \dot{u}}{\partial \theta_c}Kd_{\theta_f}\zeta\omega_n \\ k_3 &= \frac{\partial \dot{u}}{\partial \theta_f}\omega_n^2 + 2\frac{\partial \dot{u}}{\partial \theta_c}Kp_{\theta_f}\zeta\omega_n \\ k_4 &= \frac{\partial \dot{u}}{\partial q}\omega_n^2 \end{aligned} \quad (4.33)$$

Since this is a 4th order polynomial, the solution to finding the zeros of this function is not trivial. However, there are a set of 5 constraints that will yield positive constants at all multiples of s . This would ensure stability. These constraints are presented below. Unfortunately, there is no combination of controller gains that satisfies all constraints. This means that it is not possible to find the gains analytically. A proportional gain of $Kp_u = -0.02$ and a derivative gain of $Kp_u = 0.0$ is chosen.

INDI controller

Just as with the PID, Equation 4.31 holds. However, the transfer function $\frac{\theta_f}{\theta_{f_c}}$ is different. Using the same control law for u as the PID, the transfer function for $\frac{\partial u}{\partial u_c}$ can be obtained. This is, unlike with the PID, a third order transfer function, with the denominator:

$$[1 + k_1Kd_u]s^3 + [2\zeta\omega_n + k_1Kp_u + k_2Kd_u]s^2 + [\omega_n^2 + k_2Kp_u + k_3Kd_u]s + k_3Kp_u \quad (4.34)$$

With:

$$\begin{aligned}
 k_1 &= \frac{\partial \dot{u}}{\partial \theta_c} \frac{\partial \theta_c}{\partial \dot{q}} K p_q K p_{\theta_f} \\
 k_2 &= 2 \frac{\partial \dot{u}}{\partial \theta_c} \frac{\partial \theta_c}{\partial \dot{q}} K p_q K p_{\theta_f} \zeta \omega_n + \frac{\partial \dot{u}}{\partial \theta_c} \frac{\partial \theta_c}{\partial \dot{q}} K p_q \omega_n^2 + \frac{\partial \dot{u}}{\partial q} \omega_n^2 \\
 k_3 &= \frac{\partial \dot{u}}{\partial \theta_f} \omega_n^2
 \end{aligned} \tag{4.35}$$

This leads to the following set of constraints for ensuring stability:

$$\begin{aligned}
 K d_u &> -\frac{1}{k_1} \\
 K p_u &> \frac{-2\zeta \omega_n - k_2 K d_u}{k_1} \\
 K p_u &> \frac{-\omega_n^2 - k_3 K d_u}{k_2} \\
 k_3 K p_u &> 0
 \end{aligned} \tag{4.36}$$

This set does provide a region where all constraints are met. Choosing $K p_u = -0.02$ and $K d_u = 0$ meets these criteria and produces a stable result.

w controller

PID control

When observing the equation of \dot{w} in Equation 4.19, it is clear that by far the largest contribution is generated by the collective pitch. Therefore, the equation of \dot{w} can be rewritten to

$$\dot{w} \approx \frac{\partial \dot{w}}{\partial \theta_0} \theta_0 \tag{4.37}$$

Applying the following PD control law: $\theta_0 = K p_w (w_{ref} - w) + K d_w \frac{d}{dt} (w_{ref} - w)$ yields Equation 4.38 as transfer function of w

$$\frac{w(s)}{w_{ref}(s)} = \frac{K p_w + K d_w s}{s \left(1 + \frac{\partial \dot{w}}{\partial \theta_0} K d_w \right) + \frac{\partial \dot{w}}{\partial \theta_0} K p_w} \tag{4.38}$$

This is a first order system. Choosing a time constant of $\tau = 0.1$, and a derivative gain of $K d_w = 0$, yields a proportional gain of $K p_w = -0.07$.

INDI control

Here, just as with the θ_f controller, the derivative is assumed to change by control input only (this was also assumed for the PID controller due to the large contribution of the control input). Using the partial derivative in Equation 4.37 as the model inverse, the system becomes an integral and is now linear. This means that the controller has the same structure as Equation 4.28 and the same gains apply to the proportional and derivative gains for the inner \dot{w} and outer w loop respectively, meaning that they have as gains: $K p_w = \frac{\omega_n}{2\zeta}$ and $K p_{\dot{w}} = 2\zeta \omega_n$. With $\omega_n = 1.5$ and $\zeta = 0.5\sqrt{2}$, this is equal to 1.06 and 2.12 respectively.

4.2.7. Assessing Controllers

The performance of the controllers can be assessed by subjecting them to a disturbance input. For this, both controllers are simulated using the non-linear model, trimmed at a forward velocity of 1 m/s. The disturbance is a 1 degree increase in cyclic control relative to trim at the 5 second mark. After 5 more seconds, the cyclic control is brought back to the trimmed value. The controllers are turned on after 10 seconds. Also note the two vertical dotted lines. these indicate the start and end of the disturbance. The end of the disturbance also marks the start of the controllers. Additionally, note that these are 2 separate

simulations. One using the PID pitch angle controller, PID horizontal velocity controller and PID vertical velocity controller denoted by PID and one using the INDI pitch angle controller, PID horizontal velocity controller and INDI vertical velocity controller denoted by $INDI$.

Also, the control inputs are limited to $\pm 10^\circ$ and the control input rate is limited to $25^\circ/s$.

The helicopter response using both controllers is shown in Figure 4.6, with the cyclic and collective inputs in Figure 4.7 and Figure 4.8. As shown, both controllers are capable of controlling the given disturbance and have similar response. Both controllers appear to reach the limit on the cyclic control input, but on the cyclic this is not the case. The INDI controller appears to have smoother control inputs than the PID, but this could be attributed to controller tuning. Nevertheless, both controllers perform equally well.

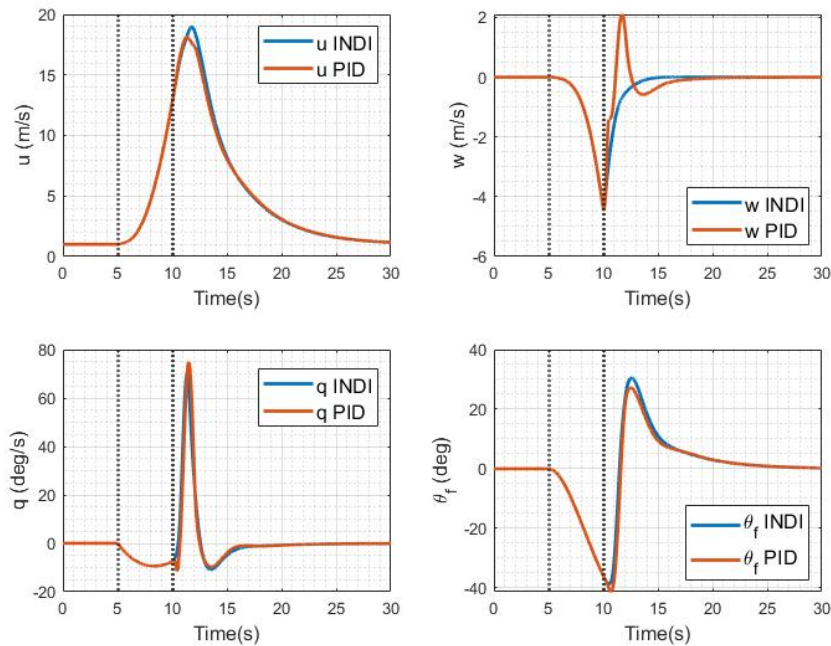


Figure 4.6: Response of controlled hovering helicopter case 3-DOF-PH-HUB-CG to input disturbance on cyclic of 1 degree for 5 seconds.

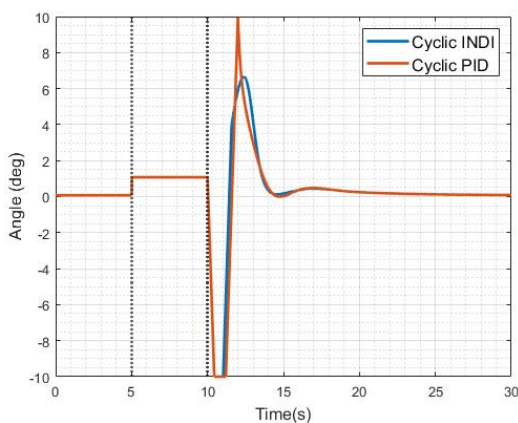


Figure 4.7: Cyclic control of the controlled hovering helicopter case 3-DOF-PH-HUB-CG to input disturbance on cyclic of 1 degree for 5 seconds.

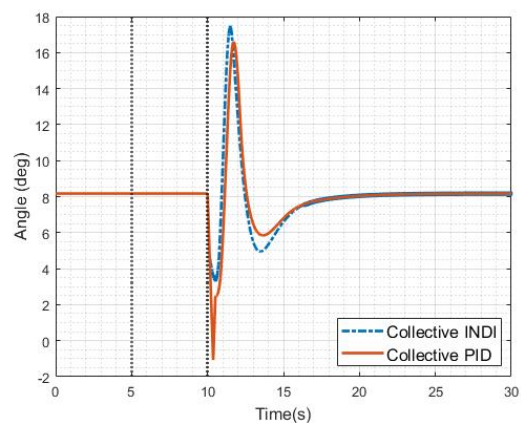


Figure 4.8: Collective control of the controlled hovering helicopter case 3-DOF-PH-HUB-CG to input disturbance on cyclic of 1 degree for 5 seconds.

4.3. Case 3-DOF-PH-HUB-OFF

4.3.1. Configuration

Typically, the rotor hub is not aligned with the c.g. of the helicopter. This means that there is an additional moment created by the position of the rotor hub in x_B direction. This is illustrated in Figure 4.9.

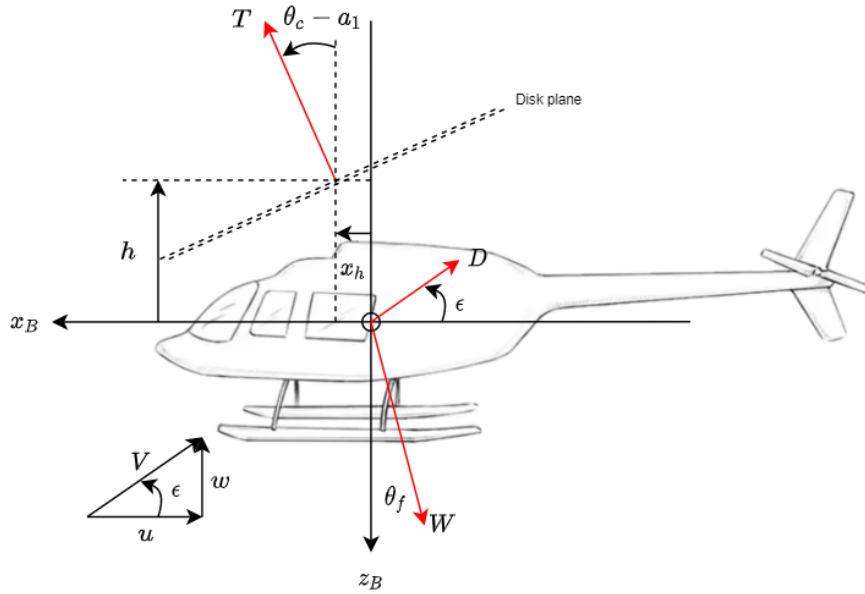


Figure 4.9: Diagram of case 3-DOF-PH-HUB-OFF in x_B frame.

4.3.2. Equations of Motion

Since the forces remain unchanged, only the \dot{q} equation changes.

$$\dot{q} = T \cos(\theta_c - a_1) \frac{x_h}{I_y} - T \sin(\theta_c - a_1) \frac{h}{I_y} \quad (4.39)$$

4.3.3. Trimming

Trimming is done via the same procedure as in case Case 3-DOF-PH-HUB-CG. The equations for this procedure are as follows:

$$\theta_c = a_1 + \tan^{-1} \left(\frac{x_h}{h} \right) \quad (4.40)$$

$$\alpha_d = \tan^{-1} \left(\frac{x_h}{h} \right) - \theta_f \quad (4.41)$$

$$\tan(\theta_f) = -\frac{Dh - Wx_h}{Wh + Dx_h} \quad (4.42)$$

$$T = \sqrt{(D \cos(\theta_f) + W \sin(\theta_f))^2 + (-D \cos(\theta_f) + W \sin(\theta_f))^2} \quad (4.43)$$

$$\begin{bmatrix} \theta_c \\ \theta_0 \end{bmatrix} = \begin{bmatrix} 1 + \frac{3}{2}\mu^2 & -\frac{8}{3}\mu \\ -\mu & \frac{2}{3} + \mu^2 \end{bmatrix}^{-1} \begin{bmatrix} -2\mu^2\alpha_d - 2\mu\lambda_i \\ \frac{4}{\sigma} \frac{C_T}{c_{l\alpha}} - \mu\theta_f + \lambda_i \end{bmatrix} + \begin{bmatrix} \tan^{-1}\left(\frac{x_h}{h}\right) \\ 0 \end{bmatrix} \quad (4.44)$$

The trim curves for different airspeeds are presented in Figure 4.10. Here, the helicopter was trimmed for multiple rotor hub locations relative to the c.g. What is clear from this diagram is that the further the hub is located backwards, the smaller the trimmed cyclic position. This makes sense, since in the trimmed condition, the fuselage is aligned such that the rotor hub is directly above the c.g. This is also visible in the collective remaining constant for each configuration. Note that for the rest of the simulation cases, $x_h = -0.08$ will be used.

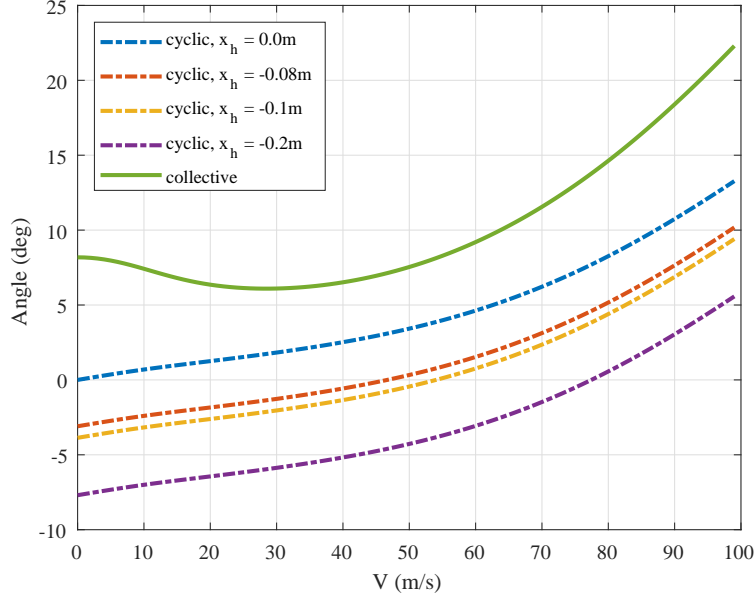


Figure 4.10: Trim curve for case 3-DOF-PH-HUB-OFF where the rotor hub is located at different offsets of x_h m in x_B direction.

4.3.4. Model Linearisation

Only the partial derivatives w.r.t. q change. Note the subscript PH_{OFF} . This indicates Pure Helicopter, with hub at OFFset, which applies to case 3-DOF-PH-HUB-OFF.

Partial Derivatives of \dot{q}

$$\left(\frac{\partial \dot{q}}{\partial u}\right)_{PH_{OFF}} = \frac{\partial T}{\partial u} \left(\frac{x_h \cos(\theta_c - a_1)}{I_y} - \frac{h \sin(\theta_c - a_1)}{I_y} \right) + \frac{\partial a_1}{\partial u} \left(\frac{T x_h}{I_y} \sin(\theta_c - a_1) + \frac{T h}{I_y} \cos(\theta_c - a_1) \right) \quad (4.45)$$

$$\left(\frac{\partial \dot{q}}{\partial w}\right)_{PH_{OFF}} = \frac{\partial T}{\partial w} \left(\frac{x_h \cos(\theta_c - a_1)}{I_y} - \frac{h \sin(\theta_c - a_1)}{I_y} \right) + \frac{\partial a_1}{\partial w} \left(\frac{T x_h}{I_y} \sin(\theta_c - a_1) + \frac{T h}{I_y} \cos(\theta_c - a_1) \right) \quad (4.46)$$

$$\left(\frac{\partial \dot{q}}{\partial q}\right)_{PH_{OFF}} = \frac{\partial a_1}{\partial q} \left(\frac{T x_h}{I_y} \sin(\theta_c - a_1) + \frac{T h}{I_y} \cos(\theta_c - a_1) \right) \quad (4.47)$$

$$\left(\frac{\partial \dot{q}}{\partial \theta_f}\right)_{PH_{OFF}} = 0 \quad (4.48)$$

$$\left(\frac{\partial \dot{q}}{\partial \theta_c}\right)_{PH_{OFF}} = \frac{\partial T}{\partial \theta_c} \left(\frac{x_h \cos(\theta_c - a_1)}{I_y} - \frac{h \sin(\theta_c - a_1)}{I_y} \right) - \left(\frac{T x_h}{I_y} \sin(\theta_c - a_1) + \frac{T h}{I_y} \cos(\theta_c - a_1) \right) \left(1 - \frac{\partial a_1}{\partial \theta_c} \right) \quad (4.49)$$

$$\left(\frac{\partial \dot{q}}{\partial \theta_0}\right)_{PHOFF} = \frac{\partial T}{\partial \theta_0} \left(\frac{x_h \cos(\theta_c - a_1)}{I_y} - \frac{h \sin(\theta_c - a_1)}{I_y} \right) + \frac{\partial a_1}{\partial \theta_0} \left(\frac{T x_h}{I_y} \sin(\theta_c - a_1) + \frac{T h}{I_y} \cos(\theta_c - a_1) \right) \quad (4.50)$$

The resultant linear system is given in Equation 4.51.

$$\begin{bmatrix} \dot{u} \\ \dot{w} \\ \dot{q} \\ \dot{\theta}_f \end{bmatrix} = \begin{bmatrix} -0.016 & -0.052 & 0.750 & -9.796 \\ -0.052 & -0.981 & 0.961 & 0.530 \\ 0.008 & 0.000 & -0.457 & 0.000 \\ 0.000 & 0.000 & 1.000 & 0.000 \end{bmatrix} \begin{bmatrix} u \\ w \\ q \\ \theta_f \end{bmatrix} + \begin{bmatrix} 9.849 & 7.837 \\ 0.453 & -142.762 \\ -6.433 & 0.079 \\ 0.000 & 0.000 \end{bmatrix} \begin{bmatrix} \theta_c \\ \theta_0 \end{bmatrix} \quad (4.51)$$

To verify the correctness of the linear model, the response of both the linear and the nonlinear model are plotted when subjected to a disturbance. This is done exactly the same way as in case 3-DOF-PH-HUB-CG. The simulation results are presented in Figure 4.11. Just as in case 3-DOF-PH-HUB-CG, the approximation is very good until around 15 seconds, after which the linear model diverges. Also the same phenomena with the body velocity w appeared. Nevertheless, the linearised model appears to approximate the system well.

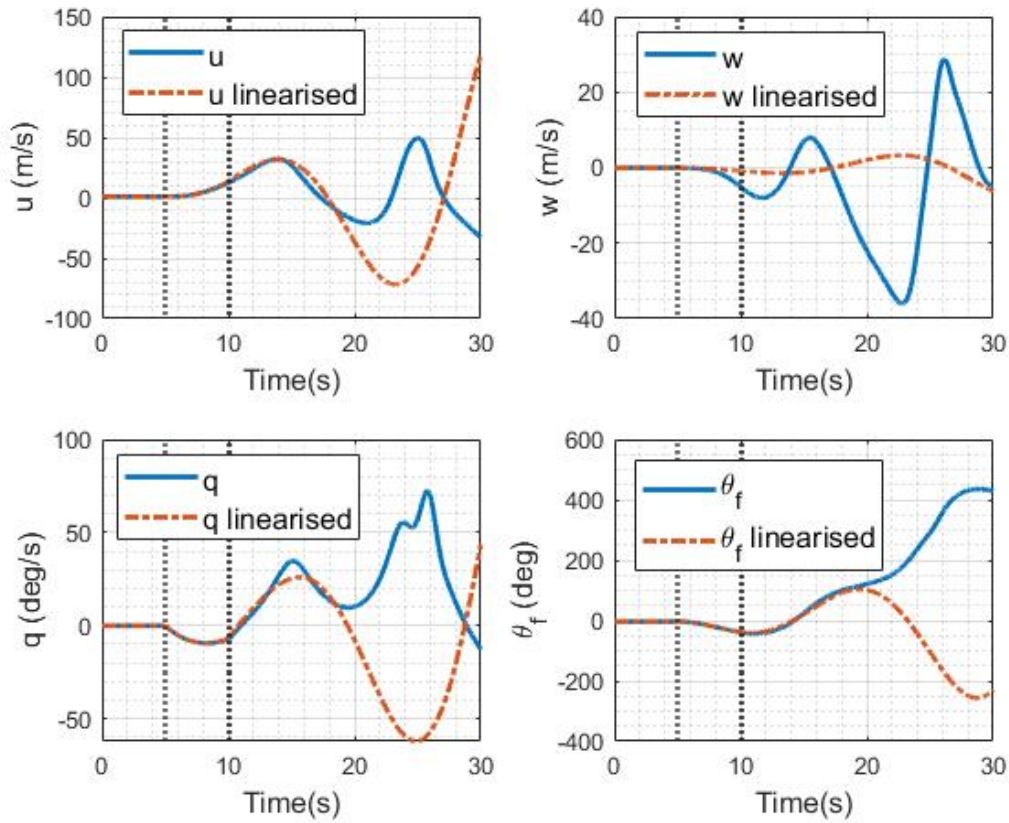


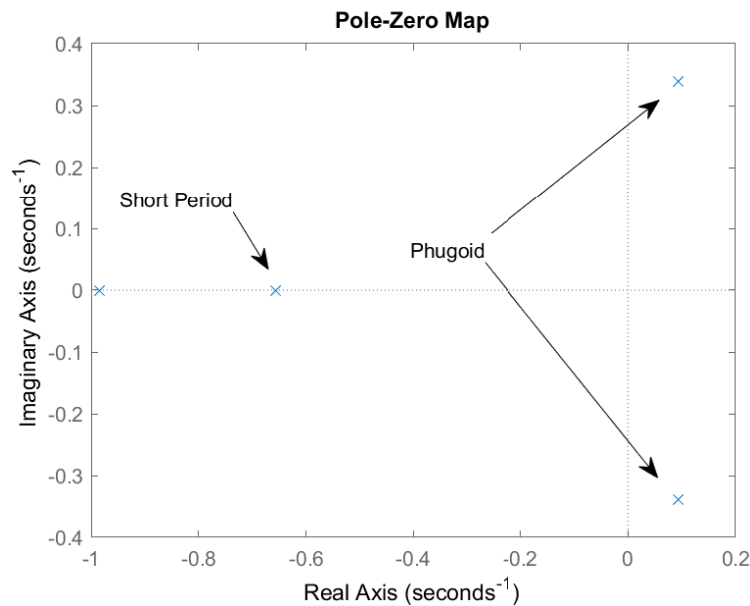
Figure 4.11: Response of linear and non-linear hovering helicopter model case 3-DOF-PH-HUB-OFF to input disturbance on cyclic of 1 degree for 5 seconds.

4.3.5. Stability Analysis

Stability of the helicopter is assessed by obtaining the poles of the linearised system. The poles of this system are given in Table 4.4, with their location plotted in Figure 4.12. Note that the phugoid mode of the helicopter model for this case is also unstable.

Table 4.4: Poles of the linearised pure helicopter model with the rotor hub offset the c.g. of the helicopter trimmed at $V = 1\text{m/s}$.

Pole	Real part	Complex part	Mode
1	-0.985	0.000	-
2	-0.657	0.000	Short Period
3	0.094	0.339	Phugoid
4	0.094	-0.339	Phugoid

**Figure 4.12:** Pole-Zero map of linearised system for case 3-DOF-PH-HUB-OFF, trimmed at $V = 1\text{ m/s}$.

4.3.6. Assessing Controllers

The controllers used for this system are exactly the same controllers as for the system in case 3-DOF-PH-HUB-CG. This is due to the fact that both systems are very similar and the controller yields a stable result. Both controllers are simulated using the same procedure as in case 3-DOF-PH-HUB-CG.

The result is presented in Figure 4.13 for the helicopter response, Figure 4.14 and Figure 4.15 for the control inputs. The response of the helicopter is very similar to that of case 3-DOF-PH-HUB-CG. However, now there is a steady state error in the horizontal body velocity u . This is caused by the offset in the hub location. The u -controller is a PID without integral component. This means that each u error corresponds to a certain attitude angle. As a result, there is a velocity error where the controller sends an attitude angle reference where the helicopter is in steady state.

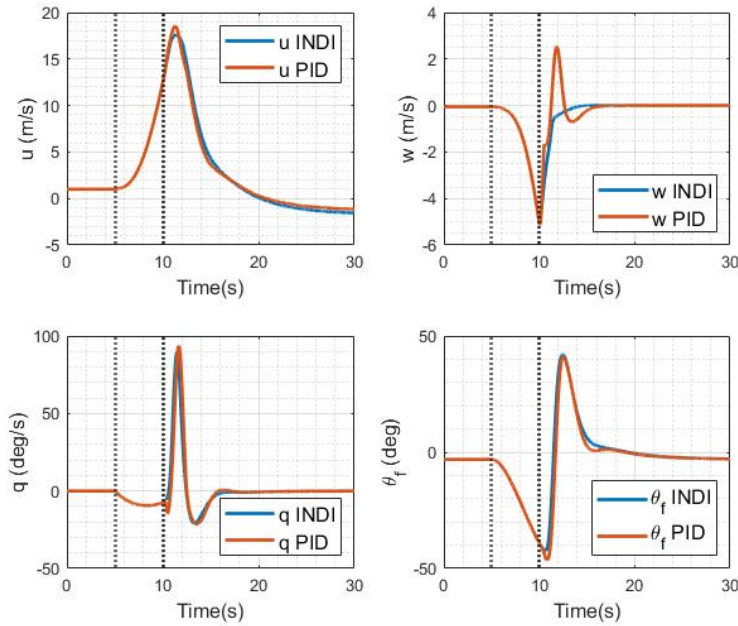


Figure 4.13: Response controlled hovering helicopter case 3-DOF-PH-HUB-OFF to input disturbance on cyclic of 1 degree for 5 seconds.

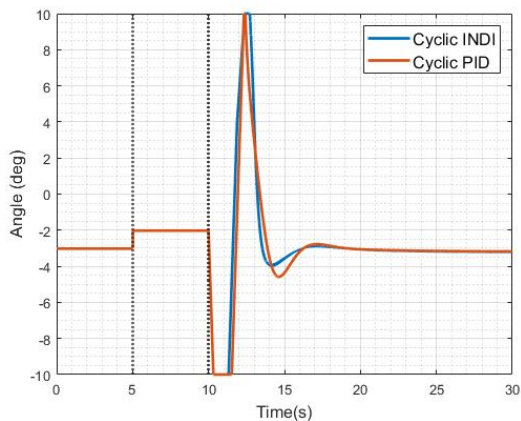


Figure 4.14: Cyclic control of the controlled hovering helicopter case 3-DOF-PH-HUB-OFF to input disturbance on cyclic of 1 degree for 5 seconds.

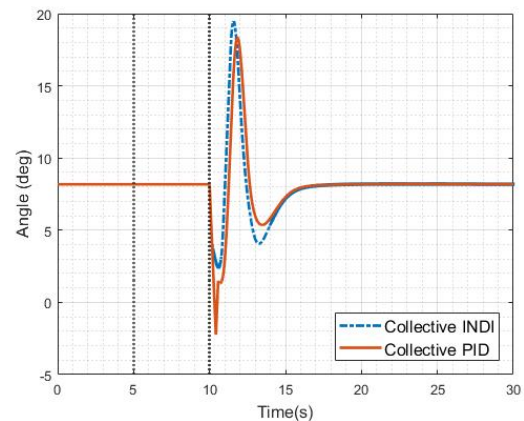


Figure 4.15: Collective control of the controlled hovering helicopter case 3-DOF-PH-HUB-OFF to input disturbance on cyclic of 1 degree for 5 seconds.

4.4. Case 3-DOF-SP-CG-HUB-OFF

4.4.1. Configuration

The configuration for case 3 where the single pendulum load is attached to the c.g. of the helicopter is shown in Figure 4.16 for the A frame and body frame respectively.

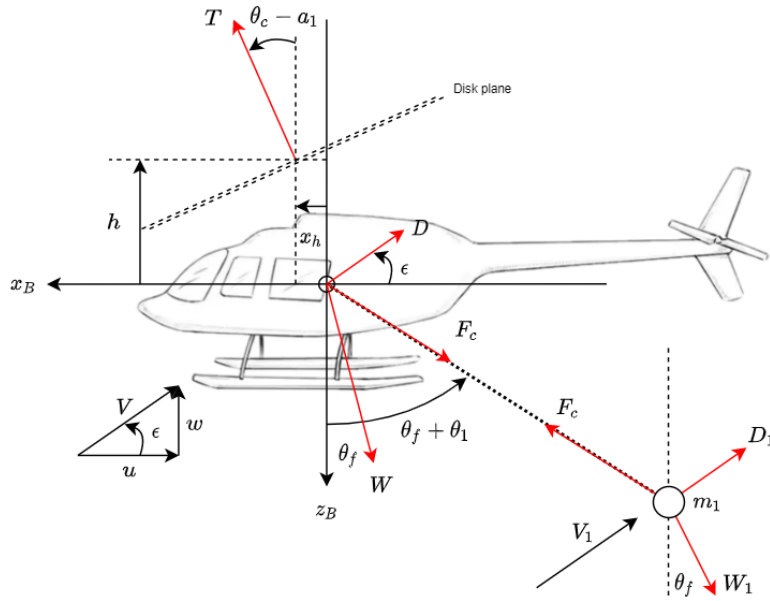


Figure 4.16: Diagram of case 3-DOF-SP-CG-HUB-OFF in x_B frame.

4.4.2. Equations of Motion

The Single pendulum model is graphically shown in Figure 4.17. The Lagrange's equation can be used to obtain the equations of motion for the system, although it can also be done with torque equilibrium. The equation of motion is presented in Equation 4.52, with the generalised drag force in Equation 4.53. Also note the subscripts 0 and 1. 0 indicates a property of the helicopter itself, whereas 1 indicates a property of the pendulum mass.

$$m_1 l_1^2 \ddot{\theta}_1 = Q_1 + m_1 l_1 [\ddot{x}_0 \cos(\theta_1) + \ddot{z}_0 \sin(\theta_1)] - W_1 l_1 \sin(\theta_1) \quad (4.52)$$

$$Q_1 = \text{sgn}(\dot{x}_1) \cdot D_{1_x} l_1 \cos(\theta_1) + \text{sgn}(\dot{z}_1) \cdot D_{1_z} l_1 \sin(\theta_1) \quad (4.53)$$

With:

$$\begin{aligned} \dot{x}_0 &= u \cos(\theta_f) + w \sin(\theta_f) \rightarrow \ddot{x}_0 = \dot{u} \cos(\theta_f) - u \sin(\theta_f)q + \dot{w} \sin(\theta_f) + w \cos(\theta_f)q \\ \dot{z}_0 &= -u \sin(\theta_f) + w \cos(\theta_f) \rightarrow \ddot{z}_0 = -\dot{u} \sin(\theta_f) - u \cos(\theta_f)q + \dot{w} \cos(\theta_f) - w \sin(\theta_f)q \end{aligned} \quad (4.54)$$

$$\begin{aligned} \dot{x}_1 &= \dot{x}_0 - l_1 \cos(\theta_1) \dot{\theta}_1 \rightarrow \ddot{x}_1 = \ddot{x}_0 - l_1 \cos(\theta_1) \ddot{\theta}_1 + l_1 \sin(\theta_1) \dot{\theta}_1^2 \\ \dot{z}_1 &= \dot{z}_0 - l_1 \sin(\theta_1) \dot{\theta}_1 \rightarrow \ddot{z}_1 = \ddot{z}_0 - l_1 \sin(\theta_1) \ddot{\theta}_1 - l_1 \cos(\theta_1) \dot{\theta}_1^2 \end{aligned} \quad (4.55)$$

$$D_{1_x} = \frac{1}{2} \rho \dot{x}_1^2 C_{D_1} S_1; D_{1_z} = \frac{1}{2} \rho \dot{z}_1^2 C_{D_1} S_1 \quad (4.56)$$

$$F_{ct_1} = m_1 l_1 \dot{\theta}_1^2 \quad (4.57)$$

$$F_c = D_{1_x} \sin(\theta_1) - D_{1_z} \cos(\theta_1) + W_1 \cos(\theta_1) + F_{ct_1} \quad (4.58)$$

Helicopter Model

$$\dot{u} = \frac{T}{m} \sin(\theta_c - \alpha_1) - \frac{D}{m} \cos(\epsilon) - g \sin(\theta_f) - qw - \frac{F_c}{m} \sin(\theta_1 + \theta_f) \quad (4.59)$$

$$\dot{w} = -\frac{T}{m} \cos(\theta_c - a_1) - \frac{D}{m} \sin(\epsilon) + g \cos(\theta_f) + qu + \frac{F_c}{m} \cos(\theta_1 + \theta_f) \quad (4.60)$$

$$\dot{q} = T \cos(\theta_c - a_1) \frac{x_h}{I_y} - T \sin(\theta_c - a_1) \frac{h}{I_y} \quad (4.61)$$

$$\dot{\theta}_f = q \quad (4.62)$$

With:

$$\sin(\epsilon) = \frac{w}{V}; \cos(\epsilon) = \frac{u}{V} \quad (4.63)$$

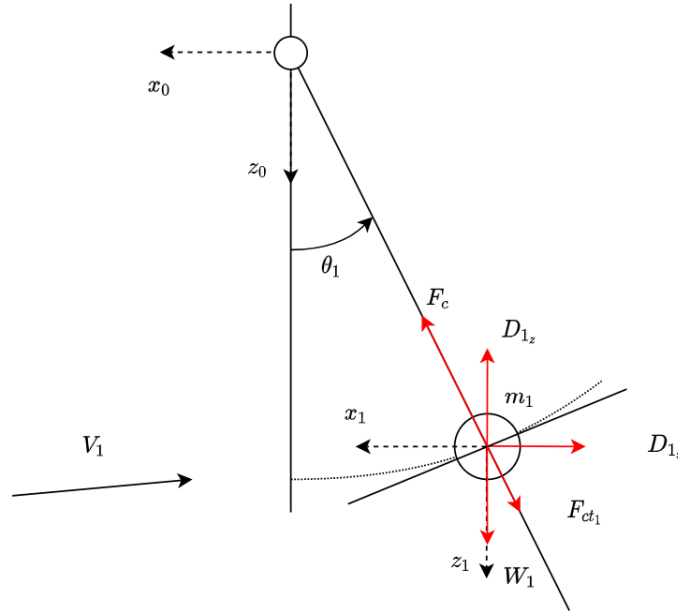


Figure 4.17: Diagram of single pendulum model.

4.4.3. Trimming

Trimming is done via the procedure in 3-DOF-PH-HUB-CG. This leads to the following expressions

$$\theta_c = a_1 + \tan^{-1} \left(\frac{x_h}{h} \right) \quad (4.64)$$

$$\tan(\theta_f) = \frac{x_h [W + F_c \cos(\theta_1)] - h [D + F_c \sin(\theta_1)]}{x_h [D + F_c \sin(\theta_1)] + h [W + F_c \cos(\theta_1)]} \quad (4.65)$$

$$T = \sqrt{([D + F_c \sin(\theta_1)] \cos(\theta_f) + [W + F_c \cos(\theta_1)] \sin(\theta_f))^2 + ([W + F_c \cos(\theta_1)] \cos(\theta_f) - [D + F_c \sin(\theta_1)] \sin(\theta_f))^2} \quad (4.66)$$

$$\tan(\theta_1) = \frac{D_1}{W_1}; F_c = \sqrt{W_1^2 + D_1^2} \quad (4.67)$$

The trimmed condition is then found using Equation 4.44. The trim curve is presented in Figure 4.18.

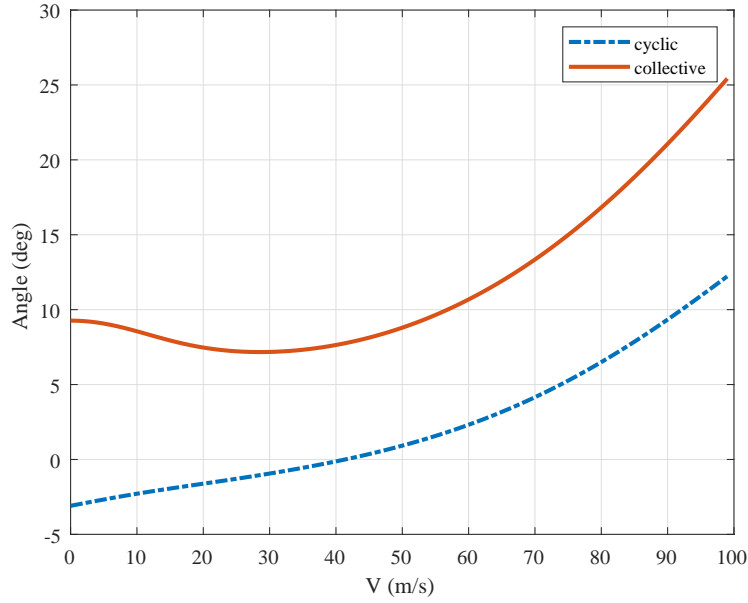


Figure 4.18: Trim curve for case 3-DOF-SP-CG-HUB-OFF.

4.4.4. Model Linearisation

For creating a linear system, two extra states are added: $\dot{\theta}_1$ and θ_1 . This leads to the linear system in Equation 4.68. This means that also the partial derivatives of these states are required as well. The derivatives of \dot{q} and θ_f are the same as for the case with the pure helicopter with offset rotor hub. Their partial derivatives with the load angle θ_1 and its rate are equal to zero. Also note the subscript SP , PH and PH_{OFF} . These indicate the partial derivative for the single pendulum, pure helicopter and pure helicopter with offset rotor hub respectively. Partial derivatives of components of the pendulum equations of motion can be found in Appendix B.

Derivatives of $\ddot{\theta}_1$

$$\begin{bmatrix} \dot{u} \\ \dot{w} \\ \dot{q} \\ \dot{\theta}_f \\ \ddot{\theta}_1 \\ \dot{\theta}_1 \end{bmatrix} = \begin{bmatrix} \frac{\partial \dot{u}}{\partial u} & \frac{\partial \dot{u}}{\partial w} & \frac{\partial \dot{u}}{\partial q} & \frac{\partial \dot{u}}{\partial \theta_f} & \frac{\partial \dot{u}}{\partial \dot{\theta}_1} & \frac{\partial \dot{u}}{\partial \theta_1} \\ \frac{\partial \dot{w}}{\partial u} & \frac{\partial \dot{w}}{\partial w} & \frac{\partial \dot{w}}{\partial q} & \frac{\partial \dot{w}}{\partial \theta_f} & \frac{\partial \dot{w}}{\partial \dot{\theta}_1} & \frac{\partial \dot{w}}{\partial \theta_1} \\ \frac{\partial \dot{q}}{\partial u} & \frac{\partial \dot{q}}{\partial w} & \frac{\partial \dot{q}}{\partial q} & \frac{\partial \dot{q}}{\partial \theta_f} & \frac{\partial \dot{q}}{\partial \dot{\theta}_1} & \frac{\partial \dot{q}}{\partial \theta_1} \\ \frac{\partial \dot{\theta}_f}{\partial u} & \frac{\partial \dot{\theta}_f}{\partial w} & \frac{\partial \dot{\theta}_f}{\partial q} & \frac{\partial \dot{\theta}_f}{\partial \theta_f} & \frac{\partial \dot{\theta}_f}{\partial \dot{\theta}_1} & \frac{\partial \dot{\theta}_f}{\partial \theta_1} \\ \frac{\partial \ddot{\theta}_1}{\partial u} & \frac{\partial \ddot{\theta}_1}{\partial w} & \frac{\partial \ddot{\theta}_1}{\partial q} & \frac{\partial \ddot{\theta}_1}{\partial \theta_f} & \frac{\partial \ddot{\theta}_1}{\partial \dot{\theta}_1} & \frac{\partial \ddot{\theta}_1}{\partial \theta_1} \\ \frac{\partial \dot{\theta}_1}{\partial u} & \frac{\partial \dot{\theta}_1}{\partial w} & \frac{\partial \dot{\theta}_1}{\partial q} & \frac{\partial \dot{\theta}_1}{\partial \theta_f} & \frac{\partial \dot{\theta}_1}{\partial \dot{\theta}_1} & \frac{\partial \dot{\theta}_1}{\partial \theta_1} \end{bmatrix} \begin{bmatrix} u \\ w \\ q \\ \theta_f \\ \dot{\theta}_1 \\ \theta_1 \end{bmatrix} + \begin{bmatrix} \frac{\partial \dot{u}}{\partial \theta_c} & \frac{\partial \dot{u}}{\partial \theta_0} \\ \frac{\partial \dot{w}}{\partial \theta_c} & \frac{\partial \dot{w}}{\partial \theta_0} \\ \frac{\partial \dot{q}}{\partial \theta_c} & \frac{\partial \dot{q}}{\partial \theta_0} \\ \frac{\partial \dot{\theta}_f}{\partial \theta_c} & \frac{\partial \dot{\theta}_f}{\partial \theta_0} \\ \frac{\partial \ddot{\theta}_1}{\partial \theta_c} & \frac{\partial \ddot{\theta}_1}{\partial \theta_0} \\ \frac{\partial \dot{\theta}_1}{\partial \theta_c} & \frac{\partial \dot{\theta}_1}{\partial \theta_0} \end{bmatrix} \begin{bmatrix} \theta_c \\ \theta_0 \end{bmatrix} \quad (4.68)$$

Partial Derivatives of \dot{u}

$$\frac{\partial \dot{u}}{\partial u_{SP}} = \frac{\partial \dot{u}}{\partial u_{PH}} - \frac{\partial F_c \sin(\theta_1 + \theta_f)}{\partial u} \frac{1}{m} \quad (4.69)$$

$$\frac{\partial \dot{u}}{\partial w_{SP}} = \frac{\partial \dot{u}}{\partial w_{PH}} - \frac{\partial F_c \sin(\theta_1 + \theta_f)}{\partial w} \frac{1}{m} \quad (4.70)$$

$$\frac{\partial \dot{u}}{\partial q_{SP}} = \frac{\partial \dot{u}}{\partial q_{PH_{OFF}}} \quad (4.71)$$

$$\frac{\partial \dot{u}}{\partial \theta_{f_{SP}}} = \frac{\partial \dot{u}}{\partial \theta_{f_{PH}}} - \frac{F_c}{m} \cos(\theta_1 + \theta_f) - \frac{\partial F_c \sin(\theta_1 + \theta_f)}{\partial \theta_f} \frac{1}{m} \quad (4.72)$$

$$\frac{\partial \dot{u}}{\partial \dot{\theta}_{1 SP}} = -\frac{\partial F_c \sin(\theta_1 + \theta_f)}{\partial \dot{\theta}_1 m} \quad (4.73)$$

$$\frac{\partial \dot{u}}{\partial \theta_{1 SP}} = -\frac{F_c}{m} \cos(\theta_1 + \theta_f) - \frac{\partial F_c \sin(\theta_1 + \theta_f)}{\partial \theta_1 m} \quad (4.74)$$

$$\frac{\partial \dot{u}}{\partial \theta_{c SP}} = \frac{\partial \dot{u}}{\partial \theta_{c PH}} \quad (4.75)$$

$$\frac{\partial \dot{u}}{\partial \theta_{0 SP}} = \frac{\partial \dot{u}}{\partial \theta_{0 PH}} \quad (4.76)$$

Partial Derivatives of \dot{w}

$$\frac{\partial \dot{w}}{\partial u_{SP}} = \frac{\partial \dot{u}}{\partial u_{PH}} + \frac{\partial F_c \cos(\theta_1 + \theta_f)}{\partial u m} \quad (4.77)$$

$$\frac{\partial \dot{w}}{\partial w_{SP}} = \frac{\partial \dot{u}}{\partial w_{PH}} + \frac{\partial F_c \cos(\theta_1 + \theta_f)}{\partial w m} \quad (4.78)$$

$$\frac{\partial \dot{w}}{\partial q_{SP}} = \frac{\partial \dot{u}}{\partial q_{PH}} \quad (4.79)$$

$$\frac{\partial \dot{w}}{\partial \theta_{f SP}} = \frac{\partial \dot{u}}{\partial \theta_{f PH}} - \frac{F_c}{m} \sin(\theta_1 + \theta_f) + \frac{\partial F_c \cos(\theta_1 + \theta_f)}{\partial \theta_f m} \quad (4.80)$$

$$\frac{\partial \dot{w}}{\partial \dot{\theta}_{1 SP}} = \frac{\partial F_c \cos(\theta_1 + \theta_f)}{\partial \dot{\theta}_1 m} \quad (4.81)$$

$$\frac{\partial \dot{w}}{\partial \theta_{1 SP}} = -\frac{F_c}{m} \sin(\theta_1 + \theta_f) + \frac{\partial F_c \cos(\theta_1 + \theta_f)}{\partial \theta_1 m} \quad (4.82)$$

$$\frac{\partial \dot{w}}{\partial \theta_{c SP}} = \frac{\partial \dot{w}}{\partial \theta_{c PH}} \quad (4.83)$$

$$\frac{\partial \dot{w}}{\partial \theta_{0 SP}} = \frac{\partial \dot{w}}{\partial \theta_{0 PH}} \quad (4.84)$$

Partial Derivatives of $\ddot{\theta}_1$

$$\frac{\partial \ddot{\theta}_1}{\partial u} = \frac{\partial \ddot{\theta}_1}{\partial Q_1} \frac{\partial Q_1}{\partial u} + \frac{\ddot{\theta}_1}{\partial \ddot{x}_0} \frac{\partial \ddot{x}_0}{\partial u} + \frac{\ddot{\theta}_1}{\partial \ddot{z}_0} \frac{\partial \ddot{z}_0}{\partial u} \quad (4.85)$$

$$\frac{\partial \ddot{\theta}_1}{\partial w} = \frac{\partial \ddot{\theta}_1}{\partial Q_1} \frac{\partial Q_1}{\partial w} + \frac{\ddot{\theta}_1}{\partial \ddot{x}_0} \frac{\partial \ddot{x}_0}{\partial w} + \frac{\ddot{\theta}_1}{\partial \ddot{z}_0} \frac{\partial \ddot{z}_0}{\partial w} \quad (4.86)$$

$$\frac{\partial \ddot{\theta}_1}{\partial q} = \frac{\ddot{\theta}_1}{\partial \ddot{x}_0} \frac{\partial \ddot{x}_0}{\partial q} + \frac{\ddot{\theta}_1}{\partial \ddot{z}_0} \frac{\partial \ddot{z}_0}{\partial q} \quad (4.87)$$

$$\frac{\partial \ddot{\theta}_1}{\partial \theta_f} = \frac{\partial \ddot{\theta}_1}{\partial Q_1} \frac{\partial Q_1}{\partial \theta_f} + \frac{\ddot{\theta}_1}{\partial \ddot{x}_0} \frac{\partial \ddot{x}_0}{\partial \theta_f} + \frac{\ddot{\theta}_1}{\partial \ddot{z}_0} \frac{\partial \ddot{z}_0}{\partial \theta_f} \quad (4.88)$$

$$\frac{\partial \ddot{\theta}_1}{\partial \dot{\theta}_1} = \frac{\partial \ddot{\theta}_1}{\partial Q_1} \frac{\partial Q_1}{\partial \dot{\theta}_1} + \frac{\ddot{\theta}_1}{\partial \ddot{x}_0} \frac{\partial \ddot{x}_0}{\partial \dot{\theta}_1} + \frac{\ddot{\theta}_1}{\partial \ddot{z}_0} \frac{\partial \ddot{z}_0}{\partial \dot{\theta}_1} \quad (4.89)$$

$$\frac{\partial \ddot{\theta}_1}{\partial \theta_1} = \frac{\partial \ddot{\theta}_1}{\partial Q_1} \frac{\partial Q_1}{\partial \theta_1} + \frac{\ddot{\theta}_1}{\partial \ddot{x}_0} \frac{\partial \ddot{x}_0}{\partial \theta_1} + \frac{\ddot{\theta}_1}{\partial \ddot{z}_0} \frac{\partial \ddot{z}_0}{\partial \theta_1} - \frac{g}{l_1} \cos(\theta_1) \quad (4.90)$$

$$\frac{\ddot{\theta}_1}{\partial \theta_c} = \frac{\ddot{\theta}_1}{\partial \ddot{x}_0} \frac{\partial \ddot{x}_0}{\partial \theta_c} + \frac{\ddot{\theta}_1}{\partial \ddot{z}_0} \frac{\partial \ddot{z}_0}{\partial \theta_c} \quad (4.91)$$

$$\frac{\ddot{\theta}_1}{\partial \theta_0} = \frac{\ddot{\theta}_1}{\partial \ddot{x}_0} \frac{\partial \ddot{x}_0}{\partial \theta_0} + \frac{\ddot{\theta}_1}{\partial \ddot{z}_0} \frac{\partial \ddot{z}_0}{\partial \theta_0} \quad (4.92)$$

Partial Derivatives of $\dot{\theta}_1$

$$\frac{\partial \dot{\theta}_1}{\partial u} = \frac{\partial \dot{\theta}_1}{\partial w} = \frac{\partial \dot{\theta}_1}{\partial q} = \frac{\partial \dot{\theta}_1}{\partial \theta_f} = \frac{\partial \dot{\theta}_1}{\partial \theta_c} = \frac{\partial \dot{\theta}_1}{\partial \theta_0} = \frac{\partial \dot{\theta}_1}{\partial \theta_1} = 0 \tag{4.93}$$

$$\frac{\partial \dot{\theta}_1}{\partial \dot{\theta}_1} = 1 \tag{4.94}$$

The resulting system when trimming for a velocity of 1 m/s is presented in Equation 4.95.

$$\begin{bmatrix} \dot{u} \\ \dot{w} \\ \dot{q} \\ \dot{\theta}_f \\ \ddot{\theta}_1 \\ \dot{\theta}_1 \end{bmatrix} = \begin{bmatrix} -0.021 & -0.053 & 0.877 & -11.577 & 0.000 & -1.781 \\ -0.052 & -0.981 & 0.954 & 0.626 & 0.000 & -0.096 \\ 0.011 & 0.000 & -0.540 & 0.000 & 0.000 & 0.000 \\ 0.000 & 0.000 & 1.000 & 0.000 & 0.000 & 0.000 \\ -0.001 & 0.000 & 0.027 & -0.386 & -0.002 & -0.386 \\ 0.000 & 0.000 & 0.000 & 0.000 & 1.000 & 0.000 \end{bmatrix} \begin{bmatrix} u \\ w \\ q \\ \theta_f \\ \dot{\theta}_1 \\ \theta_1 \end{bmatrix} + \begin{bmatrix} 11.630 & -7.859 \\ 0.357 & -142.760 \\ -7.602 & 0.093 \\ 0.000 & 0.000 \\ 0.386 & -0.005 \\ 0.000 & 0.000 \end{bmatrix} \begin{bmatrix} \theta_c \\ \theta_0 \end{bmatrix} \tag{4.95}$$

Again, the linearised model is verified by simulating it to the disturbance in 3-DOF-PH-HUB-CG. the response of the models is shown in Figure 4.19. Similarly to the previous cases, the model matches well until 15 seconds after which it diverges. Nevertheless, the linear model appears to approximate the non-linear model very well around the trimmed condition.

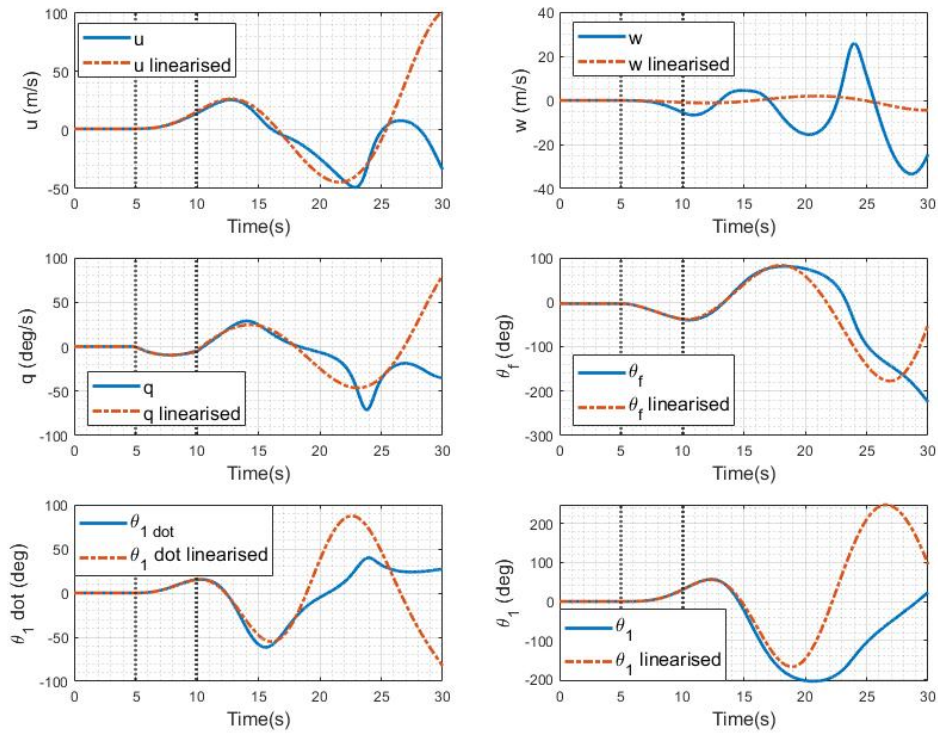


Figure 4.19: Response of linear and non-linear hovering helicopter model case 3-DOF-SP-CG-HUB-OFF to input disturbance on cyclic of 1 degree for 5 seconds.

4.4.5. Stability Analysis

Stability of the helicopter is assessed by obtaining the poles of the linearised system. The poles of this linear system are presented in Figure 4.20 with their exact location in Table 4.5. Note that the phugoid

mode of the helicopter model is still unstable. Also, there are two additional poles. These belong to the single pendulum. This pole is also unstable at the trimmed condition.

Table 4.5: Poles of case 3-DOF-SP-CG-HUB-OFF, where the linearised single pendulum model with the pendulum attached at the c.g. of the helicopter trimmed at $V = 1$ m/s.

Pole	Real part	Complex part	Mode
1	-0.985	0.000	-
2	-0.764	0.000	Short Period
3	0.019	0.632	Pendulum
4	0.019	-0.632	Pendulum
5	0.084	0.364	Phugoid
6	0.084	-0.364	Phugoid

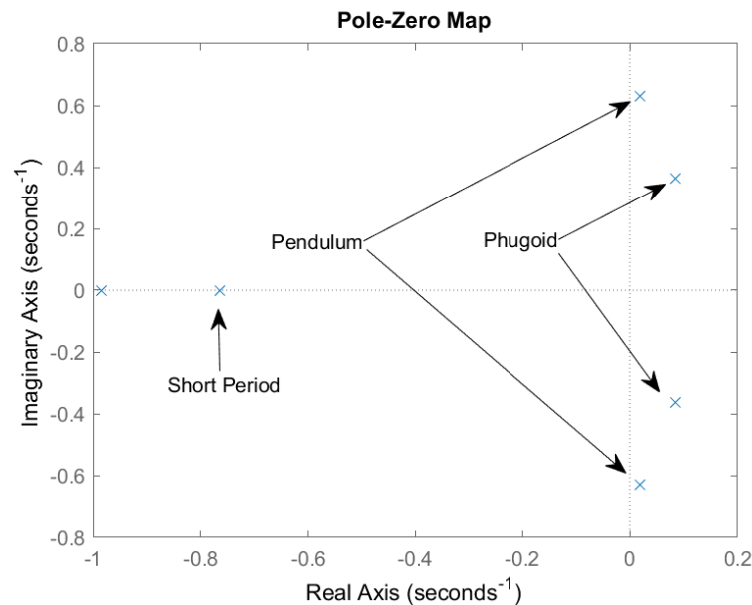


Figure 4.20: Pole-Zero map of linearised system for case 3-DOF-SP-CG-HUB-OFF, trimmed at $V = 1$ m/s.

4.4.6. Controller Design

Now that there is a load attached to the helicopter, the controller around the pitch angle θ_f controller is no longer a velocity controller for the horizontal body velocity u_x , but for a controller for the cable angle θ_1 . The controllers for the pitch angle θ_f and the vertical body velocity w will remain the same. However, the gains of the pitch angle controller PID have changed to -0.296 and 0.208 for $K_{p\theta_f}$ and $K_{d\theta_f}$ respectively. These gains have changed due to the changed partial derivatives. The gains for the INDI controllers remain the same, since this change is incorporated into the model inversion.

There will be 2 cable controllers: a PID cable controller and an INDI cable controller. The PID cable controller will be added around the PID pitch angle controller and the INDI cable controller will be added around the INDI pitch angle controller.

PID controller

The PID cable controller will be a PID controller, where the reference pitch angle is equal to $\theta_{fc} =$

$Kp_{\theta_1} e_{\theta_1} + Ki_{\theta_1} \int e_{\theta_1} dt + Kd_{\theta_1} \dot{e}_{\theta_1}$. The gains could not be obtained analytically, since this involves solving a 4th order equation. Therefore, the gains were obtained empirically, using trial and error. The gains that provided a satisfactory result are: $Kp_{\theta_1} = -0.1$, $Ki_{\theta_1} = -0.01$ and $Kd_{\theta_1} = -1.5$. During tuning, it was found that an integral component is necessary to bring the cable angle back to its reference, since steady state errors otherwise occur.

INDI controller

The INDI cable controller is a 2-loop controller, similar in structure as the INDI pitch angle controller. The inner cable angle rate loop is a PD controller and the outer cable angle loop is also a PD controller. Similarly to the PID controller, the controller gains are found empirically. The cable controller gains were tuned to: $Kp_{\theta_1} = 0.1$, $Kd_{\theta_1} = -0.6$, $Kp_{\dot{\theta}_1} = 0.1$ and $Kd_{\dot{\theta}_1} = -1.5$. Furthermore, the model inversion used was the partial derivative $\frac{\dot{\theta}_1}{\theta_f}^{-1}$. Also, it was found that, to make the controller work, the control input had to be integrated rather than summed.

4.4.7. Assessing Controllers

Subjecting both controllers to the disturbance from case 3-DOF-PH-HUB-CG, will enable the assessment of both cable controlled system. The response of the helicopter is given in Figure 4.21, with the control inputs given in Figure 4.22 and Figure 4.23. Judging from the responses, both controllers appear capable of controlling the cable and bringing the cable angle back. The INDI controller appears to stabilise the cable fast, but converges to the steady state slowly. This conclusion is based on the fact that the velocity is non-zero at $t = 30$. The PID controller appears to perform better, but behaves more aggressively. This is likely caused by the integral component of the controller. This aggressive behaviour is also visible in the control inputs.

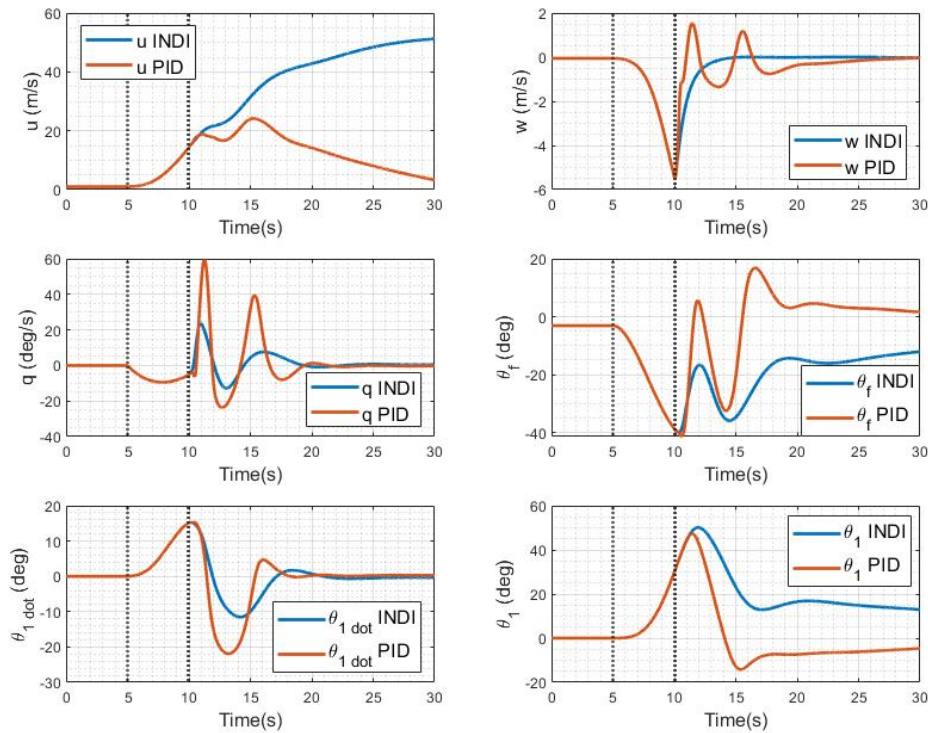


Figure 4.21: Response controlled hovering helicopter case 3-DOF-SP-CG-HUB-OFF to input disturbance on cyclic of 1 degree for 5 seconds.

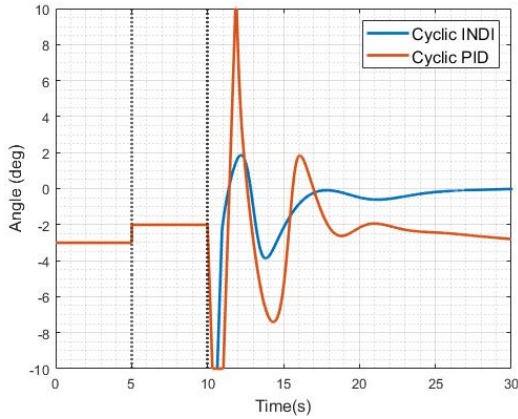


Figure 4.22: Cyclic control of the controlled hovering helicopter case 3-DOF-SP-CG-HUB-OFF to input disturbance on cyclic of 1 degree for 5 seconds.

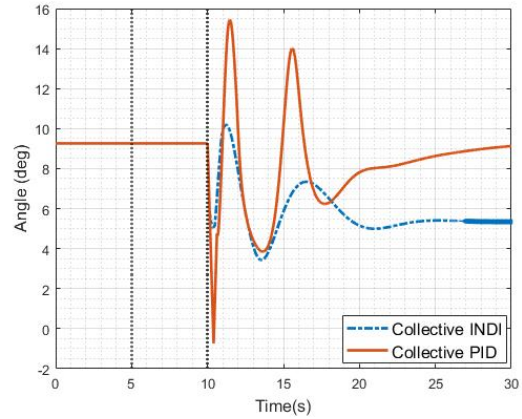


Figure 4.23: Collective control of the controlled hovering helicopter case 3-DOF-SP-CG-HUB-OFF to input disturbance on cyclic of 1 degree for 5 seconds.

4.5. Case 3-DOF-SP-OFF-HUB-OFF

4.5.1. Configuration

In this case, the configuration is changed by moving the load forward by a distance x_l as shown in Figure 4.24.

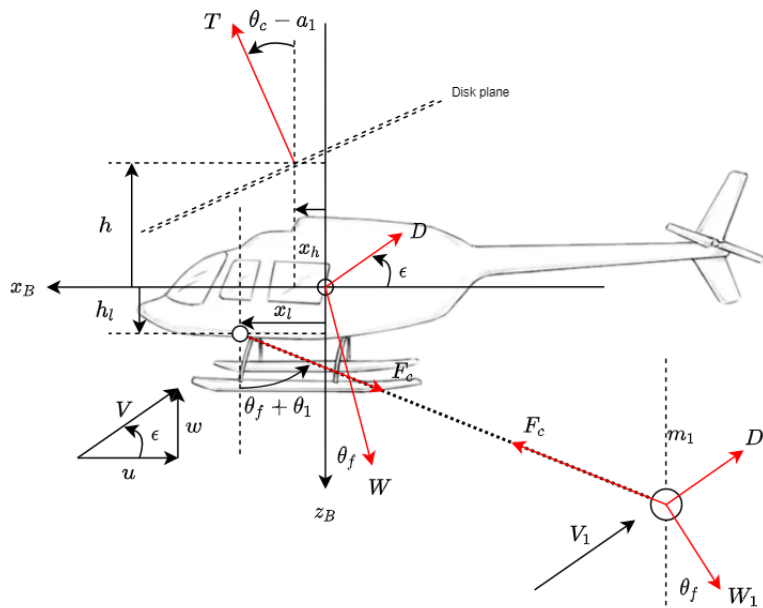


Figure 4.24: Diagram of hcase 3-DOF-SP-OFF-HUB-OFF.

4.5.2. Equations of Motion

The equations of motion for this configuration are very similar to those of case 3. The only changed equation of motion is the equation for the pitch rate. The adjusted equation for the pitch rate is given in

Equation 4.96.

$$\dot{q} = T \cos(\theta_c - a_1) \frac{x_h}{I_y} - T \sin(\theta_c - a_1) \frac{h}{I_y} - F_c \sin(\theta_1 + \theta_f) \frac{h_l}{I_y} - F_c \cos(\theta_1 + \theta_f) \frac{x_l}{I_y} \quad (4.96)$$

4.5.3. Trimming

The equations for the trimmed condition are:

$$\tan(\theta_c - a_1) = \frac{[D + F_c \sin(\theta_1)] \cos(\theta_f) + [W + F_c \cos(\theta_1)] \sin(\theta_f)}{[W + F_c \cos(\theta_1)] \cos(\theta_f) - [D + F_c \sin(\theta_1)] \sin(\theta_f)} \quad (4.97)$$

$$\tan(\theta_f) = \frac{W x_h - D h + F_c ([x_h - x_l] \cos(\theta_1) - [h + h_l] \sin(\theta_1))}{W h + D x_h + F_c ([h + h_l] \cos(\theta_1) + [x_h - x_l] \sin(\theta_1))} \quad (4.98)$$

The equation for the thrust magnitude is the same as in case 3, since the magnitude and direction of the forces has not changed. The linear system to be solved is then:

$$\begin{bmatrix} \theta_c \\ \theta_0 \end{bmatrix} = \begin{bmatrix} 1 + \frac{3}{2}\mu^2 & -\frac{8}{3}\mu \\ -\mu & \frac{2}{3} + \mu^2 \end{bmatrix}^{-1} \begin{bmatrix} -2\mu^2\alpha_d - 2\mu\lambda_i \\ \frac{4}{\sigma} \frac{C_T}{c_l \alpha} - \mu\theta_f + \lambda_i \end{bmatrix} + \begin{bmatrix} \tan^{-1}(\tan(\theta_c - a_1)) \\ 0 \end{bmatrix} \quad (4.99)$$

with:

$$\alpha_d = (\theta_c - a_1) - \theta_f \quad (4.100)$$

Choosing an x_l value of 0.5m and a h_l value of 1.0m, the trim curve is given by Figure 4.25.

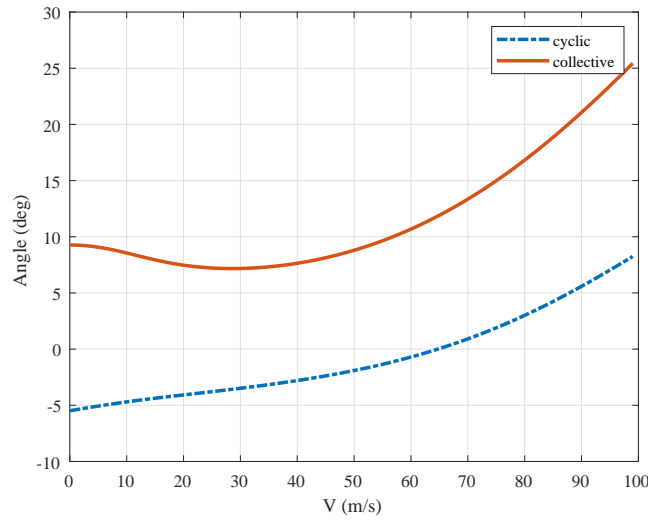


Figure 4.25: Trim curve for case 4, where the single pendulum is offset with the c.g.

4.5.4. Model Linearisation

Only the partial derivatives of q need to be found of the 2 latter terms of Equation 4.96. The other partial derivatives are found in previous cases. This leads to the following partial derivatives:

$$\frac{\partial \dot{q}}{\partial u_{SP_{OFF}}} = \frac{\partial \dot{q}}{\partial u_{PH_{OFF}}} - \frac{\partial F_c h_l \sin(\theta_1 + \theta_f)}{\partial u I_y} - \frac{\partial F_c x_l \cos(\theta_1 + \theta_f)}{\partial u I_y} \quad (4.101)$$

$$\frac{\partial \dot{q}}{\partial w_{SP_{OFF}}} = \frac{\partial \dot{q}}{\partial w_{PH_{OFF}}} - \frac{\partial F_c h_l \sin(\theta_1 + \theta_f)}{\partial w I_y} - \frac{\partial F_c x_l \cos(\theta_1 + \theta_f)}{\partial w I_y} \quad (4.102)$$

$$\frac{\partial \dot{q}}{\partial q_{SP_{OFF}}} = \frac{\partial \dot{q}}{\partial q_{PH_{OFF}}} \quad (4.103)$$

$$\frac{\partial \dot{q}}{\partial \theta_f}_{SP_{OFF}} = \frac{\partial \dot{q}}{\partial \theta_f}_{PH_{OFF}} - \frac{\partial F_c}{\partial \theta_f} \frac{h_l \sin(\theta_1 + \theta_f)}{I_y} - \frac{F_c h_l}{I_y} \cos(\theta_1 + \theta_f) - \frac{\partial F_c}{\partial \theta_f} \frac{x_l \cos(\theta_1 + \theta_f)}{I_y} + \frac{F_c x_l}{I_y} \sin(\theta_1 + \theta_f) \quad (4.104)$$

$$\frac{\partial \dot{q}}{\partial \dot{\theta}_1}_{SP_{OFF}} = -\frac{\partial F_c}{\partial \dot{\theta}_1} \frac{h_l \sin(\theta_1 + \theta_f)}{I_y} - \frac{\partial F_c}{\partial \dot{\theta}_1} \frac{x_l \cos(\theta_1 + \theta_f)}{I_y} \quad (4.105)$$

$$\frac{\partial \dot{q}}{\partial \theta_1}_{SP_{OFF}} = -\frac{\partial F_c}{\partial \theta_1} \frac{h_l \sin(\theta_1 + \theta_f)}{I_y} - \frac{F_c h_l}{I_y} \cos(\theta_1 + \theta_f) - \frac{\partial F_c}{\partial \theta_1} \frac{x_l \cos(\theta_1 + \theta_f)}{I_y} + \frac{F_c x_l}{I_y} \sin(\theta_1 + \theta_f) \quad (4.106)$$

$$\frac{\partial \dot{q}}{\partial \theta_c}_{SP_{OFF}} = \frac{\partial \dot{q}}{\partial \theta_c}_{PH_{OFF}} \quad (4.107)$$

$$\frac{\partial \dot{q}}{\partial \theta_0}_{SP_{OFF}} = \frac{\partial \dot{q}}{\partial \theta_0}_{PH_{OFF}} \quad (4.108)$$

Trimming the helicopter at a velocity of 1 m/s, and linearising the equations of motion, the following linear system in Equation 4.109 is obtained.

$$\begin{bmatrix} \dot{u} \\ \dot{w} \\ \dot{q} \\ \dot{\theta}_f \\ \ddot{\theta}_1 \\ \dot{\theta}_1 \end{bmatrix} = \begin{bmatrix} -0.027 & -0.092 & 0.916 & -11.540 & 0.000 & -1.775 \\ 0.0920 & -0.975 & 0.917 & 1.109 & 0.000 & -0.170 \\ 0.014 & 0.026 & -0.540 & -0.823 & 0.000 & -0.823 \\ 0.000 & 0.000 & 1.000 & 0.000 & 0.000 & 0.000 \\ -0.001 & 0.000 & 0.027 & -0.386 & -0.002 & -0.386 \\ 0.000 & 0.000 & 0.000 & 0.000 & 1.000 & 0.000 \end{bmatrix} \begin{bmatrix} u \\ w \\ q \\ \theta_f \\ \dot{\theta}_1 \\ \theta_1 \end{bmatrix} + \begin{bmatrix} 11.635 & -13.811 \\ -0.129 & -142.308 \\ -7.622 & 4.006 \\ 0.000 & 0.000 \\ 0.386 & -0.005 \\ 0.000 & 0.000 \end{bmatrix} \begin{bmatrix} \theta_c \\ \theta_0 \end{bmatrix} \quad (4.109)$$

Again, the linearised model is verified by simulating it to the disturbance in 3-DOF-PH-HUB-CG. the response of the models is shown in Figure 4.26. Similarly to the previous cases, the model matches well until 15 seconds after which it diverges, which is also similar to previous cases. Nevertheless, the linear model appears to approximate the non-linear model very well around the trimmed condition.

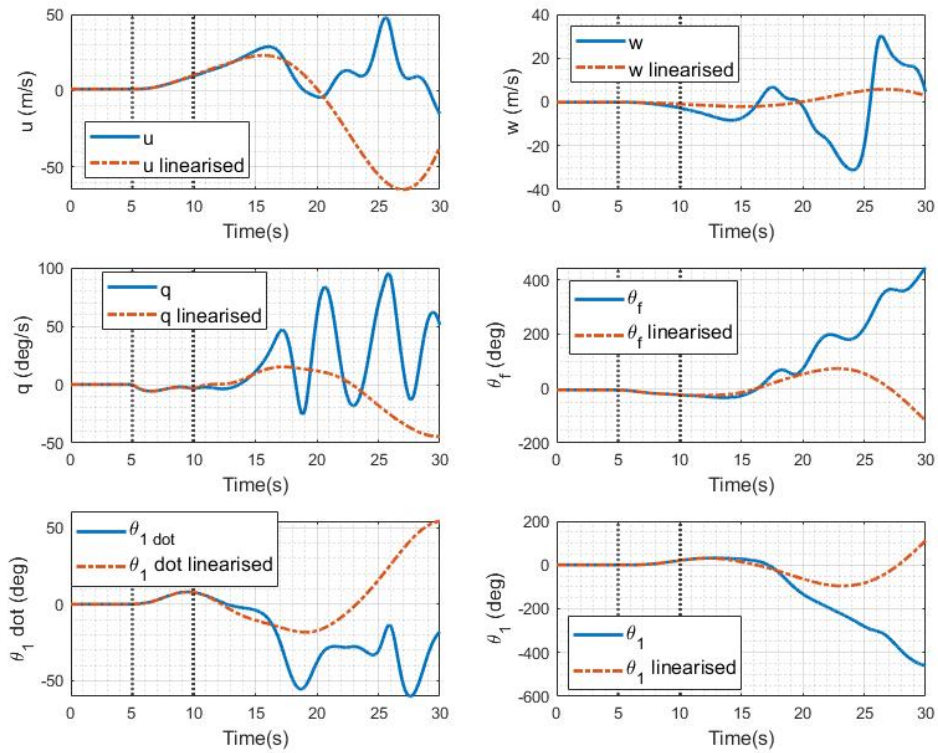


Figure 4.26: Response of linear and non-linear hovering helicopter model case 3-DOF-SP-OFF-HUB-OFF to input disturbance on cyclic of 1 degree for 5 seconds.

4.5.5. Stability Analysis

The poles of the linear system are presented in Table 4.6. Note the two stable pendulum poles (3 and 4) and the two unstable phugoid poles (5 and 6). It appears that the pendulum poles have become stable after moving the load location forward on the helicopter.

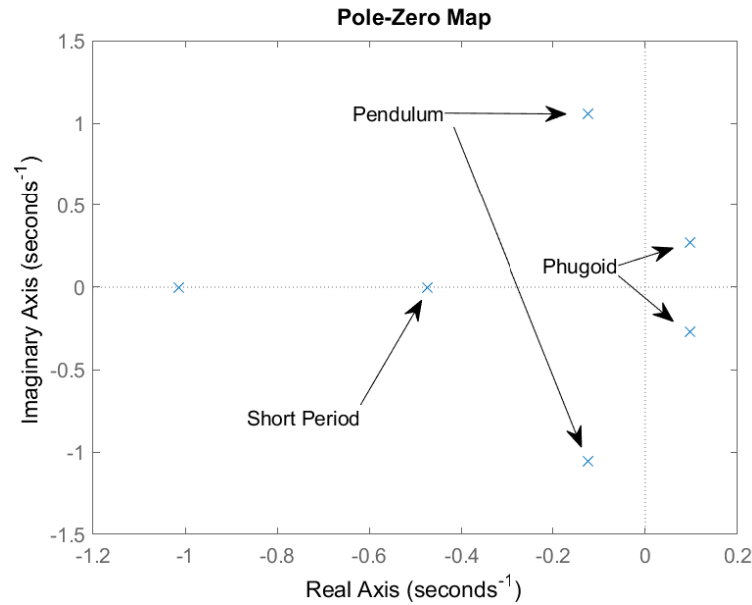


Figure 4.27: Pole-Zero map of linearised system for case 4, trimmed at $V = 1$ m/s.

Table 4.6: Poles of the linearised single pendulum model with the pendulum attached at an offset w.r.t the c.g. of the helicopter trimmed at $V = 1$ m/s.

Pole	Real part	Complex part	
1	-1.014	0.000	-
2	-0.475	0.000	Short Period
3	-0.123	1.058	Pendulum
4	-0.123	-1.058	Pendulum
5	0.096	0.274	Phugoid
6	0.096	-0.274	Phugoid

4.5.6. Assessing Controllers

For this case, the same controllers are used as in case 3-DOF-SP-CG-HUB-OFF. Assessment is done by subjecting both controllers to the disturbance from case 3-DOF-PH-HUB-CG. The response of the helicopter is given in Figure 4.28, with the control inputs in Figure 4.29 and Figure 4.30. The shape response of the helicopter is almost exactly the same as in case 3-DOF-SP-CG-HUB-OFF. However, the cable controller is less aggressive. Especially the response of the PID has improved by moving the cable load. This suggests that the helicopter-cable system became more stable by moving the load forward and down. This is backed up by the stable pendulum poles found when linearising the non-linear system. Generally, both cable controllers are capable of handling the disturbance, given that the load moved forward and down. The performance of both controllers has improved.

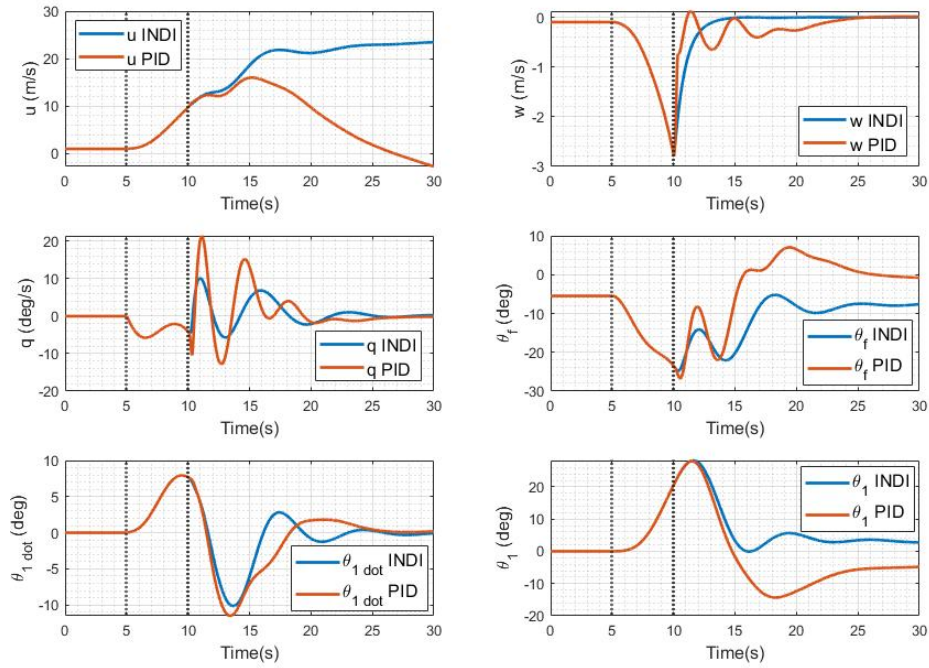


Figure 4.28: Response controlled hovering helicopter case 3-DOF-SP-OFF-HUB-OFF to input disturbance on cyclic of 1 degree for 5 seconds.

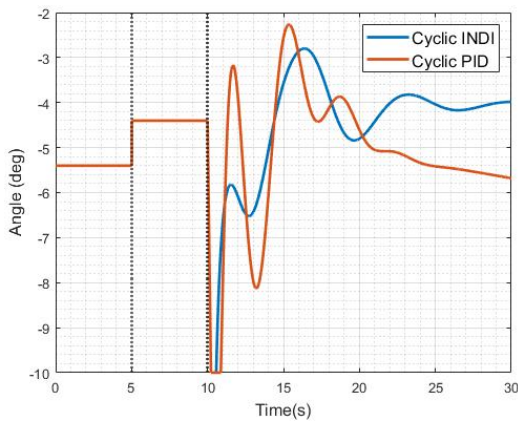


Figure 4.29: Cyclic control of the controlled hovering helicopter case 3-DOF-SP-OFF-HUB-OFF to input disturbance on cyclic of 1 degree for 5 seconds.

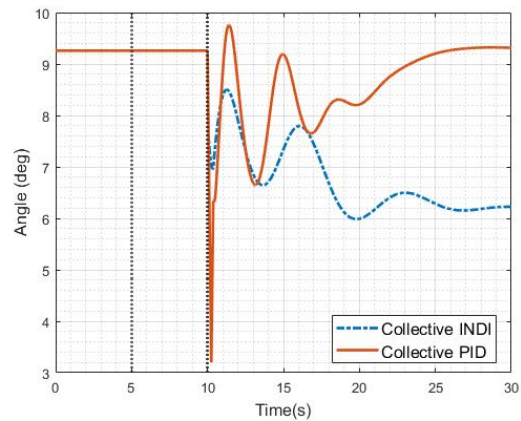


Figure 4.30: Collective control of the controlled hovering helicopter case 3-DOF-SP-OFF-HUB-OFF to input disturbance on cyclic of 1 degree for 5 seconds.

4.6. Case 3-DOF-DP-OFF-HUB-OFF

4.6.1. Configuration

With this configuration, a step is made in the direction where part of the cable is submerged, and a part emerged. For this, a double pendulum model is used where the first load is the lumped mass of the emerged cable, and the second load is the lumped mass of the submerged cable and the mass of the SONAR. For this case, the configuration is flown in the air, meaning that both loads are emerged. The configuration is shown in Figure 4.31. The double pendulum model is shown in Figure 4.32.

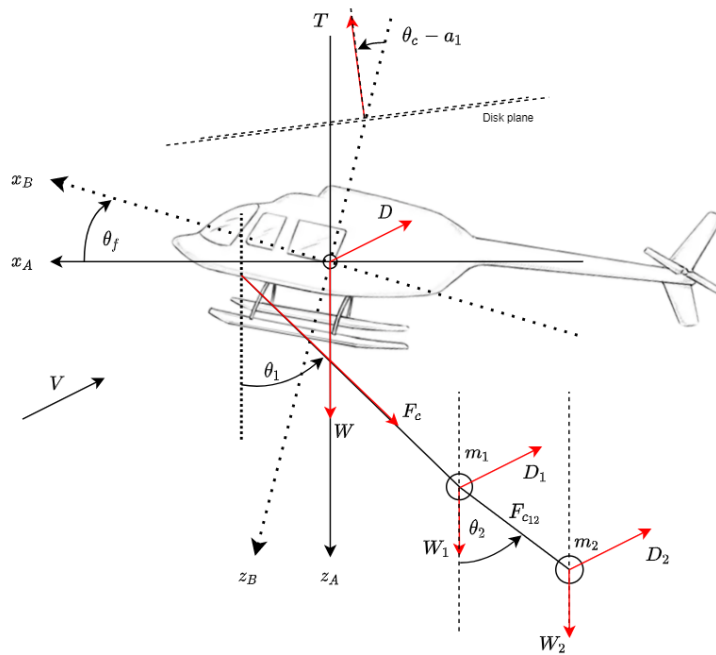


Figure 4.31: Diagram of case 3-DOF-DP-OFF-HUB-OFF.

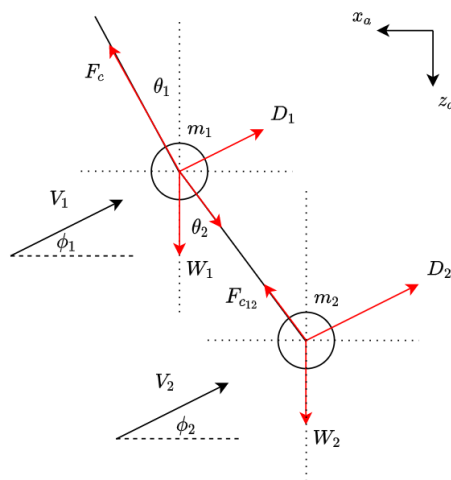


Figure 4.32: Diagram of the double pendulum model.

4.6.2. Equations of Motion

Since this is only a change in load model, the equations of motion of the helicopter do not change, hence they are the same as in Section 4.5.

Double Pendulum Model

The equations of motion for the double pendulum are given in case 3-DOF-SP-OFF-HUB-OFF. These equations of motion are derived using Lagrange's method. Here, Q_1 and Q_2 are the angular accelerations experienced due to drag. The cable force is computed using Equation 4.111 and Equation 4.112. F_{ct1} and F_{ct2} are the centrifugal forces experienced by the pendulum. These equations are derived using force equilibrium.

$$\begin{bmatrix} (m_1 + m_2) l_1^2 & 0.5 m_2 l_1 l_2 \cos(\theta_1 - \theta_2) \\ 0.5 m_2 l_1 l_2 \cos(\theta_1 - \theta_2) & m_2 l_2^2 \end{bmatrix} \begin{bmatrix} \ddot{\theta}_1 \\ \ddot{\theta}_2 \end{bmatrix} = \begin{bmatrix} (m_1 + m_2) (l_1 [\cos(\theta_1) \ddot{x}_0 + \sin(\theta_1) \ddot{z}_0] - l_1 g \sin(\theta_1)) - m_2 l_1 l_2 \dot{\theta}_2^2 \sin(\theta_1 - \theta_2) \\ m_2 (l_1 l_2 \dot{\theta}_1^2 \sin(\theta_1 - \theta_2) + l_2 [\cos(\theta_2) \ddot{x}_0 + \sin(\theta_2) \ddot{z}_0] - l_2 g \sin(\theta_2)) \end{bmatrix} + \begin{bmatrix} Q_1 \\ Q_2 \end{bmatrix} \quad (4.110)$$

$$F_c = D_{1_x} \sin(\theta_1) - D_{1_z} \cos(\theta_1) + W_1 \cos(\theta_1) + m_1 l_1 \dot{\theta}_1^2 + F_{c_{12}} \cos(\theta_1 - \theta_2) \quad (4.111)$$

$$F_{c_{12}} = F_{c_{t_2}} + D_{2_x} \sin(\theta_2) - D_{2_z} \cos(\theta_2) + W_2 \cos(\theta_2) \quad (4.112)$$

4.6.3. Trimming

Trimming is again done via the same procedure as in previous cases. The function of the thrust force is still the same as in Section 4.4. The equation for the fuselage angle and the angle $\theta_c - a_1$ are the same as in case 3-DOF-SP-OFF-HUB-OFF. The trimmed Cable force is equal to Equation 4.113 for horizontal flight. The corresponding angles θ_1 and θ_2 are given in Equation 4.114. The trim curve is presented in Figure 4.33

$$F_c = \sqrt{(W_1 + W_2)^2 + (D_{1_x} + D_{1_z})^2} \quad (4.113)$$

$$\tan(\theta_1) = \frac{D_1 + D_2}{W_1 + W_2}; \tan(\theta_2) = \frac{D_2}{W_2} \quad (4.114)$$

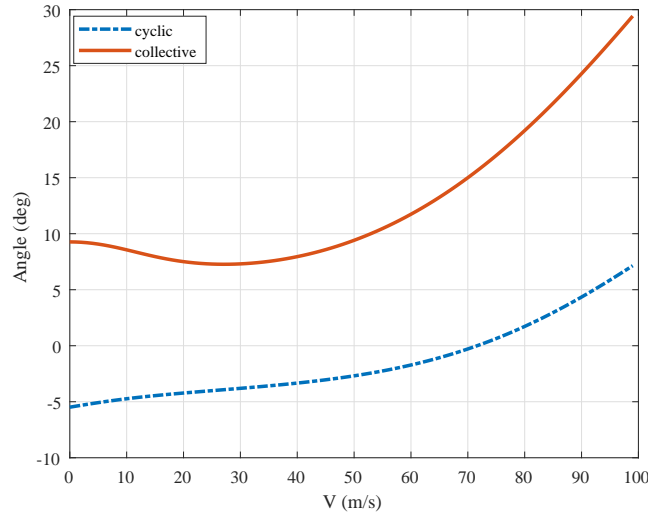


Figure 4.33: Trim curve for case 3-DOF-SP-OFF-HUB-OFF.

4.6.4. Model Linearisation

There are two new states in this system. These are the angle of the second pendulum θ_2 and its derivative $\dot{\theta}_2$. Hence, the linearised system will look like Equation 4.115. The partial derivatives of the states u , w , q and θ_f are presented below. These are only the partial derivatives that are new. The partial derivatives of the load angles θ_1 , θ_2 and their derivatives are derived and given in Appendix C this is also the case for the partial derivatives of the cable force F_c . Note subscript *DP*. This stands for "Double Pendulum" and indicates a partial derivative belonging to cases 3-DOF-SP-OFF-HUB-OFF and 3-DOF-SP-OFF-HUB-OFF-SUB, where the double pendulum is the load model.

$$\begin{bmatrix} \dot{u} \\ \dot{w} \\ \dot{q} \\ \dot{\theta}_f \\ \dot{\theta}_1 \\ \dot{\theta}_1 \\ \ddot{\theta}_2 \\ \dot{\theta}_2 \end{bmatrix} = \begin{bmatrix} \frac{\partial \dot{u}}{\partial u} & \frac{\partial \dot{u}}{\partial w} & \frac{\partial \dot{u}}{\partial q} & \frac{\partial \dot{u}}{\partial \theta_f} & \frac{\partial \dot{u}}{\partial \theta_1} & \frac{\partial \dot{u}}{\partial \theta_1} & \frac{\partial \dot{u}}{\partial \theta_2} & \frac{\partial \dot{u}}{\partial \theta_2} \\ \frac{\partial \dot{w}}{\partial u} & \frac{\partial \dot{w}}{\partial w} & \frac{\partial \dot{w}}{\partial q} & \frac{\partial \dot{w}}{\partial \theta_f} & \frac{\partial \dot{w}}{\partial \theta_1} & \frac{\partial \dot{w}}{\partial \theta_1} & \frac{\partial \dot{w}}{\partial \theta_2} & \frac{\partial \dot{w}}{\partial \theta_2} \\ \frac{\partial \dot{q}}{\partial u} & \frac{\partial \dot{q}}{\partial w} & \frac{\partial \dot{q}}{\partial q} & \frac{\partial \dot{q}}{\partial \theta_f} & \frac{\partial \dot{q}}{\partial \theta_1} & \frac{\partial \dot{q}}{\partial \theta_1} & \frac{\partial \dot{q}}{\partial \theta_2} & \frac{\partial \dot{q}}{\partial \theta_2} \\ \frac{\partial \dot{\theta}_f}{\partial u} & \frac{\partial \dot{\theta}_f}{\partial w} & \frac{\partial \dot{\theta}_f}{\partial q} & \frac{\partial \dot{\theta}_f}{\partial \theta_f} & \frac{\partial \dot{\theta}_f}{\partial \theta_1} & \frac{\partial \dot{\theta}_f}{\partial \theta_1} & \frac{\partial \dot{\theta}_f}{\partial \theta_2} & \frac{\partial \dot{\theta}_f}{\partial \theta_2} \\ \frac{\partial \dot{\theta}_1}{\partial u} & \frac{\partial \dot{\theta}_1}{\partial w} & \frac{\partial \dot{\theta}_1}{\partial q} & \frac{\partial \dot{\theta}_1}{\partial \theta_f} & \frac{\partial \dot{\theta}_1}{\partial \theta_1} & \frac{\partial \dot{\theta}_1}{\partial \theta_1} & \frac{\partial \dot{\theta}_1}{\partial \theta_2} & \frac{\partial \dot{\theta}_1}{\partial \theta_2} \\ \frac{\partial \dot{\theta}_1}{\partial u} & \frac{\partial \dot{\theta}_1}{\partial w} & \frac{\partial \dot{\theta}_1}{\partial q} & \frac{\partial \dot{\theta}_1}{\partial \theta_f} & \frac{\partial \dot{\theta}_1}{\partial \theta_1} & \frac{\partial \dot{\theta}_1}{\partial \theta_1} & \frac{\partial \dot{\theta}_1}{\partial \theta_2} & \frac{\partial \dot{\theta}_1}{\partial \theta_2} \\ \frac{\partial \ddot{\theta}_2}{\partial u} & \frac{\partial \ddot{\theta}_2}{\partial w} & \frac{\partial \ddot{\theta}_2}{\partial q} & \frac{\partial \ddot{\theta}_2}{\partial \theta_f} & \frac{\partial \ddot{\theta}_2}{\partial \theta_1} & \frac{\partial \ddot{\theta}_2}{\partial \theta_1} & \frac{\partial \ddot{\theta}_2}{\partial \theta_2} & \frac{\partial \ddot{\theta}_2}{\partial \theta_2} \\ \frac{\partial \dot{\theta}_2}{\partial u} & \frac{\partial \dot{\theta}_2}{\partial w} & \frac{\partial \dot{\theta}_2}{\partial q} & \frac{\partial \dot{\theta}_2}{\partial \theta_f} & \frac{\partial \dot{\theta}_2}{\partial \theta_1} & \frac{\partial \dot{\theta}_2}{\partial \theta_1} & \frac{\partial \dot{\theta}_2}{\partial \theta_2} & \frac{\partial \dot{\theta}_2}{\partial \theta_2} \end{bmatrix} \begin{bmatrix} u \\ w \\ q \\ \theta_f \\ \theta_1 \\ \theta_1 \\ \theta_2 \end{bmatrix} + \begin{bmatrix} \frac{\partial \dot{u}}{\partial \theta_c} & \frac{\partial \dot{u}}{\partial \theta_0} \\ \frac{\partial \dot{w}}{\partial \theta_c} & \frac{\partial \dot{w}}{\partial \theta_0} \\ \frac{\partial \dot{q}}{\partial \theta_c} & \frac{\partial \dot{q}}{\partial \theta_0} \\ \frac{\partial \dot{\theta}_f}{\partial \theta_c} & \frac{\partial \dot{\theta}_f}{\partial \theta_0} \\ \frac{\partial \dot{\theta}_1}{\partial \theta_c} & \frac{\partial \dot{\theta}_1}{\partial \theta_0} \\ \frac{\partial \dot{\theta}_1}{\partial \theta_c} & \frac{\partial \dot{\theta}_1}{\partial \theta_0} \\ \frac{\partial \ddot{\theta}_2}{\partial \theta_c} & \frac{\partial \ddot{\theta}_2}{\partial \theta_0} \\ \frac{\partial \dot{\theta}_2}{\partial \theta_c} & \frac{\partial \dot{\theta}_2}{\partial \theta_0} \end{bmatrix} \begin{bmatrix} \theta_c \\ \theta_0 \end{bmatrix} \quad (4.115)$$

Partial Derivatives \dot{u} - \dot{q} w.r.t. θ_2 and θ_2

$$\frac{\partial \dot{u}}{\partial \dot{\theta}_2_{DP}} = -\frac{\partial F_c \sin(\theta_1 + \theta_f)}{\partial \theta_2 m} \quad (4.116)$$

$$\frac{\partial \dot{u}}{\partial \theta_2_{DP}} = -\frac{\partial F_c \sin(\theta_1 + \theta_f)}{\partial \theta_2 m} \quad (4.117)$$

$$\frac{\partial \dot{w}}{\partial \dot{\theta}_2_{DP}} = \frac{\partial F_c \cos(\theta_1 + \theta_f)}{\partial \theta_2 m} \quad (4.118)$$

$$\frac{\partial \dot{w}}{\partial \theta_2_{DP}} = \frac{\partial F_c \cos(\theta_1 + \theta_f)}{\partial \theta_2 m} \quad (4.119)$$

$$\frac{\partial \dot{q}}{\partial \dot{\theta}_2_{DP}} = -\frac{\partial F_c h_l \sin(\theta_1 + \theta_f)}{\partial \theta_2 I_y} - \frac{\partial F_c x_l \cos(\theta_1 + \theta_f)}{\partial \theta_2 I_y} \quad (4.120)$$

$$\frac{\partial \dot{q}}{\partial \theta_2_{DP}} = -\frac{\partial F_c h_l \sin(\theta_1 + \theta_f)}{\partial \theta_2 I_y} - \frac{\partial F_c x_l \cos(\theta_1 + \theta_f)}{\partial \theta_2 I_y} \quad (4.121)$$

Trimming the linearised model at a velocity of 1m/s yields the linear model Equation 4.122. Subjecting it to the disturbance from 3-DOF-PH-HUB-CG will enable verification of the linear model around the trim condition. The helicopter-cable system response is shown in Figure 4.34. As in previous cases, the model fits well for the first 15 seconds of the simulation before it diverges. It appears to match the nonlinear model rather well near the trim condition.

$$\begin{bmatrix} \dot{u} \\ \dot{w} \\ \dot{q} \\ \dot{\theta}_f \\ \dot{\theta}_1 \\ \dot{\theta}_1 \\ \ddot{\theta}_2 \\ \dot{\theta}_2 \end{bmatrix} = \begin{bmatrix} -0.027 & -0.092 & 0.916 & -11.540 & 0.000 & -1.775 & 0.000 & 0.000 \\ -0.092 & -0.975 & 0.917 & 1.109 & 0.000 & 0.170 & 0.000 & 0.000 \\ 0.014 & 0.026 & -0.540 & -0.823 & 0.000 & -0.823 & 0.000 & 0.000 \\ 0.000 & 0.000 & 1.000 & 0.000 & 0.000 & 0.000 & 0.000 & 0.000 \\ 0.000 & 0.000 & 0.021 & -0.297 & -0.001 & -0.448 & 0.001 & 0.151 \\ 0.000 & 0.000 & 0.000 & 0.000 & 1.000 & 0.000 & 0.000 & 0.000 \\ 0.000 & 0.000 & 0.017 & -0.238 & -0.002 & 1.650 & -0.003 & -0.402 \\ 0.000 & 0.000 & 0.000 & 0.000 & 0.000 & 0.000 & 1.000 & 0.000 \end{bmatrix} \begin{bmatrix} u \\ w \\ q \\ \theta_f \\ \theta_1 \\ \theta_1 \\ \theta_2 \end{bmatrix} + \begin{bmatrix} 11.635 & -13.812 \\ -0.129 & -142.308 \\ -7.622 & 4.007 \\ 0.000 & 0.000 \\ 0.297 & -0.004 \\ 0.000 & 0.000 \\ 0.238 & -0.003 \\ 0.000 & 0.000 \end{bmatrix} \begin{bmatrix} \theta_c \\ \theta_0 \end{bmatrix} \quad (4.122)$$

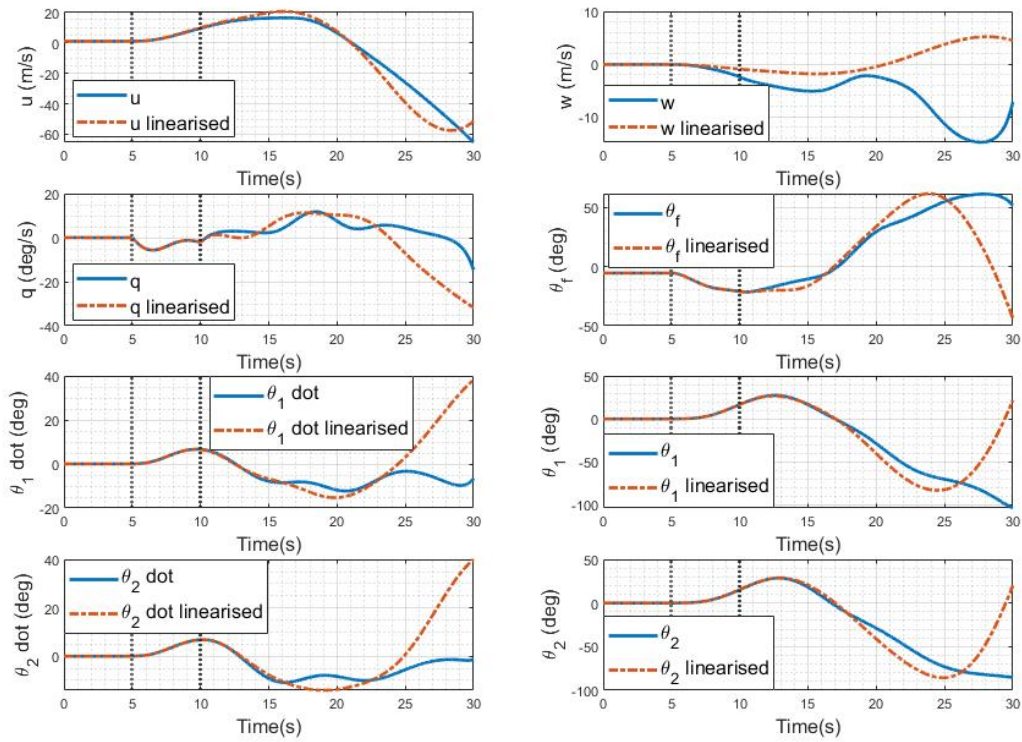


Figure 4.34: Response of linear and non-linear hovering helicopter + double pendulum model case 3-DOF-DP-OFF-HUB-OFF to input disturbance on cyclic of 1 degree for 5 seconds.

4.6.5. Stability Analysis

Stability analysis is done by analysing the poles of the linearised system. The poles of the system are presented in Figure 4.35 with their exact locations in Table 4.7. Note the addition of two stable poles (5 & 6) corresponding to the addition of the second pendulum. The helicopter phugoid is still unstable, meaning that a controller is required for stability.

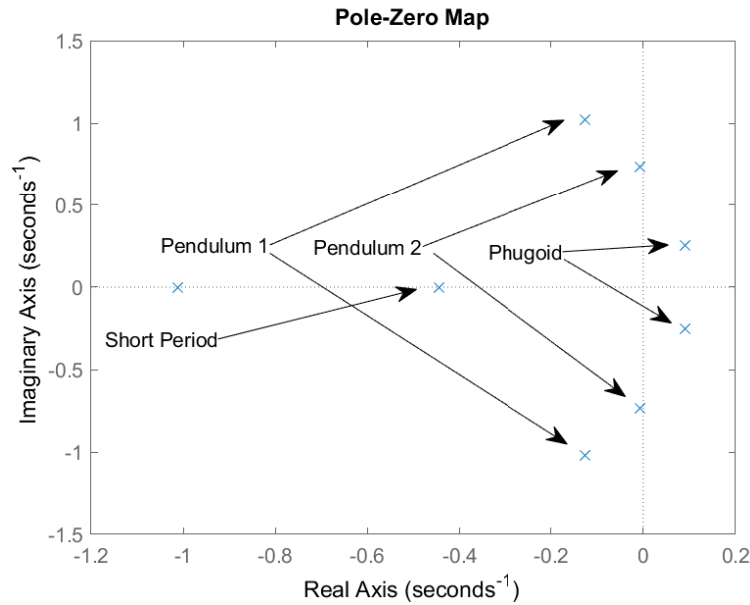


Figure 4.35: Pole-Zero map of linearised system for case 3-DOF-DP-OFF-HUB-OFF.

Table 4.7: Poles of the linearised double pendulum model case 3-DOF-DP-OFF-HUB-OFF.

Pole	Real part	Complex part	Mode
1	-1.013	0.000	-
2	-0.445	0.000	Short Period
3	-0.126	1.014	Pendulum 1
4	-0.126	-1.014	Pendulum 1
5	-0.007	0.734	Pendulum 2
6	-0.007	-0.734	Pendulum 2
7	0.090	0.254	Phugoid
8	0.090	-0.254	Phugoid

4.6.6. Controller Design

In order to control this configuration, it is assumed that the controller knows nothing about θ_2 . This means that the controller uses θ_1 and its derivative to control to stabilise the helicopter and its load. This simulates the controller using measurements from the helicopter. With this assumption, the same controller can be used as in cases 3-DOF-SP-CG-HUB-OFF and 3-DOF-SP-OFF-HUB-OFF with the same gains.

4.6.7. Assessing Controllers

Subjecting both the PID and the INDI controllers to the same disturbance as in case 3-DOF-PH-HUB-CG, yields the helicopter and cable response in Figure 4.36 and the control inputs in Figure 4.37 and Figure 4.38. Looking at the response of the helicopter and cable, the response of the helicopter and double pendulum appears stable. Also, the cable angle of the second pendulum appears to be oscillatory. This makes sense, since the helicopter only controls the cable angle of the first pendulum. Also, the control inputs are oscillatory, and more aggressive than in 3-DOF-SP-OFF-HUB-OFF, where there was only one pendulum. It appears that the addition of the second pendulum made the system more difficult to control, judging from the aggressive control inputs. Nevertheless, both controllers can control the given disturbance.

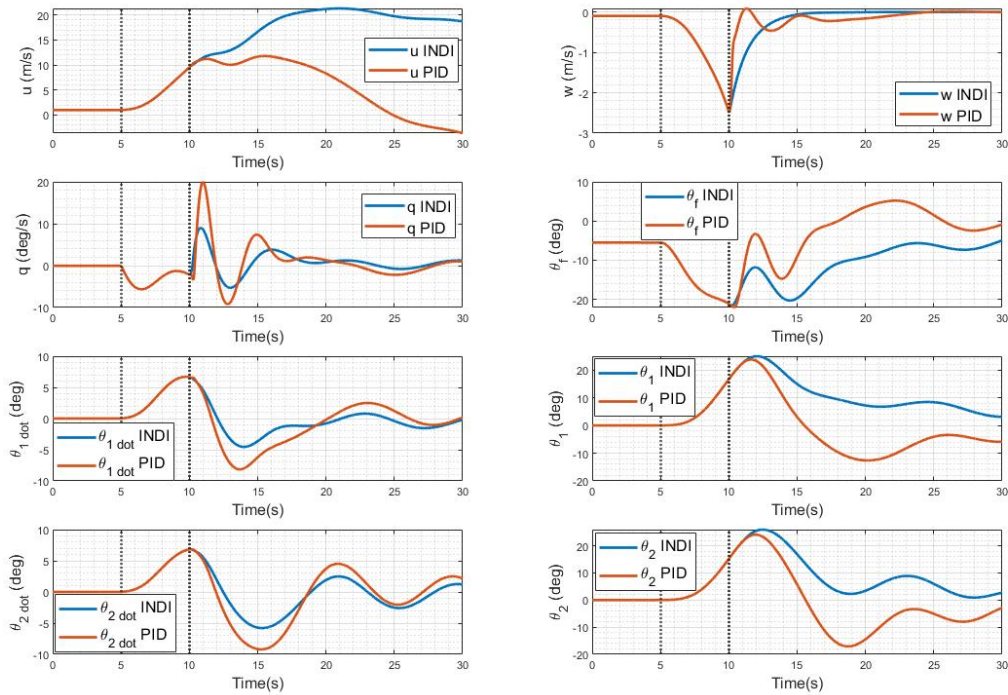


Figure 4.36: Response controlled hovering helicopter case 3-DOF-DP-OFF-HUB-OFF to input disturbance on cyclic of 1 degree for 5 seconds.

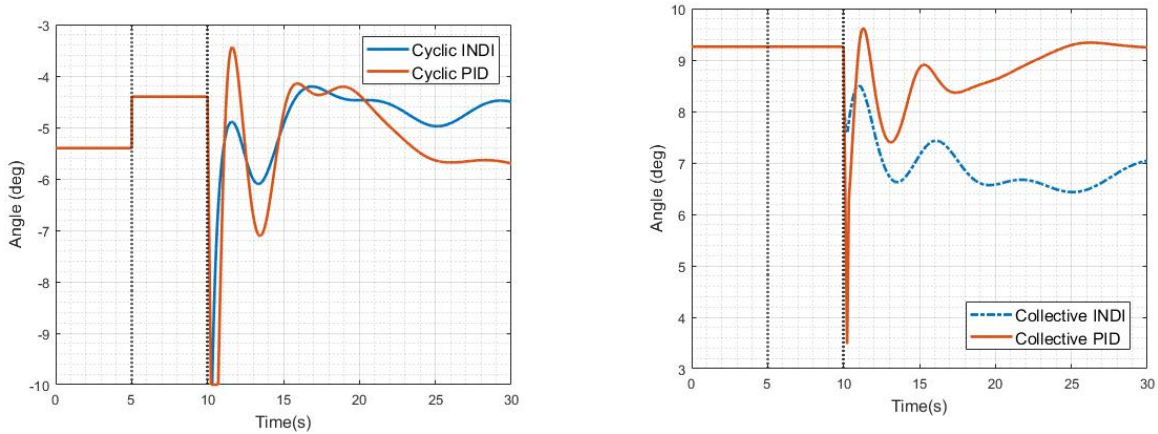


Figure 4.37: Cyclic control of controlled hovering helicopter case 3-DOF-DP-OFF-HUB-OFF to input disturbance on cyclic of 1 degree for 5 seconds.

Figure 4.38: Collective control of controlled hovering helicopter case 3-DOF-DP-OFF-HUB-OFF to input disturbance on cyclic of 1 degree for 5 seconds.

4.7. Case 3-DOF-DP-OFF-HUB-OFF-SUB

4.7.1. Configuration

The configuration of this case is exactly the same as in case 5, with the only difference being that load 2 is now submerged in the water. This has effect on the drag of this load, and therefore changes the controller gains required. The equations of motions remain unchanged, with the exception of changing the density in

the drag equations for load 2 from $\rho = 1.225$ to $\rho_w = 997 \text{ kg/m}^3$. It is assumed that the drag coefficient remains the same.

4.7.2. Stability Analysis

Trimming the same linear model as in 3-DOF-DP-OFF-HUB-OFF, but now with the water density added, to a velocity of 1 m/s , yields the linear system in Equation 4.123. Subjecting it to the disturbance from case 3-DOF-PH-HUB-CG, yields the linear model response and the nonlinear model response in Figure 4.39. The poles of this linear system are given in Figure 4.40 with their exact locations in Table 4.8. Interestingly, the linearised model is stable, whereas the nonlinear model is unstable. This is caused by the fact that the linear model is only valid in the region around the trimmed condition.

$$\begin{bmatrix} \dot{u} \\ \dot{w} \\ \dot{q} \\ \dot{\theta}_f \\ \dot{\theta}_1 \\ \dot{\theta}_1 \\ \ddot{\theta}_2 \\ \dot{\theta}_2 \end{bmatrix} = \begin{bmatrix} -0.027 & -0.098 & 0.930 & -11.535 & -0.027 & -1.785 & -0.027 & -0.001 \\ -0.078 & -0.976 & 0.911 & 1.170 & -0.572 & 0.085 & -0.571 & -0.028 \\ 0.010 & 0.030 & -0.540 & -0.808 & 0.115 & -0.808 & 0.114 & 0.006 \\ 0.000 & 0.000 & 1.000 & 0.000 & 0.000 & 0.000 & 0.000 & 0.000 \\ -0.026 & 0.002 & 0.021 & -0.297 & 0.761 & -0.447 & 0.761 & 0.151 \\ 0.000 & 0.000 & 0.000 & 0.000 & 1.000 & 0.000 & 0.000 & 0.000 \\ 0.067 & -0.009 & 0.017 & -0.237 & -2.033 & 0.169 & -2.031 & -0.409 \\ 0.000 & 0.000 & 0.000 & 0.000 & 0.000 & 0.000 & 1.000 & 0.000 \end{bmatrix} \begin{bmatrix} u \\ w \\ q \\ \theta_f \\ \theta_1 \\ \theta_1 \\ \dot{\theta}_2 \\ \theta_2 \end{bmatrix} + \begin{bmatrix} 11.635 & -14.563 \\ -0.191 & -142.233 \\ -7.625 & 4.501 \\ 0.000 & 0.000 \\ 0.298 & -0.154 \\ 0.000 & 0.000 \\ 0.239 & -0.283 \\ 0.000 & 0.000 \end{bmatrix} \begin{bmatrix} \theta_c \\ \theta_0 \end{bmatrix} \quad (4.123)$$

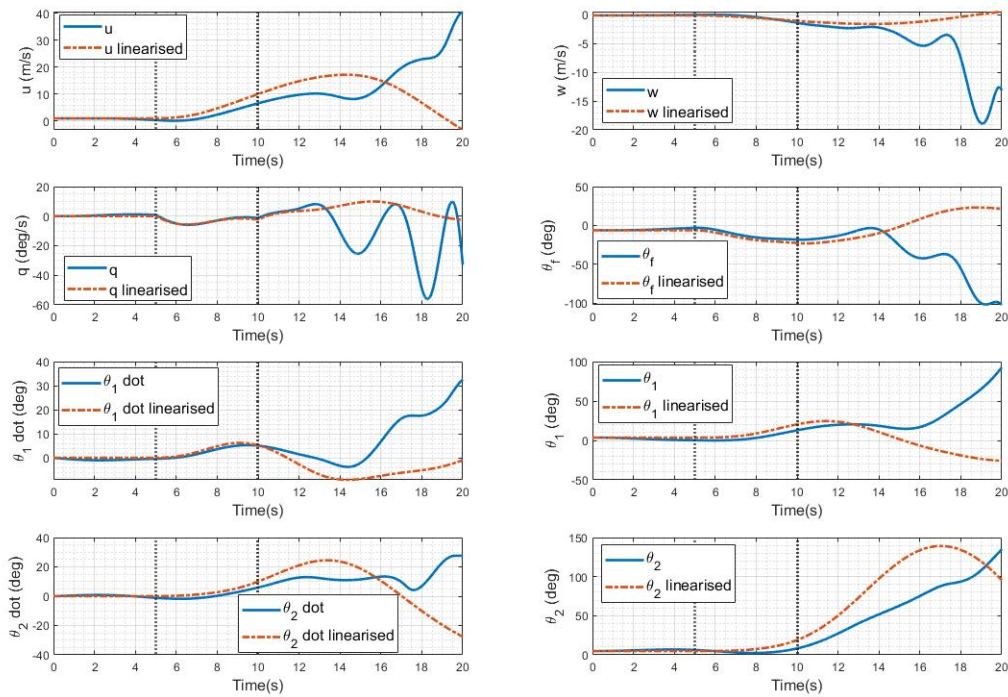


Figure 4.39: Response of linear and non-linear hovering helicopter + double pendulum model case 3-DOF-DP-OFF-HUB-OFF-SUB to input disturbance on cyclic of 1 degree for 5 seconds.

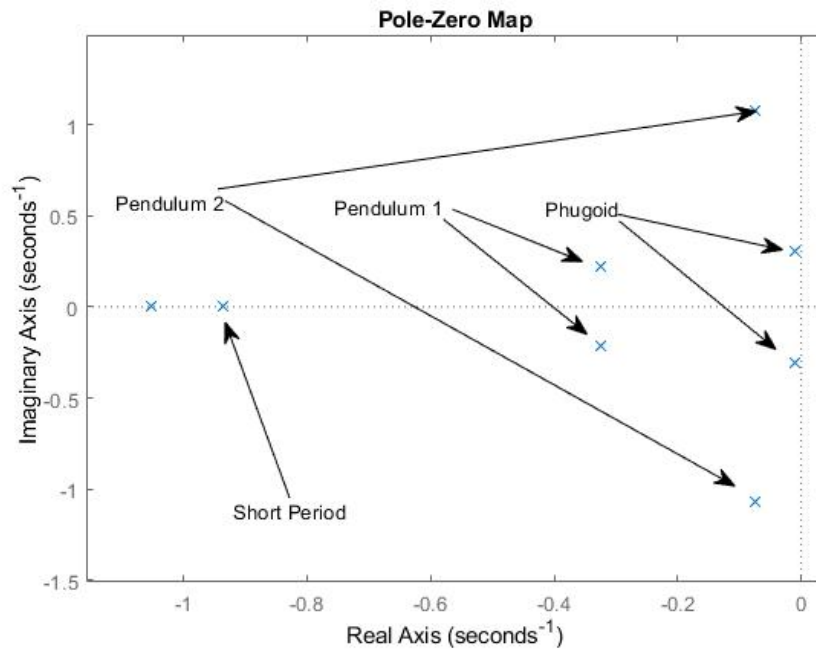


Figure 4.40: Pole-Zero map of linearised system for case 3-DOF-DP-OFF-HUB-OFF-SUB.

Table 4.8: Poles of the linearised double pendulum model with the pendulum attached at an offset w.r.t the c.g. of the helicopter trimmed at $V = 1\text{m/s}$ with load 2 submerged.

Pole	Real part	Complex part	Mode
1	-1.052	0.000	-
2	-0.937	0.000	Short Period
5	-0.326	0.218	Pendulum 1
6	-0.326	-0.218	Pendulum 1
3	-0.011	0.3052	Pendulum 2
4	-0.011	-0.3052	Pendulum 2
7	-0.076	1.072	Phugoid
8	-0.076	-1.072	Phugoid

4.7.3. Controller Design

Similar to case 3-DOF-DP-OFF-HUB-OFF, the same controllers are used as in case 3-DOF-SP-CG-HUB-OFF. However, the gains had to be re-tuned to the situation where the second pendulum is submerged. Stable gains are found for $Kp_{\theta_1} = -1$, $Ki_{\theta_1} = -0.01$ and $Kd_{\theta_1} = -2.5$ for the PID controller and $Kp_{\theta_1} = 0.1$, $Kd_{\theta_1} = -0.6$, $Kp_{\dot{\theta}_1} = 0.05$ and $Kd_{\dot{\theta}_1} = -0.3$ for the INDI controller. The gains had to be changed since the increased drag of the second pendulum would otherwise drag down the helicopter.

4.7.4. Assessing Controllers

Subjecting the controlled system to the disturbance from case 3-DOF-PH-HUB-CG yields the response in Figure 4.41. The control inputs are shown in Figure 4.42 and Figure 4.43. Looking at the response of both the PID and the INDI controllers, it appears that the INDI controller is more oscillatory than the PID controller. This is also visible in the control inputs. This was also the most difficult controller to tune. What is interesting to see is that both controllers have no residual oscillations once the first cable angle is reduced to zero. This suggests that the submerged cable could be stabilised by stabilising the emerged

cable angle. Also, the controller takes longer to stabilise the cable than in the previous case. Generally, from these two controllers, the PID performs the best. This could, however, be attributed to controller tuning, since the INDI controller was difficult to tune.

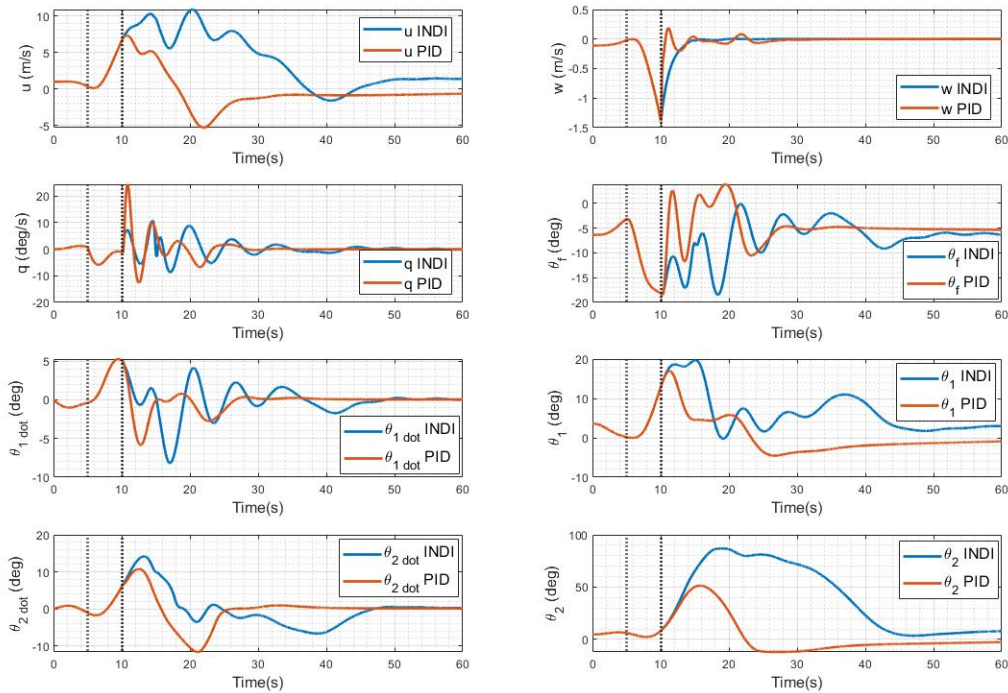


Figure 4.41: Response controlled hovering helicopter case 3-DOF-DP-OFF-HUB-OFF-SUB with double pendulum at an offset w.r.t the c.g. of the helicopter with load 2 submerged to input disturbance on cyclic of 1 degree for 5 seconds.

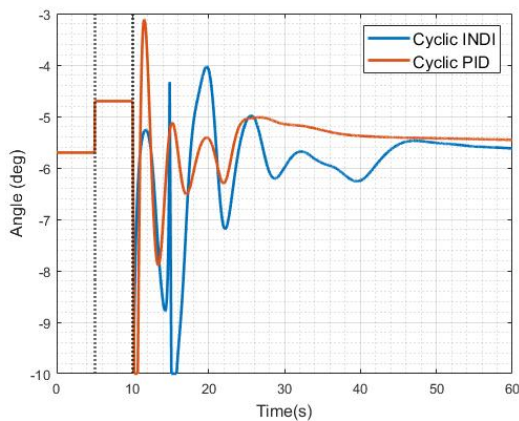


Figure 4.42: Cyclic control of controlled hovering helicopter case 3-DOF-DP-OFF-HUB-OFF-SUB with double pendulum at an offset w.r.t the c.g. of the helicopter with load 2 submerged to input disturbance on cyclic of 1 degree for 5 seconds.

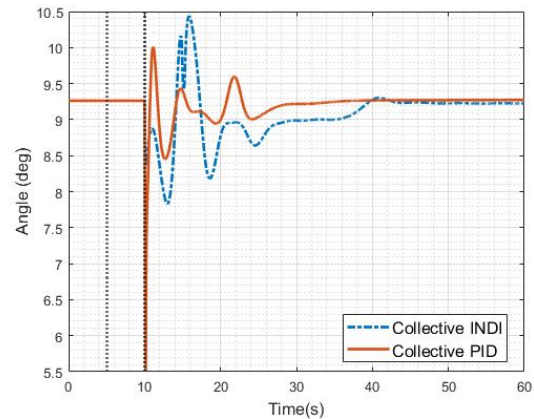


Figure 4.43: Collective control of controlled hovering helicopter case 3-DOF-DP-OFF-HUB-OFF-SUB with double pendulum at an offset w.r.t the c.g. of the helicopter with load 2 submerged to input disturbance on cyclic of 1 degree for 5 seconds.

4.8. Concluding Remarks of Preliminary Study for Helicopter Behaviour with Submerged Load

Based on simulation of the previous 6 cases, some conclusions can be drawn about the behaviour of a helicopter with a submerged hanging load. The cases analysed were:

Modelling cases for the 3-DOF model, each increasing the level of complexity.

3-DOF Model Cases				
Case	Rotor Hub Location	Load Model	Load Location	Medium
3-DOF-PH-HUB-CG	c.g.	-	-	-
3-DOF-PH-HUB-OFF	offset	-	-	-
3-DOF-SP-CG-HUB-OFF	offset	Single Pendulum	c.g.	Air
3-DOF-SP-OFF-HUB-OFF	offset	Single Pendulum	offset	Air
3-DOF-DP-OFF-HUB-OFF	offset	Double Pendulum	offset	Air
3-DOF-DP-OFF-HUB-OFF-SUB	offset	Double Pendulum	offset	Air + Water

Each case was progressively more complex than the latter, which made it easier to implement and detect interesting features about the behaviour of the helicopter. One of these features is that the helicopter is unstable to begin with, with 2 unstable phugoid poles. This is typical for helicopters, and it is a good sign that this result was found. Two controllers were designed: A PID controller and an INDI controller. This is done to practice with the two concepts in combination with helicopter control and to find out whether these control methods can control the chosen configurations when subjected to a disturbance.

For the cases where no load was attached, it was observed that the control inputs were less aggressive to stabilise the helicopter than for the cases with a load. This also makes sense, since the combined inertia of the system is higher. Also, it was found that the system is more stable when the load is moved forward relative to the c.g. of the helicopter. When submerging the second load of the double pendulum load model, it was found that the drag of the second load in combination with its attachment point (forward of the c.g. instead of aft) contributes heavily to the unstable nature of this configuration. The controller gains had to be re-tuned, and the INDI controller was very difficult to tune. In the end, both controllers are capable of controlling the configurations studied when subjected to a disturbance. Also, the INDI has smoother control inputs than the PID, except for 3-DOF-DP-OFF-HUB-OFF-SUB, when the second pendulum is submerged. Finally, it was found that no residual oscillations are present when stabilising the first pendulum in the submerged case. This suggests that the submerged cable could be stabilised by stabilising the emerged cable.

Part III

Additional Results

5

6-DOF Suspension Cable + SONAR Model

This chapter covers the development of a cable + SONAR model. This model is a discrete cable model, meaning that the cable is divided into sections, modelled as rigid links. The idea behind this is that, the more sections one has, the more the cable starts behaving like a real cable. The goal of this is to have a cable + SONAR model that can be used in combination with the helicopter model to model the effects of helicopter motion and environmental conditions on the cable and SONAR, in order to design the required controllers for the helicopter. This is done in steps: First, the Reference frames and assumptions are defined in Section 5.1 and Section 5.2. The kinematics are presented in Section 5.3. The force and moment equations are given in Section 5.4. Then, the dynamic system is solved in Section 5.5. Finally, modelling for damping and drag is done in Section 5.6 and Section 5.7.

5.1. Reference Frames

The suspension cable model makes use of two defined reference frames: The local horizontal, local vertical frame (LHLV), denoted with A and the section frame, denoted with k .

The relationship between these frames is that each cable section is rotated by an angle ϕ around the x_A axis and an angle θ around the y'_A axis. The y'_A axis is the y_A axis after the rotation ϕ around the x_A axis. A visualisation of the rotation process is shown in Figure 5.1. The section frame is presented in Figure 5.2. It is also important to mention that both reference frames are right-handed.

The reference frames are presented together with the reference frame of the helicopter in Figure 5.3. Here, the general configuration of the helicopter + SONAR is presented including the different reference frames. Note that this configuration uses 2 cable sections, hence there is a $i = 1$ and a $i = 2$. The SONAR is modelled like a cable section, with different properties than the cable sections, but the same dynamic equations.

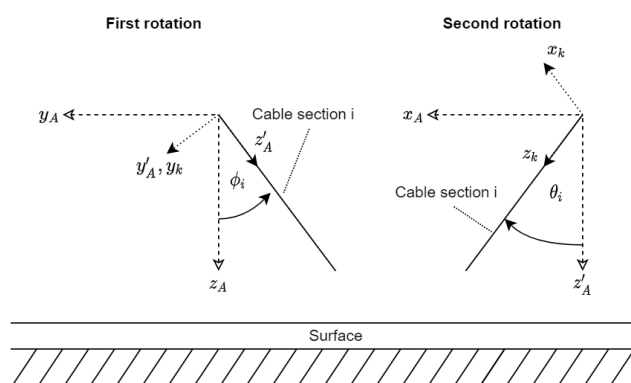


Figure 5.1: Sequence of rotations from A-frame to k-frame of a cable section i .

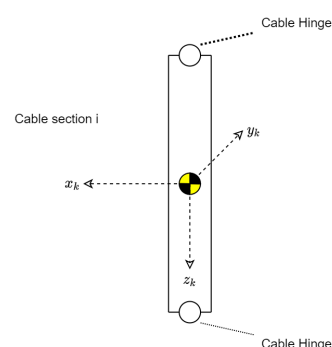


Figure 5.2: section frame of reference (k-frame) for a cable section i .

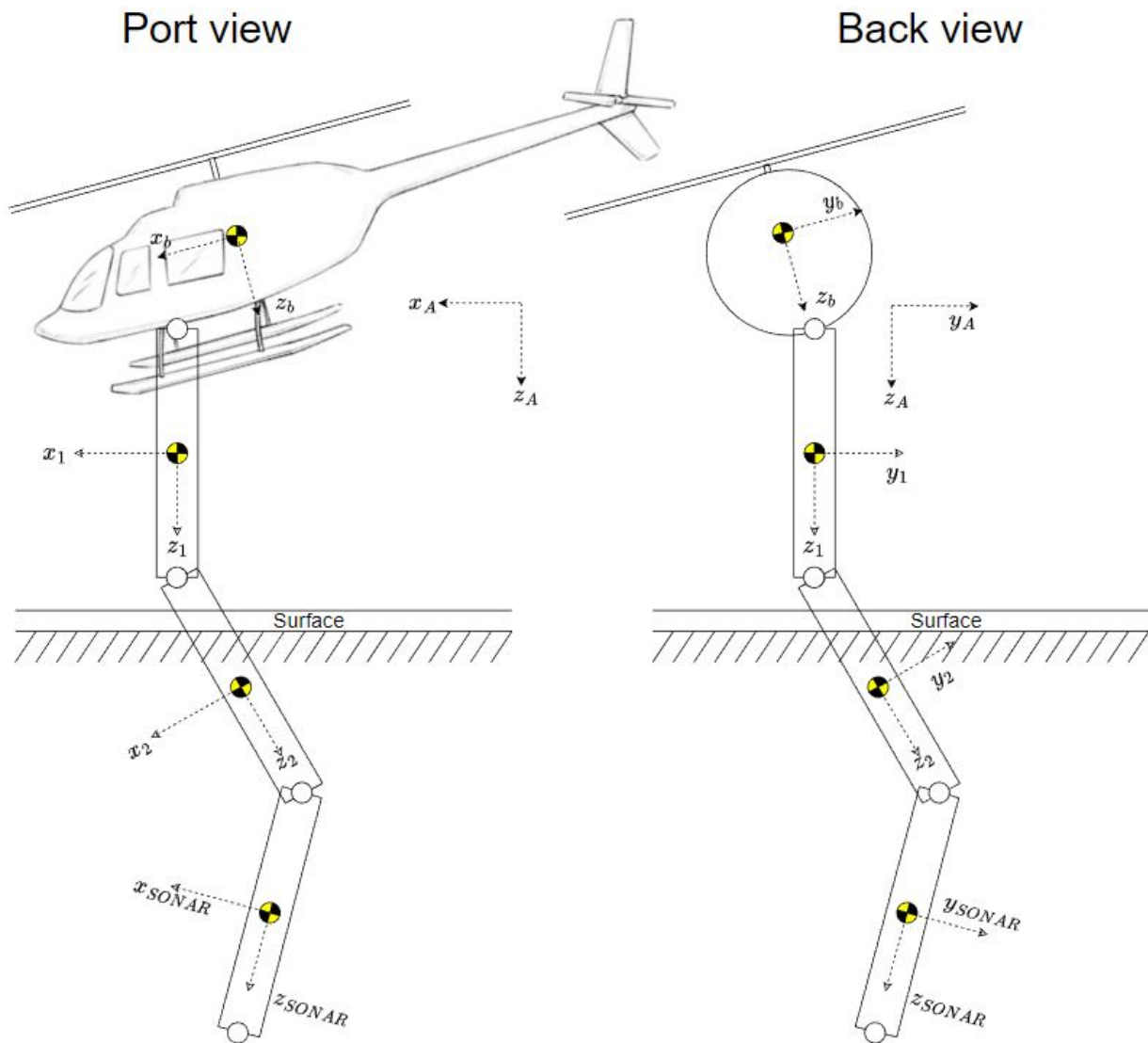


Figure 5.3: Reference frames for suspension cable with 2 sections and SONAR attached to helicopter.

5.2. Assumptions

This cable model makes use of various assumptions throughout. These are listed

1. Each cable section is assumed to be rigid. This means that rigid body dynamics apply.
2. Each cable section is assumed to have the same parameters for mass, size, shape, etc.
3. Cable stretch is assumed to be small, and is thus neglected.
4. Cable sections are assumed to rotate in two directions only. They are allowed to rotate around the lateral axes (x and y) of the cable sections and not the longitudinal axis. This essentially means that bending is modelled, but twist is not.
5. The SONAR is assumed to behave as any other cable section, albeit with different parameters. It is therefore modelled as a cable section in the dynamic system.
6. The center of mass is assumed to be in the geometric center of a cable section.
7. The cable section is assumed to be a smooth circular cylinder when computing the drag.
8. The cable attachment point is assumed to be a free hinge, meaning that no friction or damping is present here.
9. Cable hinges carry no torque, but produce a damping torque depending on relative angle and angular rate.
10. Cable damping is assumed to be linear with respect to bending angular rate and bending angle.

11. Submerged cable sections are assumed to not experience wind velocities.
12. Aerodynamic drag is assumed to act on the center of mass of the cable section.

The helicopter model provided by the thesis supervisor makes use of the following assumptions:

1. The helicopter body is modeled by subdividing it into its main components -rotor, fuselage, tailrotor, horizontal stabilizer, vertical fin- and adding the contribution of each part to the general system of forces and moments;
2. Aerodynamic forces and moments are calculated using the blade element theory;
3. The tailrotor is modeled as an actuator disc;
4. The fuselage, horizontal tail and vertical tails are modeled with linear aerodynamics;
5. Rotor disc-tilt dynamics is neglected, and only steady-state rotor disc-tilt motion is considered;
6. The dynamic inflow of both rotor and tailrotor are included in the model as state variables and can be described as a "quasi-steady dynamic inflow" by means of the time constants $\tau_{\lambda i}$ and $\tau_{\lambda i tr}$ of a value between 0.1 to 0.5 sec.;
7. The rotor is modeled with a flapping hinge situated at a distance e from the rotor hub;
8. The lead-lag motion of the blades is neglected;
9. The blades are rectangular;
10. There is no pitch-flap or pitch-lag couplings;
11. There are no tip losses;
12. The rotor is placed at the coordinates f, f_1, h from the helicopter centre of mass;
13. Gravitational forces are small compared to aerodynamic, inertial and centrifugal forces;
14. A linear twist θ_{tw} is applied;
15. The helicopter body system of reference x, y, z is assumed parallel to the rotor shaft plane;
16. The flapping and flow angles are small;
17. The rotor angular velocity is constant $\Omega = \text{const.}$ and is anticlockwise in the case of Bolkow Bo-105.
18. The longitudinal rotor disc-tilt a_1 is assumed positive when the rotor disc plane tilts backwards;
19. The lateral rotor disc-tilt b_1 is assumed positive when the rotor disc plane tilts to the azimuth $\psi=90^\circ$, this is to the right for an anticlockwise rotor;
20. The longitudinal cyclic θ_{1s} is assumed positive when the pilot moves the stick forward;
21. the lateral cyclic θ_{1c} is assumed positive when the pilot moves the stick to the right for an anticlockwise rotor;
22. No reverse flow regions are considered;
23. The flow is incompressible;
24. The blades have a uniform mass distribution with the mass centre and
25. Aerodynamic centre located on the quarter chord line

5.3. Kinematics

In this section, the kinematic relations are presented. These are the direction cosine matrix to transform from the A -frame to the section frame and the relation between the linear acceleration and the rotational rate and acceleration of the cable section.

Direction Cosine Matrix

The section frame k is (as explained in Section 5.1) a right-handed frame that is rotated by an angle ϕ around the x axis and an angle θ around the rotated y -axis. Such an order of rotations produces a direction cosine matrix (DCM) as presented in Equation 5.1. Note that each section has their own DCM based on its rotation in the A -frame.

$$R_i(\phi_i, \theta_i) = \begin{bmatrix} \cos(\theta_i) & 0 & \sin(\theta_i) \\ 0 & 1 & 0 \\ -\sin(\theta_i) & 0 & \cos(\theta_i) \end{bmatrix} \begin{bmatrix} 1 & 0 & 0 \\ 0 & \cos(\phi_i) & -\sin(\phi_i) \\ 0 & \sin(\phi_i) & \cos(\phi_i) \end{bmatrix} = \begin{bmatrix} \cos(\theta_i) & \sin(\theta_i) \sin(\phi_i) & \sin(\theta_i) \cos(\phi_i) \\ 0 & \cos(\phi_i) & -\sin(\phi_i) \\ -\sin(\theta_i) & \cos(\theta_i) \sin(\phi_i) & \cos(\theta_i) \cos(\phi_i) \end{bmatrix} \quad (5.1)$$

Derivation Linear Accelerations

In order to obtain an expression for the linear accelerations of the hinges, two variables are introduced: \bar{p}_i and \bar{r}_i . \bar{p}_i is the position vector of hinge i containing the x -, y - and z -position. The first hinge starts at the attachment point with the helicopter with \bar{p}_0 . \bar{r}_i indicates the vector connecting two hinges. The indexing

follows the logic that vector \bar{r}_i stretches over cable section i . This means that vector \bar{r}_1 is the vector from \bar{p}_0 to \bar{p}_1 . A graphic representation of these two variables is shown in Figure 5.4. Here, the vectors $\bar{r}_1 - \bar{r}_3$ are indicated by blue arrows, and $\bar{p}_0 - \bar{p}_3$ are indicated by black dots at the connection points of the different sections.

The mathematical representation of vector \bar{r}_i is given by Equation 5.2.

$$\bar{r}_i = \bar{p}_i - \bar{p}_{i-1} \quad (5.2)$$

Based on Newtonian mechanics, the velocity of hinge p_i can be defined as Equation 5.3. Variable \bar{v} indicates a linear velocity in the A -frame. The subscript indicates whether it belongs to a section i (subscript s_i) or a hinge i (subscript p_i). $\bar{\omega}_{s_i}$ indicates the rotational rate of section i in A -frame. Note the cross-product operator being used.

$$\bar{v}_{p_i} = \bar{v}_{p_{i-1}} + \bar{\omega}_{s_i} \times \bar{r}_i \quad (5.3)$$

By taking the time derivative of Equation 5.3, the linear acceleration of a hinge p_i can be found. This is shown in Equation 5.4. Variable \bar{a}_{p_i} indicates the linear acceleration of hinge p_i in A -frame. $\dot{\bar{\omega}}_{s_i}$ indicates the angular acceleration of a section i in A -frame.

$$\bar{a}_{p_i} = \bar{a}_{p_{i-1}} + \dot{\bar{\omega}}_{s_i} \times \bar{r}_i + \bar{\omega}_{s_i} \times \bar{v}_i \quad (5.4)$$

The linear acceleration of the center of mass of a section can also be found, followed from the assumption that the center of mass of a section is located in the geometric center of that section (see Figure 5.4). This means that the linear acceleration of a section i is given by Equation 5.5.

$$\bar{a}_{s_i} = \bar{a}_{p_{i-1}} + \dot{\bar{\omega}}_{s_i} \times \frac{1}{2} \bar{r}_i + \bar{\omega}_{s_i} \times \frac{1}{2} \bar{v}_i \quad (5.5)$$

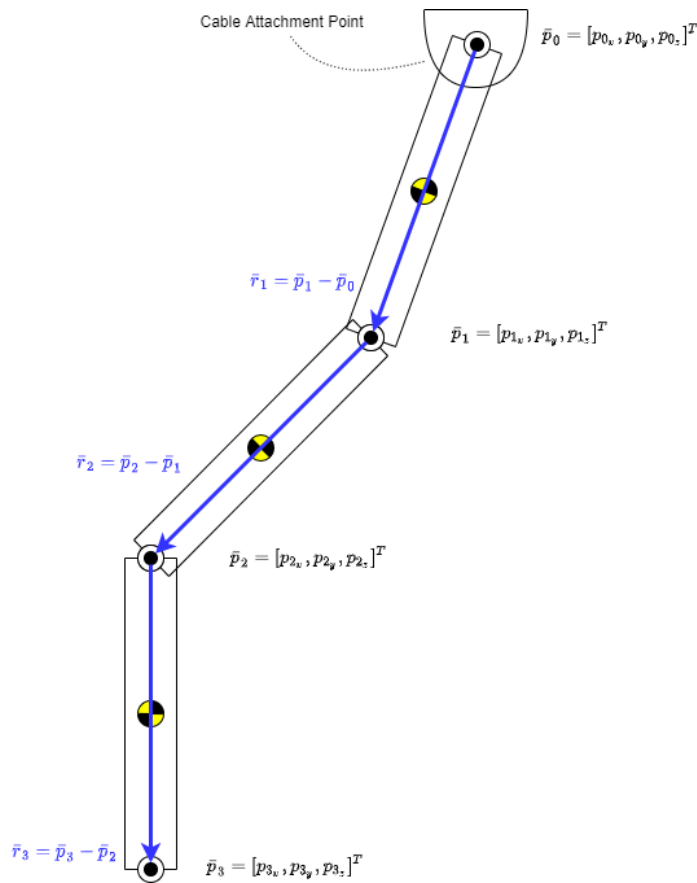


Figure 5.4: Diagram of vectors \bar{r} and hinge locations \bar{p}_i in the A-frame for three cable sections.

5.4. Force and Moment Equations

This section presents the dynamic equations of the cable model based on the force and moment equations derived from a free body diagram of the system. The free body diagram (FBD) of a suspension cable with two sections is presented in Figure 5.5. Note the location of hinges p_0 - p_2 as a reference. As shown, there are 4 different forces acting on each cable section, each having an x - and z - components respectively. Forces are indicated by red arrows.

For section 1, this is \bar{T}_0 , \bar{T}_1 , \bar{W}_1 and \bar{F}_{AE1} . Forces \bar{T}_0 and \bar{T}_1 indicate the attachment force at hinges 0 and 1 respectively. \bar{W}_1 is the weight force, which follows from the mass m_1 . This force only has a z -component in A-frame. \bar{F}_{AE1} indicates the aerodynamic force acting on the cable section. This includes aerodynamic (or hydrodynamic) drag. Note that it is assumed that the weight and aerodynamic force act at the center of mass of the section, whereas the connection forces act at the ends of the section. The letter a indicates the linear acceleration of the section and the direction is indicated by green arrows.

The subscript indicates what section or hinge the force belongs to. Subscript 1 indicates that a force belongs to section 1 or hinge 1 (if it is an attachment force \bar{T}), etc. The final force shown in the FBD is the force \bar{T}_{load} . This is the force of the attached load acting on the last cable section (and only the last cable section).

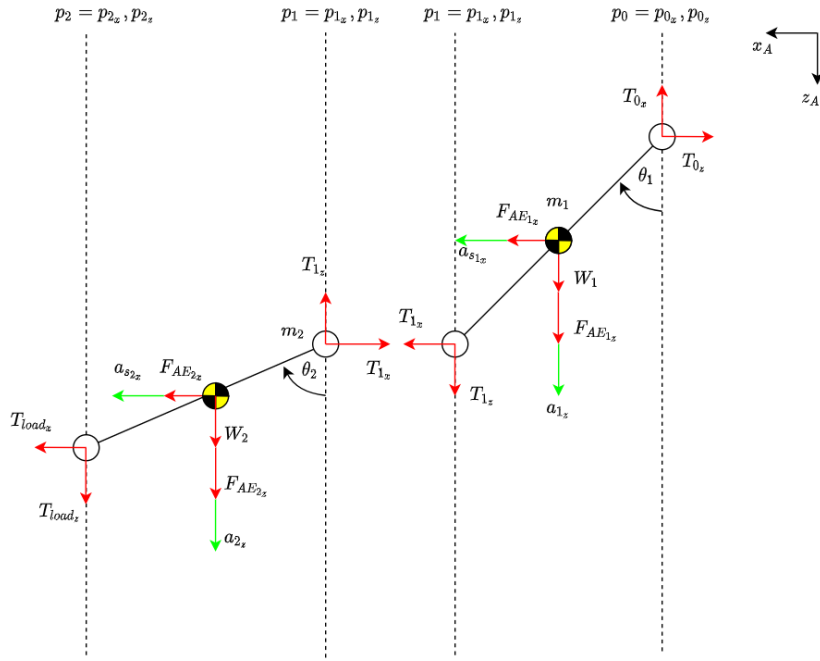


Figure 5.5: Free body diagram of 2 suspension cable sections in the x_A - z_A plane.

From the FBD, the following force equations can be obtained. These are found in Equation 5.6.

$$\begin{aligned} m_1 \bar{a}_{s1} &= \bar{T}_1 - \bar{T}_0 + \bar{W}_1 + \bar{F}_{AE1} \\ m_2 \bar{a}_{s2} &= \bar{T}_{load} - \bar{T}_1 + \bar{W}_2 + \bar{F}_{AE2} \end{aligned} \quad (5.6)$$

The torque equations can also be found in Equation 5.7. Note that the only forces not acting on the center of mass of the section are the connection forces \bar{T} . The variable $\bar{\tau}$ will be used to indicate torque. The subscript s_i indicates that this is the torque around the center of mass of section i . Again, note the cross-product. J_{s_i} indicates the inertia matrix of section i . Both equations are in the A -frame.

$$\begin{aligned} J_{s1} \dot{\bar{\omega}}_{s1} &= \bar{\tau}_{s1} - \bar{\omega}_{s1} \times J_{s1} \bar{\omega}_{s1} \\ &= \frac{1}{2} \bar{r}_1 \times (\bar{T}_0 + \bar{T}_1) - \bar{\omega}_{s1} \times J_{s1} \bar{\omega}_{s1} \\ J_{s2} \dot{\bar{\omega}}_{s2} &= \bar{\tau}_{s2} - \bar{\omega}_{s2} \times J_{s2} \bar{\omega}_{s2} \\ &= \frac{1}{2} \bar{r}_2 \times (\bar{T}_1 + \bar{T}_{load}) - \bar{\omega}_{s2} \times J_{s2} \bar{\omega}_{s2} \end{aligned} \quad (5.7)$$

Equation 5.6 and Equation 5.7 contain 12 dynamic equations. There are 18 unknowns: $[\bar{a}_{s1}, \bar{a}_{s2}, \bar{T}_0, \bar{T}_1, \bar{\tau}_{s1}, \bar{\tau}_{s2}]^T$. This means that 6 kinematic equations are needed. These are found using Equation 5.5 for \bar{a}_{s1} and \bar{a}_{s2} to make the system solvable.

Inertia

The inertia matrix of a rigid rod can be found to be equal to Equation 5.8. Note that here, the inertia is in the k -frame. Also, note that m_i is the section mass, l_i the section length and r_i the section radius.

$$J^{(k)} = \begin{bmatrix} \frac{m_i l_i^2}{12} & 0 & 0 \\ 0 & \frac{m_i l_i^2}{12} & 0 \\ 0 & 0 & \frac{m_i r_i^2}{2} \end{bmatrix} \quad (5.8)$$

5.5. Solving for Dynamic System

Solving the dynamic system is done in Appendix A from the scientific paper. From this appendix, it was found that the angular accelerations are a function of the states and the acceleration of the attachment point \bar{a}_{p_0} . This is presented in Equation 5.9.

$$\dot{\omega}_s = (A_{\dot{\omega}} - B_{\dot{\omega}} A_{\bar{a}_s})^{-1} [B_{\dot{\omega}} B_{\bar{a}_s} \bar{v}_p + B_{\dot{\omega}} C_{\bar{a}_s} \bar{a}_{p_0} + C_{\dot{\omega}} + D_{\dot{\omega}} + D_{damp}] \quad (5.9)$$

Note that all variables are taken in the A -frame of reference, meaning that conversions between frames is not necessary. However, since the sections themselves rotate within the A -frame, the inertia (as seen in the A -frame) changes as the section rotates. This means that the inertia matrix must be computed for each section individually according to Equation 5.10. This equation follows from the conservation of angular momentum.

$$J_{s_i}^{(A)} = R_i(\phi_i, \theta_i) J_{s_i}^{(k)} R_i^{-1}(\phi_i, \theta_i) \quad (5.10)$$

5.6. Modelling Damping

The suspension cable is modelled as rigid links connected by hinges. Hinges do not carry over any torque, hence additional torques are added at the hinges to model the resistance of the cable to bending. Furthermore, damping is necessary since the model will be simulated in a discrete manner. This means that occasional overshoots occur, adding energy to the system.

Damping is modelled as a torque produced by two components: A component due to the angular deflection between two sections and a torque produced due to the angular rate between two sections. The two components of the damping are given in Equation 5.11 and Equation 5.12.

$$\bar{\tau}_{d_{i_{angle}}} = D_{angle_c} (\bar{\Theta}_{s_i} - \bar{\Theta}_{s_{i-1}}) \quad (5.11)$$

$$\bar{\tau}_{d_{i_{rate}}} = D_{rate_c} (\bar{\omega}_{s_i} - \bar{\omega}_{s_{i-1}}) \quad (5.12)$$

The two damping constants D_{angle_c} and D_{rate_c} are scalars that indicate how much torque is produced for a deflection in the cable or a relative angular rate between two sections. Note that if the sections get smaller, the damping constants have to be reduced since the effect of the damping torque on the angular acceleration increases when the moment of inertia decreases. Therefore, the damping constants are reduced by a factor of n^3 when modelling more than 1 section. This is done since the moment of inertia of a cable section scales with n^{-3} . Since the SONAR size remains equal though, the damping constants of the SONAR are kept constant, with changing n .

The damping matrix is computed as in Equation 5.13. Note that the damping in the first row is zero. This is since it is assumed that the cable is free to rotate at the attachment hinge of the helicopter. However, there is a case to be made to include a damping due to angular rate, since this technically produces friction and hence damping.

$$D_{damp} = D_{angle_c} \begin{bmatrix} 0 \\ \Theta_2 - \Theta_1 \\ \Theta_3 - \Theta_2 \\ \vdots \\ \Theta_{n+1} - \Theta_n \end{bmatrix} + D_{rate_c} \begin{bmatrix} 0 \\ \bar{\omega}_2 - \bar{\omega}_1 \\ \bar{\omega}_3 - \bar{\omega}_2 \\ \vdots \\ \bar{\omega}_{n+1} - \bar{\omega}_n \end{bmatrix} \quad (5.13)$$

5.7. Modelling of Aerodynamic Forces and Hydrodynamic

The aerodynamic and hydrodynamic forces are modelled using the general equation for drag in Equation 5.15. The difference between the mediums air and water is modelled by changing the density of the fluid around the cable section. Friction is not modelled, neither is buoyancy.

1. First, the linear velocity of the center of mass of a section is computed using Equation 5.14. This follows from Equation 5.3.

$$\bar{v}_{s_i} = \bar{v}_{s_{i-1}} + \bar{\omega}_{s_i} \times \frac{1}{2} \bar{r}_i + \bar{v}_{wind} \quad (5.14)$$

Note that wind only applies to emerged cable sections.

2. Second, the velocity from step 1 is squared element wise to find the square of the velocity in their 3 directions.
3. Third, the surface area of the cable section is rotated to the A-frame. This is done because the cable sections are modelled as cylinders. Changing the orientation of the cylinder changes its surface area with respect to the incoming flow.
4. Fourth, the drag vector F_{AE_i} is computed using Equation 5.15. Note the \odot symbol, which is used to indicate element-wise multiplication. ρ_{s_i} is the effective density of the flow of the section (see conditions for submerging).

$$\bar{F}_{AE_{s_i}} = \frac{1}{2} \rho_{s_i} \bar{v}_{s_i} \odot \bar{v}_{s_i} C_{D_{s_i}} \bar{S}_{s_i_A} \quad (5.15)$$

5. Fifth, the direction of the drag force is obtained by setting the sign of the drag force equal to the opposite direction of the velocity, since the direction of the drag is lost when squaring.

Conditions for submerging

The cable sections experience drag, which is different depending on whether a cable section is submerged or not. If a cable section is submerged, the density of the fluid is higher than when emerged, which changes the drag by a large amount.

If the top hinge of the cable section is not submerged, but the bottom hinge is submerged, the amount of each section that is submerged will determine the "effective density" of the fluid the section is going through, which is the average of the amount the section is submerged. In Equation 5.16, the equation for the effective density is given. Note that this only applies to the section that is partially submerged. Sections that are emerged use the air density ρ and the sections that are submerged use the water density ρ_w . This is the case when the z-position of the bottom hinge of a section is positive or the top hinge negative. Note that in this equation, only the z-position of the hinge positions matters as this is negative if the section is emerged and positive if submerged (Hence only the third entry for p is relevant).

$$\rho_{s_i} = \frac{\rho_w \cdot p_i(3) - \rho_{air} \cdot p_{i-1}(3)}{p_i(3) - p_{i-1}(3)} \quad (5.16)$$

In previous attempts, the cable section submerging/emerging was modelled by watching whether the middle of the section left the water or not. It was decided to use a more gradual condition as it was found that sudden changes in drag send shocks through the cable. However, as the amount of cable sections increases, the difference between the two methods will go to zero.

It is also important to note that wind is only applied to sections that are emerged. If a section is submerged, it is assumed that it does not experience wind. If a section is partially submerged, the wind is applied via the same principle in Equation 5.16, where the densities are replaced by the wind velocities.

Choosing drag coefficient

The drag coefficient is estimated using data from [9]. Furthermore, a few assumptions are made:

- The temperature of both the water and the air is constant and equal to 20°C;
- The density of air and water is 1.225 kgm^{-3} and 997.0 kgm^{-3} respectively;
- A cable section is assumed to be a smooth circular cylinder.

The assumption of a cable section being a smooth cylinder could be argued about. Mostly, because it is more likely to be rough due to individual cable strands inside the cable winding. Nevertheless, for simplicity, smoothness is assumed.

In [9], the Reynolds number is defined as Equation 5.17. Here, ρ is the dimension of the fluid, V the free-stream velocity of the fluid, L the characteristic length scale (diameter of cylinder), μ the dynamic viscosity of the fluid and ν the kinematic viscosity of the fluid.

$$Re = \frac{\rho VL}{\mu} = \frac{VL}{\nu}; \nu = \frac{\mu}{\rho} \quad (5.17)$$

The viscosity of the fluid is a function of its temperature. Assuming conditions at sea level (pressure of 1 atmosphere) and a temperature of 20°C, the kinematic viscosity ν of air and water is found to be $1.51 \cdot 10^{-5}$ and $1.01 \cdot 10^{-6} \text{ m}^2 \text{ s}^{-1}$ respectively (see table 1.4 [9]). The diameter of the cable will be in the order of centimeters (10^{-2} m) and the velocity will likely remain within 100 m/s (0 to 10^2 m/s). This means that the order of magnitude for the Re for water and air will be in the order of 10^3 - 10^5 for air, and 10^4 - 10^6 for water. In Figure 5.6, the drag coefficient is shown vs. the Re for different shapes. For a smooth cylinder, the drag coefficient is approximately 1 for $10^3 < Re < 10^{5.5}$. Halfway between $10^{5.5}$ and 10^6 , the drag coefficient drops to approximately $10^{-0.5}$. For simplicity sake, the drag coefficient in air is thus taken as 1 in both air and water. The reason for this is that the velocity will likely remain well below 10^2 , meaning that an Re of 10^6 is likely not going to occur.

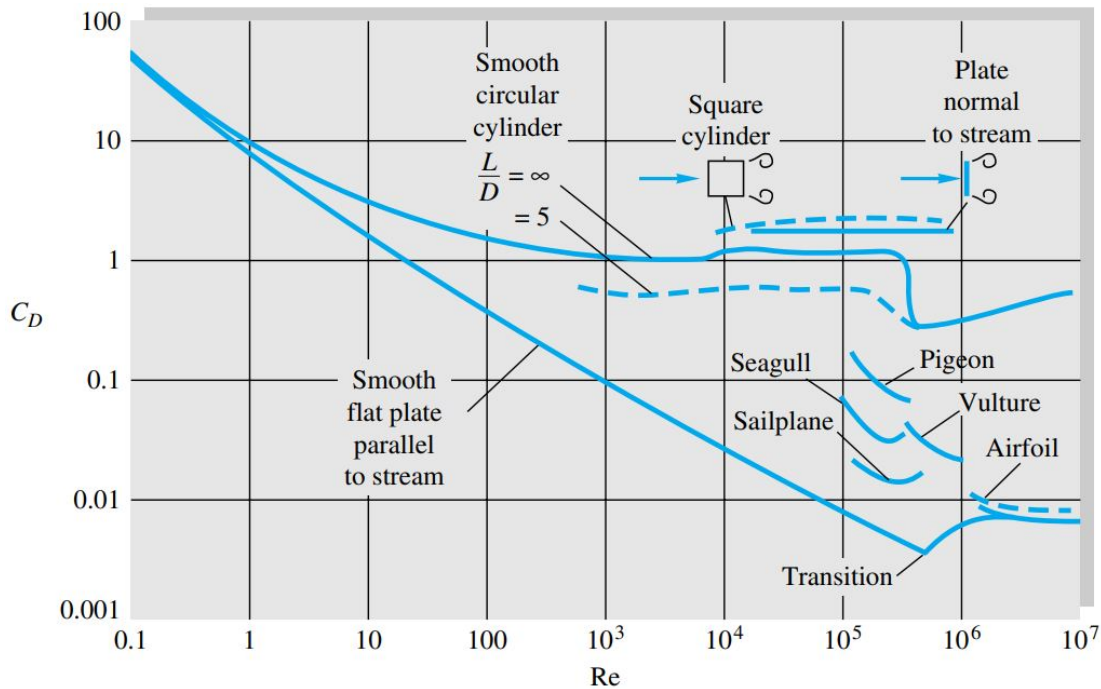


Figure 5.6: Drag coefficient for different shapes vs. Reynolds number.[9]

5.8. Cable Model Trim

Trimming the cable model is done numerically and iteratively. First, The helicopter is trimmed for the case where the cable hangs straight down. This yields a certain attitude of the helicopter, changing the position of the cable attachment point slightly, as the cable is not attached at the helicopter's center of mass.

Then, the cable is trimmed again by computing the angular acceleration of the cable sections, and moving each cable section in the direction of their acceleration according to: $\bar{\Theta}_{s_i} = \Delta \cdot \bar{\omega}_{s_i}$, where $\bar{\Theta}_{s_i}$ is the new angular position of section s_i , Δ the step size, and $\bar{\omega}_{s_i}$ the angular acceleration of a section s_i . The size of Δ was not optimized, but was taken as the $\log_{10}(\text{maximum trim error})$, with a maximum of 10^{-3} and a minimum of 10^{-4} . The maximum trim error is the largest angular rate squared from that iteration.

Once the maximum trim error reaches below a threshold, the cable is assumed to be trimmed and the helicopter is trimmed with the new trimmed cable. This operation is repeated until both the state derivative of the helicopter and the cable model reach a certain threshold.

6

6-Degrees of Freedom SONAR Control

6.1. Simulation Cases

In this chapter, 7 cases are simulated for an INDI-based control strategy and a PID-based control strategy, increasing the complexity of the system at each case. The final goal of this exercise is to have a controller capable of reducing the velocity of a hanging SONAR to zero, given a disturbance found during dipping SONAR mission conditions. At the same time, the helicopter is required to hover, but it is allowed to translate. The cases are presented in Table 6.1. The column helicopter model indicates where the main rotor hub is located along the x_b axis. The cable model column indicates how many cable sections are used. For cases 1 and 2, no load is assumed so no cable sections apply. Column Load location indicates where the attachment point of the cable is located. Medium indicates the medium in which the cable model is modelled. For cases 3-5, this is air, meaning that the cable is not submerged. For cases 6 and 7, this is water, meaning that the cable is partially submerged. The disturbance column indicates the disturbances modelled in the environment. Aerodynamic indicates inclusion of wind and gusts. Note that all cases are simulated with the helicopter starting from hover.

Table 6.1: Simulation Cases for the 6-DOF hovering helicopter controller

Case	Helicopter Model	Cable Model	Load Location	Medium	Disturbances
1	Rotor hub aligned with c.g.	-	-	-	-
2	Rotor hub at offset	-	-	-	-
3	Rotor hub at offset	Single cable section + SONAR	c.g. of helicopter	Air	-
4	Rotor hub at offset	Single cable section + SONAR	At offset	Air	-
5	Rotor hub at offset	5 cable sections + SONAR	At offset	Air	-
6	Rotor hub at offset	5 cable sections + SONAR	At offset	Air + water	-
7	Rotor hub at offset	5 cable sections + SONAR	At offset	Air + water	Aerodynamic

6.2. Simulation Data

As helicopter data, the data from the Bo105 helicopter was used and was provided by the project supervisors and is given in Appendix D. The location of the attachment point for the cable was not provided, and could not be obtained via literature. Hence, a hypothetical location of $0.5m$ in front of the c.g. of the helicopter, and $1m$ below the c.g. of the helicopter.

Data for the suspension cable is provided in Appendix D. Most important to note is that the cable length is set to a length of $30m$ for cases 3 and 4. The reason for this is that shorter cable lengths are more difficult to control. A shorter cable means a higher natural frequency, meaning that the controller must react more quickly. For cases 5-8, a longer cable of $120m$ is chosen in order to also include the effects of submerging from case 6 on.

Table 6.2: Control method control loops

Controller	INDI	PID
ACAH ψ_f	INDI	PID
ACAH θ_f	INDI	PID
ACAH ϕ_f	INDI	PID
TRC u	NDI	NDI
TRC v	NDI	NDI
TRC w	INDI	NDI
Position hold x	PID	PID
Position hold y	PID	PID
Position hold z	PID	PID

6.5.1. Case 1 Trim

The helicopter is trimmed at a velocity of 0 m/s and an altitude of 60m. The trimmed states are presented in Table 6.3

Table 6.3: Trim data Case 1

Helicopter State	Symbol	Name	Value case 1	unit
1	u	Body velocity in x	0.000	m/s
2	v	Body velocity in y	0.000	m/s
3	w	Body velocity in z	0.000	m/s
4	p	Body roll rate	0.000	deg/s
5	q	Body pitch rate	0.000	deg/s
6	r	Body yaw rate	0.000	deg/s
7	ψ_f	Fuselage heading angle	0.000	deg
8	θ_f	Fuselage pitch angle	8.6232	deg
9	ϕ_f	Fuselage roll angle	-1.6326	deg
10	x	Helicopter x position	0.000	m
11	y	Helicopter y position	0.000	m
12	z	Helicopter z position	-60.000	m
13	λ_0	Normalised uniform inflow velocity	0.0491	–
14	λ_{0tr}	Normalised uniform inflow velocity tail	0.0557	–
15	ω	Main rotor angular rate	44.400	rad/s
Control	Symbol	Name	Value case 1	unit
1	θ_{1c}	Lateral Cyclic	-0.3618	deg
2	θ_{1s}	Longitudinal Cyclic	1.5110	deg
3	θ_0	Main rotor collective	14.3681	deg
4	θ_{0tr}	Tail rotor collective	13.6380	deg

6.5.2. Tuning ACAH Controller

For the ACAH controller, either INDI or PID is used. The block diagram for these controllers are shown in Figure 6.2 and Figure 6.3 for the INDI and PID controllers respectively. Note that these are shown only for the helicopter attitude in pitch. This is done for the sake of example. The architecture of the controllers for the other attitude angles are the same.

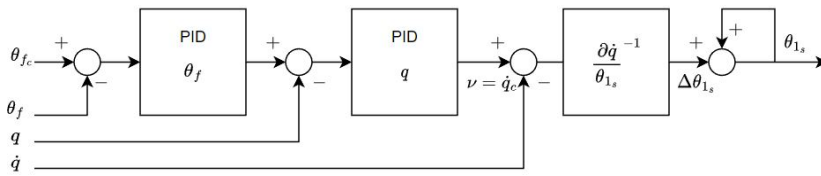


Figure 6.2: Block diagram for INDI ACAH controller

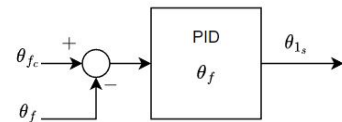


Figure 6.3: Block diagram for PID ACAH controller

The INDI attitude controller is tuned in two steps. First, the inner angular rate loop is tuned. This is tuned to a reference signal with a time constant of $\tau = 0.09$ seconds. The attitude angle loop is tuned to a reference signal with a natural frequency of $\omega_n = 5$ rad/s and a damping ratio of $\zeta = 0.9$. The latter is also the case for the PID controller.

The INDI controller response to the step input is presented in Figure 6.4 and Figure 6.5. As shown, the controller is capable of almost perfectly following the reference signal for both the inner and outer loop. The PID controller response to the step input is shown in Figure 6.6. It seems to follow the reference signal slightly worse than the INDI controller. It also appears to have steady state errors, which the INDI controller did not have. The gains for both ACAH controllers are shown in Table 6.4.

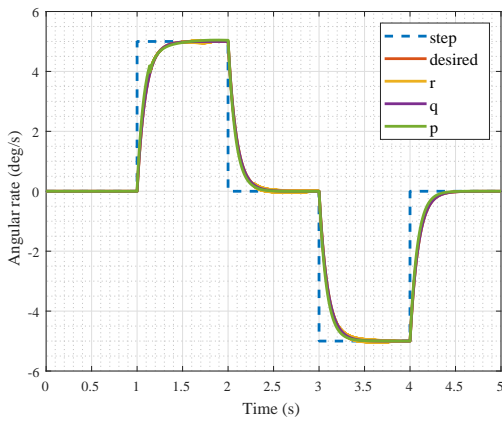


Figure 6.4: Response of inner loop INDI ACAH controller.

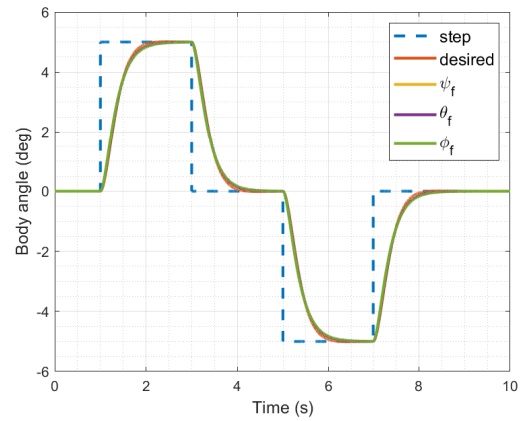


Figure 6.5: Response of outer loop INDI ACAH controller.

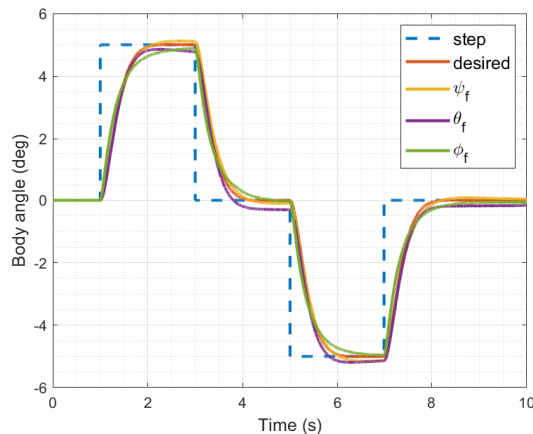


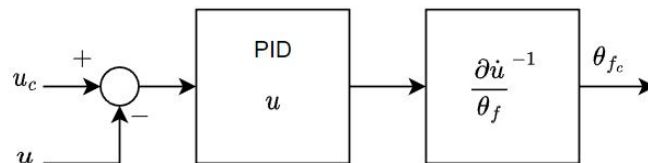
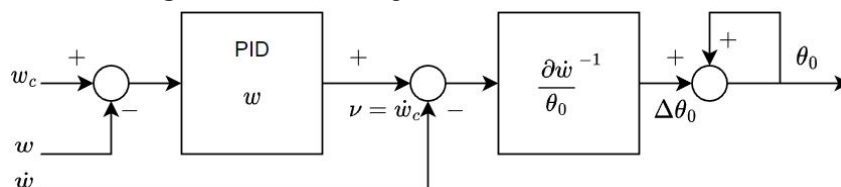
Figure 6.6: Response of PID ACAH controller.

Table 6.4: Gains for ACAH Controller Case 1.

Gain	Value INDI ACAH	Value PID ACAH	unit
K_{P_p}	12.5	-	—
K_{P_q}	11.0	-	—
K_{P_r}	11.0	-	—
$K_{P_{\phi_f}}$	2.70	0.60	s^{-1}
$K_{D_{\phi_f}}$	0.00	0.10	—
$K_{P_{\theta_f}}$	2.70	-0.53	s^{-1}
$K_{D_{\theta_f}}$	0.00	-0.11	—
$K_{P_{\psi_f}}$	2.70	-1.25	s^{-1}
$K_{D_{\psi_f}}$	0.00	-0.40	—

6.5.3. Tuning TRC Controller

The TRC controller is tuned separately for the PID ACAH and for the INDI ACAH. This way, both controllers have a TRC that works best with their ACAH, making the comparison fair. The TRC controller for the INDI ACAH is an NDI controller for body velocities u and v . For w , and INDI controller is used for the INDI ACAH inner loop, and an NDI controller is used for the PID ACAH inner loop. The decision was made to have an INDI controller in the most inner loop for the helicopter main rotor collective θ_0 as well. The block diagram for an NDI TRC controller is given in Figure 6.7 and the block diagram for an INDI TRC controller in Figure 6.8. Note that the TRC controller using NDI is applied to the other body velocities as well. However, for the sake of example, it is only shown for body velocity u .

**Figure 6.7:** Block diagram for NDI TRC controller**Figure 6.8:** Block diagram for INDI TRC controller

During tuning, it was observed that even with model inversion, the body velocities still behave somewhat like a second order system. This is strange, since model inversion should result in first order systems. For the NDI controller, it was assumed that the velocity is only dependent on the attitude. It seems that modelling errors are quite large for this assumption. Nevertheless, the controllers for u and v are tuned to show a desired response of a second order signal with a natural frequency of 1.5rad/s and a damping ratio of 0.9.

The w controller has $\frac{\partial \dot{w}}{\partial \theta_0}$ as control effectiveness for both the NDI and INDI variant. It is assumed that \dot{w} is only dependent on the main rotor collective. This controller does show behaviour of a first order system, and is tuned such that it shows a desired response of a first order signal with a time constant of 0.2 seconds. The fact that it indeed behaves as a first order signal indicates that the assumption made above is valid.

The TRC controller for the PID ACAH inner loop uses NDI for u , v and w respectively. The desired response signal is the same as for the INDI ACAH inner loop TRC controller.

The response of the tuned TRC controller for the INDI controller to step inputs for the commanded velocities is shown in Figure 6.9 for the u and v controllers and Figure 6.11 for the w controller. As shown, the u and v controllers manage to fit the desired response rather poorly. The u -controller has a steady state error. It is interesting to note that given a step command to the v -controller, the body velocity v goes down first, before increasing to the desired value. An equal but opposite effect is seen in the response of the u -controller. These behaviours are likely caused by the fact that the c.g. is above the rotation point of the helicopter in longitudinal direction, but below the rotation point of the helicopter in lateral direction. This means that as the helicopter rolls, the c.g. moves backwards in v direction (or forwards for u when pitching) before accelerating in the direction of rotation.

The response of the TRC controller tuned for the PID ACAH is shown in Figure 6.10 for the u and v controllers and Figure 6.12. This controller seems to follow the desired velocity better than the TRC controller for the INDI ACAH controller. It shows the same dip in the v -velocity and hump in u . The w -controller appears to have a steady state error. No integral terms are added to the controller to make these disappear. This will be taken care of in the position hold controller. The gains for the TRC controllers are presented in Table 6.5.

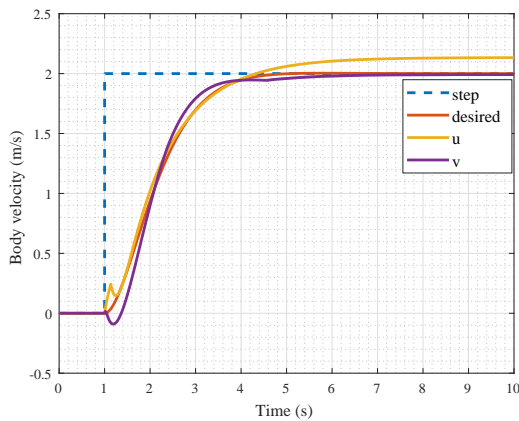


Figure 6.9: Response of u - and v -component TRC controller for INDI ACAH.

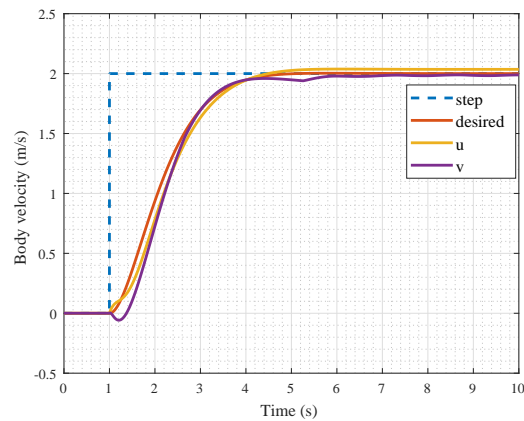


Figure 6.10: Response of u - and v -component TRC controller for PID ACAH.

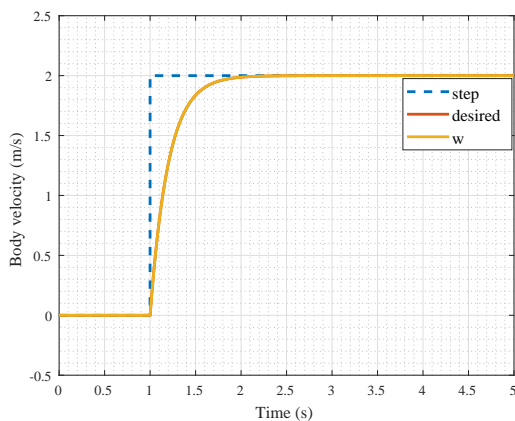


Figure 6.11: Response of w -component TRC controller for INDI ACAH.

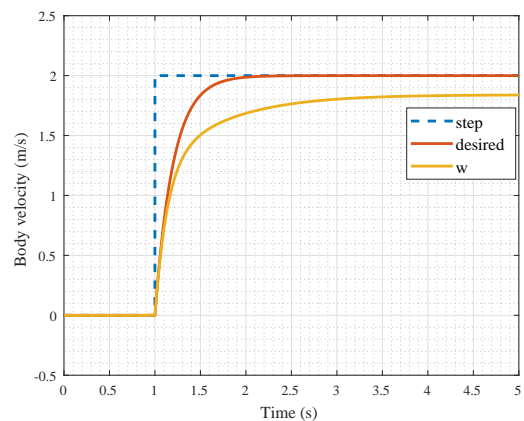


Figure 6.12: Response of w -component TRC controller for PID ACAH.

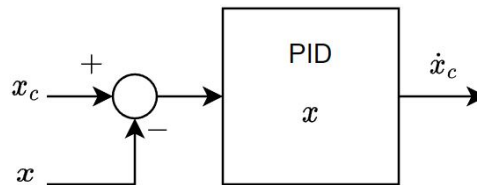
Table 6.5: Gains for TRC Controller Case 1.

Gain	Value INDI ACAH	Value PID ACAH	unit
K_{P_u}	0.75	0.85	$rad.s.m^{-1}$
K_{D_u}	0.20	0.20	$rad.s^2.m^{-1}$
K_{P_v}	0.85	0.85	$rad.s.m^{-1}$
K_{D_v}	0.10	0.10	$rad.s^2.m^{-1}$
K_{P_w}	5.00	5.00	$rad.s.m^{-1}$
K_{D_w}	0.00	0.00	$rad.s^2.m^{-1}$

6.5.4. Tuning Position hold controller

The position hold controller is tuned similar to the ACAH controller and the TRC controller and also tuned separately depending on whether the ACAH controller is a PID or INDI controller. However, the position hold controller is a PID to begin with. This is due to the fact that the relationship between velocity and position is linear to begin with. Note that the velocity from the position hold controller is rotated to the body frame before it is passed to the TRC.

For completeness, the block diagram for the position hold controller is given in Figure 6.13.

**Figure 6.13:** Block diagram position hold controller

The x - and y -position controllers are tuned to show a desired response equal to a second order signal with a natural frequency of 1.2 rad/s and a damping ratio of 0.9. The z -position controller is tuned to show a desired response equal to a first order signal with a time constant of 0.8 seconds. The response of the x -, y - and z -controllers are shown in Figure 6.14 and Figure 6.16 for the INDI ACAH and Figure 6.15 and Figure 6.17 for the PID ACAH. As shown, both z -controllers follow the desired response almost perfectly. The position hold controller has a delay with the desired response of about 0.5 seconds for both the x - and y -controllers. It is interesting to note that here too, the non-minimum phase behaviour is visible: y first decreases before it increases. Both the position hold controller with the INDI ACAH inner loop and the PID inner loop follow the desired response. The INDI ACAH has an x -controller that is slightly faster than the y -controller. For the PID ACAH, this is the other way around.

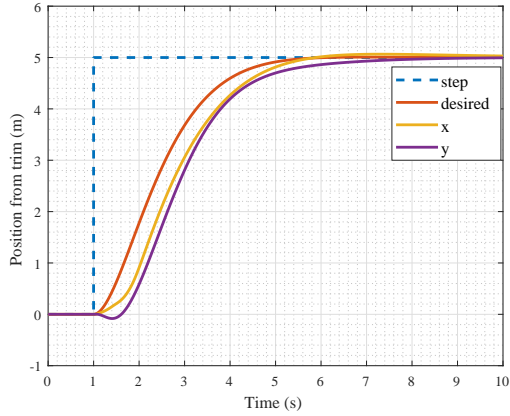


Figure 6.14: Response of position hold controller for INDI ACAH.

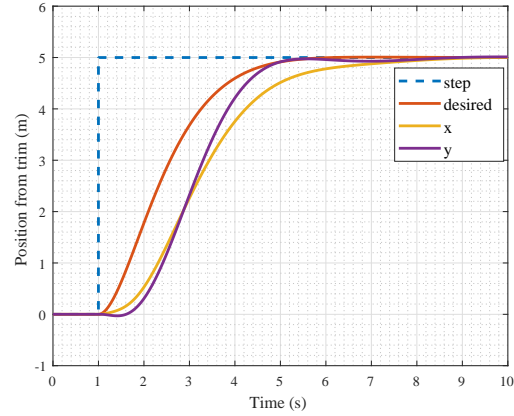


Figure 6.15: Response of position hold controller for PID ACAH.

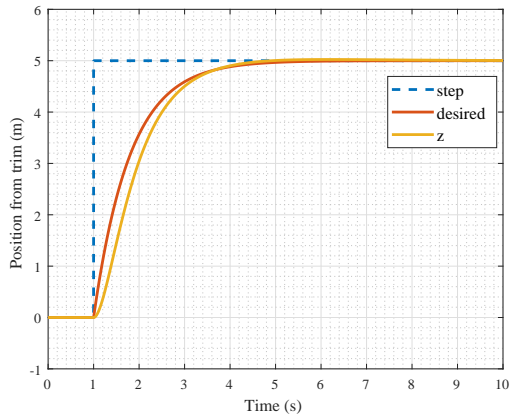


Figure 6.16: Response of position hold controller for INDI ACAH.

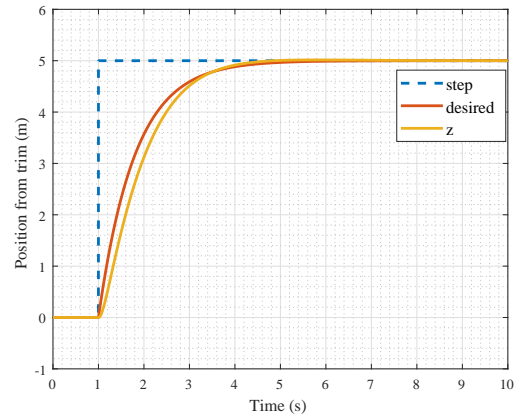


Figure 6.17: Response of position hold controller for PID ACAH.

Table 6.6: Gains for Position hold Controller Case 1.

Gain	Value INDI ACAH	Value PID ACAH	unit
K_{P_x}	0.50	0.80	s^{-1}
K_{D_x}	0.55	0.80	—
K_{P_y}	0.50	0.70	s^{-1}
K_{D_y}	0.27	0.42	—
K_{P_z}	1.00	2.00	s^{-1}
K_{D_z}	0.00	0.80	—

6.5.5. Disturbance Response

In order to compare the PID and the INDI controllers, both controllers are simulated with a filtered step input in velocity of $4kts$ at time $t = 1$ seconds. This step input in velocity represents a constant wind in x_A -direction. The filter used is given in Equation 6.1. This filter is added to smooth out the step input. For comparison between the PID and the INDI ACAH controllers, only the helicopter position, attitude and the relative control inputs are presented in Figure 6.18, Figure 6.19 and Figure 6.20 respectively. The INDI controller uses subscript $INDI$, whereas the PID controller uses PID . The first observation is that

the position appears to have a steady state error for both controllers, although it is smaller for the PID controller. This steady state error is caused by the fact that the position hold controller is a PID without an integral. This error can hence be removed using an integral component to the position hold controller. It is also interesting to see that the INDI controller generally reaches steady state quicker than the PID controller in the lateral direction. The PID reaches steady state quicker in the longitudinal direction. This is most visible in the attitude plot Figure 6.19. The reason for this is not entirely clear, but it may have something to do with the initial pitch-up of the helicopter in the first second after the disturbance hits. The INDI controller pitches back more than the PID (1.4° vs 0.2°). This could be due to the fact that at $t = 0$, the reference body velocity is 0 m/s from the position hold controller. Therefore, as soon as the wind is added, the initial response of the TRC controller is to compensate for the velocity of the wind and bring it back to zero, hence the pitch-up. The INDI controller appears to compensate for wind more quickly than the PID controller.

The final observation made is that the PID controller uses more control range than the INDI controller. The PID controller especially uses more cyclic control than the INDI controller. This also explains why the PID controller reaches steady state faster longitudinal direction. To conclude, it seems that both the PID ACAH and INDI ACAH controller are capable of handling the disturbance of $4kts$ in the x_A -direction. However, the PID does it with less steady state error in x-direction.

$$H(s) = \frac{2}{s + 2} \quad (6.1)$$

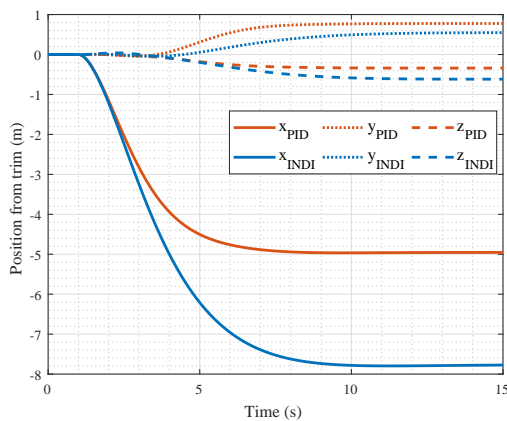


Figure 6.18: Position response of both the ACAH INDI and ACAH PID controllers to step input on disturbance velocity of $4kts$.

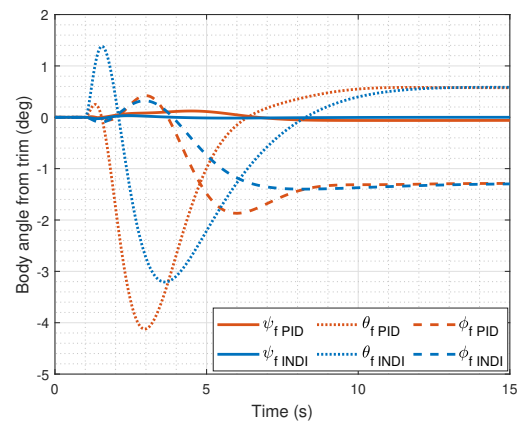


Figure 6.19: Attitude response of both the ACAH INDI and ACAH PID controllers to step input on disturbance velocity of $4kts$.

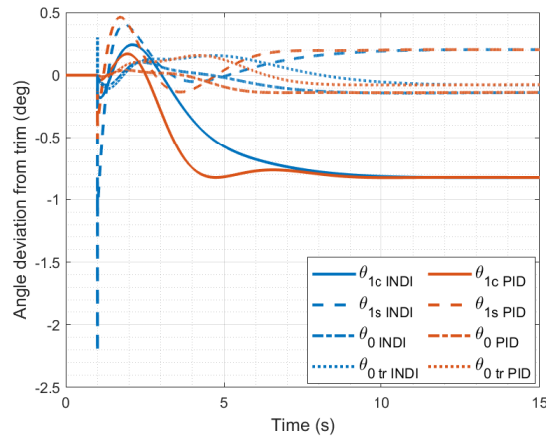


Figure 6.20: Control inputs relative to trim of both the ACAH INDI and ACAH PID controllers to step input on disturbance velocity of 4 kts .

6.6. Case 2: Pure Helicopter with Hub unaligned with C.G.

The second case places the location of the rotor hub at an offset relative to the cg of the helicopter (see Figure 6.21). This offset is in the x_B -direction of $x_h = 8\text{ cm}$ and in the y -direction $y_h = 3\text{ cm}$. (as is the x_b -location and y_b -location of the c.g. from the bo105 data). This means that the thrust also produces a pitch moment, roll moment and a yaw moment. This changes the dynamics of the helicopter.

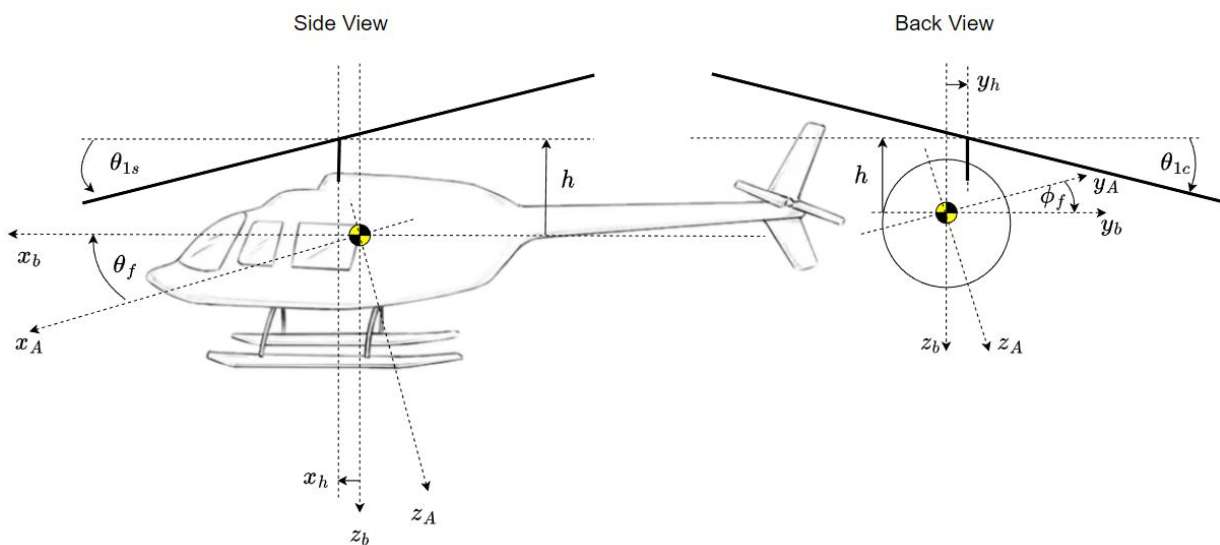


Figure 6.21: Configuration 6-DOF pure helicopter for case 2 in body frame of reference.

6.6.1. Case 2 Trim

The helicopter is, just as in case 1, trimmed at a velocity of 0 m/s and an altitude of 60 m . The trim states and control inputs are presented in Table 6.7. For clarity, the trim states and control inputs for case 1 are also given. Note that the helicopter is slightly less rolled to the left compared to case 1. This is due to the shift of the hub to the left. Since the hub moved left, the helicopter has to roll right in order to bring the hub above the c.g. again. This result hence makes sense. The helicopter is pitched up more due to moving of the hub forwards. This also makes sense as the c.g. is behind the hub and the c.g. moves forward relative to the hub when pitching up. The collective of the main and tail rotor are practically the same, whereas the cyclic is slightly different. This is to compensate for the changed attitude angles.

Table 6.7: Trim data Case 1 vs. 2

Helicopter State	Symbol	Name	Value case 1	Value case 2	unit
1	u	Body velocity in x	0.000	0.000	m/s
2	v	Body velocity in y	0.000	0.000	m/s
3	w	Body velocity in z	0.000	0.000	m/s
4	p	Body roll rate	0.000	0.000	deg/s
5	q	Body pitch rate	0.000	0.000	deg/s
6	r	Body yaw rate	0.000	0.000	deg/s
7	ψ_f	Fuselage heading angle	0.000	0.000	deg
8	θ_f	Fuselage pitch angle	8.6232	9.3449	deg
9	ϕ_f	Fuselage roll angle	-1.6326	-1.3224	deg
10	x	Helicopter x position	0.000	0.000	m
11	y	Helicopter y position	0.000	0.000	m
12	z	Helicopter z position	-60.000	-60.000	m
13	λ_0	Normalised uniform inflow velocity	0.0491	0.0491	—
14	λ_{0tr}	Normalised uniform inflow velocity tail	0.0557	0.0565	—
15	ω	Main rotor angular rate	44.400	44.400	rad/s
Control	Symbol	Name	Value case 1	Value case 5	unit
1	θ_{1c}	Lateral Cyclic	-0.3618	-0.5086	deg
2	θ_{1s}	Longitudinal Cyclic	1.5110	1.9170	deg
3	θ_0	Main rotor collective	14.3681	14.3633	deg
4	θ_{0tr}	Tail rotor collective	13.6380	13.8658	deg

6.6.2. Disturbance Response

The same controllers from case 1 are used in case 2. The reason for this is that there was not noticeable difference in the response of the controller, given the same disturbance as in case 1. This means that the conclusions from case 1 also apply to case 2.

6.7. Case 3: Helicopter with Single Cable Section at C.G.

With Case 3, a simple cable model is added to the helicopter. The goal of this case is to control the cable using helicopter motion. The cable consists of a single cable section ($n = 1$) with a length of 30m and the SONAR. It is attached at the c.g. of the helicopter. This is illustrated in Figure 6.22. Note that the cable angle θ_1 and ϕ_1 are the angle of the cable section at the attachment point to the helicopter relative to the local vertical. The SONAR is attached to the cable section and can rotate relative to it.

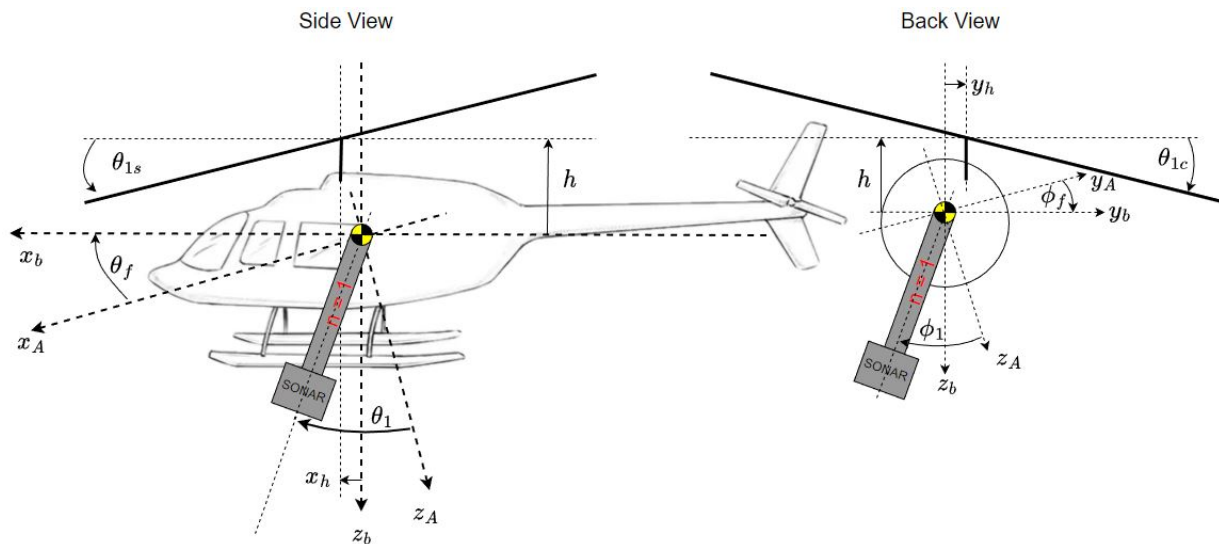


Figure 6.22: Configuration 6-DOF pure helicopter for case 3 in body frame of reference.

6.7.1. Trim Case 3

The helicopter and Cable + SONAR system is trimmed at the same conditions as in case 1 and 2. This is a trim altitude of $60m$ and a velocity of $0m/s$. The cable is set to 1 section, and has a length of $30m$. The decision was made for $30m$ to keep the cable short. Short cables are more difficult to control, due to their higher natural frequency for the pendulum motion. This demands a faster controller than if the cable were longer. The trim states are given in Table 6.8, as well as the trim controls. As shown, the pitch angle and the roll angle have increased and decreased respectively. This is caused by the added weight from the cable and SONAR. As a result, especially the collective has increased to provide more lift.

Table 6.8: Trim data Case 2 and 3

Helicopter State	Symbol	Name	Value case 2	Value case 3	unit
1	u	Body velocity in x	0.000	0.000	m/s
2	v	Body velocity in y	0.000	0.000	m/s
3	w	Body velocity in z	0.000	0.000	m/s
4	p	Body roll rate	0.000	0.000	deg/s
5	q	Body pitch rate	0.000	0.000	deg/s
6	r	Body yaw rate	0.000	0.000	deg/s
7	ψ_f	Fuselage heading angle	0.000	0.000	deg
8	θ_f	Fuselage pitch angle	9.345	11.239	deg
9	ϕ_f	Fuselage roll angle	-1.324	-1.862	deg
10	x	Helicopter x position	0.000	0.000	m
11	y	Helicopter y position	0.000	0.000	m
12	z	Helicopter z position	-60.000	-60.000	m
13	λ_0	Normalised uniform inflow velocity	0.0491	0.0520	–
14	λ_{0tr}	Normalised uniform inflow velocity tail	0.0565	0.0607	–
15	ω	Main rotor angular rate	44.400	44.400	rad/s
Cable State	Symbol	Name	Value case 2	Value case 3	unit
1	ϕ_1	Cable angle around x axis	–	0.0	deg
2	θ_1	Cable angle around y axis	–	0.0	deg
Control	Symbol	Name	Value case 2	Value case 3	unit
1	θ_{1c}	Lateral Cyclic	-0.5086	-0.5941	deg
2	θ_{1s}	Longitudinal Cyclic	1.9170	1.9045	deg
3	θ_0	Main rotor collective	14.3633	15.1087	deg
4	θ_{0tr}	Tail rotor collective	13.8658	15.1944	deg

6.7.2. Cable Controller Design

Cable Control through Helicopter Attitude

The cable controller for this case will be either an INDI controller, or a PID controller that outputs a reference attitude for the helicopter to follow. The block diagram for this control strategy is given in Figure 6.23. As shown, the cable controller is used to obtain a reference attitude in longitudinal and lateral direction. The commanded heading angle ψ_{fc} is pre-set to zero, and will stay at this value. The position hold, and the TRC controllers will produce the required main rotor collective to stay at the trim altitude. The position of the helicopter in longitudinal and lateral direction will not be controlled, and are free to move. The commanded z -position is set to the trim altitude. Note that the system using the INDI ACAH uses the INDI cable controller and the system using the PID ACAH uses the PID cable controller.

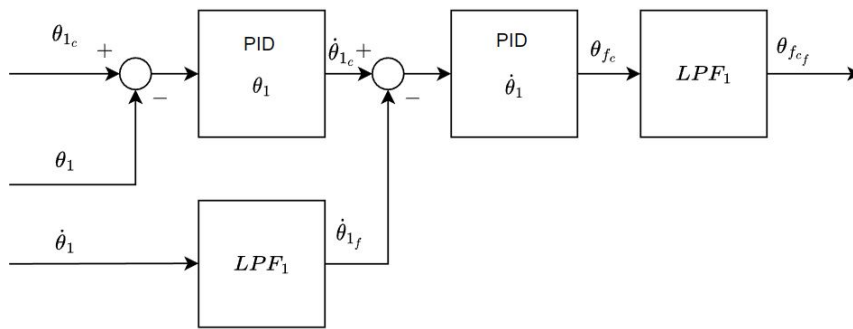


Figure 6.25: Block diagram for PID cable controller using cable control through helicopter attitude

6.7.3. Cable controller tuning

Tuning the cable controller is done using a similar procedure as the tuning for the ACAH, TRC and the position hold controller. A command cable angle is given to the controller which it has to follow. Both the INDI and PID cable controller are tuned such that the cable angle response matches a given desired response. This response is set to a natural frequency of ω_n of 0.2 rad and a damping ratio of $\zeta = 1$.

INDI Controller The cable angle response of the INDI controller is shown in Figure 6.26. Note that the subscript indicates whether the step command was in the ϕ_{1c} or the θ_{1c} direction. The transient of the response matches the desired response relatively well. After 15 seconds, the cable response no longer matches the desired response. However, no combination of gains was found that matches the cable response better to the desired response. During tuning, it was found that adding an integral component to the PID of the outer loop of the cable controller reduced the time to reach steady state. However, the overshoot increased, and the response would no longer match the desired response. The controller gains are given in Table 6.9.

PID Controller The cable angle response of the INDI controller is shown in Figure 6.27, with the controller gains in Table 6.9. Contrary to the INDI controller, an integral component was required to match the cable angle response to the desired response. The reason for this can be explained. The INDI controller has some integral-like behaviour already, since the control increments stack on top of each other. This means that if an error persists and there is a control increment, the control input increases over time as the control increments are added together. A PID controller doesn't have this naturally, and requires an integral component to do this.

What is interesting when comparing to the INDI controller is that the cross-coupling between ϕ_1 and θ_1 is much bigger for the PID controller than the INDI controller. This suggests that the INDI controller is better at decoupling the two modes. It is also interesting that the cross-coupling is more when the commanded cable angle is stepped in longitudinal direction than in lateral direction. The reason for this can be found in the fact that when the helicopter pitches, the main rotor collective has to change to produce the same amount of lift. This in turn requires a new lateral cyclic compensate for the lateral force imbalance. This causes a lateral motion of the helicopter and thus a change of the cable angle ϕ_1 . When the commanded cable angle is in lateral direction, the cable controller sends a reference roll angle. This requires a lateral cyclic, which means that the helicopter motion remains lateral. This reasoning can be backed up by observing the control inputs in Figure 6.28. Note that when there is a step in θ_{1c} (longitudinal cable angle, in blue), the longitudinal cyclic decreases to pitch the helicopter. Then, the main rotor collective changes, to compensate for lift. At the same time, the lateral cyclic changes to compensate for force imbalance. The longitudinal cyclic barely changes when the commanded cable angle is in lateral direction (in red).

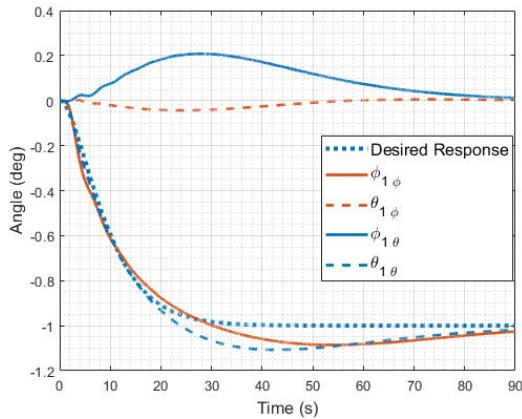


Figure 6.26: Cable angle response for INDI controller case 3, given a step input in commanded cable angle.

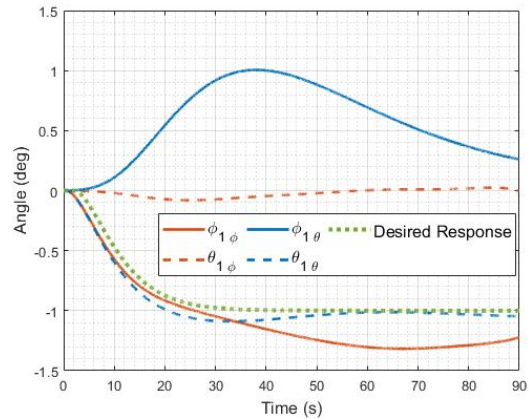


Figure 6.27: Cable angle response for PID controller case 3, given a step input in commanded cable angle.

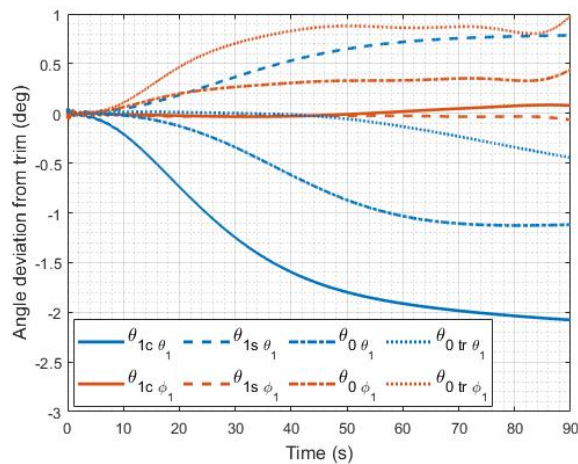


Figure 6.28: Control inputs relative to trim for PID controller case 3, given a step input in commanded cable angle.

Table 6.9: Gains for Cable Controller Case 3.

Gain	Value INDI	Value PID	unit
$K_{P\phi_1}$	0.80	2.0	s^{-1}
$K_{I\phi_1}$	0.00	0.15	s^{-2}
$K_{D\phi_1}$	1.60	12.00	—
$K_{P\dot{\phi}_1}$	0.65	0.80	s^{-1}
$K_{I\dot{\phi}_1}$	0.00	0.00	s^{-2}
$K_{D\dot{\phi}_1}$	2.60	4.00	—
$K_{P\theta_1}$	0.80	2.00	s^{-1}
$K_{I\theta_1}$	0.00	0.15	s^{-2}
$K_{D\theta_1}$	2.10	12.00	—
$K_{P\dot{\theta}_1}$	0.65	0.80	s^{-1}
$K_{I\dot{\theta}_1}$	0.00	0.00	s^{-2}
$K_{D\dot{\theta}_1}$	2.80	4.00	—

6.7.4. Disturbance Response

In order to compare the two control methods, INDI vs. PID, the helicopter-cable system is simulated given a disturbance in wind, just as in cases 1 and 2. This is done in two separate simulations with the same wind disturbance as in case 1 and 2. This is a filtered 4 kts wind at $t = 1$ seconds. The cable angle response is shown in Figure 6.29. As is visible, the cable angles diverge more when using the PID, than when using the INDI controller. The INDI controlled cable is more oscillatory. When looking at the control inputs to the helicopter in Figure 6.30, both the PID and the INDI controlled system shown oscillatory control inputs. Experimenting with controller gains found that these oscillations follow from the controller gains $K_{D\dot{\phi}_1}$ and $K_{D\dot{\theta}_1}$. Reducing these gains removes the oscillations. In order to determine whether either controller is better at performing the dipping SONAR mission, the SONAR ground velocity is presented in Figure 6.31. Here, it becomes clear that the INDI controller is better at keeping the lateral velocity low than the PID controller, given a longitudinal wind disturbance. This is consistent with the previous observation that the INDI controller is better at decoupling the longitudinal and lateral modes.

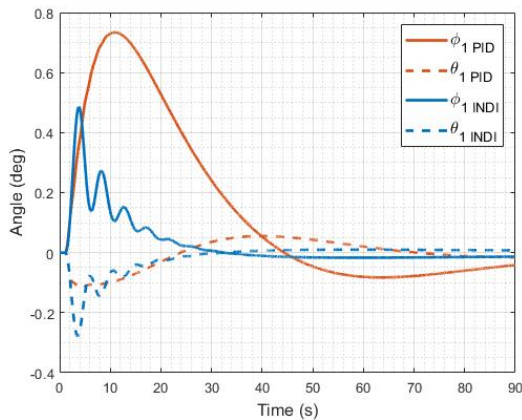


Figure 6.29: Cable angle response for disturbance case 3, given a filtered 4 kts step input in wind.

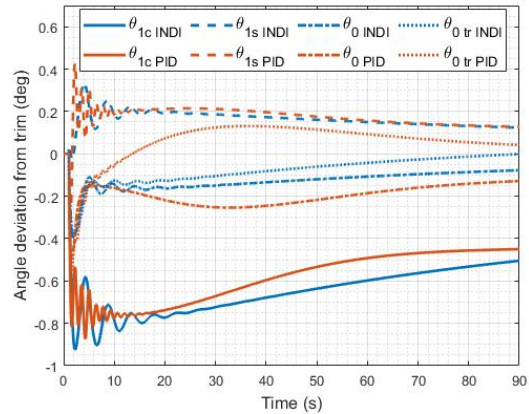


Figure 6.30: Control inputs relative to trim for disturbance case 3, given a filtered 4 kts step input in wind.

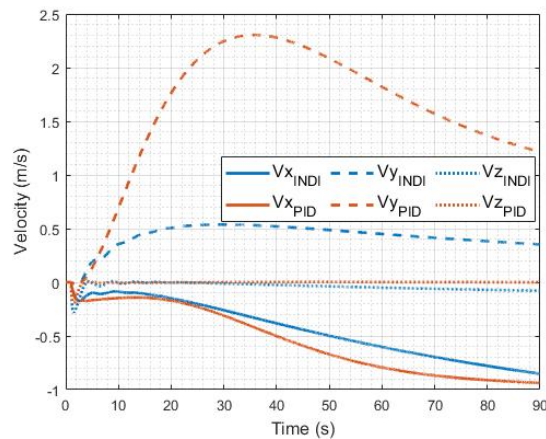


Figure 6.31: Sonar ground velocity response for disturbance case 3, given a filtered 4 kts step input in wind.

6.7.5. Conclusions case 3

In this section, a cable model consisting of a single cable section is added to the helicopter model. The goal of this section was to obtain a PID and an INDI controller that controls the cable. The two controllers were tuned via the same procedure as the ACAH, TRC and position hold and the two controllers matched the desired response with limited success. When comparing both control methods, it was found that both the PID and the INDI are capable of controlling the cable when subjected to a disturbance wind of 4 kts. However, the INDI controller is more capable of decoupling the longitudinal and lateral modes of the helicopter-cable system than the PID controller.

6.8. Case 4: Helicopter with Single Cable Section at Offset

With Case 4, the simple cable model from case 3 is put at an off-set relative to the c.g. of the helicopter. The reason for this is that the cable would realistically never be located exactly at the c.g., although it would remain close to it. For this case, the cable attachment point is put at $x_l = 0.50\text{m}$ in front of the c.g. and $h_l = 1.0\text{m}$ below the c.g. These values are somewhat arbitrary, since the Bo105 does not have a cable attachment point in reality. y_l is kept at 0 m. See Figure 6.32.

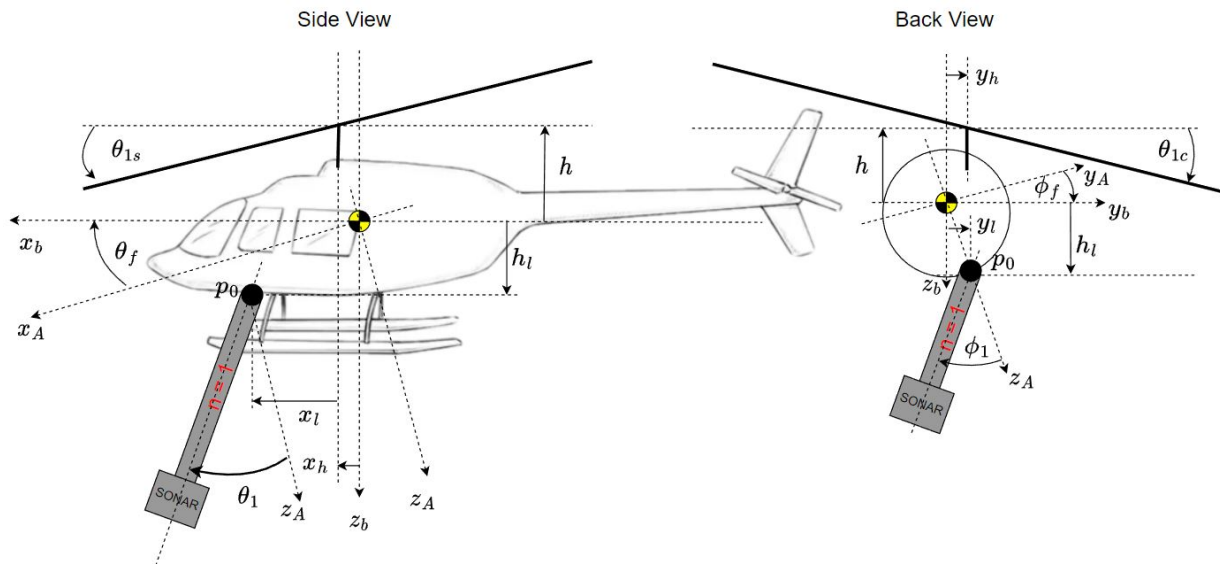


Figure 6.32: Configuration 6-DOF pure helicopter for case 4 in body frame of reference.

6.8.1. Trim Case 4

The helicopter and Cable + SONAR system is trimmed at the same conditions as in cases 1-3. This is a trim altitude of $60m$ and a velocity of $0m/s$. The trim states are given in Table 6.10, as well as the trim controls. For comparison, the trim states and controls of case 3 are shown as well. Interestingly, the fuselage pitch angle has decreased slightly. This is due to the combined c.g. of the cable tension and the helicopter has shifted forwards. The same is true for the fuselage roll angle. The control inputs are largely the same for cases 3 and 4.

Table 6.10: Trim data Case 2 and 3

Helicopter State	Symbol	Name	Value case 3	Value case 4	unit
1	u	Body velocity in x	0.000	0.000	m/s
2	v	Body velocity in y	0.000	0.000	m/s
3	w	Body velocity in z	0.000	0.000	m/s
4	p	Body roll rate	0.000	0.000	deg/s
5	q	Body pitch rate	0.000	0.000	deg/s
6	r	Body yaw rate	0.000	0.000	deg/s
7	ψ_f	Fuselage heading angle	0.000	0.000	deg
8	θ_f	Fuselage pitch angle	11.239	10.857	deg
9	ϕ_f	Fuselage roll angle	-1.862	-2.068	deg
10	x	Helicopter x position	0.000	0.000	m
11	y	Helicopter y position	0.000	0.000	m
12	z	Helicopter z position	-60.000	-60.000	m
13	λ_0	Normalised uniform inflow velocity	0.0520	0.0520	–
14	λ_{0tr}	Normalised uniform inflow velocity tail	0.0607	0.0609	–
15	ω	Main rotor angular rate	44.400	44.400	rad/s
Cable State	Symbol	Name	Value case 3	Value case 4	unit
1	ϕ_1	Cable angle around x axis	0.0	0.0	deg
2	θ_1	Cable angle around y axis	0.0	0.0	deg
Control	Symbol	Name	Value case 3	Value case 4	unit
1	θ_{1c}	Lateral Cyclic	-0.5941	-0.5950	deg
2	θ_{1s}	Longitudinal Cyclic	1.9045	1.7031	deg
3	θ_0	Main rotor collective	15.1087	15.1132	deg
4	θ_{0tr}	Tail rotor collective	15.1944	15.2621	deg

6.8.2. Disturbance Response

Using the same controllers from case 3 yields practically the same response as in case 3. However, for the PID controller to work, the derivative gains $K_{D\phi_1}$ and $K_{D\theta_1}$ in Table 6.9 have been reduced from 12.00 to 8.00. The reason for this reduction is that the cable controller was sending very oscillatory signals to the ACAH. Reducing the derivative gain removed most of these oscillations. The cable response to the disturbance from case 1-3 is shown in Figure 6.33. As shown, the response is almost exactly the same. Therefore, this case will not be discussed in more detail.

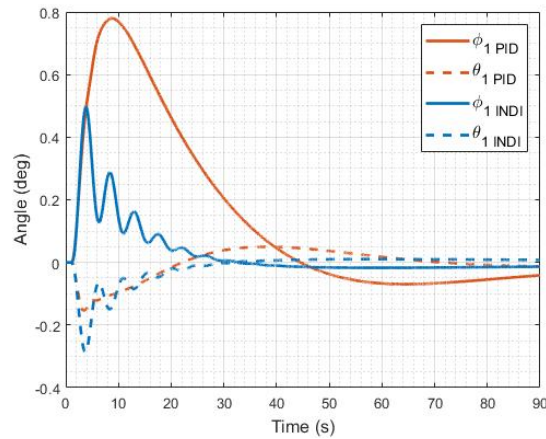


Figure 6.33: Cable angle response for disturbance case 4, given a filtered 4 kts step input in wind.

6.9. Case 5: Helicopter with Multiple Cable Sections at Offset

Case 5 is the same as case 4, yet with a longer cable and 5 cable sections ($n = 5$). The function of this case is to observe the change from a rigid to a flexible cable. The configuration is illustrated in Figure 6.34. Note that from this point, the configuration of the helicopter does not change with cases 6 and 7. In case 6, the cable model is lowered into the water and in case 7, the environmental conditions are changed.

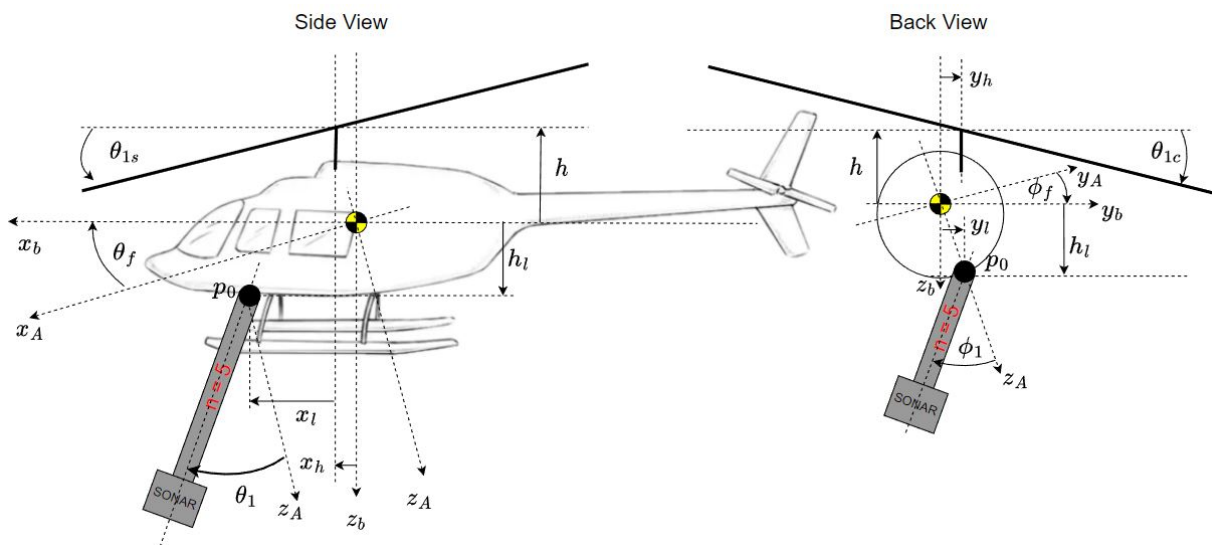


Figure 6.34: Configuration 6-DOF pure helicopter for case 5 - case 7 in body frame of reference.

6.9.1. Trim

For case 5, the helicopter is trimmed at a velocity of 0 m/s in forward direction, similar to cases 1-4. The trimming procedure is also the same. The trimmed states are presented in Table 6.11. Note that the cable angle of only the first cable section is presented. It is not necessary to add the states of the other cable sections, as the cable is still and straight down for cases 4 and 5. The only difference for trimming cases 4 and 5 is the difference in length of the cable (30m for case 4 and 120m for case 5). This means that the cable is heavier. Therefore, the trimmed states are very similar for cases 4 and 5.

Table 6.11: Trim data Case 4 vs. 5

Helicopter State	Symbol	Name	Value case 4	Value case 5	unit
1	u	Body velocity in x	0.000	0.000	<i>m/s</i>
2	v	Body velocity in y	0.000	0.000	<i>m/s</i>
3	w	Body velocity in z	0.000	0.000	<i>m/s</i>
4	p	Body roll rate	0.000	0.000	<i>deg/s</i>
5	q	Body pitch rate	0.000	0.000	<i>deg/s</i>
6	r	Body yaw rate	0.000	0.000	<i>deg/s</i>
7	ψ_f	Fuselage heading angle	0.000	0.000	<i>deg</i>
8	θ_f	Fuselage pitch angle	10.857	11.053	<i>deg</i>
9	ϕ_f	Fuselage roll angle	-2.068	-2.166	<i>deg</i>
10	x	Helicopter x position	0.000	0.000	<i>m</i>
11	y	Helicopter y position	0.000	0.000	<i>m</i>
12	z	Helicopter z position	-60.000	-60.000	<i>m</i>
13	λ_0	Normalised uniform inflow velocity	0.0520	0.0523	–
14	λ_{0tr}	Normalised uniform inflow velocity tail	0.0609	0.0614	–
15	ω	Main rotor angular rate	44.400	44.400	<i>rad/s</i>
Cable State	Symbol	Name	Value case 4	Value case 5	unit
1	ϕ_1	Cable angle around x axis	0.0	0.0	<i>deg</i>
2	θ_1	Cable angle around y axis	0.0	0.0	<i>deg</i>
Control	Symbol	Name	Value case 4	Value case 5	unit
1	θ_{1c}	Lateral Cyclic	-0.5950	-0.6030	<i>deg</i>
2	θ_{1s}	Longitudinal Cyclic	1.7031	1.6826	<i>deg</i>
3	θ_0	Main rotor collective	15.1132	15.1944	<i>deg</i>
4	θ_{0tr}	Tail rotor collective	15.2621	15.4208	<i>deg</i>

6.9.2. Cable Controller Design

The design of the cable controller is done in a different way than in cases 3 and 4. In this case, rather than using the attitude of the helicopter, the velocity of the helicopter is used. The reason for this is that the smaller cable sections have a higher frequency than the larger single cable section in case 4. As a result, the attitude of the helicopter became too oscillatory. Using the velocity instead made the controller less aggressive, since it is one integration above acceleration (which follows from attitude).

The general architecture of the controller is shown in Figure 6.35. As shown, the cable controller and the position hold controller commands are added together, to get a velocity command. This command is converted to body frame, after which the body reference velocities are sent to the TRC. This then results in an attitude command for the ACAH, which yields a certain control command to the helicopter. Note that the position hold only contains the altitude hold for this case. When setting a reference angle for the cable controller, the helicopter has to effectively accelerate to a certain velocity where the drag is such that the cable remains at its reference. Therefore, the position hold is off for horizontal motion, as it would otherwise conflict with the cable controller.

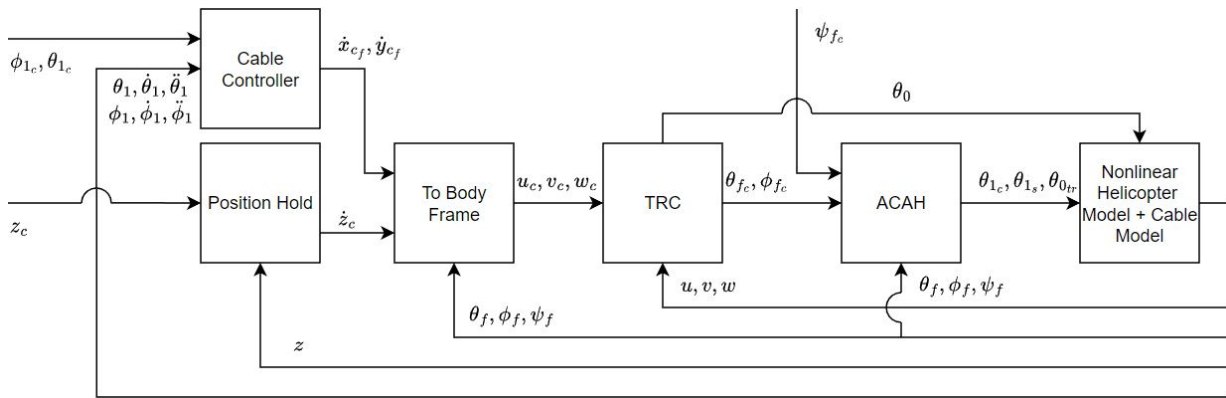


Figure 6.35: Controller architecture case 5

INDI Controller

The architecture of the cable controller of cable angle θ_1 is shown in Figure 6.36. As shown, this is an INDI controller with an inner cable rate loop and an outer cable angle loop. Notice the similarity with Figure 6.24. The model inversion used for this controller is presented in Equation 6.3. For the lateral cable angle, this is equal to l_c .

$$\frac{\partial \ddot{x}}{\partial \dot{\theta}_1} = -l_c \tag{6.3}$$

Note that there are two low pass filters (LPF) present in the controller instead of one. The low pass filter LPF_1 is a filter added to the cable angular rate and the cable angular acceleration. This is done since the cable angular rate and acceleration are very oscillatory, and are smoothed out using this filter. A time constant of $\tau_1 = 10$ seconds is used for this filter. Note that filtered signals have subscript f attached to them. To synchronise the controller with the delayed filtered signals, the same LPF is applied to the feedback of the commanded horizontal velocity. A second filter is added at the end: LPF_2 . This filter smooths the commanded velocity to remove high frequencies from the velocity commands and has a time constant of $\tau_2 = 5$ seconds. The cable controller for cable angle ϕ_1 has the same structure and filters as the cable controller for angle θ_1 .

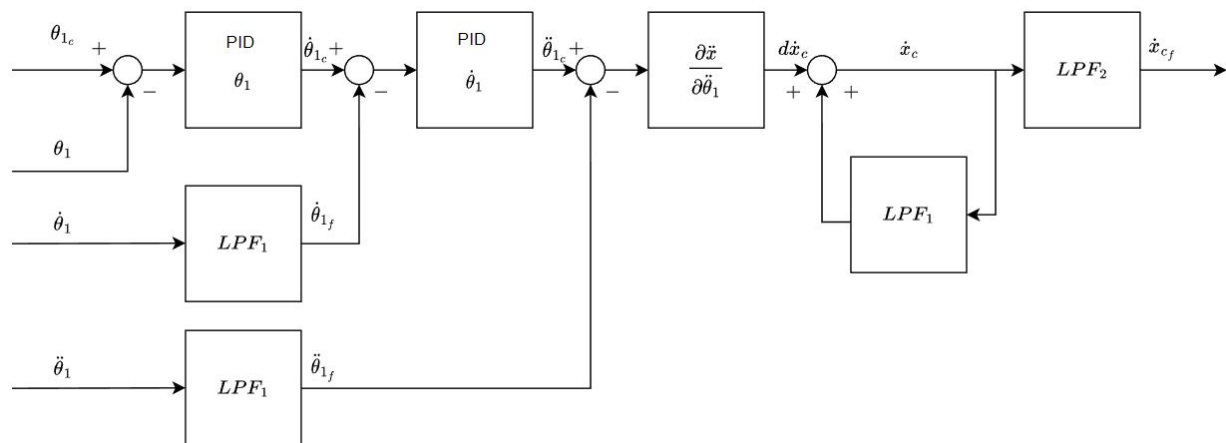


Figure 6.36: Block diagram INDI cable controller case 5

PID Controller

The architecture of the PID cable controller is shown in Figure 6.37. It is very similar to the INDI. Note that the same filters are used for the PID as for the INDI.

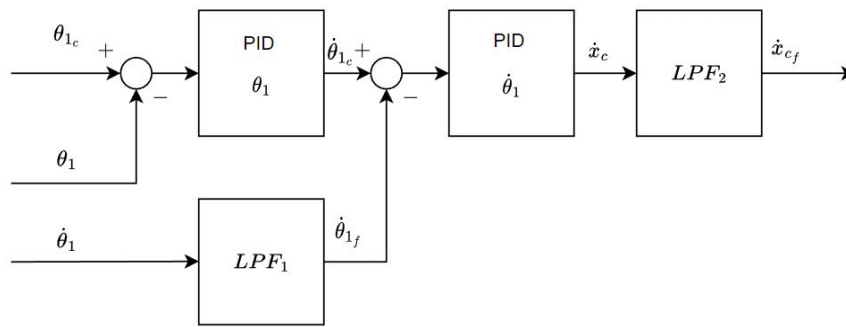


Figure 6.37: Block diagram PID cable controller case 5

6.9.3. Cable Controller Tuning

Controller tuning was done via the same approach as done in previous cases. However, during the process, it was found to be very difficult to find a set of gains that yields satisfactory results. Therefore, it was not possible to match the output of the controllers to a desired response. Nevertheless, some interesting conclusions can be drawn from this case: First, there are two distinct phases in the cable response. The first is an oscillatory transient phase and the second is a very smooth phase where the cable angle moves to its desired value. The first phase is caused by the acceleration of the helicopter. This causes a sudden excitation of the cable, which takes time to settle. At the same time, the helicopter is accelerating to the velocity that produces enough drag to have the cable displaced at the desired cable angle. Second, the controller behaviour is very different than that from case 3 and 4. Most notably, it's a slower due to it being an integral away from the acceleration of the cable.

INDI and PID Controller

The cable response of the tuned INDI and PID controllers is shown in Figure 6.38 and Figure 6.39. Both the INDI and the PID controller approach the desired cable angle very slowly. The first phase of the cable angle response is not visible in the response of the PID controller. This suggests that the PID is not able to damp the oscillation caused by the initial acceleration quickly. However, the controller gains are not optimised, so this could be due to bad gain tuning. Interestingly, the lateral-longitudinal coupling is clearly visible in the PID, whereas less so for the INDI, which is consistent with the previous cases.

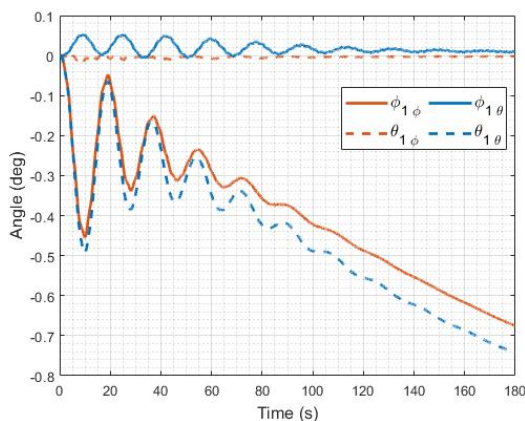


Figure 6.38: Response cable angle with INDI cable controller

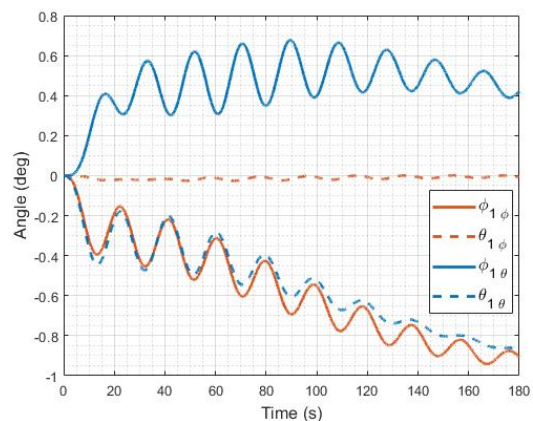


Figure 6.39: Response cable angle with PID cable controller

Table 6.12: Gains for Cable Controllers Case 5.

Gain	Value INDI	Value PID	unit
$K_{P\phi_1}$	1.00	1.50	s^{-1}
$K_{I\phi_1}$	0.00	0.30	—
$K_{D\phi_1}$	1.00	0.00	s^{-2}
$K_{P\dot{\phi}_1}$	0.20	12.00	—
$K_{I\dot{\phi}_1}$	0.00	0.00	s
$K_{D\dot{\phi}_1}$	0.10	72.00	s^{-1}
$K_{P\theta_1}$	1.00	1.50	s^{-1}
$K_{I\theta_1}$	0.00	0.30	—
$K_{D\theta_1}$	1.00	0.00	s^{-2}
$K_{P\dot{\theta}_1}$	0.20	-12.00	—
$K_{I\dot{\theta}_1}$	0.00	0.00	s
$K_{D\dot{\theta}_1}$	0.10	-72.00	s^{-1}

6.9.4. Cable Controller Disturbance Response

In order to compare the PID and the INDI controllers, both controllers are simulated with a filtered step input in the disturbance velocity of $4kts$ in x-direction at time $t = 1$ seconds as is done in previous cases. The response of the cable angle is presented in Figure 6.40. As shown, the PID controller is unstable under the given disturbance. It is not able to compensate for the added wind. The INDI controller on the other hand is capable of maintaining control. However, when observing the control inputs to the helicopter, a vibration is present. This vibration is caused by the oscillations of the first cable section. Such oscillations could be removed by making the controller slower. Either by increasing the time constant of the filters used or by reducing the gains of the controller. Furthermore, it was found that these vibrations are present when the air velocity in that direction is small. This means that drag has a damping effect on the cable sections. Nevertheless, it shows that the INDI controller is more capable of adapting to the new situation of added wind.

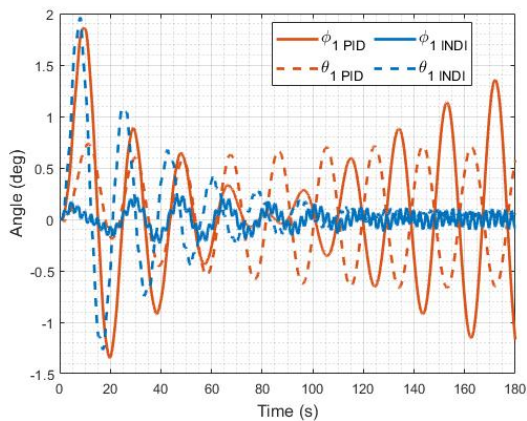


Figure 6.40: Response of cable angle with INDI and PID controller to a step input on wind of $4kts$

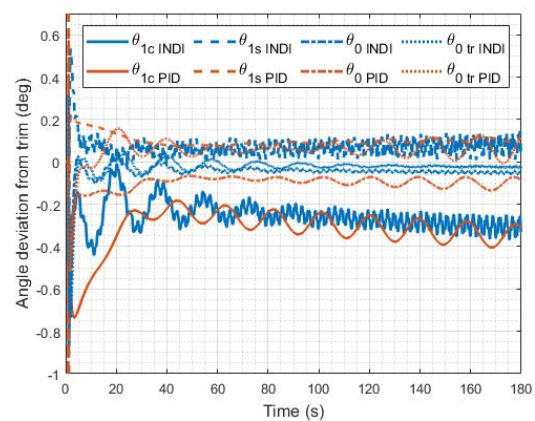


Figure 6.41: Control inputs from INDI and PID controller from a step input on wind of $4kts$

6.9.5. Conclusions case 5

From case 4 to case 5, the length of the cable was increased from 30 to 120 meters and the amount of cable sections was increased from 1 to 5. The effect of lengthening the cable on the controller is largely the lower frequency of the pendulum mode of the cable. The effect of the addition of cable sections is more pronounced: Since each cable link moves with respect to the other links, oscillations are present in

the angular rate and acceleration which find their way through the controller. This requires the addition of low-pass filters in order to smooth these out. It was also found that the drag on the cable has a stabilising effect on the cable. The expectation for case 6 is therefore that the oscillations are more damped than in case 5, due to the added drag from the water. On the topic of performance, the INDI controller was capable of stabilising the cable given a $4kts$ wind after tuning, which the PID was not capable of doing. This shows the adaptive nature of the INDI controller. There were, however, vibrations present in the response of the cable and in the control inputs to the helicopter. These could be removed by either lowering gains of the cable controller, or by increasing the time constants of the low-pass filters.

6.10. Case 6: Helicopter with Multiple Cable Sections at Offset, Partially Submerged

Case 6 adds the concept of submergence. With a trimmed altitude of 60m and a cable length of 120m, half the cable is submerged and the other half emerged in zero wind conditions. The addition of water drag, instead of air drag in case 5, will likely cause more damping to the cable, as well as a slower system to control. This will make it easier for the INDI controller, since INDI is based on the principle of the controls being faster than the states.

6.10.1. Trim

The trim is done exactly as done in case 5, and also provides the same trim states and controls as shown in Table 6.13. This makes sense, since the trimmed velocity is still $0m/s$, meaning that the cable is still straight down. The effect of the water drag is therefore not visible. Note: When trimming the cable at nonzero velocities, the cable will not have a straight shape, and will bulge out of the water. This means that the drag of the cable has an effect on the trimmed solution. From this point, trimming has become an iterative process. First, the cable must be trimmed to obtain the cable tension acting on the helicopter. Then, the helicopter is trimmed with this cable tension. This requires a certain attitude of the helicopter, slightly changing the altitude of the cable attachment point (its not at the c.g. of the helicopter. The helicopter c.g. is trimmed at the trim altitude). This changes the amount the cable is submerged, changing the drag of the cable and hence the trim tension.

Table 6.13: Trim data Case 5 vs. 6

Helicopter State	Symbol	Name	Value case 5	Value case 6	unit
1	u	Body velocity in x	0.000	0.000	m/s
2	v	Body velocity in y	0.000	0.000	m/s
3	w	Body velocity in z	0.000	0.000	m/s
4	p	Body roll rate	0.000	0.000	deg/s
5	q	Body pitch rate	0.000	0.000	deg/s
6	r	Body yaw rate	0.000	0.000	deg/s
7	ψ_f	Fuselage heading angle	0.000	0.000	deg
8	θ_f	Fuselage pitch angle	11.053	11.053	deg
9	ϕ_f	Fuselage roll angle	-2.166	-2.166	deg
10	x	Helicopter x position	0.000	0.000	m
11	y	Helicopter y position	0.000	0.000	m
12	z	Helicopter z position	-60.000	-60.000	m
13	λ_0	Normalised uniform inflow velocity	0.0523	0.0523	–
14	λ_{0tr}	Normalised uniform inflow velocity tail	0.0614	0.0614	–
15	ω	Main rotor angular rate	44.400	44.400	rad/s
Cable State	Symbol	Name	Value case 5	Value case 6	unit
1	ϕ_1	Cable angle around x axis	0.0	0.0	deg
2	θ_1	Cable angle around y axis	0.0	0.0	deg
Control	Symbol	Name	Value case 5	Value case 6	unit
1	θ_{1c}	Lateral Cyclic	-0.6030	-0.6030	deg
2	θ_{1s}	Longitudinal Cyclic	1.6826	1.6826	deg
3	θ_0	Main rotor collective	15.1944	15.1944	deg
4	θ_{0tr}	Tail rotor collective	15.4208	15.4208	deg

6.10.2. Cable Controller Design

The cable controller design is discussed in this section. For this case, however, 3 control strategies are tested in order to find out what control strategy works best for dipping SONAR missions. There 3 control strategies are: cable control through helicopter attitude, cable control through helicopter velocity and cable control through helicopter position. As the name suggests, the first strategy uses the cable controller to obtain a reference attitude for the helicopter to follow in order to control the cable. The second uses the velocity, as illustrated in case 5. The final strategy uses the controller to obtain a reference position.

Control strategy 1: Cable control through helicopter attitude

Cable control through helicopter is done the same way as in case 3 and 4. However, since part of the cable is submerged, the model inversion used is no longer the entire length of the cable, but the altitude of the helicopter is used instead. The reason for this is that it is assumed that the helicopter moves much faster than the submerged parts of the cable and the cable angle is small. For simplicity, the trimmed altitude is used, since the altitude remains roughly constant. The block diagram for this control strategy can be found in Figure 6.23, with the cable controller block diagram in Figure 6.24 and Figure 6.25. Tuning was done by setting a reference for the cable angle of -1° for ϕ_{1c} and θ_{1c} at the $t = 0$ seconds in two separate simulations, similar to previous cases. The goal was to have both cable angles follow a desired response with a natural frequency of $\omega_n = 0.2$ rad/s, a damping ratio of $\zeta = 1$ and a time delay of 2.08 seconds. The time delay is added to match the desired signal with the response of the helicopter-cable system. This is done to synchronise the responses when comparing control strategies. The gains for the controller are found in Table 6.14.

The system was simulated for 60 seconds and the response of the cable is shown in Figure 6.42. The helicopter attitude deviation from trim is shown in Figure 6.43. The body velocities and the helicopter control input deviation from trim is shown in Figure 6.44 and Figure 6.45 respectively. Again, note that the subscripts ϕ and θ indicate whether the simulation was done with the ϕ_{1c} reference of -1° or the θ_{1c} reference of -1° .

The controller appears to follow the desired response with little deviation, as it was tuned to do. The attitude deviation of the helicopter relative to trim is quite oscillatory, yet the angles are well below 1° . The body velocities and helicopter control input deviation from trim are presented for reference.

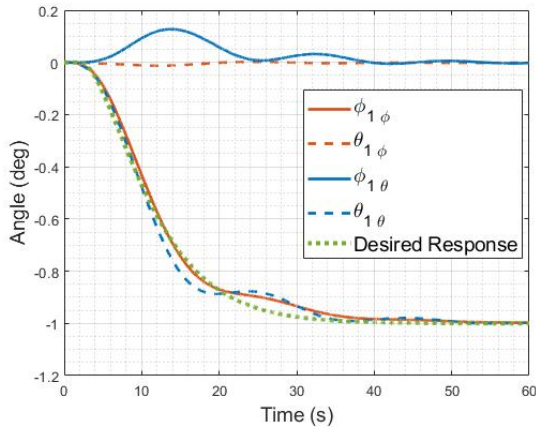


Figure 6.42: Response cable angle with INDI cable controller through attitude control

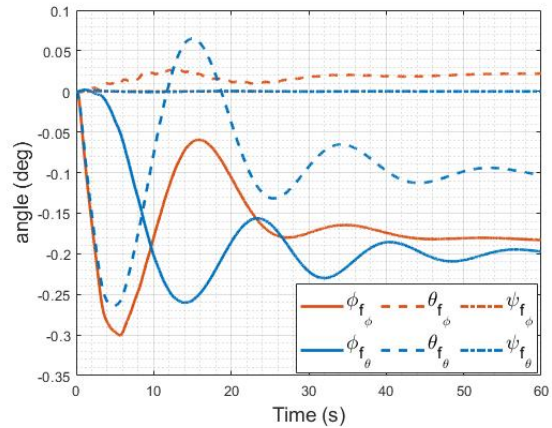


Figure 6.43: Response of helicopter attitude from trim with INDI cable controller through attitude control

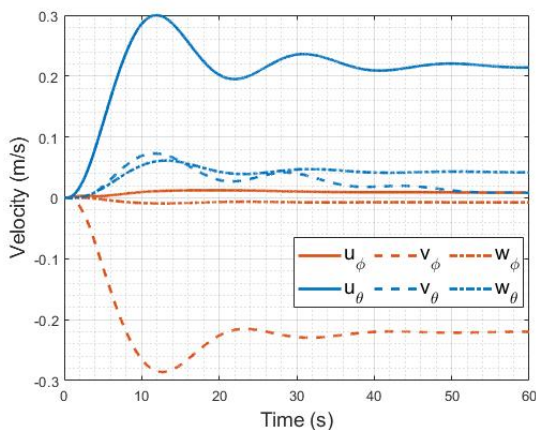


Figure 6.44: Response of body velocities with with INDI cable controller through attitude control

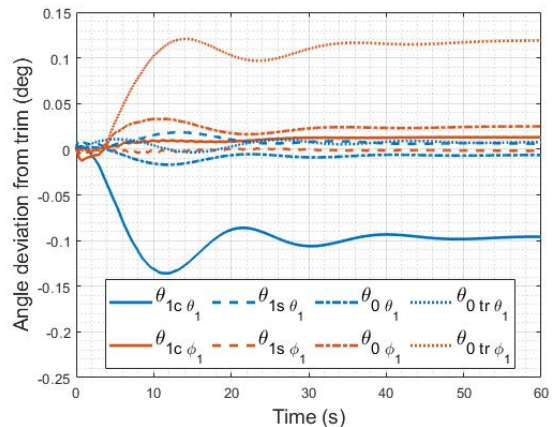


Figure 6.45: Control inputs from trim to helicopter with with INDI cable controller through attitude control

Control strategy 2: Cable control through helicopter velocity

Cable control through helicopter velocity is done exactly as in case 5. However, since part of the cable is submerged, the model inversion used is no longer the entire length of the cable, but the altitude of the helicopter is used instead. The reason for this is that it is assumed that the helicopter moves much faster than the submerged parts of the cable and the cable angle is small. The block architecture for this control strategy is found in Figure 6.36. Tuning was done using the same procedure as the control through attitude with the same desired response with a natural frequency of $\omega_n = 0.2$ rad/s, a damping ratio of $\zeta = 1$ and a time delay of 2.08 seconds. This is done in order to allow comparing the strategies in the end. The final

gains are presented in Table 6.14.

The system was simulated for 60 seconds and the response of the cable is shown in Figure 6.46. The helicopter attitude deviation from trim is shown in Figure 6.47. The body velocities and the helicopter control input deviation from trim is shown in Figure 6.48 and Figure 6.49 respectively.

The first observation that can be made is that this control strategy follows the reference better than when using the cable controller using attitude control. The reason for this is that the desired response was matched to this control strategy. Nevertheless, the response using this control strategy is different from the previous in multiple ways. The first being that the cross-coupling between the longitudinal angle θ_1 and the lateral angle ϕ_1 is smaller. This suggests that this strategy is better at decoupling these two modes. A second large difference is that the attitude response of the helicopter is smoother, and less oscillatory than when using control strategy 1. Finally, the control input deviation of the control inputs to the helicopter in Figure 6.49 are more aggressive in the first 5 seconds than in Figure 6.45 from strategy 1.

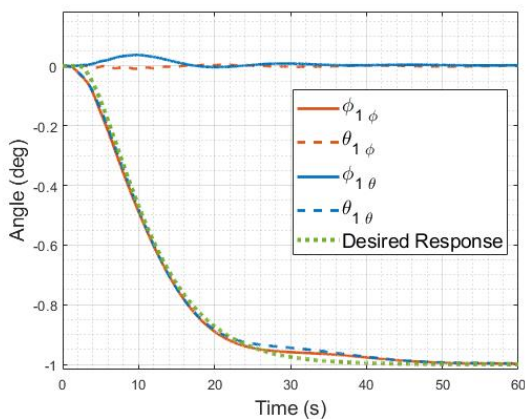


Figure 6.46: Response cable angle with INDI cable controller through velocity control

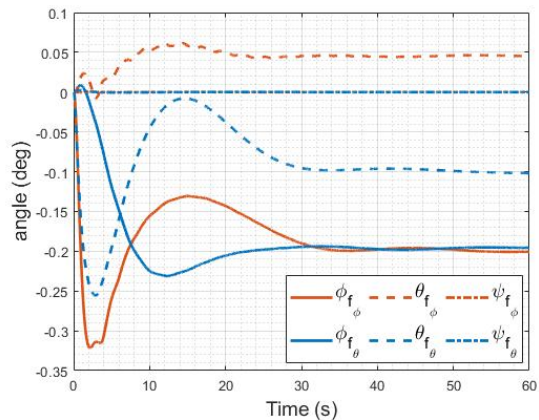


Figure 6.47: Response of helicopter attitude from trim with INDI cable controller through velocity control

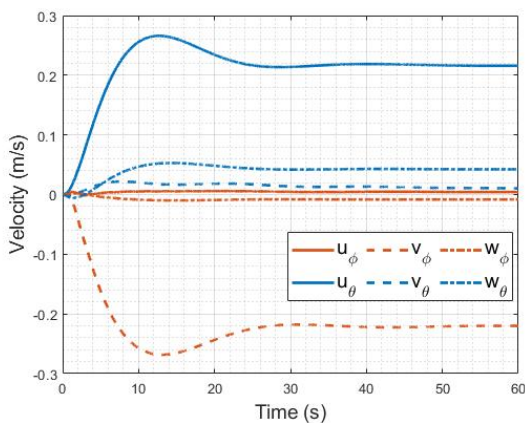


Figure 6.48: Response of body velocities with with INDI cable controller through velocity control

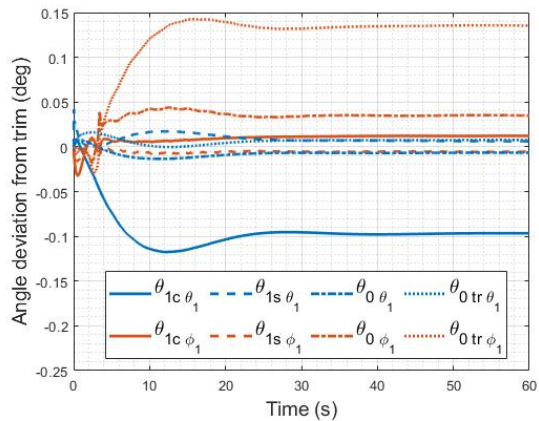


Figure 6.49: Control inputs from trim to helicopter with with INDI cable controller through velocity control

Control strategy 3: Cable control through helicopter position

Cable control through helicopter position was not presented in this work yet. The controller architecture is shown in Figure 6.50. The cable controller block diagram is given in Figure 6.51.

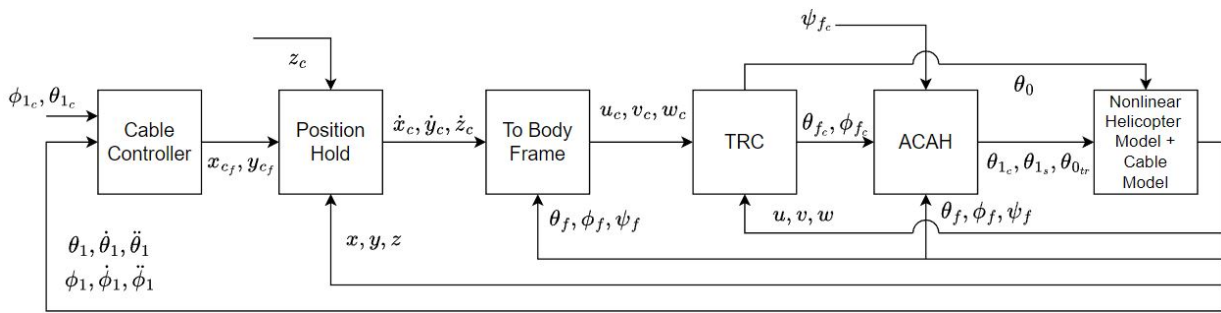


Figure 6.50: Controller architecture cable control through helicopter position

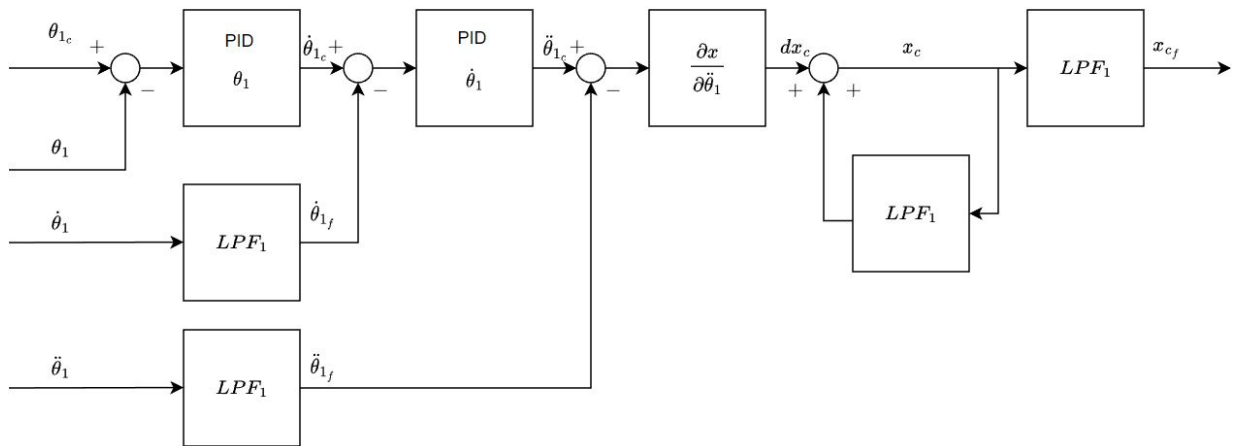


Figure 6.51: Cable controller block diagram for control through helicopter position

Tuning was done using the same procedure as the control through attitude and through velocity with the same desired response. The final gains are presented in Table 6.14.

The system was simulated for 60 seconds and the response of the cable is shown in Figure 6.52. The helicopter attitude deviation from trim is shown in Figure 6.53. The body velocities and the helicopter control input deviation from trim is shown in Figure 6.54 and Figure 6.55 respectively.

The first observation that can be made is that this control strategy follows the reference worse than when using either strategy 1 or 2. However, just like strategy 2, there is less cross-coupling present and the response is smoother than using strategy 1. It is, however, more aggressive than both strategies, when observing the control inputs in Figure 6.55.

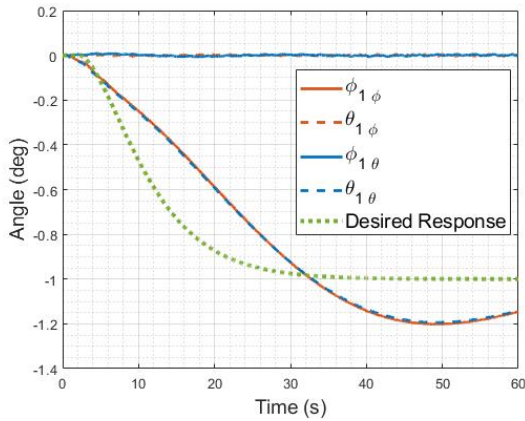


Figure 6.52: Response cable angle with INDI cable controller through position control

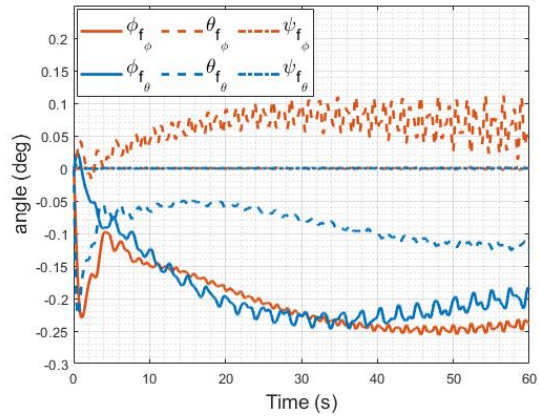


Figure 6.53: Response of helicopter attitude from trim with INDI cable controller through position control

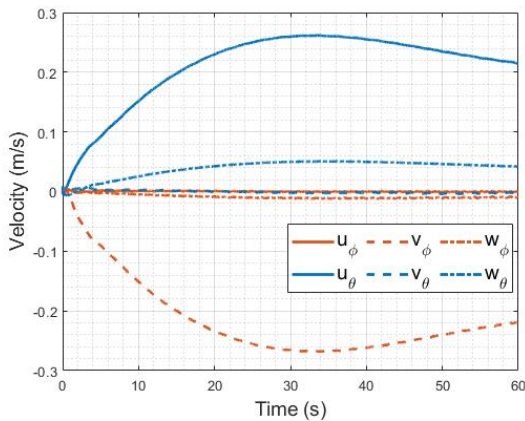


Figure 6.54: Response of body velocities with with INDI cable controller through position control

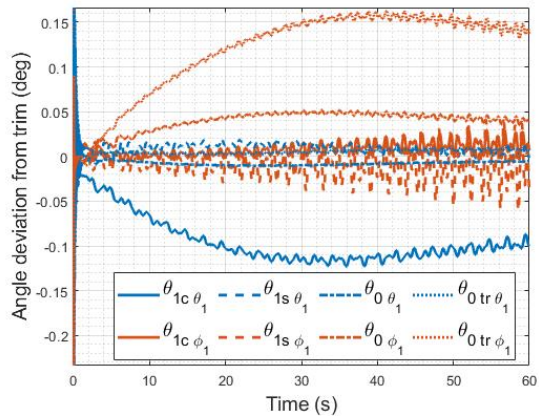


Figure 6.55: Control inputs from trim to helicopter with with INDI cable controller through position control

Control strategy comparison by disturbance response

In order to decide what control strategy is best, all 3 strategies are simulated with a wind of $4kts$ at the $t = 1$ seconds mark and a reference angle of 0° for ϕ_{1c} and θ_{1c} . The response of the cable angle, SONAR ground velocity, body velocities and helicopter attitude are presented in Figure 6.56 - Figure 6.59. To avoid cluttering, not all body velocities and attitudes are plotted. Note that the subscripts att, vel and pos indicate attitude, velocity and position. These represent the different control strategies: using attitude,

velocity and position. Observing the cable angles, it is clear that the cable controller through helicopter attitude shows the smallest angle deviation to a $4kts$ wind, yet the controller through helicopter velocity reaches a 0° angle faster. Also, the cross-coupling between the longitudinal and lateral angles appears to be larger for the control strategy using attitude control than the other strategies. This was already observed previously.

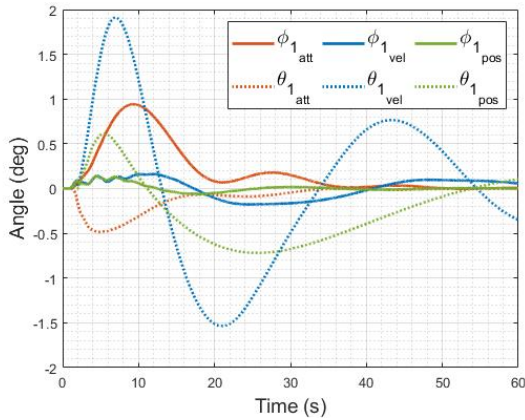


Figure 6.56: Cable angle response to a $4kts$ wind using different control strategies

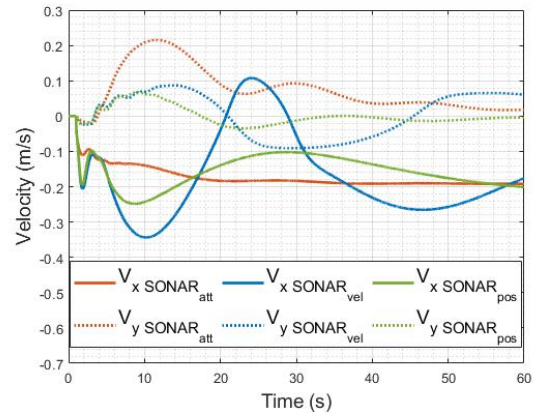


Figure 6.57: SONAR ground velocity squared response to a $4kts$ wind using different control strategies

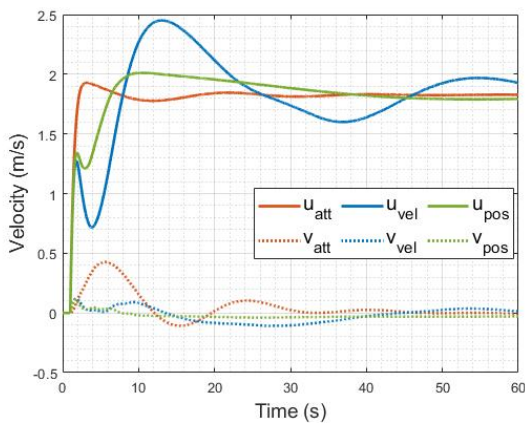


Figure 6.58: Body velocity response to a $4kts$ wind using different control strategies

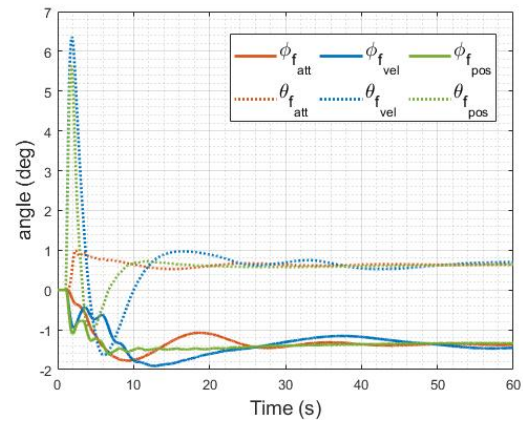


Figure 6.59: Helicopter attitude response relative to trim to a $4kts$ wind using different control strategies

Cable control strategy choice

In order to determine what strategy is best for dipping SONAR missions, it can be reasoned that the amount of velocity deviation is most important. Observing the SONAR velocity, the control strategy using helicopter attitude performs the best, by having the lowest velocity deviation. The reason why cable control through attitude control performs better, is likely due to the wind velocity not being present in the controller loop. In the other two control strategies, the body velocity is within the control loop via the TRC controller. Since there is initially no body velocity (there is no wind after all) and the cable is straight, the reference body velocity is zero. This means that once the wind hits, the reference velocity is still close to zero, meaning that the controller will move the helicopter such that the body velocity is reduced to zero, before the cable controller or position hold controller can match the wind velocity. This can be seen in Figure 6.58, where the control strategies using velocity and position decrease the body velocity initially, before matching the roughly 1.8 m/s in u direction.

6.10.3. Cable Controller Tuning

This section covers the tuning of the PID controller, since the INDI controller was tuned in the previous section. Since the decision was made to use a cable controller through attitude control for INDI, the same strategy is used for PID as well. The desired response still remains the same with a natural frequency of $\omega_n = 0.2\text{ rad/s}$, a damping ratio of $\zeta = 1$ and a time delay of 2.08 seconds. The gains are presented in

Table 6.14.

The cable angle response and the helicopter attitude deviation from trim are presented in Figure 6.60 and Figure 6.61. Note that the cable angle for $\phi_{1\theta}$ is not zero. This is due to a steady state error that is reduced to zero using an integral. It will eventually reach zero. Furthermore, the pitch angle of the helicopter vibrates for a step in ϕ_{1c} . The reason for this could be the fact that the cable angle, angular rate and angular acceleration are all close to zero, meaning that the oscillation of the cable section is most dominant.

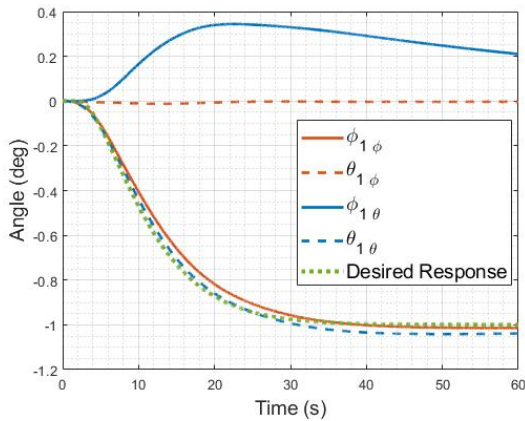


Figure 6.60: Cable angle response using PID controller for case 6

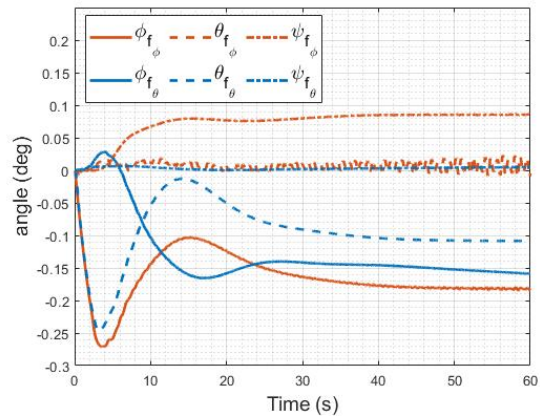


Figure 6.61: Helicopter attitude response using PID controller for case 6

6.10.4. Cable Controller Disturbance Response

The performance of the PID and the INDI controller is again assessed by adding a disturbance wind of $4kts$ at the $t = 1$ seconds mark. The response of both the PID and the INDI controllers are shown in Figure 6.62 - Figure 6.64. As shown, the INDI controller is more capable of keeping the SONAR velocity low than the PID. However, the PID controller's response is more smooth. Looking at the cable angle response, the same can be said. When looking at the control inputs relative to trim, both the PID and the INDI controller have some vibration in the first 5 seconds of the simulation. This can be attributed to the sudden change in wind. Both controllers use about the same amount of control during the disturbance response.

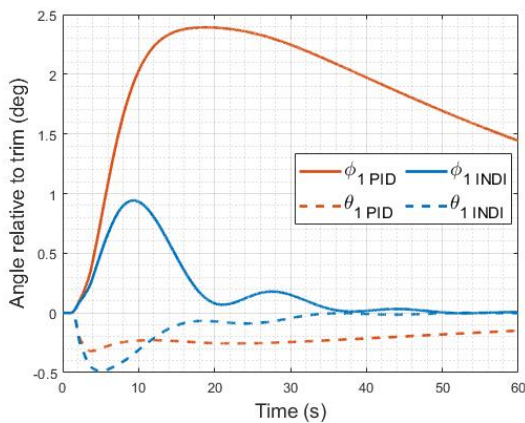


Figure 6.62: Cable angle response to a 4kts wind using PID and INDI control for case 6

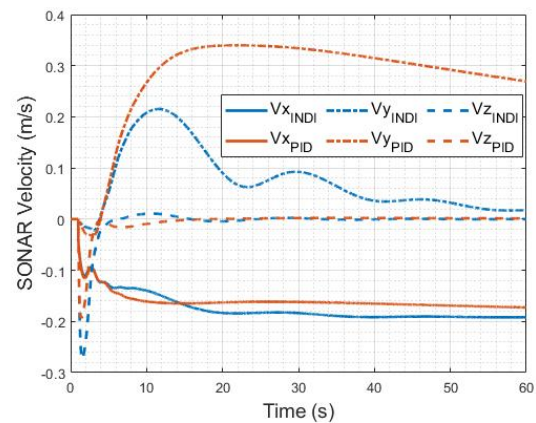


Figure 6.63: SONAR ground velocity response to a 4kts wind using PID and INDI control for case 6

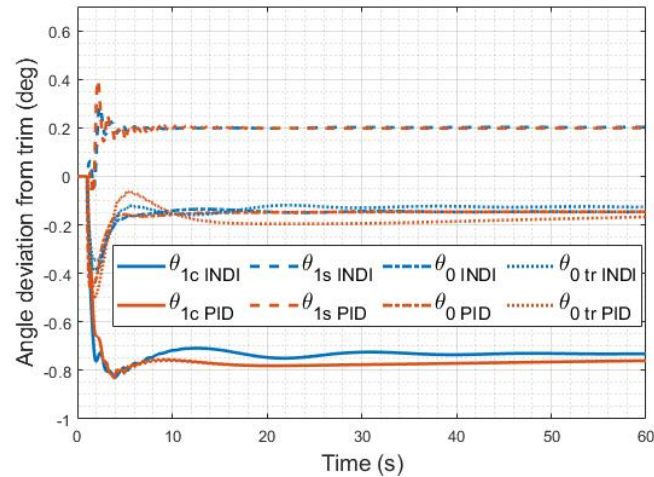


Figure 6.64: Control inputs from trim to helicopter with a 4kts wind using PID and INDI control for case 6

Table 6.14: Gains for Cable Controllers Case 6.

Gain	Value INDI _{att}	Value INDI _{vel}	Value INDI _{pos}	Value PID	unit
$K_{P\phi_1}$	0.40	0.20	0.30	1.00	s^{-1}
$K_{I\phi_1}$	0.00	0.00	0.08	0.02	—
$K_{D\phi_1}$	1.20	0.30	2.50	1.40	s^{-2}
$K_{P\dot{\phi}_1}$	0.20	1.20	1.00	0.65	—
$K_{I\dot{\phi}_1}$	0.00	0.00	0.00	0.00	s
$K_{D\dot{\phi}_1}$	1.10	0.55	0.00	8.00	s^{-1}
$K_{P\theta_1}$	0.40	0.20	0.30	1.00	s^{-1}
$K_{I\theta_1}$	0.00	0.00	0.08	0.02	—
$K_{D\theta_1}$	1.20	0.40	2.50	1.40	s^{-2}
$K_{P\dot{\theta}_1}$	0.20	1.1	1.00	0.65	—
$K_{I\dot{\theta}_1}$	0.00	0.00	0.00	0.00	s
$K_{D\dot{\theta}_1}$	1.10	0.55	0.00	8.00	s^{-1}
Time constant					
τ_1	5	5	5	5	s
τ_2	-	5	-	-	s

6.10.5. Conclusions case 6

Case 6 is different from case 5 in the way that drag is computed. In case 5, the cable was suspended in air, whereas in case 6 the cable was partially submerged. As expected, the water added damping to the cable, making it possible to use INDI for cable control through attitude control. This was not possible for case 5, due to the oscillations from the cable sections.

This case studied 3 different control strategies in order to figure out what way to best control the cable. These 3 strategies were: cable control through attitude control, cable control through velocity control and cable control through position control. After subjecting each of these controllers to a wind disturbance, it turned out that the control strategy using helicopter attitude performed best by keeping the change in SONAR ground velocity the smallest. The reason for this is that the air velocity is not present in the control loop via the TRC controller. It was therefore not attempting to bring the air velocity down to zero initially. After comparing the PID and the INDI controllers, it was found that the INDI controller was better at keeping

the SONAR ground velocity low. However, the response was more oscillatory than the PID. Both controllers use practically the same amount of control.

6.11. Case 7: Helicopter with Multiple Cable Sections at Offset, Partially Submerged with Wind

Case 7 builds on case 6 by adding atmospheric disturbance to the helicopter-cable system. A constant wind and the turbulence model are added.

6.11.1. Case 7 Trim

Case 7 is, unlike cases 1-6, trimmed at an air velocity of 10, 20 and 30 kts and a ground velocity of 0kts. This is the maximum wind expected at a sea state of 4-5. This distinction is important, since in windy conditions, the submerged cable sections should not be displaced by wind. This means that the cable will have an initial cable displacement. This is also visible in the trim states in Table 6.15. Note that the top cable sections, 1-3, have a cable displacement of around 52 degrees. The cable section that is partially submerged has a displacement that is less, since part of it is submerged. The final cable section and the SONAR are not displaced. This is to be expected. Note that the

6.11.2. Disturbance Rejection

In this section, the disturbance rejection of the two cable controllers is assessed. This is done by simulating both controllers with the wind and turbulence model from the scientific paper. The assessment is done by simulating the controlled helicopter-cable system under different wind conditions: 10kts, 20kts and 30kts.

10 kts wind

For a wind of 10 kts, the gusts are as in Figure 6.65. Simulation is done for 5 minutes, and the goal of the controller is to keep altitude, and keep the cable angle at its trimmed value. The performance metrics defined for the controllers are: standard deviation of the control inputs, mean sonar velocity and standard deviation of the SONAR velocity.

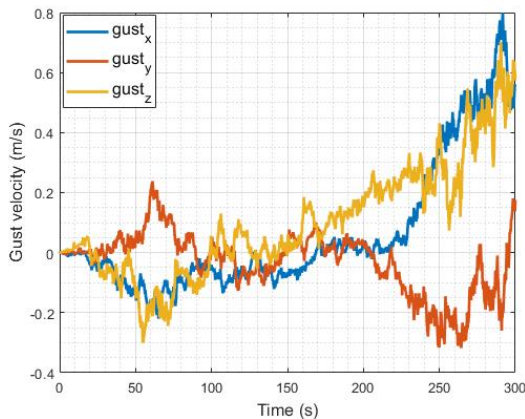


Figure 6.65: Gust velocities for a wind of 10 kts.

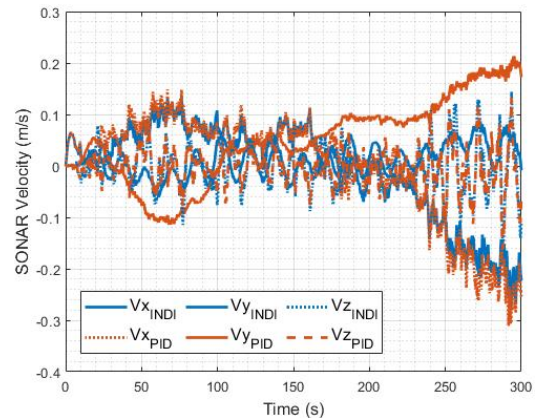


Figure 6.66: SONAR ground velocity response at 10 kts wind.

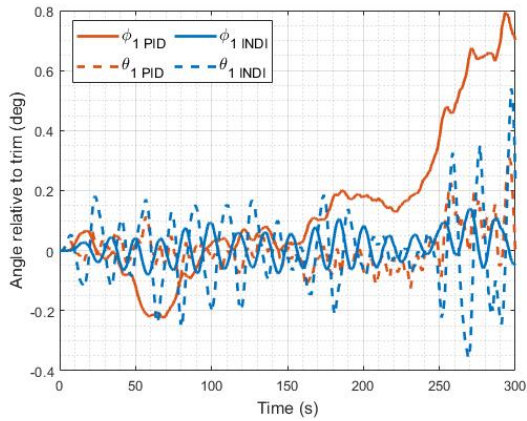


Figure 6.67: Cable angle response at 10 kts wind.

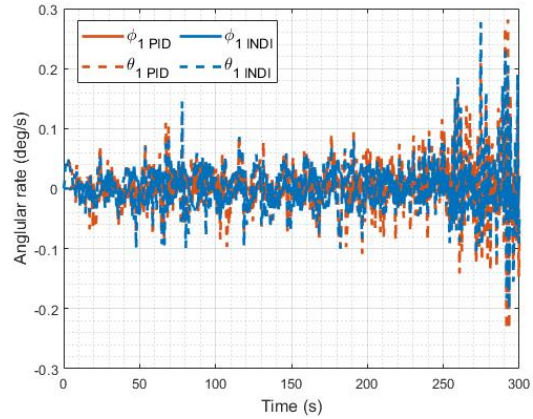


Figure 6.68: SONAR angular rate response at 10 kts wind.

The performance metrics for a velocity of 10 kts are given in Table 6.16. For reference, the SONAR ground velocity is provided in Figure 6.66. Note that this image is rather cluttered, due to the long simulation time, but the important part is to see that the SONAR velocity never exceeds 1m/s throughout the entire simulation, passing the first requirement for the controller at 10 kts.

During simulation, it was found that, although the PID controller from case 6 is capable of controlling the disturbed system, it does so using more control relative to the INDI controller, constantly oscillating. This is also clear from the performance metrics.

When looking at the standard deviation of the SONAR velocity, the PID and INDI perform roughly equal in x and z direction. However, in y direction, the INDI controller is clearly better, but the standard deviation is still very small for both controllers, with the standard deviation being in the order of centimeters per second. The mean of the SONAR velocity indicates how much the SONAR drifts. Here, both the PID and the INDI controller perform similarly.

The cable angle response and the SONAR angular rate response are provided in Figure 6.67 and Figure 6.68. As shown, the INDI controller is better capable of keeping the cable angles close to 0, especially the lateral cable angle ϕ_1 . The SONAR angular rate indicates that both controllers pass the second controller requirement to keep SONAR angular rates below $1^\circ/s$.

Generally, the INDI controller is better than the PID at keeping the SONAR stable at a wind of 10 kts. However, the cyclic control inputs are more oscillatory than the PID.

Table 6.16: Performance metrics Cable controllers for a wind of 10 kts.

standard deviation controls (deg)	$\sigma_{\theta_{1c}}$	$\sigma_{\theta_{1s}}$	σ_{θ_0}	$\sigma_{\theta_{0tr}}$
INDI	0.0494	0.0125	0.0713	0.2273
PID	0.0622	0.0239	0.0801	0.2519
standard deviation V_{SONAR} (m/s)	$\sigma_{V_{SONARx}}$	$\sigma_{V_{SONARy}}$	$\sigma_{V_{SONARz}}$	
INDI	0.0935	0.0296	0.0404	
PID	0.1049	0.0818	0.0358	
mean V_{SONAR} (m/s)	\bar{V}_{SONARx}	\bar{V}_{SONARy}	\bar{V}_{SONARz}	
INDI	-0.0062	0.0104	-0.0029	
PID	-0.0056	0.0495	-0.0026	

20 kts wind

For a wind of 20 kts, the gusts are as in Figure 6.69. Simulation is done for 5 minutes, and the goal of the controller is to keep altitude, and keep the cable angle at its trimmed value. Just as for 10 kts.

During simulation, it was found that the controller could not handle the disturbances. The controller was trying to correct for the disturbances too aggressively. To counter this, the gains for the ACAH controllers have been lowered by a factor of 3. The gains for the TRC controllers for the vertical body velocity w were lowered by a factor 5. This will hurt the performance of the ACAH and TRC controller, but it is necessary to reject the disturbance. The gains of the other controllers were left unchanged. This change was done for both the PID and the INDI controller.

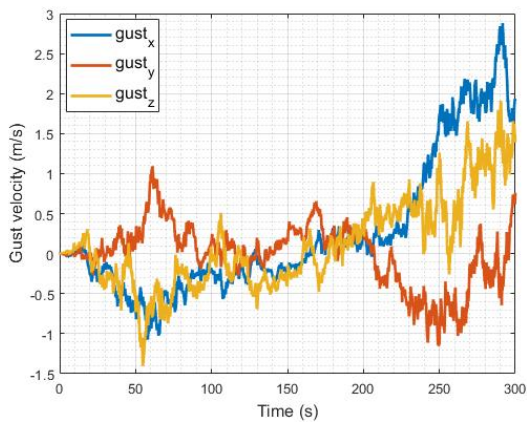


Figure 6.69: Gust velocities for a wind of 20 kts.

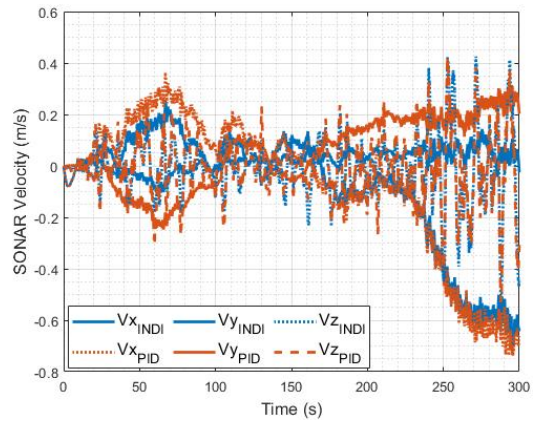


Figure 6.70: SONAR ground velocity response at 20 kts wind.

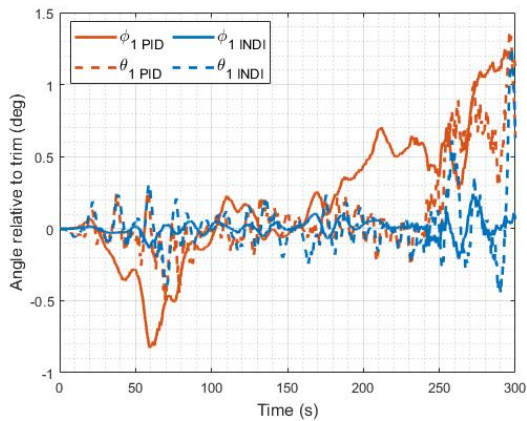


Figure 6.71: Cable angle response at 20 kts wind.

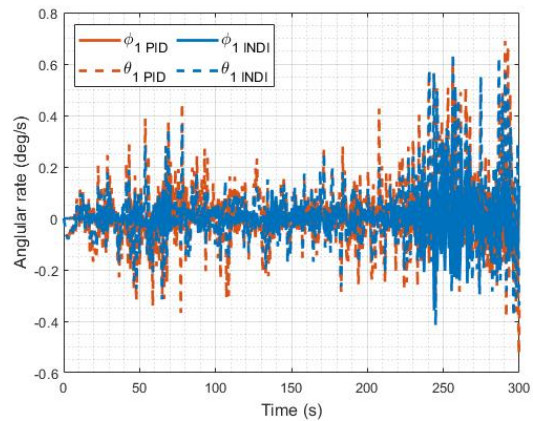


Figure 6.72: SONAR angular rate response at 20 kts wind.

When running the simulation with the re-tuned controllers, the performance metrics in Table 6.17 were found. From these metrics, it becomes clear that the performance of both the PID and the INDI controller worsened in all aspects, accompanied with a higher control use. This is also observed in Figure 6.70 and Figure 6.71, where the SONAR velocity reaches higher values, and the cable angle tracking performance has degraded. This makes sense in the way that increased disturbance is accompanied with worse controller performance. Judging by the controller performance metrics, the INDI controller performs better than the PID, except at the mean of the SONAR velocity in x-direction. However, both values are near 10

cm/s.

From Figure 6.70, it is found that the SONAR velocity does not exceed 1 m/s and from Figure 6.72, it appears that the SONAR angular rate does not exceed $1^\circ/s$, making this controller pass the first and second controller requirement.

Table 6.17: Performance metrics Cable controllers for a wind of 20 kts.

standard deviation controls (deg)	$\sigma_{\theta_{1c}}$	$\sigma_{\theta_{1s}}$	σ_{θ_0}	$\sigma_{\theta_{0tr}}$
INDI 10 kts	0.0494	0.0125	0.0713	0.2273
INDI 20 kts	0.1081	0.0608	0.2492	0.6918
PID 10 kts	0.0622	0.0239	0.0801	0.2519
PID 20 kts	0.1188	0.1228	0.2555	0.6694
standard deviation V_{SONAR} (m/s)	$\sigma_{V_{SONARx}}$	$\sigma_{V_{SONARy}}$	$\sigma_{V_{SONARz}}$	
INDI 10 kts	0.0935	0.0296	0.0404	
INDI 20 kts	0.2348	0.0399	0.1241	
PID 10 kts	0.1049	0.0818	0.0358	
PID 20 kts	0.2722	0.1357	0.1242	
mean V_{SONAR} (m/s)	\bar{V}_{SONARx}	\bar{V}_{SONARy}	\bar{V}_{SONARz}	
INDI 10 kts	-0.0062	0.0104	-0.0029	
INDI 20 kts	-0.0918	0.0196	-0.0047	
PID 10 kts	-0.0056	0.0495	-0.0026	
PID 20 kts	-0.0728	0.0525	-0.0056	

30 kts wind

30 kts wind is about the highest wind that would be encountered at a sea state of 4-5. Therefore, this wind condition is the ultimate test for the two controllers. The gusts modelled with this wind are found in Figure 6.73.

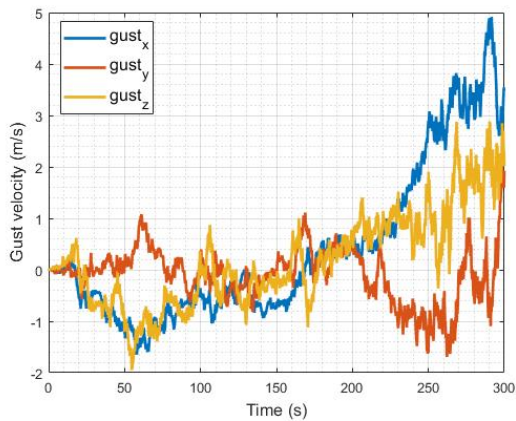


Figure 6.73: Gust velocities for a wind of 30 kts.

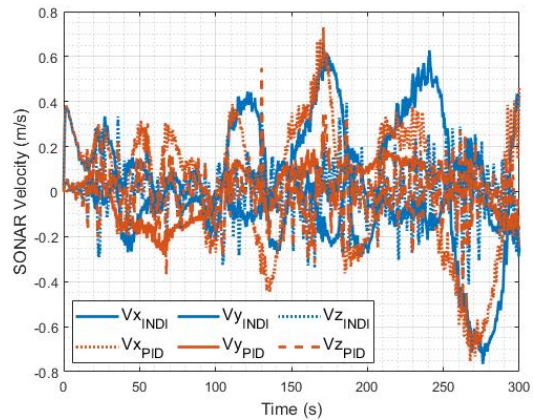


Figure 6.74: SONAR ground velocity response at 30 kts wind.

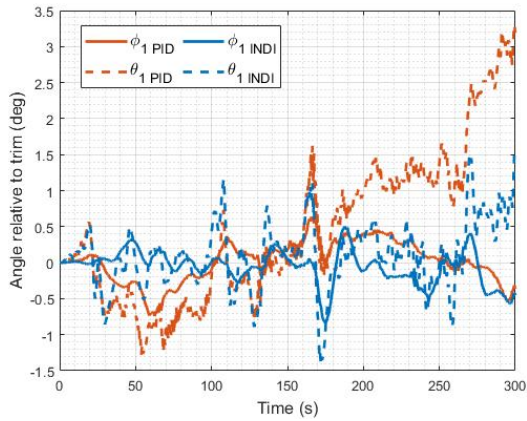


Figure 6.75: Cable angle response at 30 kts wind.

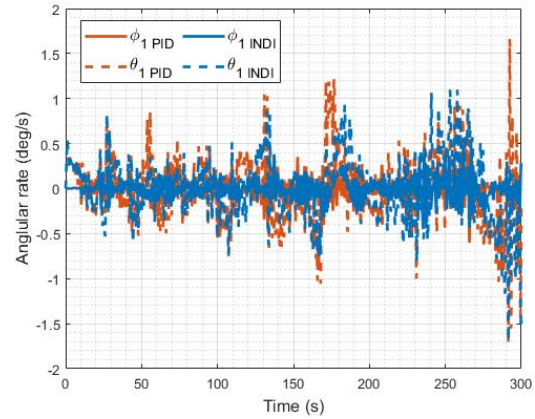


Figure 6.76: SONAR angular rate response at 30 kts wind.

During simulation, it was found that both the PID and INDI controller had trouble controlling the cable, with the INDI having more trouble than the PID and crashing earlier. Generally, there were no issues, until at some point the helicopter got blown away far from its initial position in a relatively short time. This meant that sometimes the helicopter would change position quickly, but the cable system is much slower to respond. As a result, the helicopter would pull the cable completely straight, with the cable angle changing quickly. After that, the helicopter will be pulled back by the cable, and will make corrections at the same time in an attempt to keep the cable angle constant. This results in an aggressive correction of the helicopter and cable.

The source of this behaviour was not found, but it is likely that drifting of the helicopter is the source of this behaviour, since the other two wind velocities (10 and 20 kts) did not show these issues. To figure out whether this is the case, the cable controller is disconnected and instead the position hold controller from case 2 is used for the INDI controller. The gains for the TRC and ACAH remain reduced (see 20 kts). Using this controller, the helicopter position barely drifted and the previous phenomena disappeared. This suggests that it was indeed caused by fast drifting of the helicopter relative to the cable. Also, the cable angle remained somewhat constant during this simulation. This suggests that a position hold might perform equal or better in high wind conditions. Therefore, the position hold case for INDI is included into Table 6.18, for comparison with the PID and INDI cable controller.

The performance metrics of the cable controllers given a wind disturbance of 30 kts are given in Table 6.18. From this table, some interesting results can be gathered.

With respect to control use, the position hold controller performs worst here, likely because it is fighting the wind much more than the other two controllers. This is because keeping the cable angle constant requires flying with the gusts, whereas keeping position means constant acceleration and deceleration. With respect to SONAR velocity, the position hold controller performs best, with the smallest standard deviation of the SONAR velocity and the smallest mean in almost all directions. This is because the helicopter is set to hold the same position, meaning that the mean of the SONAR motion will generally also be close to zero. The standard deviation is likely the smallest also because the helicopter stays in the same place. This means that the helicopter will not excite the submerged sections of cable and the only motion is caused by the gusts.

Generally, a position hold controller is better than a cable angle controller under the wind conditions of 30 kts. The reason being is that, when the helicopter remains static, there is no excitation of the cable due to the helicopter moving and the only excitation is by the gust and attitude changes of the helicopter (the cable is attached offset to the c.g. after all). This means that the SONAR is kept more still than when using a cable controller.

In Figure 6.74, Figure 6.75 and Figure 6.76, the SONAR velocity, cable angle and SONAR angular rate are presented for the INDI and PID cable controller. As shown, the SONAR velocity does not exceed 1 m/s during this simulation, but the SONAR angular rate does exceed $1^\circ/s$. This means that the cable controllers pass the first controller requirement, but fail the second. Also, with regards to drifting, when observing the cable angle response, one can see the cable angle increase relatively fast around the 260

seconds mark for both the PID and the INDI cable controller. This quick change in angle comes from the gusts at this time. This is also the gust that causes the helicopter to drift, resulting in the unstable behaviour mentioned before.

Table 6.18: Performance metrics Cable controllers for a wind of 30 kts.

standard deviation controls (deg)	$\sigma_{\theta_{1c}}$	$\sigma_{\theta_{1s}}$	σ_{θ_0}	$\sigma_{\theta_{0tr}}$
INDI 10 kts	0.0494	0.0125	0.0713	0.2273
INDI 20 kts	0.1081	0.0608	0.2492	0.6918
INDI 30 kts	0.1877	0.1872	0.4408	0.5618
INDI position hold 30 kts	0.2994	0.2382	0.5348	1.3591
PID 10 kts	0.0622	0.0239	0.0801	0.2519
PID 20 kts	0.1188	0.1228	0.2555	0.6694
PID 30 kts	0.2217	0.1480	0.3824	0.3706
standard deviation V_{SONAR} (m/s)	$\sigma_{V_{SONARx}}$	$\sigma_{V_{SONARy}}$	$\sigma_{V_{SONARz}}$	
INDI 10 kts	0.0935	0.0296	0.0404	
INDI 20 kts	0.2348	0.0399	0.1241	
INDI 30 kts	0.3544	0.0903	0.3715	
INDI position hold 30 kts	0.1751	0.1062	0.2839	
PID 10 kts	0.1049	0.0818	0.0358	
PID 20 kts	0.2722	0.1357	0.1242	
PID 30 kts	0.3751	0.1031	0.3208	
mean V_{SONAR} (m/s)	\bar{V}_{SONARx}	\bar{V}_{SONARy}	\bar{V}_{SONARz}	
INDI 10 kts	-0.0062	0.0104	-0.0029	
INDI 20 kts	-0.0918	0.0196	-0.0047	
INDI 30 kts	0.0397	0.0116	-0.0218	
INDI position hold 30 kts	-0.0151	-0.0006	-0.0057	
PID 10 kts	-0.0056	0.0495	-0.0026	
PID 20 kts	-0.0728	0.0525	-0.0056	
PID 30 kts	0.0744	0.0124	-0.0333	

6.11.3. Fulfillment of controller requirement 3: step response

The third controller requirement puts a limit on the allowed time to steady state of the cable of 60 seconds given a step input of 7 Bft, with the SONAR at a depth of 60m. This was simulated with a step input of 17 m/s at the 1 second mark of the simulation. Note that for this simulation, the reduced controller gains were used as for the 20 kts simulation in the previous section.

The SONAR velocity response and the cable angle response are presented in Figure 6.77 and Figure 6.78. As shown, there is a large disturbance at the 1 second mark due to the increased wind. The cable angle immediately changes to -10.5 degrees in longitudinal direction (backwards). This is followed by a response of the lateral angle, due to the helicopter motion. After approximately 40 seconds, the velocity in x-direction settles on around 2 m/s. The velocity in z-direction settles in about the same time. The velocity in y-direction settles in around a minute for the INDI controller and around 20 seconds for the PID controller in y-direction, but the INDI controller reaches 0 much faster than the PID controller. The aforementioned results mean that the PID and the INDI controller both pass the third controller requirement of reaching steady state within 60 seconds given a step input of 7 Bft in wind. The PID settles slightly faster than the INDI. The INDI on the other hand is better capable of decoupling the longitudinal and lateral motion, resulting in a zero lateral velocity faster.

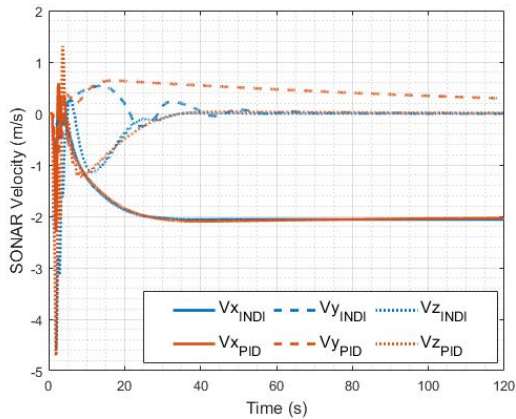


Figure 6.77: SONAR ground velocity response at 17m/s step in wind.

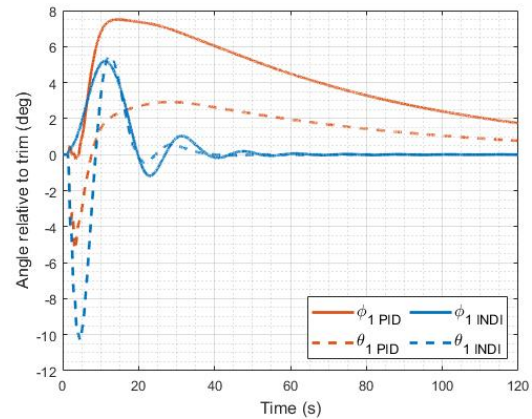


Figure 6.78: Cable angle response at 17 m/s step in wind

6.12. Conclusions

To conclude, there were 7 cases studied in this chapter:

Simulation Cases for the 6-DOF helicopter controller

Case	Helicopter Model	Cable Model	Load Location	Medium	Disturbances
1	Rotor hub aligned with c.g.	-	-	-	-
2	Rotor hub at offset	-	-	-	-
3	Rotor hub at offset	Single cable section + SONAR	c.g. of helicopter	Air	-
4	Rotor hub at offset	Single cable section + SONAR	At offset	Air	-
5	Rotor hub at offset	5 cable sections + SONAR	At offset	Air	-
6	Rotor hub at offset	5 cable sections + SONAR	At offset	Air + water	-
7	Rotor hub at offset	5 cable sections + SONAR	At offset	Air + water	Aerodynamic

For each of these cases, a PID and an INDI controller were designed with the aim of comparing their response to disturbance to each other. In cases 1 and 2, this was done without a load. In cases 3 and 4, a load was attached, consisting only of 1 cable section. Case 5 changed this to 5 sections and case 6 added water to simulate submergence. Case 7 compared both controllers when in a gusty environment.

From the first two cases, it was concluded that the PID and INDI controller for the pure helicopter (no load) responded similarly to a disturbance. In cases 3 and 4, the cable was attached, and it was found that the INDI was better at controlling the cable angle than the PID. It was especially better at decoupling the longitudinal and lateral modes. This was something that was also observed in Chapter 4. Case 5 found that when using more cable sections, oscillations appear due to them moving relative to each other. When controlling in air, this meant that INDI could not be used in combination with attitude control, but that cable control through velocity control was necessary. Here too, INDI showed more promising results by adapting itself more to changing circumstances, but the controllers could not be tuned properly, so it may not be better than a PID in this case.

In case 6, the added damping of the water meant that cable control through attitude control was possible. As a result, 3 control strategies were investigated, with the cable control through attitude control performing the best when subjected to a constant wind. The reason for its better performance was that helicopter control through attitude control did not have velocity in its control loop for the attitude of the helicopter. This made that it largely ignored it and kept the cable angle stable more quickly. When comparing the INDI controller to the PID controller, it was found that the INDI controller was better at controlling the cable angle, and also keeping the SONAR velocity low.

In case 7, 3 different wind speeds were used to compare the performance of the INDI cable controller to the PID cable controller. It was found that for wind speeds of 10 and 20 kts, the INDI controller performed

better than the PID at keeping the SONAR velocity low. However, at 30 kts this was no longer the case. It was found that there were large aggressive corrections by the helicopter when it got blown away from its position if the cable could not keep up. This meant that the helicopter would pull the cable taught, and got pulled back by it. Changing the cable controller for a position controller removed this issue entirely, which suggests that a position hold controller could perform better in high wind conditions. Nevertheless, it should be emphasized that the cable controller has a different goal than the position hold controller. The cable controller has as goal to keep the cable angle at the helicopter at the trimmed value. This means that in windy conditions, the helicopter will be told to move with the wind in order to keep the angle at the trimmed value (it ignores the wind velocity, as was shown in case 6). The position hold controller would not do this. However, with dipping SONAR missions in mind, keeping the helicopter in the same position may prove more useful than keeping the cable angle constant, as this keeps the SONAR position constant and its velocity low.

With respect to the controller requirements, it was found that the controllers were able to pass the first and second requirement of keeping the SONAR rates below 1m/s and $1^\circ/s$ in all directions up to a wind speed of 20 kts. At 30 kts, the requirement of keeping the SONAR angular rate below $1^\circ/s$ failed. The third requirement with respect to reaching steady state was passed by both the PID and the INDI controller, reaching steady state within 60 seconds after a 17 m/s step in wind. The PID controller settled slightly faster, but the INDI controller kept the longitudinal and lateral modes more decoupled.

Table 6.15: Trim data Case 6 vs. 7 trimmed at a wind of 33 kts

Helicopter State	Symbol	Name	Value case 6	Value case 7	unit
1	u	Body velocity in x	0.000	16.959	<i>m/s</i>
2	v	Body velocity in y	0.000	0.072	<i>m/s</i>
3	w	Body velocity in z	0.000	-0.760	<i>m/s</i>
4	p	Body roll rate	0.000	0.000	<i>deg/s</i>
5	q	Body pitch rate	0.000	0.000	<i>deg/s</i>
6	r	Body yaw rate	0.000	0.000	<i>deg/s</i>
7	ψ_f	Fuselage heading angle	0.000	0.000	<i>deg</i>
8	θ_f	Fuselage pitch angle	11.053	-2.576	<i>deg</i>
9	ϕ_f	Fuselage roll angle	-2.166	-5.411	<i>deg</i>
10	x	Helicopter x position	0.000	0.000	<i>m</i>
11	y	Helicopter y position	0.000	0.000	<i>m</i>
12	z	Helicopter z position	-60.000	-60.000	<i>m</i>
13	λ_0	Normalised uniform inflow velocity	0.0523	0.0316	-
14	λ_{0tr}	Normalised uniform inflow velocity tail	0.0614	0.0487	-
15	ω	Main rotor angular rate	44.400	44.400	<i>rad/s</i>
Cable State	Symbol	Name	Value case 6	Value case 7	unit
1	ϕ_1	Cable angle around x axis section 1	0.0	0.0	<i>deg</i>
2	ϕ_2	Cable angle around x axis section 2	0.0	0.0	<i>deg</i>
3	ϕ_3	Cable angle around x axis section 3	0.0	0.0	<i>deg</i>
4	ϕ_4	Cable angle around x axis section 4	0.0	0.0	<i>deg</i>
5	ϕ_5	Cable angle around x axis section 5	0.0	0.0	<i>deg</i>
6	ϕ_{SONAR}	Cable angle around x axis SONAR	0.0	0.0	<i>deg</i>
7	θ_1	Cable angle around y axis section 1	0.0	-51.5657.0	<i>deg</i>
8	θ_2	Cable angle around y axis section 2	0.0	-52.1476.0	<i>deg</i>
9	θ_3	Cable angle around y axis section 3	0.0	-52.7492.0	<i>deg</i>
10	θ_4	Cable angle around y axis section 4	0.0	-34.0085.0	<i>deg</i>
11	θ_5	Cable angle around y axis section 5	0.0	0.0	<i>deg</i>
12	θ_{SONAR}	Cable angle around y axis SONAR	0.0	0.0	<i>deg</i>
Control	Symbol	Name	Value case 6	Value case 7	unit
1	θ_{1c}	Lateral Cyclic	-0.6030	-3.2628	<i>deg</i>
2	θ_{1s}	Longitudinal Cyclic	1.6826	2.9582	<i>deg</i>
3	θ_0	Main rotor collective	15.1944	13.6436	<i>deg</i>
4	θ_{0tr}	Tail rotor collective	15.4208	12.8987	<i>deg</i>

Sensitivity Analysis 6-DOF Cable Controller

In this chapter, a sensitivity analysis is performed in order to find out how sensitive the controller performance is to changing parameters. Therefore, changes were made to the amount of cable sections as well as the length of the cable to figure out how the performance of the cable controller changes.

7.1. Sensitivity to Changing Cable Length

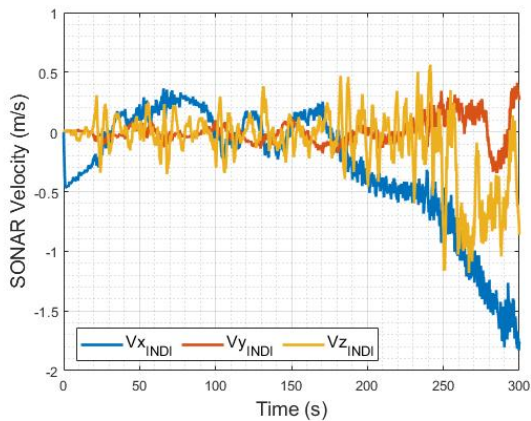
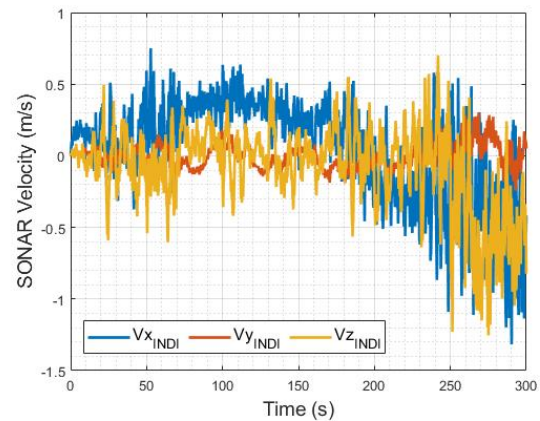
In this section, the simulations from case 7 were done with varying cable lengths of 120m, 250m, 500m and 750 meters. This was done to figure out how the performance of the cable controller varies with cable length. The system was trimmed under 30 kts headwind and is simulated for 5 minutes in gusty environment.

The performance parameters for these two additional simulations are shown in conjunction with the results from case 7 for comparison. First of all, it appears that for 250m, the amount of control used decreases, whereas for 500m and 750m it increases. This means that the control efficiency has decreased over this increase in length. The exact reason for this is not known, but it could be related to the fact that the cable sections are longer than the trimmed altitude of the helicopter. This means that the first cable section moves slower than when suspended in air, which would explain the degraded control effectiveness. With regards to SONAR velocity it seems that the standard deviation of the SONAR velocity remains roughly constant with increasing length, except at 250m where a sudden increase is observed. This is an interesting result as this suggests that the performance of the cable controller is independent of cable length. The average velocity of the SONAR also remains roughly constant with changing length.

The SONAR velocity is also plotted for the aforementioned cable lengths in Figure 7.1-Figure 7.3. From these, it appears that the SONAR velocity oscillates more, the longer the cable gets. It is thought that this is due to the first cable section being longer than the altitude of the helicopter.

Table 7.1: Performance metrics Cable controllers for a wind of 30 kts, compared to cable length.

standard deviation controls (deg)	$\sigma_{\theta_{1c}}$	$\sigma_{\theta_{1s}}$	σ_{θ_0}	$\sigma_{\theta_{0tr}}$
INDI, 120m	0.1877	0.1872	0.4408	0.5618
INDI, 250m	0.0698	0.1071	0.2914	0.7509
INDI, 500m	0.1900	0.1394	0.3054	0.5575
INDI, 750m	0.1879	0.1810	0.4276	0.5545
INDI position hold, 120m	0.2994	0.2382	0.5348	1.3591
PID, 120m	0.2217	0.1480	0.3824	0.3706
standard deviation V_{SONAR} (m/s)	$\sigma_{V_{SONARx}}$	$\sigma_{V_{SONARy}}$	$\sigma_{V_{SONARz}}$	
INDI, 120m	0.3544	0.0903	0.3715	
INDI, 250m	0.5058	0.1045	0.2848	
INDI, 500m	0.3406	0.0853	0.2901	
INDI, 750m	0.3545	0.0903	0.3658	
INDI position hold, 120m	0.1751	0.1062	0.2839	
PID, 120m	0.3751	0.1031	0.3208	
mean V_{SONAR} (m/s)	\bar{V}_{SONARx}	\bar{V}_{SONARy}	\bar{V}_{SONARz}	
INDI 120m	0.0397	0.0116	-0.0218	
INDI, 250m	-0.2884	0.0016	-0.0962	
INDI, 500m	0.0395	-0.0060	-0.0866	
INDI, 750m	0.0401	0.0110	-0.0251	
INDI position hold, 120m	-0.0151	-0.0006	-0.0057	
PID, 120m	0.0744	0.0124	-0.0333	

**Figure 7.1:** SONAR ground velocity response at 30 kts wind for 250m long cable.**Figure 7.2:** SONAR ground velocity response at 30 kts wind for 500m long cable.

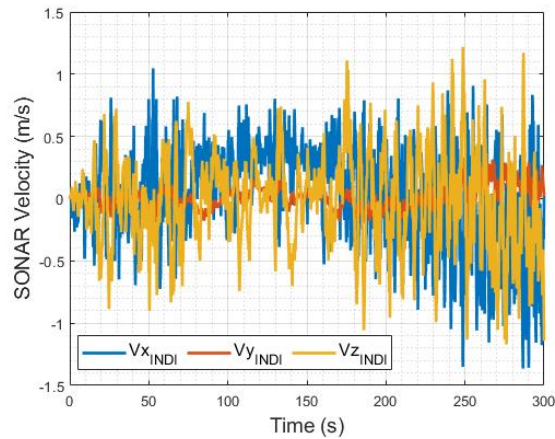


Figure 7.3: SONAR ground velocity response at 30 kts wind for 750m long cable.

7.2. Sensitivity to Amount of Cable Sections

To figure out whether the performance of the INDI cable controller changes, the amount of cable sections was increased from 5 to 25 to 75, while keeping a cable length of 750m. This means that each cable section has a length of 150 to 30 to 10m, and that the cable is more free to deform. The system is trimmed under 30 kts headwind and is simulated for 5 minutes in gusty environment.

The SONAR velocity for the 25 and 75 cable sections are presented in Figure 7.4 and Figure 7.5. From these, it becomes clear that the SONAR velocity is similar for both 25 sections and 75 sections. The main difference is that the peaks in velocity are higher for 25 sections than for 75 sections. It is also interesting to note the dominant peaks in the z-direction. This is due to the small drag modelling in the cable. Since the cable sections move straight up, the drag modelled is very low, since friction drag is not modelled. Having a more refined drag model would be necessary to find out whether these peaks remain. The performance metrics are given in Table 7.2. From this, it can be concluded that the control use first increases with cable flexibility, and then decreases. The standard deviation of the SONAR velocity decreases with cable flexibility and the mean stays roughly the same, staying well below 5 cm/s. This suggests that the response of the controller is improved if the cable is more flexible.

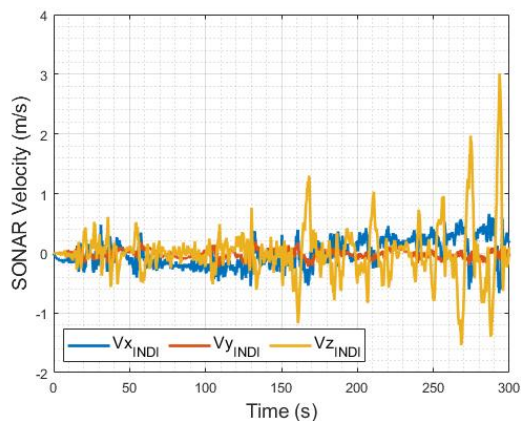


Figure 7.4: SONAR ground velocity response at 30 kts wind for 750m long cable with 25 cable sections.

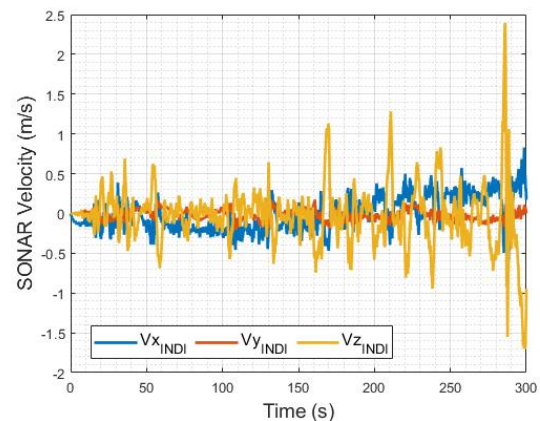


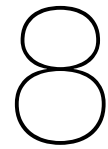
Figure 7.5: SONAR ground velocity response at 30 kts wind for 750m long cable with 75 cable sections.

Table 7.2: Performance metrics Cable controllers for a wind of 30 kts with 750m long cable, compared to better resolution cable model.

standard deviation controls (deg)	$\sigma_{\theta_{1c}}$	$\sigma_{\theta_{1s}}$	σ_{θ_0}	$\sigma_{\theta_{0tr}}$
INDI, 5 sections	0.1879	0.1810	0.4276	0.5545
INDI, 25 sections	0.1888	0.2764	0.8440	2.3755
INDI, 75 sections	0.1726	0.3429	0.7510	2.0701
standard deviation V_{SONAR} (m/s)	$\sigma_{V_{SONARx}}$	$\sigma_{V_{SONARy}}$	$\sigma_{V_{SONARz}}$	
INDI, 5 sections	0.3545	0.0903	0.3658	
INDI, 25 sections	0.2192	0.0645	0.4550	
INDI, 75 sections	0.2048	0.0624	0.3852	
mean V_{SONAR} (m/s)	\bar{V}_{SONARx}	\bar{V}_{SONARy}	\bar{V}_{SONARz}	
INDI, 5 sections	0.0401	0.0110	-0.0251	
INDI, 25 sections	-0.0009	-0.0148	-0.0029	
INDI, 75 sections	-0.0033	-0.0149	-0.0299	

7.3. Conclusions Sensitivity Analysis

In this chapter, it was looked into how sensitive the cable controller performance is to changing the cable parameters length l_c and the number of cable sections n . It was found that when lengthening the cable, the cable controller generally uses more control. However, it is thought that if the first cable section is partially submerged, the control effectiveness of the motion of the helicopter goes down due to the added drag. This could be countered by modelling more cable sections. Also, it was found that when using a longer cable, the standard deviation of the velocity of the SONAR decreases. This is a result that is expected, since the added drag of the water resists the motion of the cable. With regard to the amount of cable sections, it was found that when using more cable sections, the performance of the cable controller increases. This suggests that the cable controller performs better with a more flexible cable. It was also found that the SONAR velocity in z-direction has large peaks. It is thought that a lack of friction drag modelling causes less resistance in this direction than the others. A better drag model would be required to figure out if this is the case.



Verification and Validation

8.1. Cable Model Verification

The cable model was verified by checking the correctness of the angular acceleration calculation. This was done in Appendix E

8.2. Cable Model Validation

Validation is done by simulating the cable model in a set of environments. Three different environments have been chosen to see whether the cable behaves in a real way. All three are simulated using a cable with 4 cable sections and the SONAR. Both the cable angle and the cable shape are of interest.

Dropping the Cable

The first method is by dropping the cable from a certain angle, and have it swing through air alone. For the simulation, a cable with 4 sections and the SONAR were modelled at an altitude of 140 m, with a 120m long cable and a 5m long SONAR. This means that the SONAR will be emerged throughout the simulation. The cable is initialised at an angle of 45° for cable sections in longitudinal direction. The angular rate is set to zero.

Running the simulation yields the cable shape in Figure 8.1. Here, the cable shape is plotted for each second in the simulation up to 12 seconds. This is done since the period of a 120m long pendulum is roughly 22 seconds. Hence, half a period is shown to avoid cluttering. Note that the arrows indicate the direction of the cable. As shown, the cable remains almost perfectly straight all the way down, but doesn't reach the initial angular deflection of 45° . This is caused by the damping as well as the air drag. In Figure 8.2, the cable angle at the attachment point is plotted over a time of 60 seconds. Here, the effect of the drag is more visible.

Overall, the cable behaves as it should given this disturbance.

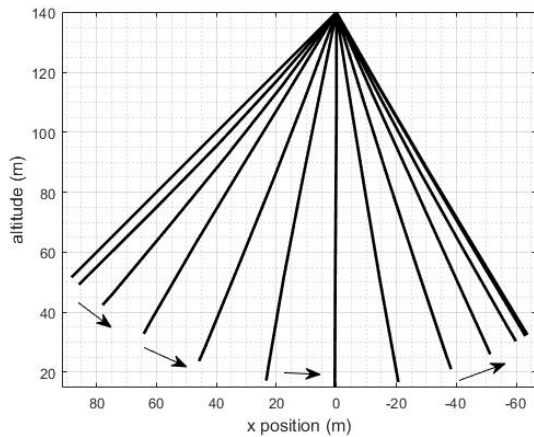


Figure 8.1: Validation cable shape when dropping cable

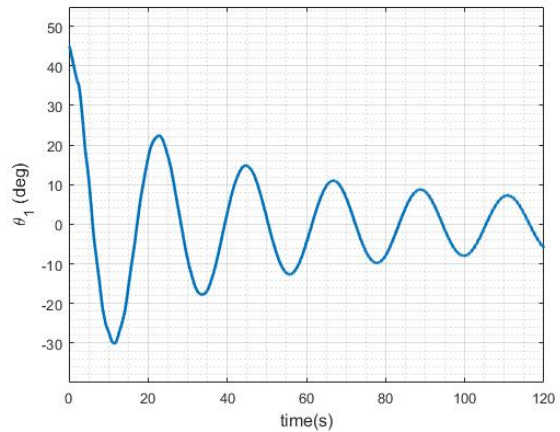


Figure 8.2: Validation cable angle when dropping cable

Blowing wind

The second method involves putting the cable into a wind disturbance of 40 m/s, while keeping the attachment point fixed. A large wind was chosen to see the cable behaviour better. The parameters of the simulation are the same as the previous simulation without the initial cable deflection.

The simulation results are shown in Figure 8.3 and Figure 8.4. In Figure 8.3, the cable shape is plotted for each second over the 60 second simulation. Note that the arrows indicate the direction the cable is travelling in. What is interesting to note is the 3 left most cable shapes. These show the cable shape in the first 3 seconds of the simulation. Note how the cable bulges back first due to the drag, before it starts to move back. This is exactly how a real cable would behave, which is a good result. The cable angle is shown in Figure 8.4. Note how there is a transient in the first couple of seconds. This is when the cable sections start moving. This sends a shock through the cable initially. The cable also appears to settle at a non-zero cable angle due to the drag. Generally, the cable behaves as intended.

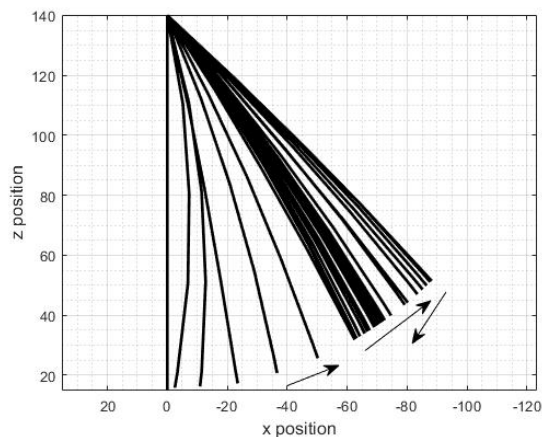


Figure 8.3: Validation cable shape when in 40 m/s wind

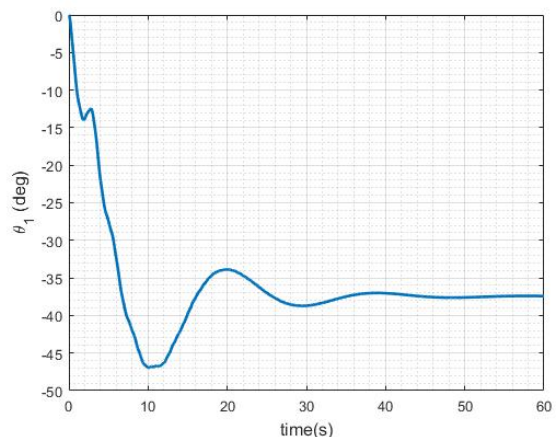


Figure 8.4: Validation cable angle when in 40 m/s wind

Blowing wind when submerged

The final method is to check how the cable behaves under the same conditions as the previous simulation of 40 m/s wind, but with submerged cable sections. The trim altitude is dropped from 140m to 60m, meaning that half the cable is submerged.

The simulation results are shown in Figure 8.5 for the cable shape and Figure 8.6 for the cable angle. The plot of the cable shape is more zoomed in on the x-axis, which gives it its warped appearance. As shown, the cable bulges back first, similar to when in air. However, the cable sections that are submerged appear to respond slower than the emerged sections. This is in line with expectations, as the water drag is much higher than the air drag. Also, the wind is not felt at sections that are submerged, which is why they are not really deflected at the steady state. The plot for the cable angle shows the cable angle at the attachment point over time. Here too, the transient is present, but more pronounced than in the previous simulation. After the transient, the cable angle moves gradually to the steady state due to the slow adjustment of the submerged cable sections.

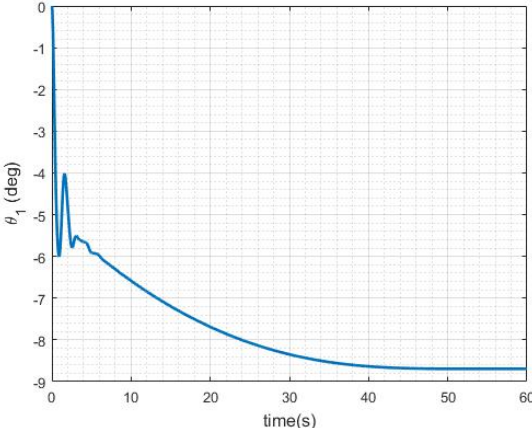
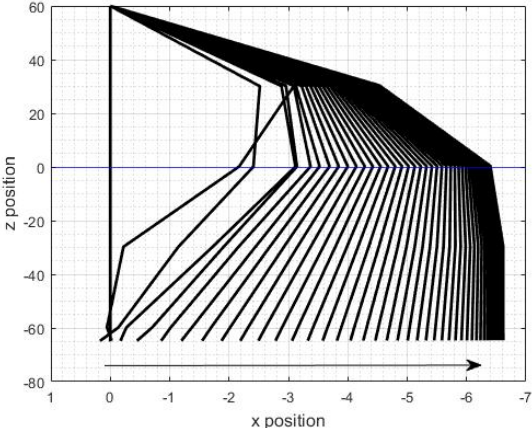


Figure 8.5: Validation cable shape when in 40 m/s wind submerged **Figure 8.6:** Validation cable angle when in 40 m/s wind submerged

After these 3 simulations, the cable appears to move in a realistic manner. Therefore, the cable model seems valid enough for the problem at hand.

Part IV

Closure

Conclusion

9.1. Closing Remarks

The goal of this thesis is to apply INDI to a hovering helicopter with a dipping SONAR. The main reason for this is that the suspension cable moves in a complex way when subjected to disturbances, due to its flexibility. Hence, a control method is desired that ignores the cable dynamics in order to control the SONAR. The method chosen for this exercise was incremental nonlinear dynamic inversion (INDI).

The main strength of INDI is that it uses minimal model knowledge in order to control a system. Only the control effectiveness of the system is required, and it is generally robust against modelling errors, given the sampling frequency of the controller is large enough. In order to assess the performance of the INDI controller, it was compared to classical PID control, which is still common in many flight control systems. Comparisons were made with respect to the control usage and the SONAR velocity when given a certain disturbance.

The main conclusion of this thesis is that cable control using INDI performs better at stabilising the SONAR than PID does under turbulent conditions with wind up to 20 kts in terms of control use and SONAR velocity. However, due to the way the cable controller is designed in this work, either controller could fail if the helicopter gets blown away too far from the cable sections that are submerged, which was the case for 30 kts.

The cable controller works by keeping the angle of the cable at the attachment point to the helicopter constant. Thus, changing wind will inevitably result into translation commands to the helicopter in order to keep this angle constant. This means that when there is a sufficiently large change in wind, the helicopter changes its velocity to keep the angle constant and starts drifting. The submerged cable sections lag behind and can drag down the helicopter.

A position controller proved to work better under the high wind and high turbulent conditions of 30 kts wind. It seems that improvements could be made by either finding a way to vary the desired cable angle based on the turbulence or to find a controller that incorporates cable control and helicopter position hold together in order to keep the helicopter position somewhat constant, yet move slightly to stabilise the cable to changing wind conditions.

Moreover, requirements were defined for both the PID and the INDI controller to fulfill. This was done in order to have something to compare the controllers to, other than each other. The controller requirements are listed below:

1. The translational rates of the SONAR shall not exceed $1m/s$ in all directions with the SONAR submerged at a depth of 60m and sea state 5 for 5 minutes.
2. The rotational rates of the SONAR shall not exceed $1^\circ/s$ in all directions with the SONAR submerged at a depth of 60m and sea state 5 for 5 minutes.
3. The SONAR shall reach steady state within 60 seconds in all axes after a step input gust of 0 to 7 Bft with the SONAR submerged at a depth of 60m.

Simulation showed that these requirements could be met by both the PID and the INDI controllers up to 20 kts wind. The second requirement failed at 30 kts wind. Both controllers passed the third requirement. It was also found that shorter cables are more limiting than longer cables. This is due to the higher drag of longer cables and the lower natural frequency of longer cables.

9.2. Research Questions

The main research question of this thesis is:

How does an INDI controller compare to PID control in keeping a dipping SONAR stationary while hanging under a hovering helicopter during a dipping SONAR mission?

The answer to this question is that INDI has a better cable angle tracking performance than the PID in turbulent conditions. It also appeared to be more robust to the disturbances than the PID controller up to winds of 20 kts. However, the INDI controller performs worse than the PID at 30 kts. Likely due to the fact that the INDI has better tracking performance, which generally reduces disturbance rejection.

From this main research question, the following sub-questions arose and have been answered:

Sub-question 1: What does a dipping SONAR mission look like?

Sub-question 1.1: **What is dipping SONAR?**

Answer: A dipping SONAR is a SONAR device that is suspended below a helicopter, and lowered into the water periodically to take measurements in order to detect submarines.

Sub-question 1.2: **What manoeuvres are expected?**

Answer: From the mission analysis, it appears that the helicopter will remain hovering at 50-300ft altitude during the process of dipping.

Sub-question 1.3: **What environmental conditions are expected?**

Answer: The exact environmental conditions at which dipping SONAR is used are not readily available. However, helicopter operations were found to occur at sea states of up to 4-5. Hence, sea state 5 was chosen as a worst case scenario.

Sub-question 1.4: **What are the requirements of the controller?**

Answer:

- i. The translational rates of the SONAR shall not exceed $1m/s$ in all directions with the SONAR submerged at a depth of 60m and sea state 5 for 5 minutes.
- ii. The rotational rates of the SONAR shall not exceed $1^\circ/s$ in all directions with the SONAR submerged at a depth of 60m and sea state 5 for 5 minutes.
- iii. The SONAR shall reach steady state within 60 seconds in all axes after a step input gust of 0 to 7 Bft with the SONAR submerged at a depth of 60m.

Sub-question 1.5: **What are the controller performance metrics?**

Answer: The performance of the controllers is assessed via the following performance metrics:

- i. Standard deviation of the velocity of the SONAR;
- ii. Mean of the velocity of the SONAR;
- iii. Standard deviation of the control inputs.

The mean will tell how much the SONAR drifts. The standard deviation tells something about the oscillatory nature of the motion.

Sub-question 2: What are the dynamic characteristics of a helicopter during a dipping SONAR mission?

Sub-question 2.1: **What are the rotor dynamics?**

Answer: The rotor flapping dynamics not included in the helicopter model. However, quasi-steady inflow dynamics were assumed.

Sub-question 2.2: **What are the actuator dynamics?**

Answer: Actuator dynamics were not modelled in this thesis, but could be approximated using a first order lag filter.

Sub-question 2.5: **What is the state of the art in helicopter modelling with a slung load?**

Answer: In literature, typically a helicopter is modelled in combination with a simple pendulum, though other models are used as well. The reason for this is that the pendulum mode is the main mode for a hanging load. Especially when moving from A to B, the pendulum mode is the most dominant. However, when remaining stationary, the pendulum mode may not be as dominant, meaning that the cable can change shape. This requires a more detailed cable model.

Sub-question 2.3: **How does a pure helicopter behave (without any suspended load)?**

Answer: The helicopter is unstable in its phugoid mode to begin with. Hence, a controller is necessary to keep it stable. With this controller, the helicopter responds relatively quick. It has good tracking performance with both the PID and INDI controllers

Sub-question 2.4: **How does a submerged load change helicopter behaviour?**

Answer: Adding a submerged load to the helicopter yields more aggressive control inputs than when no loads are attached. Also, it was found that the location of the load has a large influence on the response of the helicopter. Moving the load forwards improved performance generally. Also, the drag of the water added a lot of drag to the cable, keeping it from oscillating.

Sub-question 3: What is the state of the art in helicopter automatic flight control systems?

Sub-question 3.1: **What different control methodologies exist?**

Answer: Many different control methodologies exist to control a helicopter with a hanging load. This includes both linear and non-linear control methods.

Sub-question 3.2: **What different control modes exist?**

Answer: Attitude hold, Coupled, stability control augmentation system, attitude command attitude hold, translational rate command, position hold and altitude hold.

Sub-question 3.3: **What are their advantages/disadvantages?**

Answer: Each control methodology has their advantages and disadvantages regarding to model knowledge, complexity and robustness.

Sub-question 3.4: **Why choose INDI as control method?**

Answer: INDI is a control method that requires minimal model knowledge and is generally very robust to errors.

Sub-question 4: How to design an INDI controller for a helicopter with a dipping SONAR?

Sub-question 4.1: **How does INDI work?**

Answer: INDI is a sensor-based approach, meaning that it trades model knowledge for measurements in order to control the dynamic system.

Sub-question 4.2: **What is the controlled variable?**

Answer: The controlled variable used for SONAR control is the angle of the cable at the attachment point of the helicopter.

Sub-question 4.3: **How is INDI currently used in control systems?**

Answer: INDI is not practically applied in flight control systems yet (as to the authors knowledge). However, case studies were done to apply INDI to various vehicles, including helicopters.

Sub-question 4.4: **How to design the outer loop controller?**

Answer: The outer loop controller of the SONAR controller is a PID controller, controlling the cable angle, followed by a loop controlling the cable angular rate.

Sub-question 5: What models will be used?

Sub-question 5.1: **What model is used for the helicopter?**

Answer: An 8 degrees of freedom helicopter model is used of the Bo-105 helicopter, obtained from the thesis supervisor.

Sub-question 5.2: **What model is used for the suspension cable?**

Answer: A discrete cable model was developed in this thesis.

Sub-question 5.3: **What model is used for the SONAR?**

Answer: The SONAR is modelled as a rigid cylinder.

Sub-question 5.4: **What model is used for the environment?**

Answer: For the environment, a constant wind was used in combination with a von Karman turbulence model.

Sub-question 6: How does an INDI controller perform for a helicopter with a dipping SONAR compared to PID?

Sub-question 6.1: **What sensors are required to make it work?**

Answer: For INDI, not only the helicopter states are needed, but also their rates. This means that angular accelerations must either be measured directly, or deduced from other sensors. Rate gyros are capable of determining the attitude of the angular position of the helicopter (by integrating), the angular rate from measurements and the angular acceleration by differentiating, although errors are likely to occur here. The same is true for the cable angle measurements.

Sub-question 6.2: **What are the requirements of the sensors?**

Answer: From the basic principles of INDI, fast sensors are needed in order for the assumptions of INDI to hold. Faster sensors also make INDI more robust.

Sub-question 6.3: **How robust is INDI to flapping dynamics?**

Answer: Flapping dynamics are not assessed separately in this thesis. However, flapping dynamics are very complex and introduce time delays into the system. It is known that time delays degrade controller performance.

Sub-question 6.4: **How robust is INDI to actuator dynamics?**

Answer: In general, actuator dynamics slow down the control inputs response. This means that there is a time delay between the desired control input and the actual control input., reducing controller performance This can be mitigated by synchronising the control input signals and the control variables by using filters.

Recommendations

This chapter contains recommendations containing improvements on this research, possible future steps and ideas that came up during this project.

Rec 1 : Improvement on models

In this research, a model for a helicopter, a cable + SONAR and the wind were used. There were some things, however, that were not modelled, which could change the behavior of the controller. These are sensor measurements and actuator dynamics.

The cable model could be improved by adding a more realistic damping model. Currently, the damping is assumed to be linear and depends on the angle between cable sections and the relative angular velocity between these two. The coefficients used for damping were based on guesswork in order to ensure a stable simulation. Having a realistic damping of the cable would make the analysis of the cable model more valid. Also, the sensitivity analysis showed that there are large peaks in the vertical SONAR velocity. It is thought that a lack of drag on the cable in this direction is the cause of this. Adding a more refined drag model would show whether this is the case.

The wind model could be improved by adding varying wind with altitude, since wind and gusts are different close to the water's surface than at altitude. It would also be interesting to add a wave model, a sea current model and to have wind interact with the waves in order to see the effects this has on the cable's behaviour.

Rec 2 : Future steps

The conclusions of this report were that, although INDI cable control performed better than PID cable control in turbulent conditions, a position hold controller performed better than the cable controller in general. This follows from the fact that the cable controller follows a certain reference cable angle, which remained constant regardless of wind conditions. This meant that move commands were introduced to keep this angle constant. The next step could be finding a way to change the reference cable angle based on the incoming disturbance. Alternatively, a wash-out could be added to remove the effect of the disturbance. The general idea is to find a way to stabilise the cable, while generally staying at the same position.

Another future step could be using measurements of the SONAR states if possible and controlling the SONAR, rather than the cable angle at the helicopter. The major advantage here would be that for INDI, the complex cable dynamics could be largely ignored. The difficulty here, however, lies in determining what the control effectiveness is in such a case, as the cable shape influences the control effectiveness.

In literature, several works discussed the use of an active cargo hook, which essentially is a moving platform underneath the helicopter to which the cable is attached ([12],[53]). According to [12], this is more stable than when using the helicopter to move around. The use of an active cargo hook could be the solution to staying in the same position while stabilising the suspension cable.

It is recommended to perform a linear analysis of the controlled helicopter-cable system with the goal of finding the bandwidth of the controller. This will tell how stable the system is and would be required if any certification is done in the future.

Rec 3 : Ideas that came up

In determining the control strategy for the cable controller, 3 different options were investigated: cable control through helicopter attitude, velocity and position. It was found that cable control through attitude performed best, as this controller ignores the velocity of the helicopter. This means that when there is an aerodynamic disturbance, this is only present in the response of the cable. The other control strategies use the translational rate command, which controls the airspeed of the helicopter. This means that these control strategies have the aerodynamic disturbance twice: once in the cable response and once in the translational rate command. It would be interesting to see whether the other control strategies perform more similar, or better, when using a translational rate command that doesn't use airspeed, but ground speed instead. This should be possible by means of GPS measurements.

References

- [1] C. Adams *et al.*, “Modeling and input shaping control of a micro coaxial radio-controlled helicopter carrying a suspended load,” *International Conference on Control, Automation and Systems*, pp. 645–650, 2012.
- [2] *Armelsan Datasheet.pdf*.
- [3] T. Ashitha Varghese *et al.*, “Sliding Mode Control Based Design for a 6-DOF Miniature Helicopter in Hovering Flight Mode,” *2019 IEEE 5th International Conference on Mechatronics System and Robots, ICMSR 2019*, pp. 59–63, 2019. DOI: 10.1109/ICMSR.2019.8835471.
- [4] “Asw helicopters.” (), [Online]. Available: <https://www.globalsecurity.org/military/systems/aircraft/rotary-asw.htm>.
- [5] B. J. Bacon *et al.*, “Reconfigurable flight control using nonlinear dynamic inversion with a special accelerometer implementation,” *AIAA Guidance, Navigation, and Control Conference and Exhibit*, no. August, 2000. DOI: 10.2514/6.2000-4565.
- [6] M. Bisgaard *et al.*, “Input shaping for helicopter slung load swing reduction,” *AIAA Guidance, Navigation and Control Conference and Exhibit*, no. August, 2008. DOI: 10.2514/6.2008-6964.
- [7] M. Bisgaard *et al.*, “Modeling of generic slung load system,” *Journal of Guidance, Control, and Dynamics*, vol. 32, no. 2, pp. 573–585, 2009. DOI: 10.2514/1.36539.
- [8] M. Bisgaard *et al.*, “Swing damping for helicopter slung load systems using delayed feedback,” *AIAA Guidance, Navigation, and Control Conference and Exhibit*, no. August, 2009. DOI: 10.2514/6.2009-5795.
- [9] T. Camp *et al.*, “Fluid mechanics,” *Mechanobiology Handbook*, pp. 23–44, 2011. DOI: 10.2478/jtam-2013-0011.
- [10] M. Chen *et al.*, “Antidisturbance Control for a Suspension Cable System of Helicopter Subject to Input Nonlinearities,” *IEEE Transactions on Systems, Man, and Cybernetics: Systems*, vol. 48, no. 12, pp. 2292–2304, 2018. DOI: 10.1109/TSMC.2017.2710638.
- [11] “Dauphin helikopter.” (), [Online]. Available: <https://www.kustwacht.nl/nl/vliegend/sar>.
- [12] T. A. Dukes, *Maneuvering Heavy Sling Loads Near Hover Part I: Damping the Pendulous Motion*, 1973.
- [13] G. Ellis, “Four Types of Controllers,” in *Control System Design Guide*, Elsevier, 2012, pp. 97–119. DOI: 10.1016/b978-0-12-385920-4.00006-0.
- [14] T. Ertuğrul *et al.*, “Model reference adaptive control design for helicopters using gain scheduled reference models,” *Proceedings of the 2016 17th International Carpathian Control Conference, ICCCC 2016*, pp. 182–187, 2016. DOI: 10.1109/CarpathianCC.2016.7501090.
- [15] Federal Aviation Administration, “Helicopter Components, Sections, and Systems,” in *Helicopter Flying Handbook*, 3, vol. 1, Oklahoma City, 2019, ch. 4, p. 20. [Online]. Available: https://www.faa.gov/regulations_policies/handbooks_manuals/aviation/helicopter_flying_handbook/.
- [16] H. Gao *et al.*, “Design of sliding mode control system for automatic transition and hover of helicopter,” *2017 3rd IEEE International Conference on Control Science and Systems Engineering, ICCSSE 2017*, no. 1, pp. 102–105, 2017. DOI: 10.1109/CCSSE.2017.8087903.
- [17] A. S. Gian Pietro, “Automatic Flight Control System: Autopilot Cable Hover Mode Computer Aided Design and Assessment,” 1989.

- [18] N. Gupta *et al.*, "Automatic Control of a Helicopter with a Hanging Load," *Center For Systems Research*, 1973.
- [19] C. R. Guy *et al.*, "ASW Helicopter/SOAR Dynamics Mathematical Model," *sixth european rotorcraft and powered lift aircraft forum*, no. 45, 1980.
- [20] "Helicopter dipping sonar." (), [Online]. Available: <https://armelsan.com/files/urunler/orkun.pdf>.
- [21] "Helicopter long-range active sonar." (), [Online]. Available: <https://www.l3harris.com/sites/default/files/2021-04/ims-maritime-ocean-systems-resource-Helras.pdf>.
- [22] T. v. Holten, *Helicopter Performance, Stability and Control*. Faculty of Aerospace Engineering Delft University of Technology, 2002.
- [23] J. Hu *et al.*, "Position tracking control of a helicopter in ground effect using nonlinear disturbance observer-based incremental backstepping approach," *Aerospace Science and Technology*, vol. 81, pp. 167–178, 2018. DOI: 10.1016/j.ast.2018.08.002. [Online]. Available: <https://doi.org/10.1016/j.ast.2018.08.002>.
- [24] Y. Huang *et al.*, "Time-Delay Margin and Robustness of Incremental Nonlinear Dynamic Inversion Control," *Journal of Guidance, Control, and Dynamics*, pp. 1–11, 2021. DOI: 10.2514/1.g006024.
- [25] "Introduction: Pid controller design." (), [Online]. Available: <https://ctms.engin.umich.edu/CTMS/index.php?example=Introduction§ion=ControlPID>.
- [26] C. M. Ivler *et al.*, "Cable angle feedback control systems to improve handling qualities for helicopters with slung loads," *AIAA Guidance, Navigation, and Control Conference 2011*, no. August, pp. 1–27, 2011. DOI: 10.2514/6.2011-6686.
- [27] E. N. Johnson *et al.*, "Pseudo-control hedging: a new method for adaptive control," *Advances in Navigation Guidance and Control Technology Workshop*, pp. 1–23, 2000.
- [28] H. M. Kim, "Design of an automatic load positioning system for hoist operations," *CEAS Aeronautical Journal*, vol. 8, no. 2, pp. 335–351, 2017. DOI: 10.1007/s13272-017-0241-8.
- [29] J. Krishnamurthi *et al.*, "Helicopter slung load control using lagged cable angle feedback," *Journal of the American Helicopter Society*, vol. 60, no. 2, pp. 1–12, 2015. DOI: 10.4050/JAHS.60.022011.
- [30] D. J. Lee *et al.*, "Model-free LQ control for unmanned helicopters using reinforcement learning," *International Conference on Control, Automation and Systems*, no. 6, pp. 117–120, 2011.
- [31] M. Li *et al.*, "An Extended INDI Approach and Application to Pitch Rate Control Laws Design of an Aircraft," pp. 1–13, 2021. DOI: 10.2514/6.2021-3005.
- [32] L. Liu *et al.*, "Composite Anti-Disturbance Reference Model L_2 - L_∞ Control for Helicopter Slung Load System," *Journal of Intelligent and Robotic Systems: Theory and Applications*, vol. 102, no. 1, 2021. DOI: 10.1007/s10846-020-01276-z.
- [33] M. Lower *et al.*, "Fuzzy flight control system for helicopter intelligence in hover," *Proceedings - 5th International Conference on Intelligent Systems Design and Applications 2005, ISDA '05*, vol. 2005, pp. 370–374, 2005. DOI: 10.1109/ISDA.2005.48.
- [34] P. Lu *et al.*, "Aircraft fault-tolerant trajectory control using Incremental Nonlinear Dynamic Inversion," *Control Engineering Practice*, vol. 57, pp. 126–141, 2016. DOI: 10.1016/j.conengprac.2016.09.010. [Online]. Available: <http://dx.doi.org/10.1016/j.conengprac.2016.09.010>.
- [35] L. R. Lucassen *et al.*, "Dynamic Stability Analysis of a Hovering Helicopter with a Sling Load," *Journal of the American Helicopter Society*, vol. 10, no. 2, pp. 6–12, 1965. DOI: 10.4050/jahs.10.6.
- [36] J. Margés. "Vliegend paradepaard staat te trappelen." (), [Online]. Available: https://magazines.defensie.nl/allehens/2016/12/06_nh90-culdrose.
- [37] P. Marguerettaz *et al.*, "Simulation of helicopter dynamics with external suspended loads," *37th European Rotorcraft Forum 2011, ERF 2011*, pp. 348–359, 2011.

- [38] B. Nagabhushan, "Dynamic stability of a helicopter carrying a suspended payload," 1978. DOI: 10.2514/6.1978-1335.
- [39] "Nh90 tactical transport helicopter." (), [Online]. Available: <https://www.army-technology.com/projects/nh90-tactical-transport-helicopter/#:~:text=Performance%20of%20the%20NH90%20helicopter&text=The%20maximum%20takeoff%20weight%20of,4.45%20hours%20on%20internal%20fuel..>
- [40] "Ocean current." (), [Online]. Available: <https://www.britannica.com/science/ocean-current#ref301646>.
- [41] G. D. Padfield, *Helicopter Flight Dynamics: The Theory and Application of Flying Qualities and Simulation Modelling*, 2nd ed. Washington DC: Blackwell, 2007, vol. 266, p. 680. DOI: 10.1016/s0021-9258(19)67866-x.
- [42] M. D. Pavel, "Mathematical modeling of tandem helicopters with external sling loads for piloted simulation," *Collection of Technical Papers - 2007 AIAA Modeling and Simulation Technologies Conference*, vol. 1, no. August, pp. 570–587, 2007. DOI: 10.2514/6.2007-6617.
- [43] M. D. Pavel *et al.*, "Incremental nonlinear dynamic inversion for the apache AH-64 helicopter control," *Journal of the American Helicopter Society*, vol. 65, no. 2, pp. 1–16, 2020. DOI: 10.4050/JAHS.65.022006.
- [44] J. Potter *et al.*, "Reducing swing of model helicopter sling load using input shaping," *IEEE International Conference on Control and Automation, ICCA*, pp. 348–353, 2011. DOI: 10.1109/ICCA.2011.6138048.
- [45] J. PRASAD *et al.*, "Synthesis of a helicopter nonlinear flight controller using approximate model inversion," 1992. DOI: 10.2514/6.1992-4468.
- [46] Y. Ren *et al.*, "Boundary control for a suspension cable system of a helicopter with saturation nonlinearity using backstepping approach," *IEEE Access*, vol. 7, pp. 114 213–114 222, 2019. DOI: 10.1109/ACCESS.2019.2935899.
- [47] C. E. Riboldi *et al.*, "A model-based design framework for rotorcraft trim control laws," *43rd European Rotorcraft Forum, ERF 2017*, vol. 1, pp. 487–501, 2017.
- [48] N. A. Sahani *et al.*, "Adaptive model inversion control of a helicopter with structural load limiting," *Journal of Guidance, Control, and Dynamics*, vol. 29, no. 2, pp. 411–420, 2006. DOI: 10.2514/1.13391.
- [49] M. Sasaki *et al.*, "Learning fuzzy logic controller for hovering a helicopter," *Annual Conference of the North American Fuzzy Information Processing Society - NAFIPS*, pp. 25–28, 1998. DOI: 10.1109/NAFIPS.1998.715522.
- [50] S. Sieberling *et al.*, "Robust flight control using incremental nonlinear dynamic inversion and angular acceleration prediction," *Journal of Guidance, Control, and Dynamics*, vol. 33, no. 6, pp. 1732–1742, 2010. DOI: 10.2514/1.49978.
- [51] P. Simplício *et al.*, "An acceleration measurements-based approach for helicopter nonlinear flight control using incremental nonlinear dynamic inversion," *Control Engineering Practice*, vol. 21, no. 8, pp. 1065–1077, 2013. DOI: 10.1016/j.conengprac.2013.03.009. [Online]. Available: <http://dx.doi.org/10.1016/j.conengprac.2013.03.009>.
- [52] P. Simplício, "Helicopter Nonlinear Flight Control: An Acceleration Measurements-based Approach Using Nonlinear Dynamic Inversion," 2011.
- [53] A. Singh *et al.*, "Slung load stabilization across the flight envelope using an active cargo hook," *AIAA Scitech 2019 Forum*, no. January, 2019. DOI: 10.2514/6.2019-0821.
- [54] Thales, "FLASH & Compact FLASH dipping sonars SONICS sonobuoy processing system," 2002.
- [55] "Understanding helicopter automatic flight control systems (afcs)." (), [Online]. Available: <https://helicoptermaintenancemagazine.com/article/understanding-helicopter-automatic-flight-control-systems-afcs>.

- [56] H. Wang *et al.*, “Modeling and Simulation of a Slung-load System for the Helicopter,” *Proceedings of the 31st Chinese Control and Decision Conference, CCDC 2019*, pp. 1148–1153, 2019. DOI: 10.1109/CCDC.2019.8833478.
- [57] X. Wang *et al.*, “Design of helicopter cable-orientation control system based on finite-element modeling,” *Lecture Notes in Computer Science (including subseries Lecture Notes in Artificial Intelligence and Lecture Notes in Bioinformatics)*, vol. 7506 LNAI, no. PART 1, pp. 313–322, 2012. DOI: 10.1007/978-3-642-33509-9{_}30.
- [58] X. Wang *et al.*, “Design of hovering altitude holding control system for helicopter,” *2012 IEEE International Conference on Information and Automation, ICIA 2012*, no. June, pp. 180–183, 2012. DOI: 10.1109/ICInfA.2012.6246804.
- [59] X. Wang *et al.*, “Stability analysis for incremental nonlinear dynamic inversion control,” *Journal of Guidance, Control, and Dynamics*, vol. 42, no. 5, pp. 1116–1129, 2019. DOI: 10.2514/1.G003791.
- [60] W. Wei, “Adaptive control based flying quality design for helicopters,” *43rd European Rotorcraft Forum, ERF 2017*, vol. 1, pp. 474–486, 2017.
- [61] “What is sonar?” (), [Online]. Available: <https://oceanservice.noaa.gov/facts/sonar.html>.
- [62] “Wind.” (), [Online]. Available: <http://www.bom.gov.au/marine/knowledge-centre/reference/wind.shtml>.
- [63] K. Yan *et al.*, “Robust adaptive backstepping control for unmanned autonomous helicopter with flapping dynamics,” *IEEE International Conference on Control and Automation, ICCA*, pp. 1027–1032, 2017. DOI: 10.1109/ICCA.2017.8003202.
- [64] A. Y. Younes *et al.*, “Adaptive integral backstepping controller for an autonomous rotorcraft,” *2009 6th International Symposium on Mechatronics and its Applications, ISMA 2009*, 2009. DOI: 10.1109/ISMA.2009.5164795.
- [65] L. I. Yu *et al.*, “Control Law Design of the Surface Damage Aircraft Based on Incremental Dynamic Inversion,” *Proceedings - 2019 Chinese Automation Congress, CAC 2019*, no. 61374032, pp. 1747–1752, 2019. DOI: 10.1109/CAC48633.2019.8997433.
- [66] S. Zhang *et al.*, “An anti-windup INDI fault-tolerant control scheme for flying wing aircraft with actuator faults,” *ISA Transactions*, vol. 93, pp. 172–179, 2019. DOI: 10.1016/j.isatra.2019.02.037. [Online]. Available: <https://doi.org/10.1016/j.isatra.2019.02.037>.



Partial Derivatives T , D , V and a_1

$$V = \sqrt{u^2 + w^2}. \quad (\text{A.1})$$

$$\frac{\partial V}{\partial u} = \frac{u}{V}. \quad (\text{A.2})$$

$$\frac{\partial V}{\partial w} = \frac{w}{V}. \quad (\text{A.3})$$

$$\alpha_c = \theta_c - \tan^{-1}\left(\frac{w}{u}\right) \quad (\text{A.4})$$

$$\frac{\partial \alpha_c}{\partial u} = \frac{w}{V^2}. \quad (\text{A.5})$$

$$\frac{\partial \alpha_c}{\partial w} = -\frac{u}{V^2}. \quad (\text{A.6})$$

$$\frac{\partial \alpha_c}{\partial \theta_c} = 1. \quad (\text{A.7})$$

$$\mu = \frac{V \cos(\alpha_c)}{\Omega R}. \quad (\text{A.8})$$

$$\frac{\partial \mu}{\partial V} = \frac{\cos(\alpha_c)}{\Omega R}. \quad (\text{A.9})$$

$$\frac{\partial \mu}{\partial \alpha_c} = -\frac{V \sin(\alpha_c)}{\Omega R}. \quad (\text{A.10})$$

$$\lambda_c = \frac{V \sin(\alpha_c)}{\Omega R}. \quad (\text{A.11})$$

$$\frac{\partial \lambda_c}{\partial V} = \frac{\sin(\alpha_c)}{\Omega R}. \quad (\text{A.12})$$

$$\frac{\partial \lambda_c}{\partial \alpha_c} = \frac{V \cos(\alpha_c)}{\Omega R}. \quad (\text{A.13})$$

$$\frac{\partial \mu}{\partial u} = \frac{\partial \mu}{\partial V} \frac{\partial V}{\partial u} + \frac{\partial \mu}{\partial \alpha_c} \frac{\partial \alpha_c}{\partial u} \quad (\text{A.14})$$

$$\frac{\partial \lambda_c}{\partial u} = \frac{\partial \lambda_c}{\partial V} \frac{\partial V}{\partial u} + \frac{\partial \lambda_c}{\partial \alpha_c} \frac{\partial \alpha_c}{\partial u} \quad (\text{A.15})$$

Partial Derivatives a_1

$$a_1 = \frac{\frac{8}{3}\mu\theta_0 - 2\mu(\lambda_c + \lambda_i) - \frac{16q}{\gamma\Omega}}{1 - \frac{1}{2}\mu^2} \quad (\text{A.16})$$

$$\frac{\partial a_1}{\partial \mu} = \frac{(1 - \frac{1}{2}\mu^2) [\frac{8}{3}\theta_0 - 2(\lambda_c + \lambda_i)] + \frac{8}{3}\mu^2\theta_0 - 2\mu^2(\lambda_c + \lambda_i) - \frac{16q}{\gamma\Omega}\mu}{(1 - \frac{1}{2}\mu^2)^2} \quad (\text{A.17})$$

$$\frac{\partial a_1}{\partial \lambda_c} = \frac{-2\mu}{1 - \frac{1}{2}\mu^2} \quad (\text{A.18})$$

$$\frac{\partial a_1}{\partial \theta_0} = \frac{\frac{8}{3}\mu}{1 - \frac{1}{2}\mu^2} \quad (\text{A.19})$$

$$\frac{\partial a_1}{\partial q} = \frac{-\frac{16}{\gamma\Omega}}{1 - \frac{1}{2}\mu^2} \quad (\text{A.20})$$

$$\frac{\partial a_1}{\partial u} = \left[\frac{\partial a_1}{\partial \mu} \frac{\partial \mu}{\partial u} + \frac{\partial a_1}{\partial \lambda_c} \frac{\partial \lambda_c}{\partial u} \right] \quad (\text{A.21})$$

$$\frac{\partial a_1}{\partial w} = \left[\frac{\partial a_1}{\partial \mu} \frac{\partial \mu}{\partial w} + \frac{\partial a_1}{\partial \lambda_c} \frac{\partial \lambda_c}{\partial w} \right] \quad (\text{A.22})$$

$$\frac{\partial a_1}{\partial \theta_c} = \left[\frac{\partial a_1}{\partial \mu} \frac{\partial \mu}{\partial \alpha_c} \frac{\partial \alpha_c}{\partial \theta_c} + \frac{\partial a_1}{\partial \lambda_c} \frac{\partial \lambda_c}{\partial \alpha_c} \frac{\partial \alpha_c}{\partial \theta_c} \right] \quad (\text{A.23})$$

Partial Derivatives $C_{T_{BEM}}$

$$C_{T_{BEM}} = \frac{1}{4} c_{l_\alpha} \sigma \left[\frac{2}{3} \theta_0 \left(1 + \frac{3}{2} \mu^2 \right) - (\lambda_c + \lambda_i) \right] \quad (\text{A.24})$$

$$\frac{\partial C_{T_{BEM}}}{\partial \mu} = \frac{1}{2} c_{l_\alpha} \sigma \theta_0 \mu \quad (\text{A.25})$$

$$\frac{\partial C_{T_{BEM}}}{\partial \lambda_c} = -\frac{1}{4} c_{l_\alpha} \sigma \quad (\text{A.26})$$

$$\frac{\partial C_{T_{BEM}}}{\partial \theta_0} = \frac{1}{6} c_{l_\alpha} \sigma \left(1 + \frac{3}{2} \mu^2 \right) \quad (\text{A.27})$$

$$\frac{\partial C_{T_{BEM}}}{\partial \theta_c} = \frac{\partial C_{T_{BEM}}}{\partial \lambda_c} \frac{\partial \lambda_c}{\partial \alpha_c} \frac{\partial \alpha_c}{\partial \theta_c} + \frac{\partial C_{T_{BEM}}}{\partial \mu} \frac{\partial \mu}{\partial \alpha_c} \frac{\partial \alpha_c}{\partial \theta_c} \quad (\text{A.28})$$

Partial Derivatives Thrust

$$\frac{\partial T}{\partial u} = \rho (\Omega R) \pi R^2 \left[\frac{\partial C_T}{\partial \mu} \frac{\partial \mu}{\partial u} + \frac{\partial C_T}{\partial \lambda_c} \frac{\partial \lambda_c}{\partial u} \right] \quad (\text{A.29})$$

$$\frac{\partial T}{\partial w} = \rho (\Omega R) \pi R^2 \left[\frac{\partial C_T}{\partial \mu} \frac{\partial \mu}{\partial w} + \frac{\partial C_T}{\partial \lambda_c} \frac{\partial \lambda_c}{\partial w} \right] \quad (\text{A.30})$$

$$\frac{\partial T}{\partial \theta_c} = \rho (\Omega R) \pi R^2 \frac{\partial C_T}{\partial \theta_c} \quad (\text{A.31})$$

$$\frac{\partial T}{\partial \theta_0} = \rho (\Omega R) \pi R^2 \frac{\partial C_T}{\partial \theta_0} \quad (\text{A.32})$$

Partial Derivatives Drag

$$D = \frac{1}{2} \rho V^2 C_D S \quad (\text{A.33})$$

$$\frac{\partial D}{\partial V} = \rho V C_D S \quad (\text{A.34})$$

B

Partial Derivatives Single Pendulum

$$\dot{x}_0 = u \cos(\theta_f) + w \sin(\theta_f) \quad (\text{B.1})$$

$$\frac{\partial \dot{x}_0}{\partial u} = \cos(\theta_f); \frac{\partial \dot{x}_0}{\partial w} = \sin(\theta_f); \frac{\partial \dot{x}_0}{\partial \theta_f} = -u \sin(\theta_f) + w \cos(\theta_f) \quad (\text{B.2})$$

$$\dot{z}_0 = -u \sin(\theta_f) + w \cos(\theta_f) \quad (\text{B.3})$$

$$\frac{\partial \dot{z}_0}{\partial u} = -\sin(\theta_f); \frac{\partial \dot{z}_0}{\partial w} = \cos(\theta_f); \frac{\partial \dot{z}_0}{\partial \theta_f} = -u \cos(\theta_f) - w \sin(\theta_f) \quad (\text{B.4})$$

$$\dot{x}_1 = \dot{x}_0 - l_1 \cos(\theta_1) \dot{\theta}_1 \quad (\text{B.5})$$

$$\frac{\partial \dot{x}_1}{\partial \dot{x}_0} = 1; \frac{\partial \dot{x}_1}{\partial \dot{\theta}_1} = -l_1 \cos(\theta_1); \frac{\partial \dot{x}_1}{\partial \theta_1} = l_1 \sin(\theta_1) \dot{\theta}_1; \quad (\text{B.6})$$

$$\dot{z}_1 = \dot{z}_0 - l_1 \sin(\theta_1) \dot{\theta}_1 \quad (\text{B.7})$$

$$\frac{\partial \dot{z}_1}{\partial \dot{z}_0} = 1; \frac{\partial \dot{z}_1}{\partial \dot{\theta}_1} = -l_1 \sin(\theta_1); \frac{\partial \dot{z}_1}{\partial \theta_1} = -l_1 \cos(\theta_1) \dot{\theta}_1; \quad (\text{B.8})$$

$$D_{1_x} = \frac{1}{2} \rho \dot{x}_1^2 C_{D_1} S_1 \rightarrow \frac{\partial D_{1_x}}{\partial \dot{x}_1} = \rho \dot{x}_1 C_{D_1} S_1 \quad (\text{B.9})$$

$$D_{1_z} = \frac{1}{2} \rho \dot{z}_1^2 C_{D_1} S_1 \rightarrow \frac{\partial D_{1_z}}{\partial \dot{z}_1} = \rho \dot{z}_1 C_{D_1} S_1 \quad (\text{B.10})$$

$$\ddot{x}_0 = \dot{u} \cos(\theta_f) - u \sin(\theta_f) \dot{q} + \dot{w} \sin(\theta_f) + w \cos(\theta_f) \dot{q} \quad (\text{B.11})$$

$$\begin{aligned} \frac{\partial \ddot{x}_0}{\partial u} &= \frac{\partial \dot{u}}{\partial u} \cos(\theta_f) - \sin(\theta_f) \dot{q} + \frac{\partial \dot{w}}{\partial u} \sin(\theta_f) \\ \frac{\partial \ddot{x}_0}{\partial w} &= \frac{\partial \dot{u}}{\partial w} \cos(\theta_f) + \frac{\partial \dot{w}}{\partial w} \sin(\theta_f) + \cos(\theta_f) \dot{q} \\ \frac{\partial \ddot{x}_0}{\partial q} &= \frac{\partial \dot{u}}{\partial q} \cos(\theta_f) - u \sin(\theta_f) + \frac{\partial \dot{w}}{\partial q} \sin(\theta_f) + w \cos(\theta_f) \\ \frac{\partial \ddot{x}_0}{\partial \theta_f} &= \frac{\partial \dot{u}}{\partial \theta_f} \cos(\theta_f) - \dot{u} \sin(\theta_f) - u \cos(\theta_f) \dot{q} + \frac{\partial \dot{w}}{\partial \theta_f} \sin(\theta_f) + \dot{w} \cos(\theta_f) - w \sin(\theta_f) \dot{q} \\ \frac{\partial \ddot{x}_0}{\partial \dot{\theta}_1} &= \frac{\partial \dot{u}}{\partial \dot{\theta}_1} \cos(\theta_f) + \frac{\partial \dot{w}}{\partial \dot{\theta}_1} \sin(\theta_f) \\ \frac{\partial \ddot{x}_0}{\partial \theta_1} &= \frac{\partial \dot{u}}{\partial \theta_1} \cos(\theta_f) + \frac{\partial \dot{w}}{\partial \theta_1} \sin(\theta_f) \\ \frac{\partial \ddot{x}_0}{\partial \theta_c} &= \frac{\partial \dot{u}}{\partial \theta_c} \cos(\theta_f) + \frac{\partial \dot{w}}{\partial \theta_c} \sin(\theta_f) \\ \frac{\partial \ddot{x}_0}{\partial \theta_0} &= \frac{\partial \dot{u}}{\partial \theta_0} \cos(\theta_f) + \frac{\partial \dot{w}}{\partial \theta_0} \sin(\theta_f) \end{aligned} \quad (\text{B.12})$$

$$\ddot{z}_0 = -\dot{u} \sin(\theta_f) - u \cos(\theta_f)q + \dot{w} \cos(\theta_f) - w \sin(\theta_f)q \quad (\text{B.13})$$

$$\begin{aligned} \frac{\partial \ddot{z}_0}{\partial u} &= -\frac{\partial \dot{u}}{\partial u} \sin(\theta_f) - \cos(\theta_f)q + \frac{\partial \dot{w}}{\partial u} \cos(\theta_f) \\ \frac{\partial \ddot{z}_0}{\partial w} &= -\frac{\partial \dot{u}}{\partial w} \sin(\theta_f) + \frac{\partial \dot{w}}{\partial w} \cos(\theta_f) - \sin(\theta_f)q \\ \frac{\partial \ddot{z}_0}{\partial q} &= -\frac{\partial \dot{u}}{\partial q} \sin(\theta_f) - u \cos(\theta_f) + \frac{\partial \dot{w}}{\partial q} \cos(\theta_f) - w \sin(\theta_f) \\ \frac{\partial \ddot{z}_0}{\partial \theta_f} &= -\frac{\partial \dot{u}}{\partial \theta_f} \sin(\theta_f) - \dot{u} \cos(\theta_f) + u \sin(\theta_f)q + \frac{\partial \dot{w}}{\partial \theta_f} \cos(\theta_f) - \dot{w} \sin(\theta_f) - w \cos(\theta_f)q \\ \frac{\partial \ddot{z}_0}{\partial \theta_1} &= -\frac{\partial \dot{u}}{\partial \theta_1} \sin(\theta_f) + \frac{\partial \dot{w}}{\partial \theta_1} \cos(\theta_f) \\ \frac{\partial \ddot{z}_0}{\partial \theta_c} &= -\frac{\partial \dot{u}}{\partial \theta_c} \sin(\theta_f) + \frac{\partial \dot{w}}{\partial \theta_c} \cos(\theta_f) \\ \frac{\partial \ddot{z}_0}{\partial \theta_0} &= -\frac{\partial \dot{u}}{\partial \theta_0} \sin(\theta_f) + \frac{\partial \dot{w}}{\partial \theta_0} \cos(\theta_f) \end{aligned} \quad (\text{B.14})$$

$$F_c = D_{1_x} \sin(\theta_1) - D_{1_z} \cos(\theta_1) + W_1 \cos(\theta_1) + m_1 l_1 \dot{\theta}_1^2 \quad (\text{B.15})$$

$$\begin{aligned} \frac{\partial F_c}{\partial D_{1_x}} &= \sin(\theta_1) \\ \frac{\partial F_c}{\partial D_{1_z}} &= -\cos(\theta_1) \\ \frac{\partial F_c}{\partial u} &= \frac{\partial F_c}{\partial D_{1_x}} \frac{\partial D_{1_x}}{\partial \dot{x}_1} \frac{\partial \dot{x}_1}{\partial \dot{x}_0} \frac{\partial \dot{x}_0}{\partial u} + \frac{\partial F_c}{\partial D_{1_z}} \frac{\partial D_{1_z}}{\partial \dot{z}_1} \frac{\partial \dot{z}_1}{\partial \dot{z}_0} \frac{\partial \dot{z}_0}{\partial u} \\ \frac{\partial F_c}{\partial w} &= \frac{\partial F_c}{\partial D_{1_x}} \frac{\partial D_{1_x}}{\partial \dot{x}_1} \frac{\partial \dot{x}_1}{\partial \dot{x}_0} \frac{\partial \dot{x}_0}{\partial w} + \frac{\partial F_c}{\partial D_{1_z}} \frac{\partial D_{1_z}}{\partial \dot{z}_1} \frac{\partial \dot{z}_1}{\partial \dot{z}_0} \frac{\partial \dot{z}_0}{\partial w} \\ \frac{\partial F_c}{\partial \theta_f} &= \frac{\partial F_c}{\partial D_{1_x}} \frac{\partial D_{1_x}}{\partial \dot{x}_1} \frac{\partial \dot{x}_1}{\partial \dot{x}_0} \frac{\partial \dot{x}_0}{\partial \theta_f} + \frac{\partial F_c}{\partial D_{1_z}} \frac{\partial D_{1_z}}{\partial \dot{z}_1} \frac{\partial \dot{z}_1}{\partial \dot{z}_0} \frac{\partial \dot{z}_0}{\partial \theta_f} \\ \frac{\partial F_c}{\partial \dot{\theta}_1} &= \frac{\partial F_c}{\partial D_{1_x}} \frac{\partial D_{1_x}}{\partial \dot{x}_1} \frac{\partial \dot{x}_1}{\partial \dot{\theta}_1} + \frac{\partial F_c}{\partial D_{1_z}} \frac{\partial D_{1_z}}{\partial \dot{z}_1} \frac{\partial \dot{z}_1}{\partial \dot{\theta}_1} + 2m_1 l_1 \dot{\theta}_1^2 \\ \frac{\partial F_c}{\partial \theta_1} &= \frac{\partial F_c}{\partial D_{1_x}} \frac{\partial D_{1_x}}{\partial \dot{x}_1} \frac{\partial \dot{x}_1}{\partial \theta_1} + D_{1_x} \cos(\theta_1) + \frac{\partial F_c}{\partial D_{1_z}} \frac{\partial D_{1_z}}{\partial \dot{z}_1} \frac{\partial \dot{z}_1}{\partial \theta_1} + D_{1_z} \sin(\theta_1) - W_1 \sin(\theta_1) \\ Q_1 &= \text{sgn}(\dot{x}_1) D_{1_x} l_1 \cos(\theta_1) + \text{sgn}(\dot{z}_1) D_{1_z} l_1 \sin(\theta_1) \end{aligned} \quad (\text{B.16})$$

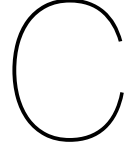
$$Q_1 = \text{sgn}(\dot{x}_1) D_{1_x} l_1 \cos(\theta_1) + \text{sgn}(\dot{z}_1) D_{1_z} l_1 \sin(\theta_1) \quad (\text{B.17})$$

Assuming both \dot{x}_1 and \dot{z}_1 are positive:

$$\begin{aligned} \frac{\partial Q_1}{\partial D_{1_x}} &= l_1 \cos(\theta_1) \\ \frac{\partial Q_1}{\partial D_{1_z}} &= l_1 \sin(\theta_1) \\ \frac{\partial Q_1}{\partial u} &= \frac{\partial Q_1}{\partial D_{1_x}} \frac{\partial D_{1_x}}{\partial \dot{x}_1} \frac{\partial \dot{x}_1}{\partial \dot{x}_0} \frac{\partial \dot{x}_0}{\partial u} + \frac{\partial Q_1}{\partial D_{1_z}} \frac{\partial D_{1_z}}{\partial \dot{z}_1} \frac{\partial \dot{z}_1}{\partial \dot{z}_0} \frac{\partial \dot{z}_0}{\partial u} \\ \frac{\partial Q_1}{\partial w} &= \frac{\partial Q_1}{\partial D_{1_x}} \frac{\partial D_{1_x}}{\partial \dot{x}_1} \frac{\partial \dot{x}_1}{\partial \dot{x}_0} \frac{\partial \dot{x}_0}{\partial w} + \frac{\partial Q_1}{\partial D_{1_z}} \frac{\partial D_{1_z}}{\partial \dot{z}_1} \frac{\partial \dot{z}_1}{\partial \dot{z}_0} \frac{\partial \dot{z}_0}{\partial w} \\ \frac{\partial Q_1}{\partial \theta_f} &= \frac{\partial Q_1}{\partial D_{1_x}} \frac{\partial D_{1_x}}{\partial \dot{x}_1} \frac{\partial \dot{x}_1}{\partial \dot{x}_0} \frac{\partial \dot{x}_0}{\partial \theta_f} + \frac{\partial Q_1}{\partial D_{1_z}} \frac{\partial D_{1_z}}{\partial \dot{z}_1} \frac{\partial \dot{z}_1}{\partial \dot{z}_0} \frac{\partial \dot{z}_0}{\partial \theta_f} \\ \frac{\partial Q_1}{\partial \dot{\theta}_1} &= \frac{\partial Q_1}{\partial D_{1_x}} \frac{\partial D_{1_x}}{\partial \dot{x}_1} \frac{\partial \dot{x}_1}{\partial \dot{\theta}_1} + \frac{\partial Q_1}{\partial D_{1_z}} \frac{\partial D_{1_z}}{\partial \dot{z}_1} \frac{\partial \dot{z}_1}{\partial \dot{\theta}_1} \\ \frac{\partial Q_1}{\partial \theta_1} &= \frac{\partial Q_1}{\partial D_{1_x}} \frac{\partial D_{1_x}}{\partial \dot{x}_1} \frac{\partial \dot{x}_1}{\partial \theta_1} - D_{1_x} l_1 \sin(\theta_1) + \frac{\partial Q_1}{\partial D_{1_z}} \frac{\partial D_{1_z}}{\partial \dot{z}_1} \frac{\partial \dot{z}_1}{\partial \theta_1} + D_{1_z} l_1 \cos(\theta_1) \end{aligned} \quad (\text{B.18})$$

$$\ddot{\theta}_1 = \frac{1}{m_1 l_1^2} Q_1 + \frac{1}{l_1} [\ddot{x}_0 \cos(\theta_1) + \ddot{z}_0 \sin(\theta_1)] - \frac{g}{l_1} \sin(\theta_1) \quad (\text{B.19})$$

$$\begin{aligned} \frac{\partial \ddot{\theta}_1}{\partial Q_1} &= \frac{1}{m_1 l_1^2} \\ \frac{\partial \ddot{\theta}_1}{\partial \ddot{x}_0} &= \frac{1}{l_1} \cos(\theta_1) \\ \frac{\partial \ddot{\theta}_1}{\partial \ddot{z}_0} &= \frac{1}{l_1} \sin(\theta_1) \end{aligned} \quad (\text{B.20})$$



Partial Derivatives Double Pendulum

$$\dot{x}_2 = \dot{x}_1 - l_2 \dot{\theta}_2 \cos(\theta_2) \quad (\text{C.1})$$

$$\frac{\partial \dot{x}_2}{\partial \dot{x}_1} = 1; \frac{\partial \dot{x}_2}{\partial \dot{\theta}_2} = -l_2 \cos(\theta_2); \frac{\partial \dot{x}_2}{\partial \theta_2} = l_2 \dot{\theta}_2 \sin(\theta_2) \quad (\text{C.2})$$

$$\dot{z}_2 = \dot{z}_1 - l_2 \dot{\theta}_2 \sin(\theta_2) \quad (\text{C.3})$$

$$\frac{\partial \dot{z}_2}{\partial \dot{z}_1} = 1; \frac{\partial \dot{z}_2}{\partial \dot{\theta}_2} = -l_2 \sin(\theta_2); \frac{\partial \dot{z}_2}{\partial \theta_2} = -l_2 \dot{\theta}_2 \cos(\theta_2) \quad (\text{C.4})$$

$$D_{2_x} = \frac{1}{2} \rho \dot{x}_2^2 C_{D_2} S_2 \rightarrow \frac{\partial D_{2_x}}{\partial \dot{x}_2} = \rho \dot{x}_2 C_{D_2} S_2 \quad (\text{C.5})$$

$$D_{2_z} = \frac{1}{2} \rho \dot{z}_2^2 C_{D_2} S_2 \rightarrow \frac{\partial D_{2_z}}{\partial \dot{z}_2} = \rho \dot{z}_2 C_{D_2} S_2 \quad (\text{C.6})$$

$$F_{ct_2} = m_2 l_2 \dot{\theta}_2^2 \rightarrow \frac{\partial F_{ct_2}}{\partial \dot{\theta}_2} = 2 m_2 l_2 \dot{\theta}_2 \quad (\text{C.7})$$

$$F_{c_{12}} = F_{ct_2} + D_{2_x} \sin(\theta_2) - D_{2_z} \cos(\theta_2) + W_2 \cos(\theta_2) \quad (\text{C.8})$$

$$\frac{\partial F_{c_{12}}}{\partial D_{2_x}} = \sin(\theta_2)$$

$$\frac{\partial F_{c_{12}}}{\partial D_{2_z}} = -\cos(\theta_2)$$

$$\frac{\partial F_{c_{12}}}{\partial u} = \frac{\partial F_{c_{12}}}{\partial D_{2_x}} \frac{\partial D_{2_x}}{\partial \dot{x}_2} \frac{\partial \dot{x}_2}{\partial \dot{x}_1} \frac{\partial \dot{x}_1}{\partial \dot{x}_0} \frac{\partial \dot{x}_0}{\partial u} + \frac{\partial F_{c_{12}}}{\partial D_{2_z}} \frac{\partial D_{2_z}}{\partial \dot{z}_2} \frac{\partial \dot{z}_2}{\partial \dot{z}_1} \frac{\partial \dot{z}_1}{\partial \dot{z}_0} \frac{\partial \dot{z}_0}{\partial u}$$

$$\frac{\partial F_{c_{12}}}{\partial w} = \frac{\partial F_{c_{12}}}{\partial D_{2_x}} \frac{\partial D_{2_x}}{\partial \dot{x}_2} \frac{\partial \dot{x}_2}{\partial \dot{x}_1} \frac{\partial \dot{x}_1}{\partial \dot{x}_0} \frac{\partial \dot{x}_0}{\partial w} + \frac{\partial F_{c_{12}}}{\partial D_{2_z}} \frac{\partial D_{2_z}}{\partial \dot{z}_2} \frac{\partial \dot{z}_2}{\partial \dot{z}_1} \frac{\partial \dot{z}_1}{\partial \dot{z}_0} \frac{\partial \dot{z}_0}{\partial w}$$

$$\frac{\partial F_{c_{12}}}{\partial q} = 0$$

$$\frac{\partial F_{c_{12}}}{\partial \theta_f} = \frac{\partial F_{c_{12}}}{\partial D_{2_x}} \frac{\partial D_{2_x}}{\partial \dot{x}_2} \frac{\partial \dot{x}_2}{\partial \dot{x}_1} \frac{\partial \dot{x}_1}{\partial \dot{x}_0} \frac{\partial \dot{x}_0}{\partial \theta_f} + \frac{\partial F_{c_{12}}}{\partial D_{2_z}} \frac{\partial D_{2_z}}{\partial \dot{z}_2} \frac{\partial \dot{z}_2}{\partial \dot{z}_1} \frac{\partial \dot{z}_1}{\partial \dot{z}_0} \frac{\partial \dot{z}_0}{\partial \theta_f} \quad (\text{C.9})$$

$$\frac{\partial F_{c_{12}}}{\partial \dot{\theta}_1} = \frac{\partial F_{c_{12}}}{\partial D_{2_x}} \frac{\partial D_{2_x}}{\partial \dot{x}_2} \frac{\partial \dot{x}_2}{\partial \dot{x}_1} \frac{\partial \dot{x}_1}{\partial \dot{\theta}_1} + \frac{\partial F_{c_{12}}}{\partial D_{2_z}} \frac{\partial D_{2_z}}{\partial \dot{z}_2} \frac{\partial \dot{z}_2}{\partial \dot{z}_1} \frac{\partial \dot{z}_1}{\partial \dot{\theta}_1}$$

$$\frac{\partial F_{c_{12}}}{\partial \theta_1} = \frac{\partial F_{c_{12}}}{\partial D_{2_x}} \frac{\partial D_{2_x}}{\partial \dot{x}_2} \frac{\partial \dot{x}_2}{\partial \dot{x}_1} \frac{\partial \dot{x}_1}{\partial \theta_1} + \frac{\partial F_{c_{12}}}{\partial D_{2_z}} \frac{\partial D_{2_z}}{\partial \dot{z}_2} \frac{\partial \dot{z}_2}{\partial \dot{z}_1} \frac{\partial \dot{z}_1}{\partial \theta_1}$$

$$\frac{\partial F_{c_{12}}}{\partial \dot{\theta}_2} = \frac{\partial F_{c_{12}}}{\partial D_{2_x}} \frac{\partial D_{2_x}}{\partial \dot{x}_2} \frac{\partial \dot{x}_2}{\partial \dot{\theta}_2} + \frac{\partial F_{c_{12}}}{\partial D_{2_z}} \frac{\partial D_{2_z}}{\partial \dot{z}_2} \frac{\partial \dot{z}_2}{\partial \dot{\theta}_2} + \frac{\partial F_{ct_2}}{\partial \dot{\theta}_2}$$

$$\frac{\partial F_{c_{12}}}{\partial \theta_2} = \frac{\partial F_{c_{12}}}{\partial D_{2_x}} \frac{\partial D_{2_x}}{\partial \dot{x}_2} \frac{\partial \dot{x}_2}{\partial \theta_2} + \frac{\partial F_{c_{12}}}{\partial D_{2_z}} \frac{\partial D_{2_z}}{\partial \dot{z}_2} \frac{\partial \dot{z}_2}{\partial \theta_2} + D_{2_x} \cos(\theta_2) + D_{2_z} \sin(\theta_2) - W_2 \sin(\theta_2)$$

$$F_c = D_{1_x} \sin(\theta_1) - D_{1_z} \cos(\theta_1) + W_1 \cos(\theta_1) + m_1 l_1 \dot{\theta}_1^2 + F_{c_{12}} \cos(\theta_1 - \theta_2) \quad (\text{C.10})$$

Note that the subscript SP stands for "Single Pendulum". This means that this partial derivative can be found in Appendix B.

$$\begin{aligned}
\frac{\partial F_c}{\partial u} &= \left(\frac{\partial F_c}{\partial u} \right)_{SP} + \frac{\partial F_{c12}}{\partial u} \cos(\theta_1 - \theta_2) \\
\frac{\partial F_c}{\partial w} &= \left(\frac{\partial F_c}{\partial w} \right)_{SP} + \frac{\partial F_{c12}}{\partial w} \cos(\theta_1 - \theta_2) \\
\frac{\partial F_c}{\partial q} &= 0 \\
\frac{\partial F_c}{\partial \theta_f} &= \left(\frac{\partial F_c}{\partial \theta_f} \right)_{SP} + \frac{\partial F_{c12}}{\partial \theta_f} \cos(\theta_1 - \theta_2) \\
\frac{\partial F_c}{\partial \dot{\theta}_1} &= \left(\frac{\partial F_c}{\partial \dot{\theta}_1} \right)_{SP} + \frac{\partial F_{c12}}{\partial \dot{\theta}_1} \cos(\theta_1 - \theta_2) \\
\frac{\partial F_c}{\partial \theta_1} &= \left(\frac{\partial F_c}{\partial \theta_1} \right)_{SP} + \frac{\partial F_{c12}}{\partial \theta_1} \cos(\theta_1 - \theta_2) - F_{c12} \sin(\theta_1 - \theta_2) \\
\frac{\partial F_c}{\partial \dot{\theta}_2} &= \frac{\partial F_{c12}}{\partial \dot{\theta}_2} \cos(\theta_1 - \theta_2) \\
\frac{\partial F_c}{\partial \theta_2} &= \frac{\partial F_{c12}}{\partial \theta_2} \cos(\theta_1 - \theta_2) + F_{c12} \sin(\theta_1 - \theta_2)
\end{aligned} \tag{C.11}$$

Partial Derivatives Load angles

$$\begin{aligned}
&\begin{bmatrix} (m_1 + m_2) l_1^2 & m_2 l_1 l_2 \cos(\theta_1 - \theta_2) \\ m_2 l_1 l_2 \cos(\theta_1 - \theta_2) & m_2 l_2^2 \end{bmatrix} \begin{bmatrix} \ddot{\theta}_1 \\ \ddot{\theta}_2 \end{bmatrix} = \\
&\left(\begin{bmatrix} (m_1 + m_2) (l_1 [\cos(\theta_1) \ddot{x}_0 + \sin(\theta_1) \ddot{z}_0] - l_1 g \sin(\theta_1)) - m_2 l_1 l_2 \dot{\theta}_2^2 \sin(\theta_1 - \theta_2) \\ m_2 (l_1 l_2 \dot{\theta}_1^2 \sin(\theta_1 - \theta_2) + l_2 [\cos(\theta_2) \ddot{x}_0 + \sin(\theta_2) \ddot{z}_0] - l_2 g \sin(\theta_2)) \end{bmatrix} \right)
\end{aligned} \tag{C.12}$$

Rewritten to:

$$\begin{bmatrix} A_{11} & A_{12} \\ A_{21} & A_{22} \end{bmatrix} \begin{bmatrix} \ddot{\theta}_1 \\ \ddot{\theta}_2 \end{bmatrix} = \begin{bmatrix} B_1 \\ B_2 \end{bmatrix} \rightarrow \begin{bmatrix} \ddot{\theta}_1 \\ \ddot{\theta}_2 \end{bmatrix} = \frac{1}{A_{11}A_{22} - A_{12}A_{21}} \begin{bmatrix} A_{22}B_1 - A_{12}B_2 \\ A_{11}B_2 - A_{21}B_1 \end{bmatrix} \tag{C.13}$$

Adding the drag components to the accelerations:

$$\begin{bmatrix} A_{11} & A_{12} \\ A_{21} & A_{22} \end{bmatrix} \begin{bmatrix} \ddot{\theta}_1 \\ \ddot{\theta}_2 \end{bmatrix} = \begin{bmatrix} B_1 \\ B_2 \end{bmatrix} \rightarrow \begin{bmatrix} \ddot{\theta}_1 \\ \ddot{\theta}_2 \end{bmatrix} = \frac{1}{A_{11}A_{22} - A_{12}A_{21}} \begin{bmatrix} A_{22}B_1 - A_{12}B_2 \\ A_{11}B_2 - A_{21}B_1 \end{bmatrix} + \begin{bmatrix} Q_1 m_1 l_1^2 \\ Q_2 m_2 l_2^2 \end{bmatrix} \tag{C.14}$$

With:

$$\begin{aligned}
Q_1 &= \text{sgn}(\dot{x}_1) D_{1_x} l_1 \cos(\theta_1) + \text{sgn}(\dot{z}_1) D_{1_z} l_1 \sin(\theta_1) \\
Q_2 &= \text{sgn}(\dot{x}_2) D_{2_x} l_2 \cos(\theta_2) + \text{sgn}(\dot{z}_2) D_{2_z} l_2 \sin(\theta_2)
\end{aligned} \tag{C.15}$$

Note that the partial derivatives of Q_1 can be found in Appendix B.

Partial Derivatives of Q_2

Assuming both \dot{x}_2 and \dot{z}_2 are positive:

$$\begin{aligned}
\frac{\partial Q_2}{\partial D_{2_x}} &= l_2 \cos(\theta_2) \\
\frac{\partial Q_2}{\partial D_{2_z}} &= l_2 \sin(\theta_2) \\
\frac{\partial Q_2}{\partial u} &= \frac{\partial Q_2}{\partial D_{2_x}} \frac{\partial D_{2_x}}{\partial \dot{x}_2} \frac{\partial \dot{x}_2}{\partial \dot{x}_1} \frac{\partial \dot{x}_1}{\partial \dot{x}_0} \frac{\partial \dot{x}_0}{\partial u} + \frac{\partial Q_2}{\partial D_{2_z}} \frac{\partial D_{2_z}}{\partial \dot{z}_2} \frac{\partial \dot{z}_2}{\partial \dot{z}_1} \frac{\partial \dot{z}_1}{\partial \dot{z}_0} \frac{\partial \dot{z}_0}{\partial u} \\
\frac{\partial Q_2}{\partial w} &= \frac{\partial Q_2}{\partial D_{2_x}} \frac{\partial D_{2_x}}{\partial \dot{x}_2} \frac{\partial \dot{x}_2}{\partial \dot{x}_1} \frac{\partial \dot{x}_1}{\partial \dot{x}_0} \frac{\partial \dot{x}_0}{\partial w} + \frac{\partial Q_2}{\partial D_{2_z}} \frac{\partial D_{2_z}}{\partial \dot{z}_2} \frac{\partial \dot{z}_2}{\partial \dot{z}_1} \frac{\partial \dot{z}_1}{\partial \dot{z}_0} \frac{\partial \dot{z}_0}{\partial w} \\
\frac{\partial Q_2}{\partial \theta_f} &= \frac{\partial Q_2}{\partial D_{2_x}} \frac{\partial D_{2_x}}{\partial \dot{x}_2} \frac{\partial \dot{x}_2}{\partial \dot{x}_1} \frac{\partial \dot{x}_1}{\partial \dot{x}_0} \frac{\partial \dot{x}_0}{\partial \theta_f} + \frac{\partial Q_2}{\partial D_{2_z}} \frac{\partial D_{2_z}}{\partial \dot{z}_2} \frac{\partial \dot{z}_2}{\partial \dot{z}_1} \frac{\partial \dot{z}_1}{\partial \dot{z}_0} \frac{\partial \dot{z}_0}{\partial \theta_f} \\
\frac{\partial Q_2}{\partial \dot{\theta}_1} &= \frac{\partial Q_2}{\partial D_{2_x}} \frac{\partial D_{2_x}}{\partial \dot{x}_2} \frac{\partial \dot{x}_2}{\partial \dot{x}_1} \frac{\partial \dot{x}_1}{\partial \dot{\theta}_1} + \frac{\partial Q_2}{\partial D_{2_z}} \frac{\partial D_{2_z}}{\partial \dot{z}_2} \frac{\partial \dot{z}_2}{\partial \dot{z}_1} \frac{\partial \dot{z}_1}{\partial \dot{\theta}_1} \\
\frac{\partial Q_2}{\partial \theta_1} &= \frac{\partial Q_2}{\partial D_{2_x}} \frac{\partial D_{2_x}}{\partial \dot{x}_2} \frac{\partial \dot{x}_2}{\partial \dot{x}_1} \frac{\partial \dot{x}_1}{\partial \theta_1} + \frac{\partial Q_2}{\partial D_{2_z}} \frac{\partial D_{2_z}}{\partial \dot{z}_2} \frac{\partial \dot{z}_2}{\partial \dot{z}_1} \frac{\partial \dot{z}_1}{\partial \theta_1} \\
\frac{\partial Q_2}{\partial \dot{\theta}_2} &= \frac{\partial Q_2}{\partial D_{2_x}} \frac{\partial D_{2_x}}{\partial \dot{x}_2} \frac{\partial \dot{x}_2}{\partial \dot{\theta}_2} + \frac{\partial Q_2}{\partial D_{2_z}} \frac{\partial D_{2_z}}{\partial \dot{z}_2} \frac{\partial \dot{z}_2}{\partial \dot{\theta}_2} \\
\frac{\partial Q_2}{\partial \theta_2} &= \frac{\partial Q_2}{\partial D_{2_x}} \frac{\partial D_{2_x}}{\partial \dot{x}_2} \frac{\partial \dot{x}_2}{\partial \theta_2} - D_{2_x} l_2 \sin(\theta_2) + \frac{\partial Q_2}{\partial D_{2_z}} \frac{\partial D_{2_z}}{\partial \dot{z}_2} \frac{\partial \dot{z}_2}{\partial \theta_2} + D_{2_z} l_2 \cos(\theta_2)
\end{aligned} \tag{C.16}$$

Partial Derivatives of \ddot{x}_0 and \ddot{z}_0 w.r.t. $\dot{\theta}_2$ and θ_2

The partial derivatives of \ddot{x}_0 and \ddot{z}_0 w.r.t. all other states have already been derived in Appendix B. Therefore, only the partial derivatives w.r.t. states $\dot{\theta}_2$ and θ_2 are presented here.

$$\begin{aligned}
\frac{\partial \ddot{x}_0}{\partial \dot{\theta}_2} &= \frac{\partial \dot{u}}{\partial \dot{\theta}_2} \sin(\theta_f) + \frac{\partial \dot{w}}{\partial \dot{\theta}_2} \cos(\theta_f) \\
\frac{\partial \ddot{x}_0}{\partial \theta_2} &= \frac{\partial \dot{u}}{\partial \theta_2} \sin(\theta_f) + \frac{\partial \dot{w}}{\partial \theta_2} \cos(\theta_f) \\
\frac{\partial \ddot{z}_0}{\partial \dot{\theta}_2} &= -\frac{\partial \dot{u}}{\partial \dot{\theta}_2} \sin(\theta_f) + \frac{\partial \dot{w}}{\partial \dot{\theta}_2} \cos(\theta_f) \\
\frac{\partial \ddot{z}_0}{\partial \theta_2} &= -\frac{\partial \dot{u}}{\partial \theta_2} \sin(\theta_f) + \frac{\partial \dot{w}}{\partial \theta_2} \cos(\theta_f)
\end{aligned} \tag{C.17}$$

Partial Derivatives of A_{ij}

$$\frac{\partial A_{12}}{\partial \theta_1} = \frac{\partial A_{21}}{\partial \theta_1} = -m_2 l_1 l_2 \sin(\theta_1 - \theta_2); \quad \frac{\partial A_{12}}{\partial \theta_2} = \frac{\partial A_{21}}{\partial \theta_2} = m_2 l_1 l_2 \sin(\theta_1 - \theta_2) \tag{C.18}$$

Partial Derivatives of B_i

$$B_1 = (m_1 + m_2) (l_1 [\cos(\theta_1) \ddot{x}_0 + \sin(\theta_1) \ddot{z}_0] - l_1 g \sin(\theta_1)) - m_2 l_1 l_2 \dot{\theta}_2^2 \sin(\theta_1 - \theta_2) \tag{C.19}$$

$$\begin{aligned}
\frac{\partial B_1}{\partial u} &= (m_1 + m_2) l_1 \left[\cos(\theta_1) \left(\frac{\partial \ddot{x}_0}{\partial u} \right)_{SP} + \sin(\theta_1) \left(\frac{\partial \ddot{z}_0}{\partial u} \right)_{SP} \right] \\
\frac{\partial B_1}{\partial w} &= (m_1 + m_2) l_1 \left[\cos(\theta_1) \left(\frac{\partial \ddot{x}_0}{\partial w} \right)_{SP} + \sin(\theta_1) \left(\frac{\partial \ddot{z}_0}{\partial w} \right)_{SP} \right] \\
\frac{\partial B_1}{\partial q} &= (m_1 + m_2) l_1 \left[\cos(\theta_1) \left(\frac{\partial \ddot{x}_0}{\partial q} \right)_{SP} + \sin(\theta_1) \left(\frac{\partial \ddot{z}_0}{\partial q} \right)_{SP} \right] \\
\frac{\partial B_1}{\partial \theta_f} &= (m_1 + m_2) l_1 \left[\cos(\theta_1) \left(\frac{\partial \ddot{x}_0}{\partial \theta_f} \right)_{SP} + \sin(\theta_1) \left(\frac{\partial \ddot{z}_0}{\partial \theta_f} \right)_{SP} \right] \\
\frac{\partial B_1}{\partial \dot{\theta}_1} &= (m_1 + m_2) l_1 \left[\cos(\theta_1) \left(\frac{\partial \ddot{x}_0}{\partial \dot{\theta}_1} \right)_{SP} + \sin(\theta_1) \left(\frac{\partial \ddot{z}_0}{\partial \dot{\theta}_1} \right)_{SP} \right] \\
\frac{\partial B_1}{\partial \theta_1} &= (m_1 + m_2) l_1 \left[\cos(\theta_1) \left(\frac{\partial \ddot{x}_0}{\partial \theta_1} \right)_{SP} + \sin(\theta_1) \left(\frac{\partial \ddot{z}_0}{\partial \theta_1} \right)_{SP} - \sin(\theta_1) \ddot{x}_0 + \cos(\theta_1) \ddot{z}_0 - g \cos(\theta_1) \right] \\
&\quad - m_2 l_1 l_2 \dot{\theta}_2^2 \cos(\theta_1 - \theta_2) \\
\frac{\partial B_1}{\partial \dot{\theta}_2} &= (m_1 + m_2) l_1 \left[\cos(\theta_1) \frac{\partial \ddot{x}_0}{\partial \dot{\theta}_2} + \sin(\theta_1) \frac{\partial \ddot{z}_0}{\partial \dot{\theta}_2} \right] - 2m_2 l_1 l_2 \dot{\theta}_2 \sin(\theta_1 - \theta_2) \\
\frac{\partial B_1}{\partial \theta_2} &= (m_1 + m_2) l_1 \left[\cos(\theta_1) \frac{\partial \ddot{x}_0}{\partial \theta_2} + \sin(\theta_1) \frac{\partial \ddot{z}_0}{\partial \theta_2} \right] + m_2 l_1 l_2 \dot{\theta}_2^2 \cos(\theta_1 - \theta_2) \\
\frac{\partial B_1}{\partial \theta_c} &= (m_1 + m_2) l_1 \left[\cos(\theta_1) \left(\frac{\partial \ddot{x}_0}{\partial \theta_c} \right)_{SP} + \sin(\theta_1) \left(\frac{\partial \ddot{z}_0}{\partial \theta_c} \right)_{SP} \right] \\
\frac{\partial B_1}{\partial \theta_0} &= (m_1 + m_2) l_1 \left[\cos(\theta_1) \left(\frac{\partial \ddot{x}_0}{\partial \theta_0} \right)_{SP} + \sin(\theta_1) \left(\frac{\partial \ddot{z}_0}{\partial \theta_0} \right)_{SP} \right]
\end{aligned} \tag{C.20}$$

$$B_2 = m_2 \left(l_1 l_2 \dot{\theta}_1^2 \sin(\theta_1 - \theta_2) + l_2 [\cos(\theta_2) \ddot{x}_0 + \sin(\theta_2) \ddot{z}_0] - l_2 g \sin(\theta_2) \right) \tag{C.21}$$

$$\begin{aligned}
\frac{\partial B_2}{\partial u} &= m_2 l_2 \left[\cos(\theta_2) \left(\frac{\partial \ddot{x}_0}{\partial u} \right)_{SP} + \sin(\theta_2) \left(\frac{\partial \ddot{z}_0}{\partial u} \right)_{SP} \right] \\
\frac{\partial B_2}{\partial w} &= m_2 l_2 \left[\cos(\theta_2) \left(\frac{\partial \ddot{x}_0}{\partial w} \right)_{SP} + \sin(\theta_2) \left(\frac{\partial \ddot{z}_0}{\partial w} \right)_{SP} \right] \\
\frac{\partial B_2}{\partial q} &= m_2 l_2 \left[\cos(\theta_2) \left(\frac{\partial \ddot{x}_0}{\partial q} \right)_{SP} + \sin(\theta_2) \left(\frac{\partial \ddot{z}_0}{\partial q} \right)_{SP} \right] \\
\frac{\partial B_2}{\partial \theta_f} &= m_2 l_2 \left[\cos(\theta_2) \left(\frac{\partial \ddot{x}_0}{\partial \theta_f} \right)_{SP} + \sin(\theta_2) \left(\frac{\partial \ddot{z}_0}{\partial \theta_f} \right)_{SP} \right] \\
\frac{\partial B_2}{\partial \dot{\theta}_1} &= m_2 l_2 \left[\cos(\theta_2) \left(\frac{\partial \ddot{x}_0}{\partial \dot{\theta}_1} \right)_{SP} + \sin(\theta_2) \left(\frac{\partial \ddot{z}_0}{\partial \dot{\theta}_1} \right)_{SP} \right] + 2m_2 l_1 l_2 \dot{\theta}_1 \sin(\theta_1 - \theta_2) \\
\frac{\partial B_2}{\partial \theta_1} &= m_2 l_2 \left[\cos(\theta_2) \left(\frac{\partial \ddot{x}_0}{\partial \theta_1} \right)_{SP} + \sin(\theta_2) \left(\frac{\partial \ddot{z}_0}{\partial \theta_1} \right)_{SP} \right] + m_2 l_1 l_2 \dot{\theta}_1^2 \cos(\theta_1 - \theta_2) \\
\frac{\partial B_2}{\partial \dot{\theta}_2} &= m_2 l_2 \left[\cos(\theta_2) \frac{\partial \ddot{x}_0}{\partial \dot{\theta}_2} + \sin(\theta_2) \frac{\partial \ddot{z}_0}{\partial \dot{\theta}_2} \right] \\
\frac{\partial B_2}{\partial \theta_2} &= m_2 l_2 \left[\cos(\theta_2) \frac{\partial \ddot{x}_0}{\partial \theta_2} + \sin(\theta_2) \frac{\partial \ddot{z}_0}{\partial \theta_2} - \sin(\theta_2) \ddot{x}_0 + \cos(\theta_2) \ddot{z}_0 - g \cos(\theta_2) \right] \\
&\quad - m_2 l_1 l_2 \dot{\theta}_1^2 \cos(\theta_1 - \theta_2) \\
\frac{\partial B_2}{\partial \theta_c} &= m_2 l_2 \left[\cos(\theta_2) \left(\frac{\partial \ddot{x}_0}{\partial \theta_c} \right)_{SP} + \sin(\theta_2) \left(\frac{\partial \ddot{z}_0}{\partial \theta_c} \right)_{SP} \right] \\
\frac{\partial B_2}{\partial \theta_0} &= m_2 l_2 \left[\cos(\theta_2) \left(\frac{\partial \ddot{x}_0}{\partial \theta_0} \right)_{SP} + \sin(\theta_2) \left(\frac{\partial \ddot{z}_0}{\partial \theta_0} \right)_{SP} \right]
\end{aligned} \tag{C.22}$$

Partial Derivatives $\ddot{\theta}_1$

$$\ddot{\theta}_1 = A_{22}B_1 - A_{12}B_2 + Q_1 \quad (\text{C.23})$$

$$\frac{\partial \ddot{\theta}_1}{\partial u} = A_{22} \frac{\partial B_1}{\partial u} - A_{12} \frac{\partial B_2}{\partial u} + \left(\frac{\partial Q_1}{\partial u} \right)_{SP}$$

$$\frac{\partial \ddot{\theta}_1}{\partial w} = A_{22} \frac{\partial B_1}{\partial w} - A_{12} \frac{\partial B_2}{\partial w} + \left(\frac{\partial Q_1}{\partial w} \right)_{SP}$$

$$\frac{\partial \ddot{\theta}_1}{\partial q} = A_{22} \frac{\partial B_1}{\partial q} - A_{12} \frac{\partial B_2}{\partial q} + \left(\frac{\partial Q_1}{\partial q} \right)_{SP}$$

$$\frac{\partial \ddot{\theta}_1}{\partial \theta_f} = A_{22} \frac{\partial B_1}{\partial \theta_f} - A_{12} \frac{\partial B_2}{\partial \theta_f} + \left(\frac{\partial Q_1}{\partial \theta_f} \right)_{SP}$$

$$\frac{\partial \ddot{\theta}_1}{\partial \dot{\theta}_1} = A_{22} \frac{\partial B_1}{\partial \dot{\theta}_1} - A_{12} \frac{\partial B_2}{\partial \dot{\theta}_1} + \left(\frac{\partial Q_1}{\partial \dot{\theta}_1} \right)_{SP}$$

$$\frac{\partial \ddot{\theta}_1}{\partial \theta_1} = A_{22} \frac{\partial B_1}{\partial \theta_1} - \frac{\partial A_{12}}{\partial \theta_1} B_2 - A_{12} \frac{\partial B_2}{\partial \theta_1} + \left(\frac{\partial Q_1}{\partial \theta_1} \right)_{SP}$$

$$\frac{\partial \ddot{\theta}_1}{\partial \theta_2} = A_{22} \frac{\partial B_1}{\partial \theta_2} - A_{12} \frac{\partial B_2}{\partial \theta_2}$$

$$\frac{\partial \ddot{\theta}_1}{\partial \theta_2} = A_{22} \frac{\partial B_1}{\partial \theta_2} - \frac{\partial A_{12}}{\partial \theta_2} B_2 - A_{12} \frac{\partial B_2}{\partial \theta_2}$$

$$\frac{\partial \ddot{\theta}_1}{\partial \theta_c} = A_{22} \frac{\partial B_1}{\partial \theta_c} - A_{12} \frac{\partial B_2}{\partial \theta_c}$$

$$\frac{\partial \ddot{\theta}_1}{\partial \theta_f} = A_{22} \frac{\partial B_1}{\partial \theta_0} - A_{12} \frac{\partial B_2}{\partial \theta_0}$$

(C.24)

Partial Derivatives $\ddot{\theta}_2$

$$\ddot{\theta}_1 = A_{11}B_2 - A_{21}B_1 + Q_2 \quad (\text{C.25})$$

$$\frac{\partial \ddot{\theta}_1}{\partial u} = A_{11} \frac{\partial B_2}{\partial u} - A_{21} \frac{\partial B_1}{\partial u} + \frac{\partial Q_2}{\partial u}$$

$$\frac{\partial \ddot{\theta}_1}{\partial w} = A_{11} \frac{\partial B_2}{\partial w} - A_{21} \frac{\partial B_1}{\partial w} + \frac{\partial Q_2}{\partial w}$$

$$\frac{\partial \ddot{\theta}_1}{\partial q} = A_{11} \frac{\partial B_2}{\partial q} - A_{21} \frac{\partial B_1}{\partial q} + \frac{\partial Q_2}{\partial q}$$

$$\frac{\partial \ddot{\theta}_1}{\partial \theta_f} = A_{11} \frac{\partial B_2}{\partial \theta_f} - A_{21} \frac{\partial B_1}{\partial \theta_f} + \frac{\partial Q_2}{\partial \theta_f}$$

$$\frac{\partial \ddot{\theta}_1}{\partial \dot{\theta}_1} = A_{11} \frac{\partial B_2}{\partial \dot{\theta}_1} - A_{21} \frac{\partial B_1}{\partial \dot{\theta}_1}$$

$$\frac{\partial \ddot{\theta}_1}{\partial \theta_1} = A_{11} \frac{\partial B_2}{\partial \theta_1} - \frac{\partial A_{21}}{\partial \theta_1} B_1 - A_{21} \frac{\partial B_1}{\partial \theta_1}$$

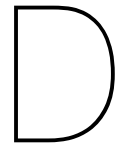
$$\frac{\partial \ddot{\theta}_1}{\partial \theta_2} = A_{11} \frac{\partial B_2}{\partial \theta_2} - A_{21} \frac{\partial B_1}{\partial \theta_2} + \frac{\partial Q_2}{\partial \theta_2}$$

$$\frac{\partial \ddot{\theta}_1}{\partial \theta_2} = A_{11} \frac{\partial B_2}{\partial \theta_2} - \frac{\partial A_{21}}{\partial \theta_2} B_1 - A_{21} \frac{\partial B_1}{\partial \theta_2} + \frac{\partial Q_2}{\partial \theta_2}$$

$$\frac{\partial \ddot{\theta}_1}{\partial \theta_c} = A_{11} \frac{\partial B_2}{\partial \theta_c} - A_{21} \frac{\partial B_1}{\partial \theta_c}$$

$$\frac{\partial \ddot{\theta}_1}{\partial \theta_0} = A_{11} \frac{\partial B_2}{\partial \theta_0} - A_{21} \frac{\partial B_1}{\partial \theta_0}$$

(C.26)



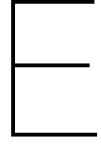
Simulation Data

Table D.1: Simulation data Bö-105 Helicopter obtained from supervisor

Variable name	Symbol	Value	Unit
Mass helicopter	M_{hel}	2096	kg
Mass rotorblade	m_{bl}	27.3	kg
	\bar{f}	-0.00155	-
	\bar{h}	0.1924	-
	\bar{f}_1	0.0061	-
Number of main rotorblades	N	4	-
Main rotor radius	R	4.91	m
Main rotor blade chord	c_{mr}	0.27	m
Main rotor liftgradient	C_{l_α}	5.73	rad ⁻¹
Main rotor speed	Ω_{mr}	424	rot/min
Helicopter moment of inertia around x-axis	I_x	1803	kgm ²
Helicopter moment of inertia around y-axis	I_y	4892	kgm ²
Helicopter moment of inertia around z-axis	I_z	4428	kgm ²
Helicopter product of inertia	I_{xz}	660	kgm ²
Rotor blade moment of inertia	I_{bl}	231.7	kgm ²
Number of tail rotorblades	N_{tr}	2	-
Tail rotor radius	R_{tr}	0.95	m
Tail rotor blade chord	c_{tr}	0.18	m
	$l_{tr} - f$	6.01726	m
	$h_{tr} - h$	0.1095	m
Tail rotor liftgradient	C_{l_α}	5.7	rad ⁻¹
Tail rotor speed	Ω_{tr}	1350	rot/min
Surface area horizontal stabilizer	S_{ht}	0.809	m ²
Horizontal stabilizer surface area	$C_{l_{ht_\alpha}}$	4	rad ⁻¹
Initial incline horizontal stabilizer	α_{0ht}	0	deg
	$l_{ht} - f$	4.556	m
	$h_{ht} - h$	0.989144	m
Fuselage equivalent drag area	F_0	1.3	m ²
Horizontal stabilizer downwash factor	K_{ht}	1.5	-
Fuselage correction coefficient	K_{fus}	0.83	-
Frontal fuselage drag area	S_{fus}	$F_0/0.2$	-
Fuselage length	l_{fus}	8.509	m
equivalent volume of circular body in lateral view	$(Vol_{fus})_n$	$(\pi/4) \times 25(AR)$	-
	S_{vt}	0	-
Time constant main rotor	$\tau_{\lambda i}$	0.1	-
Time constant tail rotor	$\tau_{\lambda itr}$	0.3	-
	$\bar{t} = \frac{M_{hel}}{\rho A \Omega R}$	0.103625	-

Table D.2: Cable and SONAR Data used throughout 6-DOF simulations. Note that when a variable has multiple values, different values are used for this variable throughout the cases.

Variable Name	Symbol	Value	Unit
Cable Specific:			
Number of cable sections	n	1,5,30	–
Length cable	l_c	30,120	m
Diameter cable	d_c	0.00955	m
Specific mass cable	$m_{c_{spec}}$	0.3477	kgm^{-1}
Damping cable rate	D_{rate_c}	-500,-50/n ³	Nms/rad
Damping cable angle	D_{angle_c}	-5,-1/n ³	Nm/deg
Drag coefficient in x direction cable section	CD_{c_x}	1	–
Drag coefficient in y direction cable section	CD_{c_y}	1	–
Drag coefficient in z direction cable section	CD_{c_z}	1	–
SONAR Specific:			
Length SONAR	l_s	5	m
Diameter SONAR	d_s	1	m
Mass SONAR	m_s	270	kg
Damping sonar rate	D_{rate_s}	-500	Nms/rad
Damping sonar angle	D_{angle_s}	-5	Nm/deg
Drag coefficient in x direction SONAR	CD_{s_x}	0.32	–
Drag coefficient in y direction SONAR	CD_{s_y}	0.32	–
Drag coefficient in z direction SONAR	CD_{s_z}	0.32	–
Environment Specific:			
Density air	ρ	1.225	kgm^{-3}
Density water	ρ_w	997	kgm^{-3}



Cable Model Verification

In this appendix, the computation of the angular acceleration of the cable model is verified by case study. For this, the cable is assumed to be 20 meters long, consisting of 2 10m long cable sections with the SONAR attached at the bottom. The top cable section is rotated an angle 20° around the x-axis and an angle of 10° around the y-axis. The second cable section is rotated an angle of 40° and 30° around the x- and y-axis. Both cable sections also have an initial angular rate. The rate around the x- and y-axis is $5^\circ/s$ for the first cable section and $1^\circ/s$ for the second cable section. The SONAR has no initial angular displacement, nor angular velocity. The damping constants used are $500Nm/s/rad$ for the angular rate and $5Nm/^\circ$.

The Rotation matrices from the LVLH frame to the section frame for the cable sections and the SONAR given the initial states are:

$$R_1(20^\circ, 10^\circ) = \begin{bmatrix} 0.9848 & 0.0594 & 0.1632 \\ 0 & 0.9397 & -0.3420 \\ -0.1736 & 0.3368 & 0.9254 \end{bmatrix} \quad (E.1)$$

$$R_2(40^\circ, 30^\circ) = \begin{bmatrix} 0.8660 & 0.3214 & 0.3830 \\ 0 & 0.7660 & -0.6428 \\ -0.5000 & 0.5567 & 0.6634 \end{bmatrix} \quad (E.2)$$

$$R_{SONAR}(0^\circ, 0^\circ) = \begin{bmatrix} 1 & 0 & 0 \\ 0 & 1 & 0 \\ 0 & 0 & 1 \end{bmatrix} \quad (E.3)$$

The inertia of the cable sections and the SONAR in their section frame are:

$$J^{(k)}_c = \begin{bmatrix} 28.9750 & 0 & 0 \\ 0 & 28.9750 & 0 \\ 0 & 0 & 0.0000 \end{bmatrix} \quad (E.4)$$

$$J^{(k)}_{SONAR} = \begin{bmatrix} 562.5000 & 0 & 0 \\ 0 & 562.5000 & 0 \\ 0 & 0 & 33.7500 \end{bmatrix} \quad (E.5)$$

Rotating them to the LVLH frame yields:

$$J^{(A)}_{s1} = \begin{bmatrix} 28.2035 & 1.6171 & -4.3754 \\ 1.6171 & 25.5856 & 9.1709 \\ -4.3754 & 9.1709 & 4.1610 \end{bmatrix} \quad (E.6)$$

$$J^{(A)}_{s2} = \begin{bmatrix} 24.7242 & 7.1337 & -7.3626 \\ 7.1337 & 17.0032 & 12.3559 \\ -7.3626 & 12.3559 & 16.2226 \end{bmatrix} \quad (E.7)$$

$$J^{(A)}_{SONAR} = \begin{bmatrix} 562.5000 & 0 & 0 \\ 0 & 562.5000 & 0 \\ 0 & 0 & 33.7500 \end{bmatrix} \quad (E.8)$$

With an initial altitude of the helicopter of 60m and the rotation matrices, the hinge positions of the cable and SONAR can be computed starting from the top to the bottom:

$$p_0 = \begin{bmatrix} 0 \\ 0 \\ 0 \end{bmatrix}, p_1 = \begin{bmatrix} 1.6318 \\ -3.4202 \\ -50.7458 \end{bmatrix}, p_2 = \begin{bmatrix} 5.4620 \\ -9.8481 \\ -44.1117 \end{bmatrix}, p_3 = \begin{bmatrix} 5.4620 \\ -9.8481 \\ -39.1117 \end{bmatrix}, \quad (\text{E.9})$$

Note that the z-direction is defined positive downwards, meaning that the z-direction increases from -trim altitude with decreasing altitude.

The P -matrices (see App A from scientific paper) can then be computed as:

$$P_{0 \rightarrow 1} = \begin{bmatrix} 0 & -9.2542 & -3.4202 \\ 9.2542 & 0 & -1.6318 \\ 3.4202 & 1.6318 & 0 \end{bmatrix} \quad P_{1 \rightarrow 2} = \begin{bmatrix} 0 & -6.6341 & -6.4279 \\ 6.6341 & 0 & -3.8302 \\ 6.4279 & 3.8302 & 0 \end{bmatrix} \quad P_{2 \rightarrow 3} = \begin{bmatrix} 0 & -5 & 0 \\ 5 & 0 & 0 \\ 0 & 0 & 0 \end{bmatrix} \quad (\text{E.10}) \quad (\text{E.11}) \quad (\text{E.12})$$

The $\bar{\Omega}$ -matrices (see App A from scientific paper) can then be computed as:

$$\bar{\Omega}_{s1} = \begin{bmatrix} 0 & 0 & 0.0873 \\ 0 & 0 & -0.0873 \\ -0.0873 & 0.0873 & 0 \end{bmatrix} \quad \bar{\Omega}_{s2} = \begin{bmatrix} 0 & 0 & 0.0175 \\ 0 & 0 & -0.0175 \\ -0.0175 & 0.0175 & 0 \end{bmatrix} \quad \bar{\Omega}_{SONAR} = \begin{bmatrix} 0 & 0 & 0 \\ 0 & 0 & 0 \\ 0 & 0 & 0 \end{bmatrix} \quad (\text{E.13}) \quad (\text{E.14}) \quad (\text{E.15})$$

The linear velocity of the cable hinges are:

$$\nu_0 = \begin{bmatrix} 0 \\ 0 \\ 0 \end{bmatrix}, \nu_1 = \begin{bmatrix} 0.8076 \\ -0.8076 \\ -0.4409 \end{bmatrix}, \nu_2 = \begin{bmatrix} 0.9234 \\ -0.9234 \\ -0.6199 \end{bmatrix}, \nu_3 = \begin{bmatrix} 0.9234 \\ -0.9234 \\ -0.6199 \end{bmatrix}, \quad (\text{E.16})$$

With the linear velocity at the c.g.'s of the sections being:

$$\nu_{s1} = \begin{bmatrix} 0.4038 \\ -0.4038 \\ -0.2204 \end{bmatrix}, \nu_{s2} = \begin{bmatrix} 0.8655 \\ -0.8655 \\ -0.5304 \end{bmatrix}, \nu_{SONAR} = \begin{bmatrix} 0.9234 \\ -0.9234 \\ -0.6199 \end{bmatrix}, \quad (\text{E.17})$$

The surface area of the cable and SONAR in their section frame equals:

$$S_c^{(k)} = \begin{bmatrix} 0.0955 \\ 0.0955 \\ 0.0001 \end{bmatrix} \quad (\text{E.18}) \quad S_{SONAR}^{(k)} = \begin{bmatrix} 5.0000 \\ 5.0000 \\ 0.7854 \end{bmatrix} \quad (\text{E.19})$$

Rotating it to the LVLH frame yields:

$$S_{s1}^{(A)} = \begin{bmatrix} 0.0940 \\ 0.0954 \\ -0.0170 \end{bmatrix}, S_{s2}^{(A)} = \begin{bmatrix} 0.0827 \\ 0.1039 \\ -0.0248 \end{bmatrix}, S_{SONAR}^{(A)} = \begin{bmatrix} 5.0000 \\ 5.0000 \\ 0.7854 \end{bmatrix}, \quad (\text{E.20})$$

The drag on the cable sections can then be computed as:

$$\bar{F}_{AE_{s1}} = \begin{bmatrix} -0.0094 \\ 0.0095 \\ 0.0005 \end{bmatrix}, \bar{F}_{AE_{s2}} = \begin{bmatrix} -0.0379 \\ 0.0477 \\ 0.0043 \end{bmatrix}, \bar{F}_{AE_{SONAR}} = \begin{bmatrix} -0.8356 \\ 0.8356 \\ 0.0592 \end{bmatrix}, \quad (\text{E.21})$$

Now, the Matrices can be assembled to compute the angular acceleration of the cable sections. These matrices are provided below:

$$A_{\dot{\omega}} = \begin{bmatrix} 28.2035 & 1.6171 & -4.3754 & 0 & 0 & 0 & 0 & 0 & 0 \\ 1.6171 & 25.5856 & 9.1709 & 0 & 0 & 0 & 0 & 0 & 0 \\ -4.3754 & 9.1709 & 4.1610 & 0 & 0 & 0 & 0 & 0 & 0 \\ 0 & 0 & 0 & 24.7242 & 7.1337 & -7.3626 & 0 & 0 & 0 \\ 0 & 0 & 0 & 7.1337 & 17.0032 & 12.3559 & 0 & 0 & 0 \\ 0 & 0 & 0 & -7.3626 & 12.3559 & 16.2226 & 0 & 0 & 0 \\ 0 & 0 & 0 & 0 & 0 & 0 & 562.5000 & 0 & 0 \\ 0 & 0 & 0 & 0 & 0 & 0 & 0 & 562.5 & 0 \\ 0 & 0 & 0 & 0 & 0 & 0 & 0 & 0 & 33.75 \end{bmatrix} \quad (\text{E.22})$$

$$B_{\dot{\omega}} = \begin{bmatrix} 0 & 16.088 & 5.946 & 0 & 32.177 & 11.892 & 0 & 2498.6 & 923.45 \\ -16.088 & 0 & 2.8368 & -32.177 & 0 & 5.6736 & -2498.6 & 0 & 440.57 \\ -5.946 & -2.8368 & 0 & -11.892 & -5.6736 & 0 & -923.45 & -440.57 & 0 \\ 0 & 0 & 0 & 0 & 11.534 & 11.175 & 0 & 1791.2 & 1735.5 \\ 0 & 0 & 0 & -11.534 & 0 & 6.6588 & -1791.2 & 0 & 1034.2 \\ 0 & 0 & 0 & -11.175 & -6.6588 & 0 & -1735.5 & -1034.2 & 0 \\ 0 & 0 & 0 & 0 & 0 & 0 & 0 & 675 & 0 \\ 0 & 0 & 0 & 0 & 0 & 0 & -675 & 0 & 0 \\ 0 & 0 & 0 & 0 & 0 & 0 & 0 & 0 & 0 \end{bmatrix} \quad (\text{E.23})$$

$$C_{\dot{\omega}} = \begin{bmatrix} -0.03652 \\ 0.03652 \\ 0.019937 \\ -0.001521 \\ 0.001521 \\ 0.0023519 \\ 0 \\ 0 \\ 0 \end{bmatrix} \quad (\text{E.24}) \quad D_{\dot{\omega}} = \begin{bmatrix} -9239.4 \\ -4412.3 \\ -1.5546 \\ -17135 \\ -10213 \\ -2.2011 \\ -2.0889 \\ -2.0889 \\ 0 \end{bmatrix} \quad (\text{E.25})$$

$$A_{\bar{a}_s} = \begin{bmatrix} 0 & 4.6271 & 1.7101 & 0 & 0 & 0 & 0 & 0 & 0 \\ -4.6271 & 0 & 0.81588 & 0 & 0 & 0 & 0 & 0 & 0 \\ -1.7101 & -0.81588 & 0 & 0 & 0 & 0 & 0 & 0 & 0 \\ 0 & 9.2542 & 3.4202 & 0 & 3.3171 & 3.2139 & 0 & 0 & 0 \\ -9.2542 & 0 & 1.6318 & -3.3171 & 0 & 1.9151 & 0 & 0 & 0 \\ -3.4202 & -1.6318 & 0 & -3.2139 & -1.9151 & 0 & 0 & 0 & 0 \\ 0 & 9.2542 & 3.4202 & 0 & 6.6341 & 6.4279 & 0 & 2.5 & 0 \\ -9.2542 & 0 & 1.6318 & -6.6341 & 0 & 3.8302 & -2.5 & 0 & 0 \\ -3.4202 & -1.6318 & 0 & -6.4279 & -3.8302 & 0 & 0 & 0 & 0 \end{bmatrix} \quad (\text{E.26})$$

$$B_{\bar{a}_s} = \begin{bmatrix} 0 & 0 & 0.043633 & 0 & 0 & 0 & 0 & 0 & 0 & 0 \\ 0 & 0 & -0.043633 & 0 & 0 & 0 & 0 & 0 & 0 & 0 \\ -0.043633 & 0.043633 & 0 & 0 & 0 & 0 & 0 & 0 & 0 & 0 \\ 0 & 0 & 0.087266 & 0 & 0 & 0.0087266 & 0 & 0 & 0 & 0 \\ 0 & 0 & -0.087266 & 0 & 0 & -0.0087266 & 0 & 0 & 0 & 0 \\ -0.087266 & 0.087266 & 0 & -0.0087266 & 0.0087266 & 0 & 0 & 0 & 0 & 0 \\ 0 & 0 & 0.087266 & 0 & 0 & 0.017453 & 0 & 0 & 0 & 0 \\ 0 & 0 & -0.087266 & 0 & 0 & -0.017453 & 0 & 0 & 0 & 0 \\ -0.087266 & 0.087266 & 0 & -0.017453 & 0.017453 & 0 & 0 & 0 & 0 & 0 \end{bmatrix} \quad (\text{E.27})$$

$$D_{damp} = \begin{bmatrix} 0 \\ 0 \\ 0 \\ 34.876 \\ 34.876 \\ 0 \\ 8.7876 \\ 8.7723 \\ 0 \end{bmatrix} \quad (\text{E.28})$$

The angular acceleration vector $\dot{\bar{\omega}}_s$ is then found to be:

$$\dot{\bar{\omega}}_s = \begin{bmatrix} 1.0202 \\ -87543 \\ 0.30588 \\ 0.74442 \\ 1.4691e + 05 \\ 0.1886 \\ 0.09347 \\ -1.5163e + 05 \\ 0 \end{bmatrix} \quad (\text{E.29})$$